

ISSUE: 31
SCOPUS

UNIVERSIDAD POLITÉCNICA SALESIANA ECUADOR

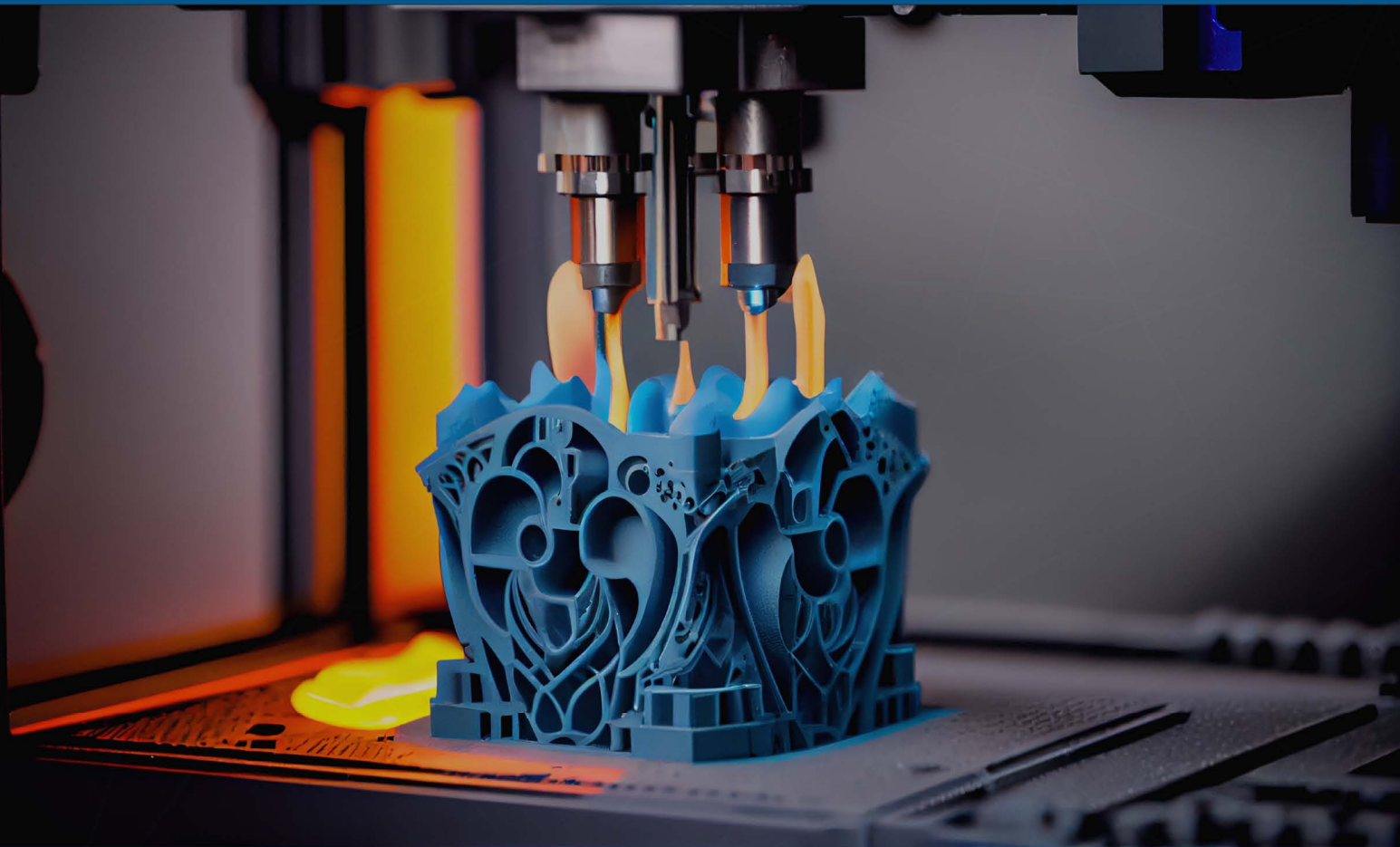
pISSN: 1390-650X

eISSN: 1390-860X

January / June 2024

INGENIUS

Revista de Ciencia y Tecnología



- Tensile/Compressive Response of 316L Stainless Steel Fabricated by Additive Manufacturing

Pag. 9

- Electric substation inspection: YOLOv5 in hotspot detection through thermal imaging.

Pag. 43

- Liquefied Petroleum Gas Systems: A Review On Design And Sizing Guidelines.

Pag. 81

- Incidence of automotive air conditioning on the index of fuel consumption in spark ignition vehicle on a route in the Ecuadorian Amazon.

Pag. 115

Indexed in: **SCOPUS**

INGENIUS

INGENIUS • Special Issue 31 • january/june 2024. Journal of Science and Tecnology of the Universidad Politécnica Salesiana of Ecuador. Publication dedicated to studies related to the Sciences of Mechanical Engineering, Electrical Engineering, Electronic Engineering, Mechatronic Engineering, Systems Engineering and Industrial Engineering.

Editors Board

RAFAEL ANTONIO BALART GIMENO, PHD, Universidad Politécnica de Valencia, España – Editor-in-chief.

JOHN IGNACIO CALLE SIGÜENCIA, PHD, Universidad Politécnica Salesiana, Ecuador – Editor-in-chief.

ESTEBAN MAURICIO INGA ORTEGA, PHD, Universidad Politécnica Salesiana, Ecuador – Associate Editor.

MARLON XAVIER QUINDE ABRIL, MSC, Universidad Politécnica Salesiana, Ecuador – Associate Editor.

TEODIANO FREIRE BASTOS FILHO, PHD, (Universidade Federal do Espírito Santo, Brasil – Associate Editor.

Scientific board

JUAN LÓPEZ MARTÍNEZ, PHD, Universidad Politécnica de Valencia, España.

ELENA FORTUNATI, PHD, Universidad de Perugia, Italia.

GUSTAVO ROVELO RUIZ, PHD, Hasselt University, Diepenbeek, Bélgica.

FRANKLIN GAVILANEZ ALVAREZ, PHD, American University, Estados Unidos.

PIEDAD GAÑAN ROJO, PHD, Universidad Pontificia Bolivariana, Colombia.

JOSÉ ALEX RESTREPO, PHD, Universidad Simón Bolívar, Venezuela.

SERGIO LUJAN MORA, PHD, Universidad de Alicante, España.

MARTHA ZEQUERA DÍAZ, PHD, Pontificia Universidad Javeriana, Colombia.

GROVER ZURITA, PHD, Universidad Privada Boliviana, Bolivia.

VLADIMIR ROBLES, PHD, Universidad Politécnica Salesiana, Ecuador.

GERMÁN ARÉVALO, PHD, Universidad Politécnica Salesiana, Ecuador.

WILBERT AGUILAR, PHD, Universidad de las Fuerzas Armadas, ESPE, Ecuador.

JACK BRAVO TORRES, PHD, Universidad Politécnica Salesiana, Ecuador.

WALTER OROZCO, PHD, Universidad Politécnica Salesiana, Ecuador.

MARIELA CERRADA, PHD, Universidad Politécnica Salesiana, Ecuador.

JULIO CÉSAR VIOLA, PHD, Universidad Politécnica Salesiana, Ecuador.

SERGIO GAMBOA SÁNCHEZ, PHD, Universidad Nacional Autónoma de México, México.

ROGER ABDÓN BUSTAMANTE PLAZA, PHD, Universidad de Chile, Chile.

CHRISTIAN BLUM, PHD, Consejo Superior de Investigaciones Científicas, España.

SILVIA NOEMI SCHIAFFINO, PHD, Universidad Nacional del Centro de la Provincia de Buenos Aires, Argentina.

ANALÍA ADRIANA AMANDI, PHD, Universidad Nacional del Centro de la Provincia de Buenos Aires, Argentina.

RUBÉN DE JESÚS MEDINA MOLINA, PHD,

Universidad de Los Andes, Venezuela.

JOHNNY JOSUÉ BULLÓN TORREALBA, PHD, Universidad de Los Andes, Venezuela.

RODRIGO PALMA HILLERNS, PHD, Universidad de Chile, Chile.

GERARDO ESPINOZA PÉREZ, PHD, Universidad Nacional Autónoma de México, México.

ALEXANDRE MENDES ABRÃO, PHD, Universidad Federal de Minas Gerais, Brasil.

KAMLA ABDEL RADI ISMAIL, PHD, Universidad Estatal de Campinas Unicamp, Brasil.

ARNALDO DA SILVA, PHD, Universidad Estatal de Campinas Unicamp, Brasil.

ÁLVARO ROCHA, PHD, Universidad de Coimbra, Portugal.

JOSÉ ANTENOR POMILIO, PHD, Universidad Estatal de Campinas Unicamp, Brasil.

LUIS PAULO REIS, PHD, Universidad de Minho, Portugal.

LUÍS FERNANDES, PHD, Escuela Superior Náutica Infante d. Henrique, Portugal.

ANÍBAL TRAÇA DE ALMEIDA, PHD, Universidad de Coimbra, Portugal.

JORGE SÁ SILVA, PHD, Universidad de Coimbra, Portugal.

PEDRO MANUEL SOARES MOURA, PHD, Universidad de Coimbra, Portugal.

SÉRGIO MANUEL RODRIGUES LOPES, PHD, Universidad de Coimbra, Portugal.

RICARDO MADEIRA SOARES BRANCO, PHD, Universidad de Coimbra, Portugal.

CARLOS ALEXANDRE BENTO CAPELA, PHD, Universidad de Coimbra, Portugal.

FILIFE ARAUJO, PHD, Universidad de Coimbra, Portugal.

LUIS MANUEL GUERRA SILVA ROSA, PHD, Universidad de Lisboa, Portugal.

HÉLDER DE JESUS FERNANDES, PUGA, PHD, Universidad de Minho, Portugal.

FILIFE SAMUEL, PEREIRA DA SILVA, PHD, Universidad de Minho, Portugal.

CÉSAR SEQUEIRA, PHD, Universidad de Lisboa, Portugal.

JOSÉ TEIXEIRA ESTÊVÃO FERREIRA, PHD,

Universidad de Coimbra, Portugal.

NUNO LARANJEIRO, PHD, Universidad de Coimbra, Portugal.

LUÍS AMARAL, PHD, Universidad de Lisboa, Portugal.

JORGE HENRIQUES, PHD, Universidad de Coimbra, Portugal.

WILLIAM IPANAQUE, PHD, Universidad de Piura, Perú.

LORENZO LEIJA SALAS, PHD, Centro de Investigación y Estudios Avanzados del Instituto Politécnico Nacional, México.

VALERI KONTOROVICH MAZOVER, PHD, Centro de Investigación y de Estudios Avanzados del Instituto Politécnico Nacional, México.

ALEJANDRO ÁVILA GARCÍA, PHD, Centro de Investigación y de Estudios Avanzados del Instituto Politécnico Nacional, México.

PAOLO BELLAVISTA, PHD, Universidad de Bologna, Italia.

CARLOS RUBIO, PhD, Centro de Ingeniería y Desarrollo Industrial, México.

FERNANDO HERNÁNDEZ SÁNCHEZ, PhD, Centro de Investigación Científica de Yucatán, México.

EMILIO MUÑOZ SANDOVAL, PhD, Instituto Potosino de Investigación Científica y Tecnológica, México.

YASUHIRO MATSUMOTO KUWABARA, PhD, Centro de Investigación y de Estudios Avanzados del Instituto Politécnico Nacional, México.

DAVID ZUMOFFEN, PhD, Centro Internacional Franco Argentino de Ciencias de la Información y de Sistemas, Argentina.

VICENTE RODRÍGUEZ GONZÁLEZ, PhD, Instituto Potosino de Investigación Científica y Tecnológica, México.

ALEJANDRO RODRÍGUEZ ÁNGELES, PhD, Centro de Investigación y de Estudios Avanzados del Instituto Politécnico Nacional, México.

ALISTAIR BORTHWICK, PhD, Universidad de Edimburgo, Reino Unido.

Reviewers board

FEDERICO DOMINGUEZ, PHD, Escuela Superior Politécnica del Litoral, Ecuador.

ENRIQUE CARRERA, PHD, Universidad de las Fuerzas Armadas, ESPE, Ecuador.

ANDRÉS TELLO, MSc, Universidad de Cuenca, Ecuador.

CRISTIAN GARCÍA BAUZA, PHD, Universidad Nacional del Centro de la Provincia de Buenos Aires, Argentina.

OSVALDO AÑÓ, PHD, Universidad Nacional de San Juan, Argentina.

THALÍA SAN ANTONIO, PHD, Universidad Técnica de Ambato, Ecuador.

VICTOR SAQUICELA, PHD, Universidad de Cuenca, Ecuador.

GONZALO OLMEDO, PHD, Universidad de las Fuerzas Armadas, ESPE, Ecuador.

ROMÁN LARA, PHD, Universidad de las Fuerzas Armadas, ESPE, Ecuador.

GUILLERMO SORIANO, PHD, Escuela Superior Politécnica del Litoral, Ecuador.

MARÍA FERNANDA GRANDA, PHD, Universidad de Cuenca, Ecuador.

RICARDO CAYSSIALS, PHD, Universidad Tecnológica Nacional, Argentina.

LEONARDO SOLAQUE GUZMAN, PHD, Universidad Militar Nueva Granada, Colombia.

JOSÉ DI PAOLO, PHD, Universidad Nacional de Entre Ríos, Argentina.

ASTRID RUBIANO FONSECA, PHD, Universidad Militar Nueva Granada, Colombia.

ROBINSON JIMÉNEZ, PHD, Universidad Militar Nueva Granada, Colombia.

ALFONSO ZOZAYA, PHD, Universidad de Carabobo, Venezuela.

MAURICIO MAULEDOUX, PHD, Universidad Militar Nueva Granada, Colombia.

LUIS MEDINA, PHD, Universidad Simón Bolívar, Venezuela.

ERNESTO CUADROS-VARGAS, PHD, Universidad Católica San Pablo, Perú.

SAMUEL SEPÚLVEDA CUEVAS, PHD, Universidad de la Frontera, Chile.

CARLOS CARES, PHD, Universidad de la Frontera, Chile.

RAFAEL SOTELO, PHD, Universidad de Montevideo, Uruguay.

OMAR LOPEZ, PHD, Universidad de Los Andes, Colombia.

JOB FLORES-GODOY, PHD, Universidad Católica del Uruguay, Uruguay.

LUIS MARIO MATEUS, PHD, Universidad de los Andes, Colombia.

AMADEO ARGÜELLES CRUZ, PHD, Instituto Politécnico Nacional, México.

SANTIAGO BENTANCOURT PARRA, PHD, Universidad Pontificia Bolivariana, Colombia.

GERMÁN ZAPATA, PHD, Universidad Nacio-

nal de Colombia, Colombia.

PEDRO GARCÍA, PHD, Universidad Autónoma de Barcelona, España.

ARTURO CONDE ENRÍQUEZ, PHD, Universidad Autónoma de Nuevo León, México.

ALBERTO CAVAZOS GONZÁLEZ, PHD, Universidad Autónoma de Nuevo León, México.

ERNESTO VÁZQUEZ MARTÍNEZ, PHD, Universidad Autónoma de Nuevo León, México.

MIGUEL DÍAZ RODRIGUEZ, PHD, Universidad de Los Andes, Venezuela.

EFRAÍN ALCORTA GARCÍA, PHD, Universidad Autónoma de Nuevo León, México.

LUIS CHIRINOS GARCIA, PHD, Pontificia Universidad Católica de Perú, Perú.

OSCAR AVILÉS, PHD, Universidad Militar Nueva Granada, Colombia.

DORA MARTÍNEZ DELGADO, PHD, Universidad Autónoma de Nuevo León, México.

DAVID OJEDA, PHD, Universidad Técnica del Norte, Ecuador.

IRENE BEATRÍZ STEINMANN, PHD, Universidad Tecnológica Nacional, Argentina.

MARIO SERRANO, Universidad Nacional de San Juan, Argentina.

CORNELIO POSADAS CASTILLO, PHD, Universidad Autónoma Nuevo León, México.

MARIO ALBERTO RIOS MESIAS, PHD, Universidad de Los Andes, Colombia.

YUDITH CARDINALE VILLARREAL, PHD, Universidad Simón Bolívar, Venezuela.

JOSE EDUARDO OCHOA LUNA, PHD, Universidad Católica San Pablo, Perú.

DANTE ANGEL ELIAS GIORDANO, PHD, Pontificia Universidad Católica de Perú, Perú.

MANUEL PELAEZ SAMANIEGO, PHD, Universidad de Cuenca, Ecuador.

JUAN ESPINOZA ABAD, PHD, Universidad de Cuenca, Ecuador.

PIETRO CODARA, PHD, Universidad de Milan, Italia.

ALBERTO SORIA, PHD, Centro de Investigación y de Estudios Avanzados del Instituto Politécnico Nacional, México.

JOSÉ M. ALLER, PHD, Universidad Politécnica Salesiana, Ecuador.

FERNEY AMAYA F., PHD, Universidad Pontificia Bolivariana, Medellín, Colombia.

SANTIAGO ARANGO ARAMBURO, PHD, Universidad Nacional de Colombia, Colombia.

DIEGO ARCOS-AVILÉS, PHD, Universidad de las Fuerzas Armadas, ESPE, Ecuador.

PABLO AREVALO, PHD, Universidad Politécnica Salesiana, Ecuador.

ROBERTO BELTRAN, MSc, Universidad de las Fuerzas Armadas, ESPE, Ecuador.

LEONARDO BETANCUR, PHD, Universidad Pontificia Bolivariana, Medellín, Colombia.

ROBERTO GAMBOA, PHD, Universidad de Lisboa, Portugal.

PAULO LOPES DOS SANTOS, PHD, Universidad do Porto, Portugal.

PEDRO ANDRÉ DIAS PRATES, PHD, Universidad de Coimbra, Portugal.

JOSÉ MANUEL TORRES FARINHA, PHD, Universidad de Coimbra, Portugal.

CELSO DE ALMEIDA, PHD, Universidad Estatal de Campinas Unicamp, Brasil.

RAMON MOLINA VALLE, PHD, Universidad Federal de Minas Gerais, Brasil.

CRISTINA NADER VASCONCELOS, PHD, Universidad Federal Fluminense, Brasil.

JOÃO M. FERREIRA CALADO, PHD, Universidad de Lisboa, Portugal.

GUILHERME LUZ TORTORELLA, PHD, Universidad Federal de Santa Catarina, Brasil.

MAURO E. BENEDET, PHD, Universidad Federal de Santa Catarina, Brasil.

ARTEMIS MARTI CESCHIN, PHD, Universidade de Brasilia, Brasil.

GILMAR BARRETO, PHD, Universidad Estatal de Campinas Unicamp, Brasil.

RICARDO EMILIO F. QUEVEDO NOGUEIRA, PHD, Universidad Federal de Ceará, Brasil.

WESLEY LUIZ DA SILVA ASSIS, PHD, Universidad Federal Fluminense, Brasil.

ANA P. MARTINAZZO, PHD, Universidad Federal Fluminense, Brasil.

JORGE BERNARDINO, PHD, Universidad de Coimbra, Portugal.

LUIS GERALDO PEDROSO MELONI, PHD, Universidad Estatal de Campinas Unicamp, Brasil.

FACUNDO ALMERAYA CALDERÓN, PHD, Universidad Autónoma de Nuevo León, México.

FREDDY VILLAO QUEZADA, PHD, Escuela Superior Politécnica del Litoral, Ecuador.

JOSE MANRIQUE SILUPU, MSc, Universidad de Piura, Perú.

GERMÁN ARIEL SALAZAR, PHD, Instituto de Investigaciones en Energía no Convencional, Argentina.

JOSÉ MAHOMAR JANANÍAS, PHD, Universidad del BIOBIO, Chile.

ARNALDO JÉLVEZ CAAMAÑO, PHD, Universidad del BIOBIO, Chile.

JORGE ANDRÉS URIBE, MSc, Centro de Ingeniería y Desarrollo Industrial, México.

RICARDO BELTRAN, PHD, Centro de Investigación en Materiales Avanzados, México.

ADI CORRALES, MSc, Centro de Ingeniería y Desarrollo Industrial, México.

JORGE URIBE CALDERÓN, PHD, Centro de Investigación Científica de Yucatán, México.

JOSÉ TRINIDAD HOLGUÍN MOMACA, MSc, Centro de Investigación en Materiales Avan-

zados, México.

JUAN MANUEL ALVARADO OROZCO, PhD, Centro de Ingeniería y Desarrollo Industrial, México.

ARNALDO JÉLVEZ CAAMAÑO, PHD, Universidad del BIOBIO, Chile.

JAVIER MURILLO, PHD, Centro Internacional Franco Argentino de Ciencias de la Información y de Sistemas, Argentina.

LUCAS DANIEL TERRISSI, PHD, Universidad Nacional de Rosario, Argentina.

RENE VINICIO SANCHEZ LOJA, MSC, Universidad Politécnica Salesiana, Ecuador.

FREDDY LEONARDO BUENO PALOMEQUE, MSC, Universidad Politécnica Salesiana, Ecuador.

DIEGO CABRERA MENDIETA, MSC, Universidad Politécnica Salesiana, Ecuador.

EDWUIN JESUS CARRASQUERO, PHD, Universidad Técnica de Machala, Ecuador.

CARLOS MAURICIO CARRILLO ROSERO, MSC, Universidad Técnica de Ambato, Ecuador.

DIEGO CARRION GALARZA, MSC, Universidad Politécnica Salesiana, Ecuador.

CARMEN CELI SANCHEZ, MSC, Universidad Politécnica Salesiana, Ecuador.

DIEGO CHACON TROYA, MSC, Universidad Politécnica Salesiana, Ecuador.

PAUL CHASI, MSC, Universidad Politécnica Salesiana, Ecuador.

JUAN CHICA, MSC, Universidad Politécnica Salesiana, Ecuador.

DIEGO MARCELO CORDERO GUZMÁN, MSC, Universidad Católica de Cuenca, Ecuador.

LUIS JAVIER CRUZ, PHD, Universidad Pontificia Bolivariana, Medellín, Colombia.

FABRICO ESTEBAN ESPINOZA MOLINA, MSC, Universidad Politécnica Salesiana, Ecuador.

JORGE FAJARDO SEMINARIO, MSC, Universidad Politécnica Salesiana, Ecuador.

PATRICIA FERNANDEZ MORALES, PHD, Universidad Pontificia Bolivariana, Medellín, Colombia.

MARCELO FLORES VAZQUEZ, MSC, Universidad Politécnica Salesiana, Ecuador.

CARLOS FLORES VÁZQUEZ, MSC, Universidad Católica de Cuenca, Ecuador.

CARLOS FRANCO CARDONA, PHD, Universidad Nacional de Colombia, Colombia.

CRISTIAN GARCÍA GARCÍA, MSC, Universidad Politécnica Salesiana, Ecuador.

TEONILA GARCÍA ZAPATA, PHD, Universidad Nacional Mayor de San Marcos, Perú.

LUIS GARZÓN MÑOZ, PHD, Universidad Politécnica Salesiana, Ecuador.

NATALIA GONZALEZ ALVAREZ, MSC, Universidad Politécnica Salesiana, Ecuador.

ERNESTO GRANADO, PHD, Universidad Simón Bolívar, Venezuela.

ADRIANA DEL PILAR GUAMAN, MSC, Universidad Politécnica Salesiana, Ecuador.

JUAN INGA ORTEGA, MSC, Universidad Politécnica Salesiana, Ecuador.

ESTEBAN INGA ORTEGA, PHD, Universidad Politécnica Salesiana, Ecuador.

PAOLA INGAVÉLEZ, MSC, Universidad Politécnica Salesiana, Ecuador.

CESAR ISAZA ROLDAN, PHD, Universidad Pontificia Bolivariana.

NELSON JARA COBOS, MSC, Universidad Politécnica Salesiana, Ecuador.

RUBEN JERVES, MSC, Universidad Politécnica Salesiana, Ecuador.

VICTOR RAMON LEAL, PHD, Investigador de PDVSA, Venezuela

GABRIEL LEON, MSC, Universidad Politécnica Salesiana, Ecuador.

EDILBERTO LLANES, PHD, Universidad Internacional SEK, Ecuador.

LUIS LÓPEZ, MSC, Universidad Politécnica Salesiana, Ecuador.

CARLOS MAFLA YÉPEZ, MSC, Universidad Técnica del Norte, Ecuador.

HADER MARTÍNEZ, PHD, Universidad Pontificia Bolivariana, Medellín, Colombia

JAVIER MARTÍNEZ, PHD, Instituto Nacional de Eficiencia Energética y Energías Renovables, Ecuador.

ALEX MAYORGA, MSC, Universidad Técnica de Ambato, Ecuador.

JIMMY MOLINA, MSC, Universidad Técnica de Machala, Ecuador.

ANDRES MONTERO, PHD, Universidad de Cuenca, Ecuador.

VICENTE MORALES, MSC, Universidad Técnica de Ambato, Ecuador.

FABIÁN MORALES, MSC, Universidad Técnica de Ambato, Ecuador.

DIEGO MORALES, MSC, Ministerio de Electricidad y Energías Renovables del Ecuador.

YOANDRYS MORALES TAMAYO, PHD, Universidad Técnica de Cotopaxi, Cotopaxi

OLENA LEONIDIVNA NAIDIUK, MSC, Universidad Politécnica Salesiana, Ecuador.

OSCAR NARANJO, MSC, Universidad del Azuay, Ecuador.

PAUL NARVAEZ, MSC, Universidad Politécnica Salesiana, Ecuador.

HERNÁN NAVAS OLMEDO, MSC, Universidad Técnica de Cotopaxi, Ecuador.

CESAR NIETO, PHD, Universidad Pontificia Bolivariana, Medellín, Colombia

FABIO OBANDO, MSC, Universidad Politécnica Salesiana, Ecuador.

LUIS ORTIZ FERNANDEZ, MSC, Universidade Federal de Rio Grande del Norte, Brasil

PABLO PARRA, MSC, Universidad Politécnica Salesiana, Ecuador.

PAULO PEÑA TORO, PHD, Ministerio de Productividad, Ecuador.

PATSY PRIETO VELEZ, MSC, Universidad Politécnica Salesiana, Ecuador.

DIEGO QUINDE FALCONI, MSC, Universidad Politécnica Salesiana, Ecuador.

DIANA QUINTANA ESPINOZA, MSC, Universidad Politécnica Salesiana, Ecuador.

WILLIAM QUITIAQUEZ SARZOSA, MSC, Universidad Politécnica Salesiana, Ecuador.

FLAVIO QUIZHPI PALOMEQUE, MSC, Universidad Politécnica Salesiana, Ecuador.

WASHINGTON RAMIREZ MONTALVAN, MSC, Universidad Politécnica Salesiana, Ecuador.

FRAN REINOSO AVECILLAS, MSC, Universidad Politécnica Salesiana, Ecuador.

NÉSTOR RIVERA CAMPOVERDE, MSC, Universidad Politécnica Salesiana, Ecuador.

JORGE ROMERO CONTRERAS, MSC, Universidad de Carabobo, Venezuela

FABIAN SAENZ ENDERICA, MSC, Universidad de las Fuerzas Armadas, ESPE, Ecuador.

LUISA SALAZAR GIL, PHD, Universidad Simón Bolívar, Venezuela

GUSTAVO SALGADO ENRÍQUEZ, MSC, Universidad Central del Ecuador., Ecuador.

JUAN CARLOS SANTILLÁN LIMA, MSC, Universidad Nacional de Chimborazo

JONNATHAN SANTOS BENÍTEZ, MSC, Universidad Politécnica Salesiana, Ecuador.

ANDRÉS SARMIENTO CAJAMARCA, MSC, Universidad Federal de Santa Catarina, Brasil

LUIS SERPA ANDRADE, MSC, Universidad Politécnica Salesiana, Ecuador.

CRISTIAN TIMBI SISALIMA, MSC, Universidad Politécnica Salesiana, Ecuador.

MILTON TIPAN SIMBAÑA, MSC, Universidad Politécnica Salesiana, Ecuador.

PAUL TORRES JARA, MSC, Universidad Politécnica Salesiana, Ecuador.

RODRIGO TUFÍÑO CÁRDENAS, MSC, Universidad Politécnica Salesiana, Ecuador.

FERNANDO URGILES ORTÍZ, MSC, Universidad Politécnica Salesiana, Ecuador.

JUAN VALLADOLID QUITOISACA, MSC, Universidad Politécnica Salesiana, Ecuador.

EFRÉN VÁZQUEZ SILVA, PHD, Universidad Politécnica Salesiana, Ecuador.

JULIO VERDUGO, MSC, Universidad Politécnica Salesiana, Ecuador.

MARY VERGARA PAREDES, PHD, Universidad de los Andes, Merida, Venezuela

JENNIFER YEPEZ ALULEMA, MSC, Universidad Politécnica Salesiana, Ecuador.

JULIO ZAMBRANO ABAD, MSC, Universidad Politécnica Salesiana, Ecuador.

PATRICIA ZAPATA MOLINA, MSC, Universidad Politécnica Salesiana, Ecuador.

Publications board

JUAN CÁRDENAS TAPIA, SDB, PHD
JOSÉ JUNCOSA BLASCO, PHD
JUAN PABLO SALGADO GUERRERO, PHD
ANGLE TORRES TOUKOUMIDIS, PHD
JAIME PADILLA VERDUGO, PHD
SHEILA SERRANO VINCENTI, MSC
JORGE CUEVA ESTRADA, MSC
JOHN CALLE SIGÜENCIA, PHD
FLORALBA AGUILAR GORDÓN, PHD
BETTY RODAS SOTO, MSC
MÓNICA RUIZ VÁSQUEZ, MSC
JORGE ALTAMIRANO SÁNCHEZ, MSC
DAVID ARMENDÁRIZ GONZÁLEZ, MSC

General Editor

ANGEL TORRES TOUKOUMIDIS, PHD

Technical board

DRA. MARCIA PEÑA, Style Reviewer,
Centro Gráfico Salesiano - Editorial Don Bosco
MSC. MARLON QUINDE ABRIL, Diagramming and layout
BSC. ANDRES LOPEZ, Community Manager - Diagramming and layout
BSC. MARÍA JOSÉ CABRERA, Marcalyc Support
BSC. CHRISTIAN ARPI, Community Managers Coordinator's team

Publications Service

HERNÁN HERMOSA (General Coordination)
MARCO GUTIÉRREZ (OJS Layout)
PAULINA TORRES (Style Editing)
RAYSA ANDRADE (Layout)
MARTHA VINUEZA (Layout)
ADRIANA CURIEL AVILA, (Translation)

Editorial

Editorial Abya Yala (Quito-Ecuador),
Av. 12 de octubre N422 y Wilson,
Bloque A, UPS Quito, Ecuador.
Casilla 17-12-719 Teléfonos: (593-2) 3962800 ext. 2638
email: editorial@abyayala.org

Printing: 800 copies

Typographic system used in the composition of this document L^AT_EX.

INGENIUS

REVISTA DE CIENCIA Y TECNOLOGIA

Special Issue 31: Additive Manufacturing

january – june 2024

ISSN impreso 1390-650X / ISSN electrónico 1390-860X

The administration of the journal is done through the following parameters:

The journal uses the academic anti-plagiarism system  

The articles have an identification code (Digital Object Identifier) 

The editorial process is managed through the Open Journal System 

It is an open access publication (Open Access) licensed Creative Commons



The politics copyright of use postprint, are published in the Self-Archive Policy Repository

Sherpa/Romeo. 

The articles of the present edition can be consulted in

<http://revistas.ups.edu.ec/index.php/ingenius>



UNIVERSIDAD POLITÉCNICA SALESIANA DEL ECUADOR

INGENIUS Journal, is indexed in the following Databases and scientific information systems:

SELECTIVE DATABASES



Scopus



Google
scholar

SciELO Ecuador

BASE

EBCOhost
Fuente Académica Plus

Scientific Indexing Services

EuroPub

REVIEWS EVALUATION PLATFORMS

MIAR

Quality Open Access Market



SELECTIVE DIRECTORIES

latindex

Journal Seeker
Research Bible

AcademicKeys
UNLOCKING ACADEMIC CAREERS

SCIENCE LIBRARY INDEX

ULRICHSWEB™
GLOBAL SERIALS DIRECTORY

SELECTIVE SERIAL LIBRARY

reDalyc.org

REDIB
Red Iberoamericana
de Innovación y Conocimiento Científico

refseek™

SCIENTIFIC LITERATURE SEARCHERS OPEN ACCESS

DOAJ
DIRECTORY OF
OPEN ACCESS
JOURNALS

EXALEAD

WORLDWIDE SCIENCE.ORG
The World's Open Access Journal

Journals for Free

OTHER BIBLIOGRAPHICAL DATABASES

Dialnet

Journal
TOCs
The latest Journal Tables of Contents

PKP|INDEX

CATALOG OF INTERNATIONAL UNIVERSITY LIBRARIES



UNIVERSITÄT BAMBERG



Dear readers,

On the horizon of technological innovation, additive manufacturing emerges as a beacon, illuminating the path towards new advancements in multiple fields. In this edition, we delve into the depths of this fascinating world, exploring how the response to tension/compression of stainless steel 316L, manufactured through this method, triggers significant transformations. Additionally, delving into predictions of abrasive wear and the surface hardness of printed parts through technologies like SLA (stereolithography apparatus), we envision a future where precision and efficiency converge. Electrical engineering, the driving force of progress, presents us with dizzying contributions. From evaluating nonlinear optimization models for the economic dispatch of isolated microgrids to the application of artificial intelligence algorithms like YOLOv5 in identifying hotspots in electrical substations through thermal images, we witness an era in which technology redefines the boundaries of what is possible. The classification of vital elements in electrical systems based on centrality measures in networks and linegraph transformation represents a crucial step towards energy efficiency and safety. Computer engineering becomes the symphony that blends logic and innovation. Creating custom algorithms for dynamic optimization in last-mile delivery route planning opens doors to unprecedented operational efficiency. This field, in constant evolution, challenges us to rethink how we interact with information and how machines can facilitate and enhance our daily lives. Mechanical engineering, a cornerstone of the industry, invites us to reflect on sustainability and

optimization. From the comprehensive review of design guidelines and sizing in liquefied petroleum gas systems to the reuse of electric vehicle batteries for a second life in renewable energy systems, solutions that combine efficiency and environmental responsibility are outlined. The proposal for improvement in the structural system of a rigid mountain bike frame and the analysis of the impact of automotive air conditioning on fuel consumption underscore how mechanical engineering converges with ecology and resource optimization. In this interdisciplinary framework, synergies emerge, propelling us towards an innovative and sustainable future. The synaptic connection between additive manufacturing, electrical engineering, computing, and mechanics generates a space of infinite possibilities. This issue of our magazine is a tribute to the symphony of knowledge, where each note represents a significant advancement in our journey towards a brighter tomorrow. As we navigate these pages brimming with knowledge, we invite you to contemplate the transformative power of collaboration between seemingly disparate disciplines. It is at the intersection of these areas where innovation comes to life, where boundaries blur, and solutions take shape. In this ongoing journey towards the future, science and technology become our most powerful allies. May this edition inspire, guide, and awaken innovative curiosity in each of our readers. Let us advance together towards a future full of possibilities. Challenges will always be present, and synergistic work will be the fundamental tool to overcome them.

John Calle-Sigüencia, PhD

Editor in Chief

ÍNDICE

Tensile/Compressive Response of 316L Stainless Steel Fabricated by Additive Manufacturing	9
Respuesta a la tensión/compresión del acero inoxidable 316L fabricado por manufactura aditiva Germán Omar Barrionuevo, Iván La Fé-Perdomo, Esteban Cáceres-Brito, Wilson Navas-Pinto	
Prediction of abrasive wear and surface hardness of printed parts by SLA technology	19
Predicción de desgaste abrasivo y dureza superficial de partes impresas por tecnología SLA P. Muñoz-Valverde, O. Villena-López, L. Mayorga-Ases, C. Pérez-Salinas, D. Moya	
A non-linear optimization model assessment for the economic dispatch of isolated microgrids	32
Evaluación de un modelo de optimización no lineal para el despacho económico de microrredes aisladas Carlos Veloz, Diego L. Jiménez J., Verónica C. Almache B., Roberto Salazar Achig	
Electric substation inspection: YOLOv5 in hotspot detection through thermal imaging	43
Inspección de subestaciones eléctricas: YOLOv5 en la identificación de puntos calientes mediante imágenes térmicas Daniel A. Pérez-Aguilar, Jair M. Pérez-Aguilar, Andy P. Pérez-Aguilar, Redy H. Risco-Ramos, Manuel E. Malpica-Rodríguez	
Network centrality measures for classifying important components in electrical power systems based on linegraph transformation	55
Clasificación de elementos importantes en sistemas eléctricos de potencia según medidas de centralidad en redes y transformación linegraph José A. Moronta R., Claudio M. Rocco S.	
Optimization algorithms for adaptative route sequencing on real-world last-mile deliveries	64
Algoritmos de optimización para secuenciación adaptativa de rutas reales en entregas de última milla Fernando Hernández Gobertti, Rafael Sotelo, Marcelo Forets	
Liquefied Petroleum Gas Systems: A Review On Desing And Sizing Guidelines	81
Sistemas de gas licuado de petróleo: una revisión sobre lineamientos de diseño y dimensionamiento Diego Venegas-Vásconez, César Ayabaca-Sarria, Salvatore Reina-Guzmán, Luis Tipanluisa-Sarchi, Óscar Farías-Fuentes	
Reuse of Electrical Vehicle Batteries for Second Life Applications in Power Systems with a High Penetration of Renewable Energy: A Systematic Literature Review	95
Reutilización de baterías de vehículos eléctricos para aplicaciones de segunda vida en sistemas eléctricos de potencia con una alta penetración de energía renovable: una revisión sistemática de la literatura Jorge Campoverde-Pillco, Danny Ochoa-Correa, Edisson Villa-Ávila, Patricio Astudillo-Salinas	
Improvement proposal in the structural system of a 15” R29 rigid mountain bike frame, with fea and geometric optimization	106
Propuesta de mejora en el sistema estructural de un cuadro rígido de bicicleta de montaña de 15” R29, mediante FEA y optimización geométrica Juan P. Guamán, Hugo E. Crespo, César A. Paltán, Jorge I. Fajardo	
Incidence of automotive air conditioning on the index of fuel consumption in spark ignition vehicle on a route in the ecuadorian amazon	115
Incidencia del aire acondicionado automotriz en el índice de consumo de combustible en vehículo de encendido provocado en una ruta de la Amazonía ecuatoriana Edilberto Antonio Llanes-Cedeño, Shayan Fredy Grefa Shiguango, Jaime Vinicio Molina-Osejos, Juan Carlos Rocha-Hoyos	
Normas editoriales	127
Guidelines	



TENSILE/COMPRESSIVE RESPONSE OF 316L STAINLESS STEEL FABRICATED BY ADDITIVE MANUFACTURING

RESPUESTA A LA TENSIÓN/COMPRESIÓN DEL ACERO INOXIDABLE 316L FABRICADO POR MANUFACTURA ADITIVA

Germán Omar Barrionuevo^{1,*}, Iván La Fé-Perdomo^{2,3}, Esteban Cáceres-Brito¹, Wilson Navas-Pinto^{1,4}

Received: 01-10-2023, Received after review: 28-11-2023, Accepted: 12-12-2023, Published: 01-01-2024

Abstract

Additive manufacturing has evolved from a rapid prototyping technology to a technology with the ability to produce highly complex parts with superior mechanical properties than those obtained conventionally. The processing of metallic powders by means of a laser makes it possible to process any type of alloy and even metal matrix composites. The present work analyzes the tensile and compressive response of 316L stainless steel processed by laser-based powder bed fusion. The resulting microstructure was evaluated by optical microscopy. Regarding the mechanical properties, the yield strength, ultimate tensile strength, percentage of elongation before breakage, compressive strength and microhardness were determined. The results show that the microstructure is constituted by stacked micro molten pools, within which cellular sub-grains are formed due to the high thermal gradient and solidification rate. The compressive strength (1511.88 ± 9.22 MPa) is higher than the tensile strength (634.80 ± 11.62 MPa). This difference is mainly associated with strain hardening and the presence of residual stresses. The initial microhardness was 206.24 ± 11.96 HV; after the compression test, the hardness increased by 23%.

Keywords: Additive manufacturing, Laser powder bed fusion, Mechanical properties, Stainless steel, Strain hardening

Resumen

La manufactura aditiva pasó de ser una tecnología de prototipado rápido a una tecnología con la capacidad de producir piezas de gran complejidad y con propiedades mecánicas superiores a las obtenidas convencionalmente. El procesamiento de polvos metálicos a través de un láser permite procesar cualquier tipo de aleación e incluso materiales compuestos. En el presente trabajo se analiza la respuesta a tracción y compresión del acero inoxidable 316L procesado mediante fusión selectiva láser. Se analizó la microestructura resultante mediante microscopía óptica; respecto a las propiedades mecánicas se determinó la resistencia a la fluencia, resistencia última a la tracción, porcentaje de elongación antes de la rotura, resistencia a la compresión y microdureza. Los resultados obtenidos muestran que la microestructura está constituida por micropiletas fundidas apiladas, dentro de las cuales se generan subgranos celulares, producto del elevado gradiente térmico y la alta tasa de solidificación. La resistencia a la compresión (1511.88 ± 9.22 MPa) es mayor a la resistencia a tracción (634.80 ± 11.62 MPa). Esta diferencia está asociada principalmente al endurecimiento por deformación y la presencia de esfuerzos residuales. La microdureza inicial fue de 206.24 ± 11.96 HV; posterior al ensayo de compresión la dureza se incrementó un 23%.

Palabras clave: manufactura aditiva, fusión selectiva láser, propiedades mecánicas, acero inoxidable, endurecimiento por deformación

^{1,*}Departamento de Ciencias de la Energía y Mecánica, Universidad de las Fuerzas Armadas ESPE, Quito, Ecuador.
Corresponding author ✉: gobarrionuevo@uc.cl.

²Departamento de Ingeniería Mecánica y Metalúrgica, Escuela de Ingeniería, Pontificia Universidad Católica de Chile, Santiago, Chile.

³Study Centre on Advanced and Sustainable Manufacturing, University of Matanzas, Matanzas, Cuba

⁴Department of Mechanical Engineering, University of Saskatchewan, Saskatoon, Canada.

Suggested citation: Barrionuevo, G. O.; La Fé-Perdomo, I.; Cáceres-Brito, E.; Navas-Pinto, W. "Tensile/Compressive Response of 316L Stainless Steel Fabricated by Additive Manufacturing," *Ingenius, Revista de Ciencia y Tecnología*, N.º 31, pp. 9-18, 2024, DOI: <https://doi.org/10.17163/ings.n31.2024.01>.

1. Introduction

Additive manufacturing (AM) technology emerged as a rapid prototyping technique. Although initially focused on polymer processing with techniques such as stereolithography (SLA) and fused deposition modeling (FDM) in the 1980s, it was later extended to the processing of metals, ceramics, and composites [1, 2].

AM came from the minds of two chemical engineers who developed a toy for their daughter, which deposited a polymer layer by layer [3]. They patented their invention in 1986. A few years later, they consolidated one of the most successful additive manufacturing companies to date, Stratasy. Already in the 1990s, the first developments in metal processing appeared, with technologies such as selective laser melting (SLM) and selective laser sintering (SLS) [4, 5]. It is worth noting that all these developments went hand in hand with universities and research centers, which accelerated technological development.

The last few years have seen great advances in processing various types of materials [6]. Manufacturers have expanded their product portfolio to include equipment, raw materials, and consumables. In addition, extensive research has been developed to investigate the potential benefits of AM in different fields. For instance, several opportunities as possible cost and lead time reductions, the possibility of unique design solutions, and the consolidation of multiple components, have been identified [7]. However, additive manufacturing is not yet a plug-and-play technology. It requires a thorough knowledge of the material to be processed, suitable processing parameters, and environmental conditions, among others [5]. Furthermore, AM also requires substantial work and research in order to obtain diverse certifications and standards required in different fields to demonstrate its efficiency in manufacturing complex parts and assure their repeatability and quality [7].

FDM technology is one of the most widely used technologies, mainly due to its ease of installation and work [8–11]. In contrast, metal fabrication requires expensive and more complex equipment. Metal AM is classified into directed energy deposition (DED) [12–14] and powder bed fusion (PBF) [15, 16]; within DED, the technology that stands out for its versatility and processing capability is wire arc additive manufacturing (WAAM) [17–20]. On the other hand, in PBF, the best option for the manufacture of parts of great geometric complexity and reduced size is laser-based powder bed fusion (LPBF) [21].

LPBF uses a medium-power laser (100-400 W) to melt metal powders, which change phase in microseconds, creating repetitive cycles of melting and solidification that produce microstructures never seen before [22, 23]. One of the notable features is the formation of smaller grains compared to the same material

processed conventionally. In addition, micro-molten pools are created within which cellular subgrains are formed. These peculiar microstructures give rise to different mechanical properties [24, 25], which require multiple mechanical tests to determine their suitability for use as load-bearing structural elements or in dynamic environments under varying loads.

Regarding the mechanical properties, a significant improvement in different mechanical properties of specimens manufactured by means of LPBF has been observed. For instance, Röttger et al. [26] compared the mechanical properties of specimens manufactured with 316L austenitic steel processed by SLM technology and specimens manufactured through a regular casting process. After performing tensile tests, it was observed that the tensile strength increased by approximately 20 % in samples produced by AM. Moreover, Kurzynowski et al. [27] carried out tensile tests on 316L stainless steel specimens manufactured by SLM with different process parameters and compared the results with the mechanical properties of samples made from rolled sheet AISI SS316L. An improvement in the yield strength and Young's modulus was observed after testing. In addition, Liverani et al. [28] studied the effect of different process parameters on the microstructure and mechanical properties of specimens produced by SLM. After performing tensile and fatigue tests, the experimental results suggest the possibility of an improvement of the ultimate tensile strength and the percentage of elongation of the specimens when compared to conventionally manufactured AISI316L samples. In a different study, Liverani et al. [29] reported a yield strength (σ_Y) of around 400 MPa and an ultimate tensile strength (σ_{UTS}) between 500-600 MPa. Larimian et al. [30] obtained similar results, highlighting the effect of processing parameters and the scanning strategy on the resulting strength. The lowest and highest σ_Y was 148 and 462 MPa, respectively. While, the σ_{UTS} values were around 178 and 584 MPa. It is worth noting that to obtain an adequate mechanical response, it is essential to obtain samples with the maximum relative density.

In the case of compressive response, Güden et al. [31] investigated the influence of the strain rate during compression tests of selective laser melted 316L stainless steel and reported ultimate true compression stresses in the range of 1400 to 1600 MPa with strain rates ranging from 2800 to 3250 s^{-1} , respectively. Li et al. [32] developed a constitutive model to predict the compressive stress-strain of 316L stainless steel processed by LPBF and compared the results with specimens manufactured with SLM equipment at different scanning speeds. An average compressive stress of 1400 MPa and a strain of 23 % were obtained.

Therefore, the present work is focused on determining the tensile and compressive response of 316L stainless steel processed by laser powder bed fusion technol-

ogy under specific conditions. As the microstructure plays a fundamental role in comprehending the resulting mechanical properties, an in-depth analysis is carried out of the microstructural features as well as the relative density.

2. Materials and Methods

The material used to fabricate the samples was 316L stainless steel, whose nominal chemical composition is detailed in Table 1.

Table 1. Nominal chemical composition of the AISI 316L stainless steel powders.

Elements (wt%)				
Fe	Cr	Ni	Mo	Mn
Bal.	16.5-18	10-13	2-2.5	0-2
	Si	C	P	S
	0-1	0-0.03	0-0.04	0-0.03

The selective laser melting process was carried out in a Concept Laser machine (MLAB 200R) equipped with a 200W fiber laser (Nb:YAG) with a wavelength of 1064 nm. The powders were deposited on a 16 mm thick 316L stainless-steel support plate. The processing parameters were a laser power of 160 W, a scanning speed of 800 mm/s, hatch spacing of 60 μm and a layer thickness of 30 μm (Figure 1); these parameters were chosen to maximize the relative density, reducing the porosity of the printed samples.

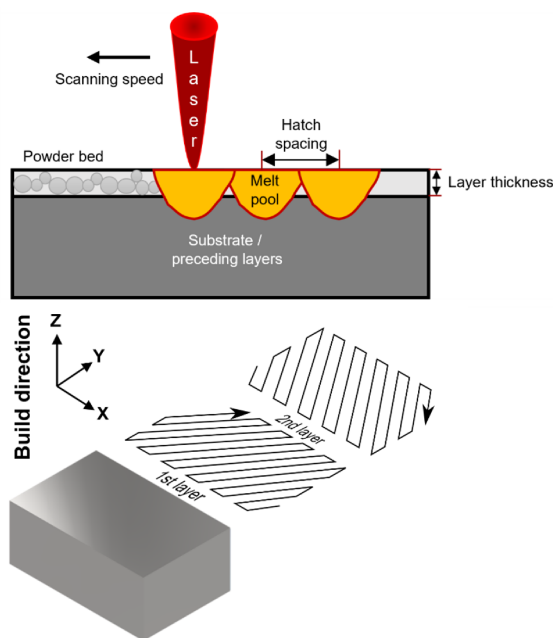


Figure 1. Schematic representation of the laser-based powder bed fusion process, identifying the key processing parameters and the scanning strategy.

Flat dog-bone geometry specimens agreeing to ASTM E8/8M-21 and prismatic samples of 16x10x7

mm were fabricated with a meander scanning strategy with a 67° rotation after each deposited layer. After manufacturing, all the samples were cut from the build platforms by wire-electrical discharge machining.

For the metallographic inspection, the samples were first planar ground using SiC paper, starting from 120 to 2000 grit to roughly polish the sample surface. Then, finely polished using alumina and posteriorly diamond paste. The material microstructure was revealed by chemical etching immersion in Aqua regia solution (20 ml HNO₃ and 60 ml HCl) for 30 s. The material surface morphology was inspected by means of optical microscopy (OM) (MEIJI IM 7200). The OM micrographs were processed and analyzed using Fiji software (National Institutes of Health, USA) to determine microstructural features and evaluate porosity by means of image analysis.

Tensile tests following the ASTM E8/8M-21 were carried out using a universal tensile tester machine (Instron 3368, Zwick) with a 50 kN load cell and a 2 mm/min speed to fracture and a gauge length of 50 mm with an extensometer. According to ASTM E9-09, compressive tests were carried out using the prismatic specimens. Four prismatic specimens were tested, and the average results were reported. In addition, the elastic modulus was calculated according to ASTM E111.

Microhardness was measured using a Vickers hardness tester (METKON DUROLINE-M), using a 500 g force and 10 s as dwell time, according to ASTM E384 standard. Mean values were recorded through five measurements and then reported.

3. Results and discussion

Figure 2 shows the manufactured test specimens. It is worth noting that both the powder and the support plate must be manufactured from the same material to obtain proper adhesion between the two parts and avoid errors or displacements during the additive manufacturing process.



Figure 2. Additively manufactured samples for microstructure and mechanical evaluation. Base plate dimension: 100 x 100 x 16 mm.

In order to determine the relative density, the surface defects obtained by optical microscopy were evaluated (Figure 3). By means of image analysis, a relative density of 99.7 % was obtained.

Obtaining parts with a relative density greater than 99 % is essential to obtain comparable mechanical properties to parts manufactured by conventional methods. As can be seen in Figure 3, there are still circular porosities, which are associated with the gas trapped inside the metal powder [33]. However, most of the surface is free of pores, which ensures the suitable performance of the manufactured samples and the proper selection of the chosen processing parameters.

3.1. Microstructure analysis

Figure 4 presents the 3D assembly of optical micrographs obtained in different manufacturing planes. It is possible to appreciate that the scanning strategy used can be distinguished in the upper plane. At the same time, it is possible to observe the stacking of micro-molten pools in the lateral planes. Figure 5a shows in more detail the arrangement of molten pools, where it is possible to extract that, on average, the molten pool has a depth of approximately $50 \mu\text{m}$ and an extension of $140 \mu\text{m}$. Figure 5b shows the detail of a molten pool within which cellular sub-grains appear, as reported in previous research work [34–37].

Cellular grains can be distinguished within the molten pool (Figure 5b); these sub-grains are produced due to the high thermal gradient and solidification rate [38]. As the fusion-solidification process is generated layer by layer, the molten pool deforms slightly due to the presence of residual stresses [39, 40]. The scanning strategy also causes the molten pool to deform; the rotation of the printing angle modifies the thermal gradient, modifying the geometry of the micro molten pools.

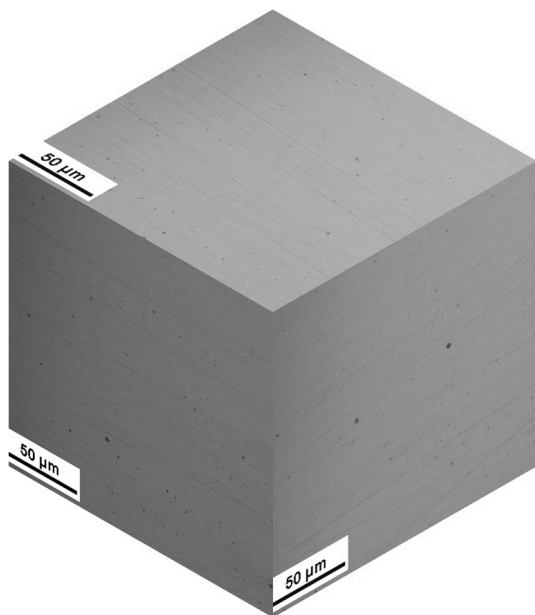


Figure 3. Optical micrograph to assess the internal porosity.



Figure 4. 3D assembly of optical micrographs of the 316 L stainless steel processed by LPBF.



(a)



(b)

Figure 5. Optical micrograph of the additively processed 316L stainless steel a) 200x, b) 1000x highlighting the molten pool.

3.2. Mechanical response

Figure 6 shows the stress-strain curve of 316L stainless steel subjected to a tensile test. The yield stress was 512.32 ± 7.84 MPa, the ultimate tensile stress was 634.80 ± 11.62 MPa, and the deformation before rupture was 31.61 ± 1.40 %.

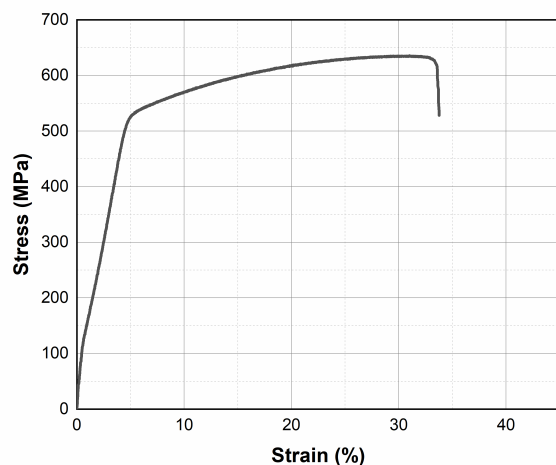


Figure 6. Tensile evaluation of LPBF 316L stainless steel.

As can be seen in Figure 6, the material shows a ductile response with a large deformation after exceeding the elastic limit region. In addition, the yield strength for the material has been determined to be around 512.32 MPa, corresponding to an engineering strain of 0.05. Accordingly, the ultimate tensile strength is around 634.80 MPa at a strain of approximately 0.32. For the manufactured group of specimens, the elastic modulus was determined to be around 229.12 ± 2.14 GPa. In addition, once the plastic deformation has begun, it is possible to observe a stable strain hardening stage followed by a necking region that leads to the fracture of the specimen. Even though the ductile response is associated with the absence of porosity, if there is a low relative density, the material tends to fracture in a brittle manner [41] due to the presence of defects such as trapped gas, unstable melting pools or lack of fusion [42].

Figure 7 shows the necking that occurs in the sample before breakage. The necking and area reduction is a typical indicator of the ductile response of the tested material. Additionally, it can be observed that the fracture occurs at an angle of about 45° .

The failure mechanism of 316L stainless steel fabricated by additive manufacturing may be associated with the microvoid coalescence fracture, which occurs when the material contains small pores or inclusions that grow and coalesce under tensile stress, forming internal microcracks.

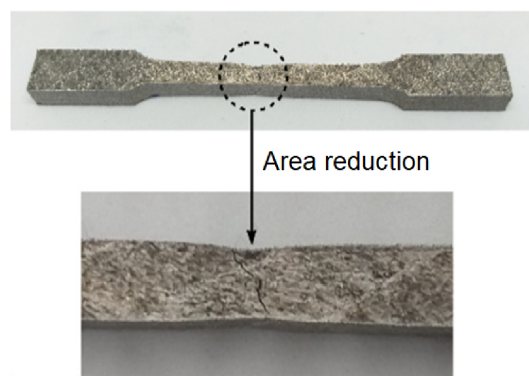


Figure 7. Area reduction of the specimen used in the tensile test.

Figure 8 shows the compressive response of the additively manufactured stainless steel specimens. The compressive strength (1511.88 ± 9.22 MPa) is higher than the tensile strength (634.80 ± 11.62 MPa). This difference is mainly associated with strain hardening and residual stresses [?, 39], [43]. As can be seen in Figure 8, when the stress exceeds 500 MPa, the material starts to harden. Strain hardening makes the material capable of withstanding high stresses before failure occurs. In addition, the crystalline structure of austenitic stainless steel (FCC) typically contains planes of atoms that can slide past each other more easily under shear forces (such as in compression) than they can be pulled apart under tensile forces. In other words, the crystal structure of the 316L SS is more resistant to compression and shear forces.

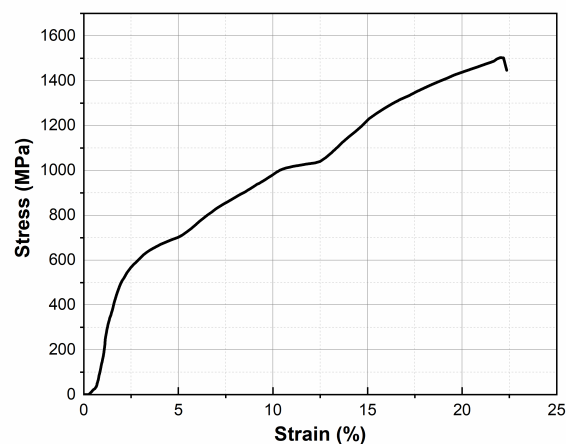


Figure 8. Compressive response of LPBF 316L stainless steel.

When subjected to compressive stress, the deformation of the material causes strain hardening. Therefore, the hardness was evaluated before and after the compression test (Figure 9).

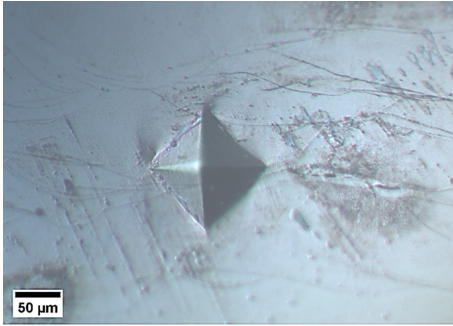


Figure 9. Microhardness evaluation of the 316L stainless steel processed by LPBF.

The initial microhardness was $206.24 \pm 11.96HV_{0.5}$ in the as-built condition. After the compression test, microhardness increases to $253.32 \pm 11.12HV_{0.5}$.

Figure 10 shows the deformation produced after the compression test, where it is evident how the molten pools have been deformed. The compression process acts as a strain-hardening treatment. It has been observed that the molten pools are deformed, which generates a kind of cold working treatment. Internally, the grains are compressed, reducing their size, which increases the hardness. The microhardness has increased by 23 %.

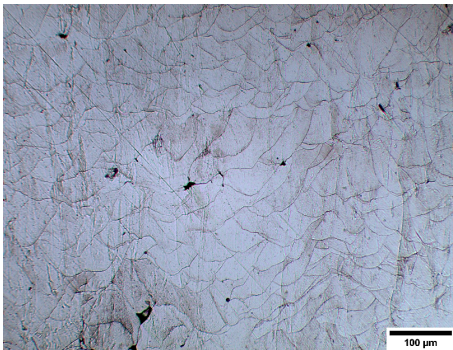


Figure 10. Compressed molten pools after compression test.

Table 2 summarizes the mechanical response of additively manufactured 316L stainless steel. The results obtained in the present work coincide with those reported in the literature [24], [26], [28], [30], [32], [41]. Therefore, it is possible to affirm that the SLM technology is reaching maturity, and work should begin on standards for its approval.

The tensile and compressive response of 316L stainless steel processed by SLM showed a mechanical response above its conventionally processed counterpart [24]. The higher strength is attributed to the microstructure. Within the molten pool, sub-grains of less than one micron were found due to the high thermal gradient resulting from the cyclic laser's interaction with the metal powders.

Additive manufacturing has a number of advantages in terms of design and flexibility. However, to ensure its use in engineering applications, it is necessary to further study its mechanical properties by varying process parameters and scanning strategies.

Table 2. Mechanical properties of the AISI 316L stainless steel additively manufactured.

Properties	Value
Yield strength (MPa)	512.32 ± 7.84
Tensile strength (MPa)	634.80 ± 11.62
Elastic modulus (GPa)	229.12 ± 2.14
Compressive strength (MPa)	1511.88 ± 9.22
Elongation (%)	31.61 ± 1.40
Microhardness (HV)	206.24 ± 11.96

4. Conclusions

In the present work, the tensile and compressive response of laser-processed 316L stainless steel has been evaluated. The main conclusions drawn are detailed below:

- Proper selection of processing parameters is essential to obtain parts with minimum porosity. The higher the relative density, the higher the mechanical properties, as the pores act as stress concentrators, reducing the mechanical strength. In this work, a relative density of 99.7 % was obtained.
- Additive manufacturing offers the possibility to control the microstructure and thus to customize certain mechanical properties. For example, the dimensions of the molten pool or the relative density. It is worth noting that the scanning strategy and the specimen geometry affect the thermal gradient and, thus, the resulting microstructure. Further research on these parameters and their effect on the mechanical properties is needed.
- Tensile and compression tests showed a ductile performance of the material obtained additively. In the case of the tensile test, the following results were obtained: a yield strength of 512.32 ± 7.84 MPa, an ultimate tensile strength of 635 MPa, and an elastic modulus of 229.12 ± 2.14 GPa. In addition, the stress-strain curve shows a ductile response of the material, which is associated with a high relative density and low porosity.

- A compressive strength of approximately 1511.88 ± 9.22 MPa was observed in the corresponding tests. The significant difference between the tensile and compression response could be attributed to the presence of residual stress produced during the manufacturing process and a strain hardening mechanism caused by the deformation of the sample and confirmed by the distortion observed in the molten pools after the compression test was performed.
- The microhardness test confirmed an increase of approximately 23 % in the results obtained after a specimen was subjected to a compression test in contrast to the results of the specimens as manufactured.

References

- [1] N. Li, S. Huang, G. Zhang, R. Qin, W. Liu, H. Xiong, G. Shi, and J. Blackburn, "Progress in additive manufacturing on new materials: A review," *Journal of Materials Science & Technology*, vol. 35, no. 2, pp. 242–269, 2019, recent Advances in Additive Manufacturing of Metals and Alloys. [Online]. Available: <https://doi.org/10.1016/j.jmst.2018.09.002>
- [2] T. J. Gordelier, P. R. Thies, L. Turner, and L. Johanning, "Optimising the FDM additive manufacturing process to achieve maximum tensile strength: a state-of-the-art review," *Rapid Prototyping Journal*, vol. 25, no. 6, pp. 953–971, Jan 2019. [Online]. Available: <https://doi.org/10.1108/RPJ-07-2018-0183>
- [3] T. J. Wallin, J. H. Pikul, S. Bodkhe, B. N. Peele, B. C. Mac Murray, D. Therriault, B. W. McEnerney, R. P. Dillon, E. P. Giannelis, and R. F. Shepherd, "Click chemistry stereolithography for soft robots that self-heal," *J. Mater. Chem. B*, vol. 5, pp. 6249–6255, 2017. [Online]. Available: <http://dx.doi.org/10.1039/C7TB01605K>
- [4] C.-m. Liu, H.-b. Gao, L.-y. Li, J.-d. Wang, C.-h. Guo, and F.-c. Jiang, "A review on metal additive manufacturing: modeling and application of numerical simulation for heat and mass transfer and microstructure evolution," *China Foundry*, vol. 18, no. 4, pp. 317–334, Jul 2021. [Online]. Available: <https://doi.org/10.1007/s41230-021-1119-2>
- [5] N. Haghdadadi, M. Laleh, M. Moyle, and S. Primig, "Additive manufacturing of steels: a review of achievements and challenges," *Journal of Materials Science*, vol. 56, no. 1, pp. 64–107, Jan 2021. [Online]. Available: <https://doi.org/10.1007/s10853-020-05109-0>
- [6] K. R. Ryan, M. P. Down, and C. E. Banks, "Future of additive manufacturing: Overview of 4D and 3D printed smart and advanced materials and their applications," *Chemical Engineering Journal*, vol. 403, p. 126162, 2021. [Online]. Available: <https://doi.org/10.1016/j.cej.2020.126162>
- [7] B. Blakey-Milner, P. Gradl, G. Snedden, M. Brooks, J. Pitot, E. Lopez, M. Leary, F. Berto, and A. du Plessis, "Metal additive manufacturing in aerospace: A review," *Materials & Design*, vol. 209, p. 110008, 2021. [Online]. Available: <https://doi.org/10.1016/j.matdes.2021.110008>
- [8] M. Vishwas and C. Basavaraj, "Studies on optimizing process parameters of fused deposition modelling technology for ABS," *Materials Today: Proceedings*, vol. 4, no. 10, pp. 10994–11003, 2017, advanced Materials, Manufacturing, Management and Thermal Science (AMMMT 2016) September 23-24, 2016. [Online]. Available: <https://doi.org/10.1016/j.matpr.2017.08.057>
- [9] Z. Liu, Y. Wang, B. Wu, C. Cui, Y. Guo, and C. Yan, "A critical review of fused deposition modeling 3D printing technology in manufacturing polylactic acid parts," *The International Journal of Advanced Manufacturing Technology*, vol. 102, no. 9, pp. 2877–2889, Jun 2019. [Online]. Available: <https://doi.org/10.1007/s00170-019-03332-x>
- [10] G. O. Barrionuevo and J. A. Ramos-Grez, "Machine learning for optimizing technological properties of wood composite filament-timberfill fabricated by fused deposition modeling," in *Applied Technologies*, M. Botto-Tobar, M. Zambrano Vizueté, P. Torres-Carrión, S. Montes León, G. Pizarro Vásquez, and B. Durakovic, Eds. Cham: Springer International Publishing, 2020, pp. 119–132. [Online]. Available: https://doi.org/10.1007/978-3-030-42520-3_10
- [11] J. Chacón, M. Caminero, E. García-Plaza, and P. Núñez, "Additive manufacturing of PLA structures using fused deposition modelling: Effect of process parameters on mechanical properties and their optimal selection," *Materials & Design*, vol. 124, pp. 143–157, 2017. [Online]. Available: <https://doi.org/10.1016/j.matdes.2017.03.065>
- [12] A. Saboori, D. Gallo, S. Biamino, P. Fino, and M. Lombardi, "An overview of additive manufacturing of titanium components by directed energy deposition: Microstructure and mechanical properties," *Applied Sciences*, vol. 7, no. 9, 2017. [Online]. Available: <https://doi.org/10.3390/app7090883>
- [13] Z. Xia, J. Xu, J. Shi, T. Shi, C. Sun, and D. Qiu, "Microstructure evolution and

- mechanical properties of reduced activation steel manufactured through laser directed energy deposition,” *Additive Manufacturing*, vol. 33, p. 101114, 2020. [Online]. Available: <https://doi.org/10.1016/j.addma.2020.101114>
- [14] S. Gao, R. Liu, R. Huang, X. Song, and M. Seita, “A hybrid directed energy deposition process to manipulate microstructure and properties of austenitic stainless steel,” *Materials & Design*, vol. 213, p. 110360, 2022. [Online]. Available: <https://doi.org/10.1016/j.matdes.2021.110360>
- [15] G. O. Barrionuevo, M. Walczak, J. Ramos-Grez, and X. Sánchez-Sánchez, “Microhardness and wear resistance in materials manufactured by laser powder bed fusion: Machine learning approach for property prediction,” *CIRP Journal of Manufacturing Science and Technology*, vol. 43, pp. 106–114, 2023. [Online]. Available: <https://doi.org/10.1016/j.cirpj.2023.03.002>
- [16] S. Chowdhury, N. Yadaiah, C. Prakash, S. Ramakrishna, S. Dixit, L. R. Gupta, and D. Buddhi, “Laser powder bed fusion: a state-of-the-art review of the technology, materials, properties & defects, and numerical modelling,” *Journal of Materials Research and Technology*, vol. 20, pp. 2109–2172, 2022. [Online]. Available: <https://doi.org/10.1016/j.jmrt.2022.07.121>
- [17] S. W. Williams, F. Martina, A. C. Addison, G. P. J. Ding, and P. Colegrove, “Wire + arc additive manufacturing,” *Materials Science and Technology*, vol. 32, no. 7, pp. 641–647, 2016. [Online]. Available: <https://doi.org/10.1179/1743284715Y.0000000073>
- [18] W. Jin, C. Zhang, S. Jin, Y. Tian, D. Wellmann, and W. Liu, “Wire arc additive manufacturing of stainless steels: A review,” *Applied Sciences*, vol. 10, no. 5, 2020. [Online]. Available: <https://doi.org/10.3390/app10051563>
- [19] J. L. Z. Li, M. R. Alkahari, N. A. B. Rosli, R. Hasan, M. N. Sudin, and F. R. Ramli, “Review of wire arc additive manufacturing for 3D metal printing,” *International Journal of Automation Technology*, vol. 13, no. 3, pp. 346–353, 2019. [Online]. Available: <https://doi.org/10.20965/ijat.2019.p0346>
- [20] T. A. Rodrigues, V. Duarte, R. M. Miranda, T. G. Santos, and J. P. Oliveira, “Current status and perspectives on wire and arc additive manufacturing (WAAM),” *Materials*, vol. 12, no. 7, 2019. [Online]. Available: <https://doi.org/10.3390/ma12071121>
- [21] X. Zhang, C. J. Yocom, B. Mao, and Y. Liao, “Microstructure evolution during selective laser melting of metallic materials: A review,” *Journal of Laser Applications*, vol. 31, no. 3, p. 031201, May 2019. [Online]. Available: <https://doi.org/10.2351/1.5085206>
- [22] W. M. Tucho, V. H. Lysne, H. Austbø, A. Sjolyst-Kverneland, and V. Hansen, “Investigation of effects of process parameters on microstructure and hardness of SLM manufactured SS316L,” *Journal of Alloys and Compounds*, vol. 740, pp. 910–925, 2018. [Online]. Available: <https://doi.org/10.1016/j.jallcom.2018.01.098>
- [23] M. Tang, L. Zhang, and N. Zhang, “Microstructural evolution, mechanical and tribological properties of TiC/Ti6Al4V composites with unique microstructure prepared by SLM,” *Materials Science and Engineering: A*, vol. 814, p. 141187, 2021. [Online]. Available: <https://doi.org/10.1016/j.msea.2021.141187>
- [24] J. Fu, S. Qu, J. Ding, X. Song, and M. Fu, “Comparison of the microstructure, mechanical properties and distortion of stainless steel 316 L fabricated by micro and conventional laser powder bed fusion,” *Additive Manufacturing*, vol. 44, p. 102067, 2021. [Online]. Available: <https://doi.org/10.1016/j.addma.2021.102067>
- [25] W. H. Kan, L. N. S. Chiu, C. V. S. Lim, Y. Zhu, Y. Tian, D. Jiang, and A. Huang, “A critical review on the effects of process-induced porosity on the mechanical properties of alloys fabricated by laser powder bed fusion,” *Journal of Materials Science*, vol. 57, no. 21, pp. 9818–9865, Jun 2022. [Online]. Available: <https://doi.org/10.1007/s10853-022-06990-7>
- [26] A. Röttger, K. Geenen, M. Windmann, F. Binner, and W. Theisen, “Comparison of microstructure and mechanical properties of 316L austenitic steel processed by selective laser melting with hot-isostatic pressed and cast material,” *Materials Science and Engineering: A*, vol. 678, pp. 365–376, 2016. [Online]. Available: <https://doi.org/10.1016/j.msea.2016.10.012>
- [27] T. Kurzynowski, K. Gruber, W. Stopyra, B. Kuznicka, and E. Chlebus, “Correlation between process parameters, microstructure and properties of 316L stainless steel processed by selective laser melting,” *Materials Science and Engineering: A*, vol. 718, pp. 64–73, 2018. [Online]. Available: <https://doi.org/10.1016/j.msea.2018.01.103>

- [28] E. Liverani, S. Toschi, L. Ceschini, and A. Fortunato, "Effect of selective laser melting (SLM) process parameters on microstructure and mechanical properties of 316L austenitic stainless steel," *Journal of Materials Processing Technology*, vol. 249, pp. 255–263, 2017. [Online]. Available: <https://doi.org/10.1016/j.jmatprotec.2017.05.042>
- [29] E. Liverani, A. H. A. Lutey, A. Ascari, and A. Fortunato, "The effects of hot isostatic pressing (HIP) and solubilization heat treatment on the density, mechanical properties, and microstructure of austenitic stainless steel parts produced by selective laser melting (SLM)," *The International Journal of Advanced Manufacturing Technology*, vol. 107, no. 1, pp. 109–122, Mar 2020. [Online]. Available: <https://doi.org/10.1007/s00170-020-05072-9>
- [30] T. Larimian, M. Kannan, D. Grzesiak, B. Al-Mangour, and T. Borkar, "Effect of energy density and scanning strategy on densification, microstructure and mechanical properties of 316l stainless steel processed via selective laser melting," *Materials Science and Engineering: A*, vol. 770, p. 138455, 2020. [Online]. Available: <https://doi.org/10.1016/j.msea.2019.138455>
- [31] M. Güden, S. Enser, M. Bayhan, A. Taşdemirci, and H. Yavaş, "The strain rate sensitive flow stresses and constitutive equations of a selective-laser-melt and an annealed-rolled 316l stainless steel: A comparative study," *Materials Science and Engineering: A*, vol. 838, p. 142743, 2022. [Online]. Available: <https://doi.org/10.1016/j.msea.2022.142743>
- [32] Y. Li, Y. Ge, J. Lei, and W. Bai, "Mechanical properties and constitutive model of selective laser melting 316L stainless steel at different scanning speeds," *Advances in Materials Science and Engineering*, vol. 2022, p. 2905843, Apr 2022. [Online]. Available: <https://doi.org/10.1155/2022/2905843>
- [33] B. Zhang, Y. Li, and Q. Bai, "Defect formation mechanisms in selective laser melting: A review," *Chinese Journal of Mechanical Engineering*, vol. 30, no. 3, pp. 515–527, May 2017. [Online]. Available: <https://doi.org/10.1007/s10033-017-0121-5>
- [34] X. Ao, H. Xia, J. Liu, and Q. He, "Simulations of microstructure coupling with moving molten pool by selective laser melting using a cellular automaton," *Materials & Design*, vol. 185, p. 108230, 2020. [Online]. Available: <https://doi.org/10.1016/j.matdes.2019.108230>
- [35] W. Yuan, H. Chen, T. Cheng, and Q. Wei, "Effects of laser scanning speeds on different states of the molten pool during selective laser melting: Simulation and experiment," *Materials & Design*, vol. 189, p. 108542, 2020. [Online]. Available: <https://doi.org/10.1016/j.matdes.2020.108542>
- [36] P. Tang, H. Xie, S. Wang, X. Ding, Q. Zhang, H. Ma, J. Yang, S. Fan, M. Long, D. Chen, and X. Duan, "Numerical analysis of molten pool behavior and spatter formation with evaporation during selective laser melting of 316l stainless steel," *Metallurgical and Materials Transactions B*, vol. 50, no. 5, pp. 2273–2283, Oct 2019. [Online]. Available: <https://doi.org/10.1007/s11663-019-01641-w>
- [37] G. O. Barrionuevo, J. Ramos-Grez, M. Walczak, and I. La Fé-Perdomo, "Numerical analysis of the effect of processing parameters on the microstructure of stainless steel 316L manufactured by laser-based powder bed fusion," *Materials Today: Proceedings*, vol. 59, pp. 93–100, 2022, third International Conference on Recent Advances in Materials and Manufacturing 2021. [Online]. Available: <https://doi.org/10.1016/j.matpr.2021.10.209>
- [38] G. O. Barrionuevo, J. A. Ramos-Grez, M. Walczak, X. Sánchez-Sánchez, C. Guerra, A. Debut, and E. Haro, "Microstructure simulation and experimental evaluation of the anisotropy of 316L stainless steel manufactured by laser powder bed fusion," *Rapid Prototyping Journal*, vol. 29, no. 3, pp. 425–436, Jan 2023. [Online]. Available: <https://doi.org/10.1108/RPJ-04-2022-0127>
- [39] H. Zhang, M. Xu, Z. Liu, C. Li, P. Kumar, Z. Liu, and Y. Zhang, "Microstructure, surface quality, residual stress, fatigue behavior and damage mechanisms of selective laser melted 304l stainless steel considering building direction," *Additive Manufacturing*, vol. 46, p. 102147, 2021. [Online]. Available: <https://doi.org/10.1016/j.addma.2021.102147>
- [40] S. Mohanty, M. Arivarasu, N. Arivazhagan, and K. Phani Prabhakar, "The residual stress distribution of CO2 laser beam welded AISI 316 austenitic stainless steel and the effect of vibratory stress relief," *Materials Science and Engineering: A*, vol. 703, pp. 227–235, 2017. [Online]. Available: <https://doi.org/10.1016/j.msea.2017.07.066>
- [41] I. La Fé-Perdomo, J. A. Ramos-Grez, I. Jeria, C. Guerra, and G. O. Barrionuevo, "Comparative analysis and experimental validation of statistical and machine learning-based regressors for modeling the surface roughness and mechanical properties of 316l stainless steel specimens produced by selective laser melting," *Journal of Manufacturing Processes*,

- vol. 80, pp. 666–682, 2022. [Online]. Available: <https://doi.org/10.1016/j.jmapro.2022.06.021>
- [42] A. G. Amir Mahyar Khorasani, Ian Gibson and A. Ghaderi, “A comprehensive study on variability of relative density in selective laser melting of Ti-6Al-4V,” *Virtual and Physical Prototyping*, vol. 14, no. 4, pp. 349–359, 2019. [Online]. Available: <https://doi.org/10.1080/17452759.2019.1614198>
- [43] A. Eliasu, S. H. Duntu, K. S. Hukpati, M. Y. Amegadzie, J. Agyapong, F. Tetteh, A. Czekanski, and S. Boakye-Yiadom, “Effect of individual printing parameters on residual stress and tribological behaviour of 316L stainless steel fabricated with laser powder bed fusion (L-PBF),” *The International Journal of Advanced Manufacturing Technology*, vol. 119, no. 11, pp. 7041–7061, Apr 2022. [Online]. Available: <https://doi.org/10.1007/s00170-021-08489-y>



PREDICTION OF ABRASIVE WEAR AND SURFACE HARDNESS OF PRINTED PARTS BY SLA TECHNOLOGY

PREDICCIÓN DE DESGASTE ABRASIVO Y DUREZA SUPERFICIAL DE PARTES IMPRESAS POR TECNOLOGÍA SLA

P. Muñoz-Valverde¹ , O. Villena-López² ,
 L. Mayorga-Ases^{2,*} , C. Pérez-Salinas³ , D. Moya³

Received: 15-05-2023, Received after review: 11-07-2023, Accepted: 19-10-2023, Published: 01-01-2024

Abstract

In the present study, a prediction of hardness deterioration and abrasive wear was performed through a neural network using artificial intelligence on a material printed in SLA. This article aims to predict the mechanical properties, wear resistance and surface hardness of parts manufactured by SLA stereolithography printing. A full factorial DOE was used to associate the peculiar parameters (print orientation, cure time, layer height) to perform experiments. The mechanical properties were evaluated according to ASTM regulations, with the objective of obtaining feeding data and validation of the predictions of the Taber Wear Index and hardness using an artificial neural network. The experimental results are in good agreement with the measured data with satisfactory prediction errors with a mean square error (MSE) of 0.01 corresponding to abrasive wear using the clear resin and a mean absolute error (MSE) of 0.09 with an R2 of 0.756, the prediction with the neural network with a mean square error (MSE) of 2.47 corresponding to abrasive wear using the tough resin and a mean absolute error (MSE) of 14.3 with an R2 of 0.97. It was shown that the accuracy of the prediction is reasonable, and the network has the potential to be improved if the experimental database for training the network could be expanded. Therefore, wear and hardness mechanical properties can be predicted appropriately with an ANN.

Keywords: 3D printing, SLA Stereolithography, Taber wear index, surface hardness, artificial neural network, light-curing resins

Resumen

En el presente estudio se realizó una predicción del deterioro de la dureza y el desgaste abrasivo a través de una red neuronal utilizando inteligencia artificial sobre un material impreso en SLA. Esta investigación tiene como objetivo predecir las propiedades mecánicas de resistencia al desgaste y dureza superficial de piezas fabricadas mediante impresión por estereolitografía (SLA). Para realizar los experimentos se utilizó un diseño factorial de dos niveles o DOE factorial completo y así asociar los parámetros peculiares (orientación de impresión, tiempo de curado, altura de la capa). Las propiedades mecánicas fueron evaluadas según normativas ASTM, con el objetivo de obtener datos de alimentación y validación de las predicciones del índice de desgaste Taber y la dureza empleando una red neuronal artificial. Los resultados experimentales concuerdan con los datos medidos con errores de predicción satisfactorios con un error cuadrático medio (MSE) de 0,01 correspondiente al desgaste abrasivo utilizando la resina transparente y un error absoluto medio (MSE) de 0,09 con un R2 de 0,76. La predicción con la red neuronal tiene un error cuadrático medio (MSE) de 2,47 perteneciente al desgaste abrasivo utilizando la resina resistente y un error absoluto medio (MSE) de 14,3 con un R2 de 0,97. Se demostró que la precisión de la predicción es razonable, y que la red tiene potencial para mejorar si se pudiera ampliar la base de datos experimental para entrenar la red. Por lo tanto, las propiedades mecánicas de desgaste y dureza se pueden predecir, adecuadamente, con una RNA.

Palabras clave: impresión 3D, estereolitografía SLA, índice de desgaste Taber, dureza superficial, red neuronal artificial, resinas fotocurables

¹Departamento de Ciencias Exactas, Universidad de las Fuerzas Armadas ESPE, Ecuador.

^{2,*}Laboratorio de Materiales y Manufactura, Universidad Técnica de Ambato, Ecuador.

Corresponding author ✉: la.mayorga@uta.edu.ec.

³Grupo de Investigación e Innovación en Ingeniería Mecánica GIM-FICM, Universidad Técnica de Ambato, Ecuador.

1. Introduction

In recent years, additive manufacturing techniques have experienced accelerated progress in the development of prototyping and manufacturing in different fields [1–3]. Polymer printing has played a key role in this progress because its technology is widely available to developers. The new generation of printers has greatly boosted innovation, reducing the time and cost of product development. In addition, the use of additive manufacturing techniques in industry has become a field of great interest due to their high performance and ease of fabrication of complex three-dimensional geometrie.

The relatively low cost of commercially available 3D printers of different types allows the use of a wide range of materials with varying quality, precision, and resolution. Among the most common technologies, SLA (stereolithography) stands out, offering several advantages in precision applications, such as easy-to-use interfaces, resolution, and relatively fast printing speed [4–6].

The properties of SLA printed parts are intimately derived from the SLA process and post-process. In recent years, the mechanical properties obtained from SLA printed parts have been studied in the different light-curing resins available in the market. Even the improvement of the resins has been studied by evaluating the light curing process [7–9]. Properties such as tensile strength, tensile modulus, compressive strength were usually studied [10–12]. However, information on hardness and wear properties is scarce.

The surface hardness of polymeric materials is an important factor in their resistance to abrasive and adhesive wear. A polymeric material with a higher surface hardness will have a higher wear resistance, as it will be less prone to deformation, adhesion and material transfer during contact with abrasive or adhesive surfaces [13]. However, it is also important to consider other factors, such as the chemical structure of the polymer and its resistance to sliding and deformation, for a complete understanding of its tribological behavior [14]. SLA printed parts are increasingly used for engineering applications, where the wear phenomenon is an important aspect to consider. As hardness is a property that is related to the wear process, its inclusion in the analysis is also necessary. Studying the correlation between wear, hardness and SLA printing process parameters is important to design suitable compounds to meet various special requirements.

The prediction of mechanical properties is fundamental in the design of parts and components to ensure their proper functioning. The use of artificial neural networks (ANNs) to predict mechanical properties of materials has proven to be a very useful and powerful tool in engineering in different fields of manufacturing and specifically in wear-related issues [10], [15, 16].

ANNs can learn complex and nonlinear patterns from large data sets and therefore can accurately predict the mechanical properties of materials from limited information. This is especially useful when experimental data on the mechanical properties of a particular material is not available or when it is desired to reduce the time and costs associated with traditional mechanical testing. In summary, using ANN to predict mechanical properties is a valuable tool that can help engineers design more efficient and safer parts and components.

Neural network (NN) approaches are widely used methodologies reported in the literature among various machine learning techniques [17]. The ability of artificial NN to capture complex relationships between input and output data is valuable in manufacturing processes where it is difficult and expensive to obtain large experimental data for process modeling. In addition, NN models show an improvement in experimental error from 40% to 70% [18].

This paper studies the prediction of abrasion wear and hardness obtained from experimental tests on parts printed with thermosetting resins (tough and transparent resins) using SLA. The structure of this paper is as follows. First, the compilation on the technological properties of printed resins and the basics of printing is presented. Secondly, the analysis of hardness resistance and wear resistance of 3D printing by SLA stereolithography is provided by experiments. Finally, the abrasive wear during the 3D printing process is estimated using an artificial neural network based on the experimental data.

2. Materials and Methods

The presentation of this section is (1) the materials and their characteristics, (2) the experimental design, (3) the process of obtaining the printed material, (4) wear and hardness analysis of the tested items and (5) ANN prediction, as shown in the flowchart in Figure 1.

2.1. Materials

Two types of resins were used for property evaluation, Clear and Tough from *FormlabsTM*. brand. Clear FLGPCL04 resin is used to print materials with high resolution and a smooth and soft finish [19]. Whereas Tough FLT0TL05 resin is used for solid prototyping because it balances strength and functionality. Both the manufacturer and printing service companies recommend its use in elements that are subjected to short periods of stress or fatigue [20], e.g., assemblies, press-type configurations and robust prototypes require the use of the aforementioned resin.

Table 1 summarizes the mechanical behavior of the material before and after curing, considering a treatment time of 60 min 60 °C, with a UV radiation of

1.25 mW/cm² and a wavelength of 405 nm for each type of resin. Nine properties are provided for Clear and Tough resin, the table is divided into three cate-

gories, cured, uncured and the testing method used to determine each property.

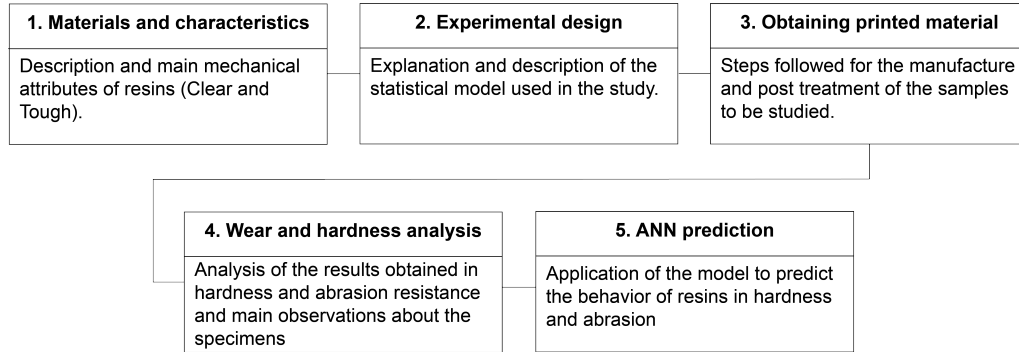


Figure 1. Flow chart of the applied methodology.

Table 1. Mechanical properties of clear and tough resin [20, 21].

PARAMETERS	CLEAR RESIN			TOUGH RESIN		
	Uncured	Post - Cured	Method	Uncured	Post - Cured	Method
Ultimate Tensile Strength	38 MPa	65 MPa	ASTM D 638 - 10	34.1 MPa	55.7 MPa	ASTM D 638 - 14
Tensile Modulus	1.6 GPa	2.8 GPa	ASTM D 638 - 10	1.7 GPa	2.7 GPa	ASTM D 638 - 14
Flexural Stength at 5% Strain				42%	24%	ASTM D 638 - 14
Elongation at Failure	12%	6.2 %	ASTM D 638 - 10	20.8 MPa	60.6 MPa	ASTM C 790 - 15
Flexural Modulus	1.25 GPa	2.2 GPa	ASTM D 790 - 10	0.6 GPa	1.6 GPa	ASTM C 790 - 15
Notched IZOD	16 J/m	25 J/m	ASTM D 256 - 10	32.6 J/m	38 J/m	ASTM D 256 - 10
Heat Deflection Temperature (64 psi)	42.7 °C	58.4 °C	ASTM D 648 - 07	32.8 °C	45.9 °C	ASTM D 648 - 16
Heat Deflection Temperature (66 psi)	49.7 °C	73.1 °C	ASTM D 648 - 07	40.4 °C	48.5 °C	ASTM D 648 - 16
Thermal Expansion (23 - 50 °C)				1597 μm/m/°C	119.4 μm/m/°C	ASTM E 831 - 13

The considered mechanical properties are ultimate tensile strength, tensile modulus, flexural strength at 5% strain, elongation at failure, flexural modulus, notched IZOD, thermal deflection temperature at 64 Psi and 66 Psi and thermal expansion. The evaluation of the technological properties corresponds to the fluid absorption capabilities of the 3D printed parts, such as water, acetone or diesel. Fluid absorption is an important property of materials for medical devices due to their possible use as containers, flow conductors, etc.

Table 2 shows other properties such as the percentage weight gain from a 1x1x1 cm cube, the data correspond to the two resins in 24 hours of immersion in different solvents.

The tensile behaviour of the two resins considering different curing times is shown in Figure 2. Due to their good tensile behaviour, both resins can be used for printing mechanical parts. For example, the Tough resin is used to print gears for RC prototypes, [22]. On the other hand, Clear resin, thanks to its high surface quality, offers the possibility of being used on visually exposed elements. In addition, replacement on

any device is easier, as the affected elements can be replaced in a short time with a new one thanks to this printing technology.

Table 2. Percentage weight gain of the two resins in 24 hours of immersion in different fluids of a 1x1x1 cm cube, [20, 21].

SOLVENT	CLEAR	TOUGH
	Gain (%)	
Strong Acid (HCl)	Distores	Distored
Xylene	< 1	< 1
Water	< 1	1.6
Sodium hydroxide (0.0025% - PH = 10)	< 1	1.5
Salt Water (3.5%)	< 1	1.5
Mineral Oil (Heavy)	< 1	< 1
Mineral Oil (Ligth)	< 1	< 1
Isooctane	< 1	< 1
Hydrogen Peroxide (3%)	< 1	2.1
Acetic Acid (5%)	< 1	2.8
Acetone	Sample cracked	Sample cracked
Isopropyl Acetate	< 1	2.1
Bleach (5% aprox)	< 1	1.7
Butyl Acetane	< 1	1.6
Diesel	< 1	< 1
Diethyl glycol monomethyl ether	1.7	6.6
Hydraulic Oil	< 1	< 1
Skydrol 5	1	1.2

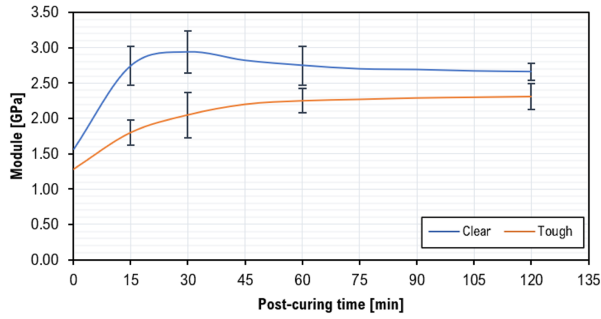


Figure 2. Young modulus vs post cured time for the Clear and Tough Resin

2.2. Experimental design

The orthogonal matrix, in the context of a statistical study, is a tool used to study and analyse all variables independently and simultaneously. It allows the analysis of one variable to be unaffected by the other variables in the study, making it easier to study each variable separately and understand its individual impact. This is due to the independence of data in the study.

By analysing variables independently, the possibility of introducing bias or confounding between them is reduced. This helps to obtain more reliable and accurate results because each variable is examined in isolation and potential sources of error can be better identified and controlled.

Consequently, an orthogonal matrix experimental design was applied in which two quantitative variables (curing time and impression orientation) and a qualitative variable corresponding to resin type were used with three levels as presented in Table 3.

Table 3. Experimental design

FACTORS	UNIT	LEVEL 1		LEVEL 2		LEVEL 3	
		T	C	T	C	T	C
Curing time	[min]	0	0	15	60	30	120
Print orientation	[°]	0		45		-	
Resin type	-	Tough (T)		Clear (C)		-	

In this analysis, a distribution of the data from a full factorial model was used. The number of experimental runs was set to 5. 100 combinations of experimental data were obtained. The data were cleaned for the existence of null values, especially for the Tough resin with 15 and 30 minutes curing times and the Clear resin with 60 and 120 minutes curing times.

2.3. Process of obtaining printed material

Figure 3 shows a SIPOC diagram of the process carried out for the printing of the specimens with the material proposed for the analysis. The graph details the steps (1) to (5) that correspond to the inputs and prototyping, while step (6) details the tests that were carried out for the analysis and data collection that fed the neural network.

Initially, the resins are in a liquid state, stored and supplied from cartridges (1). The specimens were then modelled using design software (2). For printing, the parameters specified by the manufacturer were followed [23] and the variables described in the experimental design were set (3).

The fabrication of each specimen from the SLA process was carried out by means of the printing phase in the Form 2 SLA machine considering the experimental design guidelines, the washing phase was carried out in the Form Wash machine with isopropyl alcohol solvent for a period of 10 to 20 minutes (4) and finally, the curing was carried out in the Form Cure machine.

For the curing stage of the specimens, a time span of 0 to 30 minutes was taken into consideration for the Clear resin and 0 to 120 minutes for the Tough resin as specified in Table 3 (5). An estimate of the time that can be spent per layer can be obtained from Equation (1). The forming time (T_c) depends on the area of the layer to be formed (A_c), the speed (v) and the diameter (D) of the beam, plus the repositioning time for layer materialisation (T_r). The sum of the formation time of each layer gives the total processing time, [24].

$$T_c = \frac{A_c}{vD} + T_r \quad (1)$$

In general terms, the SLA 3D printing process can be mathematically defined by relationships such as the depth of cure, the width of the cure line and the laser exposure at any point.

The depth of cure ratio (Equation (2)) is related by the laser penetration depth (D_p), the exposure energy at the resin surface (E_o) and the minimum energy to gel the resin (E_c) [24]. The width of the cured line (L_w) is expressed by Equation (3). In this relation, D is equivalent to the diameter of the laser in use in the printing machine.

$$Cd = D_p \ln \left(\frac{E_o}{E_c} \right) \quad (2)$$

$$L_w = D \sqrt{\frac{Cd}{2D_p}} \quad (3)$$

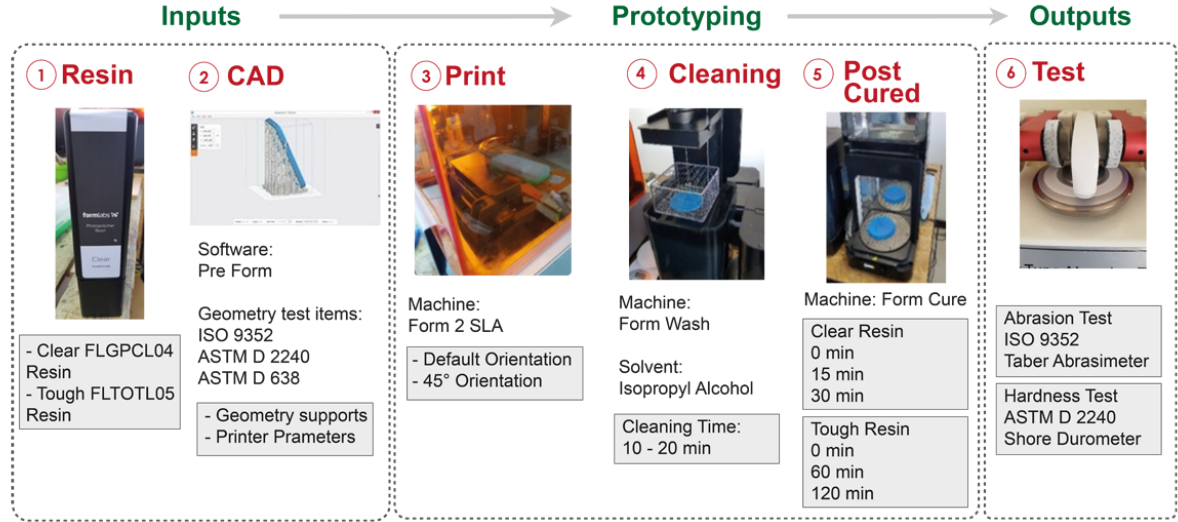


Figure 3. Stages in obtaining printed material for analysis

Considering that the laser has motions in all 3 axes (X - Y - Z), the laser exposure at any point (E (x, y, z)) is determined by Equation (4). The point (x, y) represents the distance from the centre to the beam, (z) the depth at which it is located, (Pl) is equal to the laser power, the Gaussian mean width (Wo) Vs the laser scanning speed and (Dp) the laser penetration depth, [25].

$$E(x, y, z) = \sqrt{\frac{2}{\pi}} \frac{Pl}{WoVs} e^{-\frac{2y^2}{Wo^2}} e^{-\frac{z}{Dp}} \quad (4)$$

Isotropy is a critical characteristic that relates to the parameters defined by Equations 1-4. Isotropy is one of the consequences of post-curing, which strengthens the bonds by forming covalent bonds. At the micro level, there is no marked difference between molecules arranged in the X - Y - Z planes. This makes its mechanical performance predictable and therefore better than other types of 3D printing. On the other hand, impermeability is another characteristic that outperforms the material after curing. This distinctive feature is one of the reasons why this type of printing is often used when dealing with fluids.

2.4. Wear and hardness analysis of tested items

Following the indications set out in the ISO 9352 standard. A load of 1000 grams and 1000 cycles were applied at a speed of 72 rpm. The type of grinding wheel used was intermediate grade H22. The reported result is the Taber Wear Index (TWI), Equation (5), where A is the weight of the sample before the test, B is the weight of the sample after the test and C is equal to the number of cycles used in the test.

$$TWI = \frac{[(A - B)1000]}{C} \quad (5)$$

Each test specimen was tested, and the results are expressed in terms of a Shore D hardness unit, which represents the resistance of the material to penetration by the test needle. On the Shore D scale, lower hardness values correspond to softer materials and higher values correspond to harder materials. The Shore D scale is particularly suitable for rigid materials, with a typical hardness range of 20 to 90 Shore D.

2.5. Artificial neural network (ANN) analysis methods

A neural network is a technique inspired by the biological nervous system, which aims to replicate the way humans learn to solve a wide variety of complex scientific problems. Neural networks consist of several layers of neurons connected with synaptic weights to simulate the human brain. A simplified network consists of an input layer with a number of neurons depending on the input variables (3 in this study), followed by one or more hidden layers that transform those variables for final use in the output layer [26, 27].

Overfitting is a problem related to neural network training. According to research [28–30], determine that too few neurons lead to underfitting, while too many neurons can contribute to overfitting.

Figure 4 shows the neural scheme used, where W is the synaptic weight from each neuron to another neuron in the next layer.

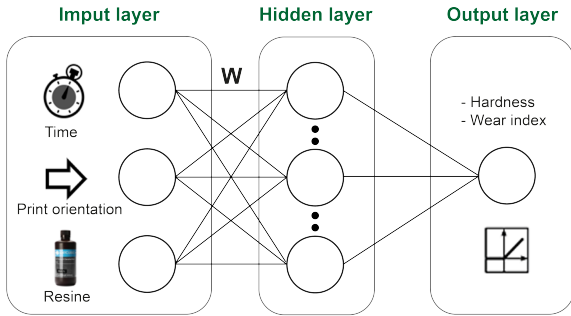


Figure 4. Neural network architecture with three layers implemented from the input to the output layer.

The multilayer feed forward network architecture used in this study consists of three neurons for the input layer, which are ordered according to the number of input variables. One neuron is in the output layer (abrasive wear) and two are hidden layers with ninety-six neurons each. The selected number of neurons in the hidden layer is determined by a trial and error procedure. To decrease the difficulty of training and to balance the importance of each parameter during the training process, the experimental database was normalised between the values 0 and 1.

The scaling of the input and output variables in the interval is determined by the ratio of the difference of the input and output variables. The scaling of the input and output variables in the interval is determined by the ratio of the difference of the input data to the mean and standard deviation (Equation (6)), where x is a data point, μ is the mean and σ is the standard deviation.

$$z = \frac{x - \mu}{\sigma} \quad (6)$$

The output of each neuron of the hidden and output layers is given by the function ReLU. This function represents the activation fusion (Equation (7)). Adam's optimisation algorithm was used together with the backpropagation training algorithm [31] to train the multilayer neural network and calculate the gradient required for weight adjustment.

$$\sigma(x) = \begin{cases} x & \text{si } x \geq 0; \\ 0 & \text{si } x < 0; \end{cases} \quad (7)$$

The training phase of the ANN determines the connection weights needed to give the desired response. The first step is to assign random weight values to all links between neurons. Next, the parameter values of the k -th experiment from the training data list are passed through the network. The estimated value is compared with the desired value using the functions: mean square error (MSE) and mean absolute error (MAE).

The different weights connecting the elements in the neural network are adjusted and approached to the target output value. Equation (8) represents the update of the synaptic weights, based on the calculated error in each neuron.

$$w'_{ji}(n) = w_{ji}(n) + \Delta w_{ji}(n) \quad (8)$$

Where $w'_{ji}(n)$ represent the adjusted weights, $w_{ji}(n)$ are the previous weights and $\Delta w_{ji}(n)$ is the synaptic weight correction. After updating all weights according to the training error, an epoch (n) is completed. An epoch is when all training trials (60 for this study) are evaluated. If the MSE is not lower than a specific target, the process is repeated by updating the weights and increasing the number of epochs required until the target is reached.

3. Results and discussion

The results are reported in two stages, (1) experimental analysis of influential factors on the output variables (Taber wear index and hardness) and (2) wear prediction by neural network.

3.1. Experimental analysis of output variables

Figure 5 details the specimens subjected to the abrasion test where the topology of the specimens has undergone a noticeable change. The main evidence is shown in the quality of the track left by the grinding wheel. This is consistent with the results presented, which indicate that there is a 70% difference in mass loss between the white (Clear Resin) and blue (Tough Resin) specimens. The latter being the most resistant to abrasion.

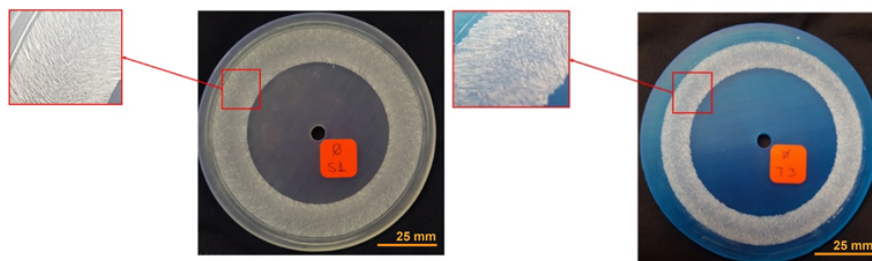


Figure 5. Tested specimens - wear resistance.

On the other hand, regarding the hardness test, it can be said that the hardness scale of the resins increases as the curing time increases. In other words, there is a directly proportional relationship. The Clear resin presents its maximum peak of Shore D hardness at 15 minutes of curing with an average of 88.4, being

the highest among the two resins used in the study. The Tough resin presents its maximum peak at 60 minutes of cure with an average hardness scale of 78.6.

Table 4 shows the distribution of the data from a full factorial model.

Table 4. Training data. Full Factorial model with 5 experimental runs

N°	CURED [min]	ORIENTATION [°]	ABRASION	CLEAR RESIN	TOUGH RESIN	N°	CURED [min]	ORIENTATION [°]	ABRASION	CLEAR RESIN	TOUGH RESIN
1	30	0	0.73	1.00	0.00	31	60	45	0.06	0.00	1.00
2	30	45	0.43	1.00	0.00	32	60	45	0.08	0.00	1.00
3	120	45	0.11	0.00	1.00	33	0	45	0.06	1.00	0.00
4	15	0	0.69	1.00	0.00	34	60	45	0.12	0.00	1.00
5	120	0	0.57	0.00	1.00	35	0	45	0.64	1.00	0.00
6	60	0	0.36	0.00	1.00	36	15	0	0.45	1.00	0.00
7	0	45	0.64	1.00	0.00	37	30	0	0.52	1.00	0.00
8	0	0	11.80	1.00	0.00	38	0	0	11.80	1.00	0.00
9	30	0	0.52	1.00	0.00	39	30	45	0.31	1.00	0.00
10	0	0	0.74	0.00	1.00	40	0	45	0.31	0.00	1.00
11	0	0	0.88	0.00	1.00	41	0	0	0.64	0.00	1.00
12	120	45	0.06	0.00	1.00	42	30	45	0.36	1.00	0.00
13	0	0	0.90	0.00	1.00	43	120	0	0.48	0.00	1.00
14	15	45	0.33	1.00	0.00	44	15	45	0.41	1.00	0.00
15	60	0	0.43	0.00	1.00	45	15	45	0.45	1.00	0.00
16	30	45	0.50	1.00	0.00	46	0	45	0.27	0.00	1.00
17	0	0	11.80	1.00	0.00	47	15	0	0.43	1.00	0.00
18	120	45	0.10	0.00	1.00	48	30	0	0.70	1.00	0.00
19	0	45	0.64	1.00	0.00	49	15	0	0.96	1.00	0.00
20	0	45	0.29	0.00	1.00	50	0	0	11.80	1.00	0.00
21	60	45	0.14	0.00	1.00	51	120	0	0.41	0.00	1.00
22	120	45	0.08	0.00	1.00	52	120	45	0.09	0.00	1.00
23	15	45	0.49	1.00	0.00	53	0	0	0.72	0.00	1.00
24	120	0	0.48	0.00	1.00	54	60	45	0.15	0.00	1.00
25	30	0	0.47	1.00	0.00	55	0	45	0.18	0.00	1.00
26	15	45	0.49	1.00	0.00	56	0	45	0.21	0.00	1.00
27	60	0	0.37	0.00	1.00	57	60	0	0.50	0.00	1.00
28	0	45	0.64	1.00	0.00	58	30	45	0.45	1.00	0.00
29	15	0	0.43	1.00	0.00	59	0	0	11.80	1.00	0.00
30	60	0	0.49	0.00	1.00	60	120	0	0.33	0.00	1.00

Figure 6 shows the experimental results for the main effects of hardness and wear rate at 5% significance level. For hardness (Figure 6a), it is observed that both resin type and curing time are incident variables (p-value < 0.01 for the two factors in the ANOVA analysis). Impression orientation is not incident (p-

value > 0.01). On the other hand, figure 6b shows that all factors (resin type, curing time and impression orientation) are incident on abrasion resistance (p-value < 0.01) for all factors. For both response variables, the resin with the highest performance is Clear resin.

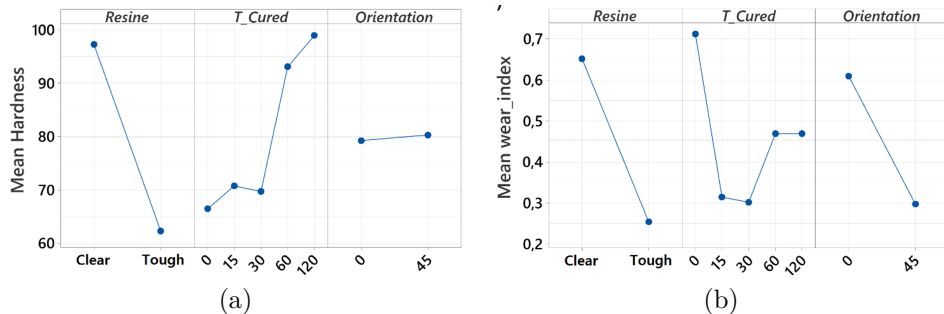


Figure 6. Main effects plot. a) Hardness, b) Abrasion resistance - Tabber test

Figure 7 shows the hardness behaviour of the two resins (Clear, Tough Resin) as a function of curing time; (figure 7a), corresponding to the Clear resin, shows a higher hardness. However, the highest values are in the range of 15 to 30 minutes. On the other hand, a similar behaviour is observed in the Tough resin (figure 7b), where it is evident that the longer the curing time, the higher the hardness. To achieve these results, a curing range of 60 minutes is necessary. It is also observed that the recommended curing time should not be exceeded because it does not improve

the hardness of the material.

Figure 8 shows the abrasion results. The two resins have a distinct pattern of behaviour. As they are not cured, they do not show good stability (low strength). The abrasion resistance increases when the two resins are cured for the first time. Regardless of the time, it is observed that the change is noticeable between 0 min and 5 min (Resin Clear 8a). Thereafter, as shown by the tensile strength results, the values do not show noticeable changes. In other words, the longer the curing time, the higher the abrasion resistance.

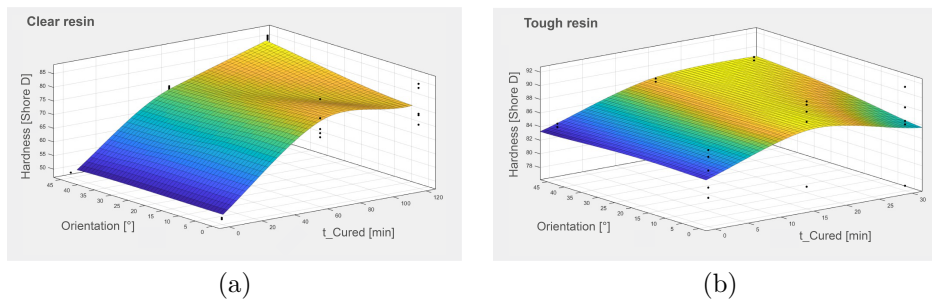


Figure 7. Experimental results. (a) Clear Resin: Hardness vs Orientation vs Post – Cured (b) Tough Resin. Hardness vs Post Cured time Vs Orientation.

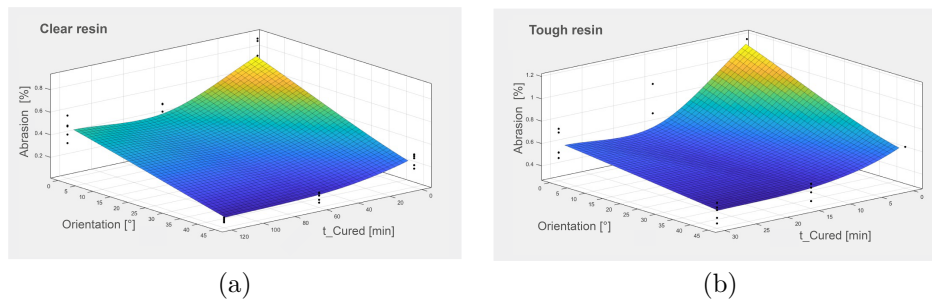


Figure 8. Experimental results. (a) Clear Resin: Wear resistance vs Orientation vs Post – Cured (b) Tough Resin. Wear resistance vs Post Cured time Vs Orientation.

3.2. Abrasive wear and hardness prediction by artificial neural network

A neural model was developed to estimate the Taber wear rate (TDI) and hardness based on different combinations of stereolithographic 3D printing. The database was obtained through laboratory tests. The experimental data used for the training stage was divided by cross-validation into 80% for training and 20% for validation. It was developed with a feed - forward and back propagation neural scheme on a total of 60 experimental data.

The best performing model was the 5-96-96-1 architecture. The activation function ReLu was used for both the hidden layers and the output layer. Figure 9 shows the relationship between the values obtained by neural training and the values obtained experimentally.

The evolution of the MAE and MSE with the epochs for the designed neural network is presented in Figure 10, where the convergence of the results is observed. The MAE at the end of the abrasive wear training procedure resulted to be 0.09 using Clear resin and an MSE value of 0.01. To measure the accuracy of the ANN, the correlation coefficient (R2) between the results and the targets was calculated. In this case, $R2 = 0.75$ represents a correlation between experimental and estimated values. The MAE is 2.47 using tough resin and an MSE value of 14.3. The correlation coefficient (R2) between the results and the targets was calculated. In this case, $R2 = 0.97$.

MAE evaluated the predictive performance of the model, MSE and R2 values. Previous research [26], [32, 33] recommends that the model should have high

R2 and low MAE and MSE for the neural model to have high efficiency. Figure 11 shows the results of the ANN training process after reaching the minimum gradient. Table 5 presents the results of MAE and MSE after network training.

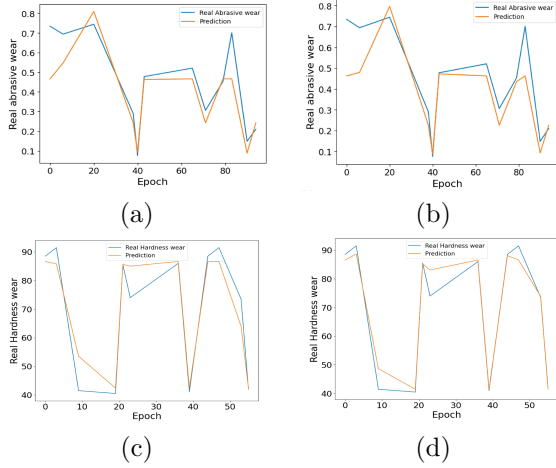


Figure 9. Overall comparison between predicted and experimental values of abrasive wear. a) Abrasive wear with Clear Resin b) Abrasive wear with Tough Resin c) Hardness with Clear Resin d) Hardness with Tough Resin

Table 5. MAE, MSE and R2 statistics of the neural model

DATA SET	MAE	MSE	R ²
Abrasive wear of Clear resin			
Training	0.06	0.01	0.75
Validation	0.09	0.01	
Tough resin abrasive wear			
Training	0.06	0.01	0.69
Validation	0.09	0.02	
Clear resin hardness			
Training	3.88	33.48	0.92
Validation	4.28	35.46	
Tough resin hardness			
Training	2.17	14.41	0.97
Validation	2.47	14.33	

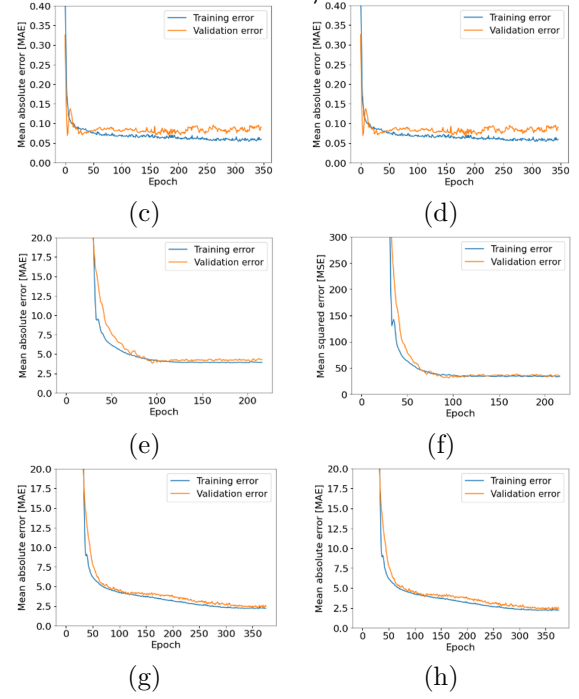


Figure 10. Evolution of the mean absolute error and evolution of the mean squared error with the number of epochs. a) MAE of abrasive wear with Clear Resin b) MSE of abrasive wear with Clear Resin c) MAE of abrasive wear with Tough Resin d) MSE of abrasive wear with Tough Resin e) MAE of hardness with Clear Resin f) MSE of hardness with Clear Resin g) MAE of hardness with Tough Resin h) MSE of hardness with Tough Resin

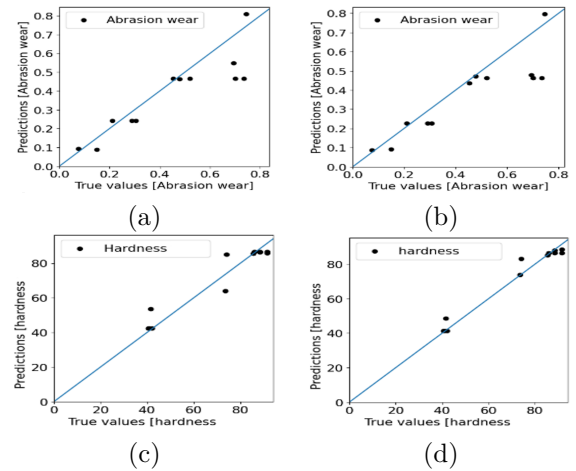
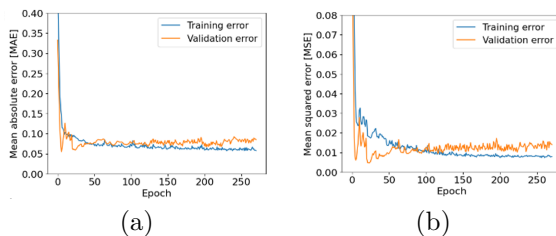


Figure 11. Regression between the data presented by the neural network and the real values obtained experimentally for abrasive wear. a) Abrasive wear with Clear Resin b) Abrasive wear with Tough Resin c) Hardness with Clear Resin d) Hardness with Tough Resin

Table 6 presents the best hyperparameter settings for the neural model, considering the statistical results and computational cost.

Figure 12 illustrates the distribution of the residuals of the model. Most of the residuals are close to zero, which determines the satisfactory performance of the proposed neural network model. The residuals are not close to a normal curve. This behavior may be due to the small sample size considered for training.

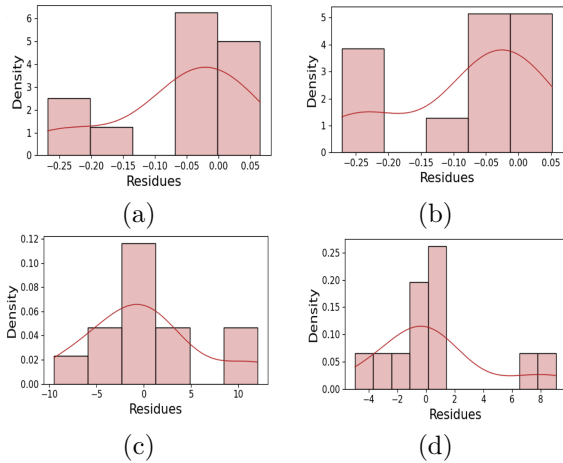


Figure 12. The distribution plot of residuals tends to a Gaussian curve, i.e. most of the residuals tend to approach the value of zero. a) Abrasive wear Clear Resin b) Abrasive wear with Tough Resin c) Hardness with Clear Resin d) Hardness with Tough Resin

Table 6. Hyperparameters of the neural network model

PARAMETER	VALUE
Network architecture	5 - 96 - 96 - 1
Input parameters	- Resin type - Curing time - Print orientation
Output parameters	Taber wear index (IWT) and hardness
Activation function	ReLu
Optimiser	Adán
Performance function	- Mean square error (MSE) - Mean absolute error (MAE) - Coefficient of determination (R2)
Learning rate	0.001
Number of iterations	500
Batch size	10

The prediction of the network was determined through the estimated values during the validation of the neural network model. However, it is observed that several values do not agree with the real data. This problem could be caused by the following three factors: type of material, lack of sampling accuracy and the architecture of the neural network.

Table 7 represents the percentage error presented by the network on each validation data. The results indicate the similarities between the experimental studies and the neural model, supporting the reliability of the model.

Table 7. Abrasion rate of the prediction error compared to actual values

DATA SET	% ERROR
Clear resin abrasive wear	19.34
Tough resin abrasive wear	19.60
Clear resin hardness	6.87
Tough resin hardness	3.92

4. Conclusions

The first objective is related to the analysis of the mechanical properties of the resins, it was determined that hardness and stress increase as a function of the post-curing time of each resin. The Tough and Clear resins have shown a definite pattern in their behavior, especially in hardness and abrasion. When uncured, their properties are lower than when cured at 60 min, which is in line with the manufacturer's recommendations. This jump is very noticeable especially in hardness and tensile strength. If the curing time is increased, their properties have a negligible increase. After the maximum curing time of 120 min, there will be no appreciable improvement in properties.

The neural network model successfully predicted the experimental results with a mean square error of 0.014 and a mean absolute error of 0.085 using clear resin. The MAE is 2.27 using tough resin and an MSE value of 14.33. The correlation coefficient (R2) between the results and the targets was calculated. In this case, $R2 = 0.97$. This shows that the predicted results agree with the measured values. It is also verified that the artificial neural network model is reliable and that the predicted results provide useful information for developing new abrasive wear resistant materials.

The visual surface diagrams constructed with the network results can be used to monitor the impact of wear evolution, reduce damage, and prevent component fracture. Finally, it is concluded that SLA 3D printing with Clear and Tough resins are good alternatives for use in the printing of emerging components due to their hardness and good abrasive wear behavior.

The abrasion experiment is limited to a medium grade. Due to the use of grinding wheels of the type mentioned above. As there is a specific degree of abrasion, the experimental conditions are limited to those proposed by the ISO 9352 abrasion standard. If it is necessary to know the behavior of the material under high and low abrasion, it is advisable to conduct experiments using grinding wheels that meet the requirements.

Acknowledgements

This research was funded by the Directorate of Research and Development of the Technical University of Ambato - DIDE through grant code UTA-CONIN-2020-0306-R and by the Bilateral Cooperation Fund for the response to COVID-19 of the British Embassy in Quito. Research support from the Mechanical Engineering Research Innovation Group (GI3M).

References

- [1] T. D. Ngo, A. Kashani, G. Imbalzano, K. T. Nguyen, and D. Hui, "Additive manufacturing (3D printing): A review of materials, methods, applications and challenges," *Composites Part B: Engineering*, vol. 143, pp. 172–196, 2018. [Online]. Available: <https://doi.org/10.1016/j.compositesb.2018.02.012>
- [2] A. I. Pérez Sanpablo, E. Romero Avila, and A. González Mendoza, "Three-dimensional printing in healthcare," *Revista Mexicana de Ingeniería Biomedica*, vol. 42, no. 2, pp. 32–48, 2021. [Online]. Available: <https://doi.org/10.17488/RMIB.42.2.3>
- [3] T. Wohlers, *Rapid Prototyping & Tooling State of the Industry Annual Worldwide Progress Report Wohlers Report*. Wohlers Associates, 2001. [Online]. Available: <https://bit.ly/46DJYlv>
- [4] E. J. Hurst, "3D printing in healthcare: Emerging applications," *Journal of Hospital Librarianship*, vol. 16, no. 3, pp. 255–267, 2016. [Online]. Available: <https://doi.org/10.1080/15323269.2016.1188042>
- [5] S. Mishra, "Application of 3D printing in medicine," *Indian Heart Journal*, vol. 68, no. 1, pp. 108–109, 2016. [Online]. Available: <https://doi.org/10.1016/j.ihj.2016.01.009>
- [6] J. W. Stansbury and M. J. Idacavage, "3D printing with polymers: Challenges among expanding options and opportunities," *Dental Materials*, vol. 32, no. 1, pp. 54–64, 2016. [Online]. Available: <https://doi.org/10.1016/j.dental.2015.09.018>
- [7] A. C. Uzcategui, A. Muralidharan, V. L. Ferguson, S. J. Bryant, and R. R. McLeod, "Understanding and improving mechanical properties in 3D printed parts using a dual-cure acrylate-based resin for stereolithography," *Advanced Engineering Materials*, vol. 20, no. 12, p. 1800876, 2018. [Online]. Available: <https://doi.org/10.1002/adem.201800876>
- [8] C. Mendes-Felipe, D. Patrocínio, J. M. Laza, L. Ruiz-Rubio, and J. L. Vilas-Vilela, "Evaluation of postcuring process on the thermal and mechanical properties of the Clear02 resin used in stereolithography," *Polymer Testing*, vol. 72, pp. 115–121, 2018. [Online]. Available: <https://doi.org/10.1016/j.polymertesting.2018.10.018>
- [9] A. Bardelcik, S. Yang, F. Alderson, and A. Gadsden, "The effect of wash treatment on the mechanical properties and energy absorption potential of a 3D printed polymethyl methacrylate (pmma)," *Materials Today Communications*, vol. 26, p. 101728, 2021. [Online]. Available: <https://doi.org/10.1016/j.mtcomm.2020.101728>
- [10] Z. Jiang, Z. Zhang, and K. Friedrich, "Prediction on wear properties of polymer composites with artificial neural networks," *Composites Science and Technology*, vol. 67, no. 2, pp. 168–176, 2007, modelling and Characterization of Composites. [Online]. Available: <https://doi.org/10.1016/j.compscitech.2006.07.026>
- [11] A. D. Tura, H. G. Lemu, H. B. Mamo, and A. J. Santhosh, "Prediction of tensile strength in fused deposition modeling process using artificial neural network and fuzzy logic," *Progress in Additive Manufacturing*, vol. 8, no. 3, pp. 529–539, Jun 2023. [Online]. Available: <https://doi.org/10.1007/s40964-022-00346-y>
- [12] M. Tayyab, S. Ahmad, M. J. Akhtar, P. M. Sathikh, and R. M. Singari, "Prediction of mechanical properties for acrylonitrile-butadiene-styrene parts manufactured by fused deposition modelling using artificial neural network and genetic algorithm," *International Journal of Computer Integrated Manufacturing*, vol. 36, no. 9, pp. 1295–1312, 2023. [Online]. Available: <https://doi.org/10.1080/0951192X.2022.2104462>
- [13] U. S. Tewari, S. K. Sharma, and P. Vasudevan, "Polymer tribology," *Journal of Macromolecular Science, Part C*, vol. 29, no. 1, pp. 1–38, 1989. [Online]. Available: <https://doi.org/10.1080/07366578908055162>
- [14] B. Gupta, "3 - friction and wear mechanism of polymers, their composites and nanocomposites," in *Tribology of Polymers, Polymer Composites, and Polymer Nanocomposites*, ser. Elsevier Series on Tribology and Surface Engineering, S. C. George, J. T. Haponiuk, S. Thomas, R. Reghunath, and S. P. S., Eds. Elsevier, 2023, pp. 51–117. [Online]. Available: <https://doi.org/10.1016/B978-0-323-90748-4.00012-1>
- [15] E. Ezugwu, S. Arthur, and E. Hines, "Tool-wear prediction using artificial neural networks," *Journal of Materials Processing Technology*, vol. 49,

- no. 3, pp. 255–264, 1995. [Online]. Available: [https://doi.org/10.1016/0924-0136\(94\)01351-Z](https://doi.org/10.1016/0924-0136(94)01351-Z)
- [16] C. F. Pérez-Salinas, A. del Olmo, and L. N. López de Lacalle, “Estimation of drag finishing abrasive effect for cutting edge preparation in broaching tool,” *Materials*, vol. 15, no. 15, p. 5135, Jul 2022. [Online]. Available: <http://dx.doi.org/10.3390/ma1515135>
- [17] G. Radhakrishnan, C. Kesavan, V. Ramesh, and T. Anandan, “Application of artificial neural network (ANN) for predicting the wear behaviour of Al 2219-SiCp composite,” in *Mechanical Engineering Design*, ser. Applied Mechanics and Materials, vol. 852. Trans Tech Publications Ltd, 10 2016, pp. 397–401. [Online]. Available: <https://doi.org/10.4028/www.scientific.net/AMM.852.397>
- [18] B. A. Shuvho, M. A. Chowdhury, and U. K. Debnath, “Analysis of artificial neural network for predicting erosive wear of nylon-12 polymer,” *ASTM*, vol. 8, no. 1, 2019. [Online]. Available: <https://doi.org/10.1520/MPC20180164>
- [19] E. Van der Giessen, L. Kubin, and S. Forest, “Jp - foreword,” in *Journal De Physique. IV.*, 2001. [Online]. Available: <https://bit.ly/48YEgMF>
- [20] FormLabs, *Tough Resin for Rugged Prototyping*. FormLabs Material Properties, 2018. [Online]. Available: <https://bit.ly/45Fi73c>
- [21] —, *Standard Materials for High-Resolution Rapid Prototyping*. FormLabs Material Properties, 2017. [Online]. Available: <https://bit.ly/407ySTI>
- [22] B. Sen-Crowe, M. Sutherland, M. McKenney, and A. Elkbuli, “A closer look into global hospital beds capacity and resource shortages during the covid-19 pandemic,” *Journal of Surgical Research*, vol. 260, pp. 56–63, 2021. [Online]. Available: <https://doi.org/10.1016/j.jss.2020.11.062>
- [23] V. R. Sastri, “4 - material requirements for plastics used in medical devices,” in *Plastics in Medical Devices (Third Edition)*, third edition ed., ser. Plastics Design Library, V. R. Sastri, Ed. William Andrew Publishing, 2022, pp. 65–112. [Online]. Available: <https://doi.org/10.1016/B978-0-323-85126-8.00008-4>
- [24] P. Jacobs, “Fundamentals of stereolithography,” *3D Systems Inc.*, pp. 196–210, 1992. [Online]. Available: <https://bit.ly/491P2BH>
- [25] J. H. Lee, R. K. Prud’homme, and I. A. Aksay, “Cure depth in photopolymerization: Experiments and theory,” *Journal of Materials Research*, vol. 16, no. 12, pp. 3536–3544, Dec 2001. [Online]. Available: <https://doi.org/10.1557/JMR.2001.0485>
- [26] K. Abd El-Aziz, D. Saber, and A. A. Megahed, “Investigation and prediction of abrasive wear rate of heat-treated HCCIs with different Cr/C ratios using artificial neural networks,” *International Journal of Metalcasting*, vol. 15, no. 4, pp. 1149–1163, Oct 2021. [Online]. Available: <https://doi.org/10.1007/s40962-020-00547-7>
- [27] A. Sagbas, F. Kahraman, and U. Esme, “Modeling and predicting abrasive wear behaviour of poly oxy methylenes using response surface methodology and neural networks,” *Metalurgija*, vol. 48, no. 2, pp. 117–120, 2009. [Online]. Available: <https://bit.ly/46WkGif>
- [28] N. Srivastava, G. Hinton, A. Krizhevsky, I. Sutskever, and R. Salakhutdinov, “Dropout: A simple way to prevent neural networks from overfitting,” *Journal of Machine Learning Research*, vol. 15, no. 56, pp. 1929–1958, 2014. [Online]. Available: <https://bit.ly/45y1l5W>
- [29] K. Cho, B. van Merriënboer, D. Bahdanau, and Y. Bengio, “On the properties of neural machine translation: Encoder–decoder approaches,” in *Proceedings of SSST-8, Eighth Workshop on Syntax, Semantics and Structure in Statistical Translation*. Doha, Qatar: Association for Computational Linguistics, Oct. 2014, pp. 103–111. [Online]. Available: <http://dx.doi.org/10.3115/v1/W14-4012>
- [30] C. Zhang, S. Bengio, M. Hardt, B. Recht, and O. Vinyals, “Understanding deep learning (still) requires rethinking generalization,” *Commun. ACM*, vol. 64, no. 3, pp. 107–115, feb 2021. [Online]. Available: <https://doi.org/10.1145/3446776>
- [31] Y. Zeng, K. Jiang, and J. Chen, “Automatic seismic salt interpretation with deep convolutional neural networks,” in *Proceedings of the 2019 3rd International Conference on Information System and Data Mining*. ACM, apr 2019. [Online]. Available: <https://doi.org/10.1145/2F3325917.3325926>
- [32] M. Hawryluk and B. Mrzyglod, “A system of analysis and prediction of the loss of forging tool material applying artificial neural networks,” *Journal of Mining and Metallurgy*, vol. 54, no. 3, pp. 323–337, 2018. [Online]. Available: <https://doi.org/10.2298/JMMB180417023H>
- [33] S. Sardar, S. Dey, and D. Das, “Modelling of tribological responses of composites using integrated ANN-GA technique,” *Journal of Composite Materials*, vol. 55, no. 7, pp. 873–896, 2021. [Online]. Available: <https://doi.org/10.1177/0021998320960520>



A NON-LINEAR OPTIMIZATION MODEL ASSESSMENT FOR THE ECONOMIC DISPATCH OF ISOLATED MICROGRIDS

EVALUACIÓN DE UN MODELO DE OPTIMIZACIÓN NO LINEAL PARA EL DESPACHO ECONÓMICO DE MICRORREDES AISLADAS

Carlos Veloz¹ , Diego L. Jiménez J.^{1,*} ,
 Verónica C. Almache B.² , Roberto Salazar Achig¹

Received: 16-11-2023, Received after review: 12-12-2023, Accepted: 19-12-2023, Published: 01-01-2024

Abstract

The present research work presents the optimal energy management of an isolated microgrid based on unconventional renewable energy sources. For this purpose, an economic dispatch problem is proposed that seeks to supply the electrical demand at the lowest possible operating cost, based on a mixed integer nonlinear optimization problem. The nonlinearity of the algorithm is presented by including the characteristic equation that describes the real operation of the generating set in the optimization model. The input data to the economic dispatch, such as solar radiation and wind speed, were obtained from the NASA platform located on the Santa Cruz Island, Galapagos province, Ecuador. In addition, the electricity demand data was obtained from real measurements of the area. The economic dispatch problem has been solved for 12, 24 and 168 hours, obtaining a proportional energy distribution for each case of 50.40% supplied by the photovoltaic generator, 23.92% by the diesel generator, 17.14% by the battery bank and 5.53% by the wind generator; therefore, the demand was totally supplied, meeting the objective that the generating set does not exhibit intermittencies and obtaining the lowest operating cost of the system.

Keywords: Economic dispatch, mixed-integer nonlinear optimization problem, non-conventional renewable energy, isolated microgrid.

Resumen

El presente trabajo de investigación muestra la gestión óptima de la energía de una microrred aislada basada en fuentes de energía renovable no convencional. Para lo cual se plantea un problema de despacho económico que busca abastecer la demanda eléctrica al menor costo de operación posible, a partir de un problema de optimización no lineal entero mixto. La no linealidad del algoritmo se presenta al incluir la ecuación característica del funcionamiento real del grupo electrógeno en el modelo de optimización. Los datos de entrada al despacho económico como radiación solar y velocidad del viento fueron obtenidos de la plataforma de la NASA situada sobre la isla Santa Cruz, provincia de Galápagos, Ecuador. Además, los datos de la demanda eléctrica fueron obtenidos de mediciones reales del sector. El problema de despacho económico se ha resultado para 12, 24 y 168 horas respectivamente, obteniendo una distribución energética proporcional para cada caso del 50.40 % suministrada por el generador fotovoltaico, 23.92 % por el generador diésel, 17.14 % por el banco de baterías y 5.53 % por el generador eólico, por lo que la demanda fue abastecida en su totalidad cumpliendo con el objetivo de que el grupo electrógeno no presente intermitencias y obteniendo el menor costo de operación del sistema.

Palabras clave: despacho económico, problema de optimización no lineal entero mixto, energía renovable no convencional, microrred aislada

^{1,*}Facultad de Ciencias de la Ingeniería y Aplicadas, Universidad Técnica de Cotopaxi, Ecuador.
 Corresponding author ✉: diego.jimenez@utc.edu.ec

²Facultad de Ciencias de la Ingeniería en Sistemas, Electrónica e Industrial, Universidad Técnica de Ambato, Ecuador.

Suggested citation: Veloz, C.; Jiménez J., D. L.; Almache B., V. C.; Salazar A., R. "A non-linear optimization model assessment for the economic dispatch of isolated microgrids," *Ingenius, Revista de Ciencia y Tecnología*, N.º 31, pp. 32-42, 2024, DOI: <https://doi.org/10.17163/ings.n31.2024.03>.

1. Introduction

At present, the population growth has led to a significant increase in the electrical consumption rate, and conventional generation units are not capable of completely fulfilling the power demand of large cities. In addition, these resources do not reach the entire population, due to either the distance from the electric network to the end user, or to economic conditions that do not allow to extend transmission lines to supply isolated areas [1–3]. This led to the alternative of initiating supply projects based of unconventional renewable energy sources, such as solar, wind, biomass, among others. These projects seek to supply the electrical demand of isolated areas or are a supplement for the general energy sector [4, 5].

The implementation of small electric generation plants has gained strength in recent years, due to the electric power supply shortfalls in the region, and especially in Ecuador, where the electric demand of its continental territory is mainly supplied by hydroelectric generation, but it maintains a deficit in the electric supply in the island territory, thus widely relying on polluting generation units such as diesel generators [6, 7].

In light of the electrical energy deficit in the island region and the increasing use of generation units based on alternative energy sources, the idea arises to supply the electrical demand of isolated areas through unconventional renewable energy [8, 9]. For this purpose, it is necessary to develop an energy management system that solves the economic dispatch problem through an association between operating costs and power generated, optimally and efficiently balancing the supply of the electrical demand [10, 11].

In this context, this research presents the evaluation of an optimization model that seeks to supply the electrical demand of an isolated microgrid using unconventional renewable energy. It incorporates a quadratic equation that models the real operation of the diesel generator in the objective function, enabling the solution of a mixed-integer nonlinear economic dispatch problem for 24, 48, and 168 hours of operation

under various constraints.

1.1. Related works

A literature review of different research works about economic dispatch of isolated microgrids is presented below.

The use of quadratic programming for solving economic dispatch problems is promoted in [12], where the quadratic function is determined using the variable scaling method to minimize system operating costs. On the other hand, [13] presents a predictive control strategy that employs an algorithm based on fuzzy logic to address an economic dispatch problem, considering different variables and potential scenarios of load and renewable energy generation capacity.

The issue of the uncertainty associated to unconventional renewable energies, which limits their usage, is addressed in [14]. However, a parameter simplification approach can be used to tackle the stochastic nature of these energies. In addition, [15, 16] propose the inclusion and solution of the uncertainty of unconventional renewable energies, by means of a consensus algorithm through centralized and distributed economic dispatch, highlighting the importance of these constraint conditions to enhance the performance of the final dispatch.

On the other hand, the use of quadratic dynamic programming is proposed in [17, 18], as a solution aimed at improving the control of load losses in the economic dispatch. In addition, in [19] it is sought to ensure the supply of electrical energy for an isolated microgrid, using prediction algorithms that enable to identify load data as input to the economic dispatch. Using a batch processing method, the performance of the model is enhanced.

Finally, Table 1 presents a literature review of the last three years, analyzing various research works that validate the possibility of posing a mixed-integer nonlinear optimization problem, seeking to minimize system operating costs with the purpose of completely supplying the electrical demand, considering different dispatchable and non-dispatchable generation units from unconventional renewable energy sources and a model of a generating set.

Table 1. Literature review

Publication year	Authors	Description	Reference
1	2022	E. López-Garza, R. F. Domínguez-Cruz, F. Martell-Chávez, and I. Salgado-Tránsito	[20]
2	2020	H. Xu, Z. Meng, and Y. Wang	[21]
3	2020	L. Jian, Z. Qian, Z. Liangang, and Y. Mengkai	[22]
4	2022	K. Chen, Z. Zhu, and J. Wang	[23]
5	2022	Xu, F., Zhang, X., Ma, X., Mao, X., Lu, Z., Wang, L., and Zhu, L.	[24]

1.2. Nomenclature

Objective function

- T : Evaluation horizon.
- t : Time.
- C_D : Diesel generator cost.
- Q_{dt} : Diesel consumption from the power as a function of time.
- C_{ENS} : Unsupplied power cost.
- P_{ENS_t} : Unsupplied power as a function of time.
- C_{SH} : Spillage power cost.
- P_{SH_t} : Spillage power as a function of time.
- CU_{BESS} : Battery bank usage cost.
- $P_{B_t}^C$: Power of the batteries in charge mode as a function of time.
- $P_{B_t}^D$: Power of the batteries in discharge mode as a function of time.
- η^C : Efficiency of the batteries in charge mode.
- η^D : Efficiency of the batteries in discharge mode.

Equation of the battery bank costs

- CI_{BESS} : BESS investment cost.
- E_{max} : Maximum energy.
- N_{ciclos} : Number of battery cycles.

Balance equation

- P_{D_t} : Diesel power as a function of time.
- P_{S_T} : Solar power as a function of time.
- P_{W_t} : Wind power as a function of time.

- D_t : Demand as a function of time.

Diesel power constraint equation

- $P_{D_{min}}$: Minimum diesel power.
- $P_{D_{max}}$: Maximum diesel power.

Diesel quadratic equation

- A : First constant of the quadratic equation.
- a : Second constant of the quadratic equation.
- c : Third constant of the quadratic equation.

BESS constraint equation

- E_t : Energy of the battery bank as a function of time.
- E_0 : Initial energy of the battery bank.
- E_{t-1} : Energy as a function of time that determines the actual conditions of the battery bank.
- E_{min} : Minimum energy.

Equation of the BESS binary variables

- X_t^C : Battery charge mode as a function of time.
- X_t^D : Battery discharge mode as a function of time.

SOC equations

- SOC_t : Battery state of charge as a function of time.
- SOC_{min} : Minimum battery state of charge.
- SOC_{max} : Maximum battery state of charge.

2. Materials and methods

Economic dispatch ensures the optimal operation of all generation units, by supplying electrical demand at the lowest operating cost [25, 26]. Figure 1 displays the methodology to carry out the proposed economic dispatch problem. First, it is essential to gather the input data that enable to supply the demand of the isolated microgrid. Then, the mixed-integer nonlinear optimization problem must be defined and, finally, it is necessary to evaluate the response of the economic dispatch to obtain different results.

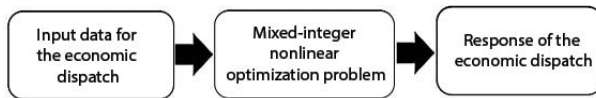


Figure 1. Economic dispatch methodology

2.1. Input data for the economic dispatch

The input data for the economic dispatch are depicted in the block diagram in Figure 2, where the solar power aims to supply most of the electrical demand, given that the Galápagos province experiences the highest values of solar irradiation in the country, as evidenced in Ecuador’s solar map [27]. This map identifies the maximum value of global solar irradiation scale at around 6 kWh/m²day, as shown in Figure 3.

Next, it is shown the behavior of the unconventional renewable energy generation units used, as input data for economic dispatch. The solar irradiation and wind speed values were obtained from [28], then converted into electrical power based on the needs of the case study and plotted for the 168 hours. Figure 4 depicts the solar power behavior over a 24-hour period, while Figure 5 displays the wind power behavior throughout the same 24-hour period. It can be observed that solar power reaches a maximum value of 70 kW, whereas wind power only reaches a maximum of 3 kW.

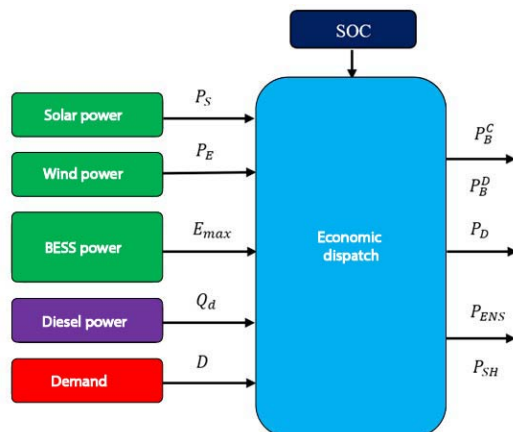


Figure 2. Block diagram used in economic dispatch

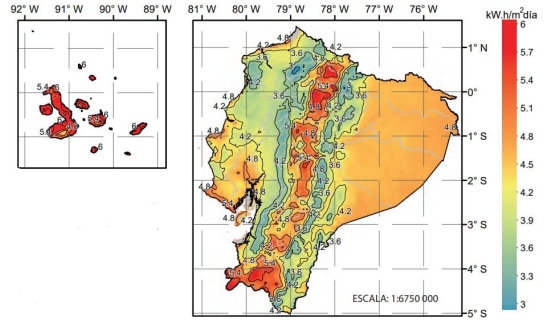


Figure 3. Global Solar Irradiation in Ecuador [27]

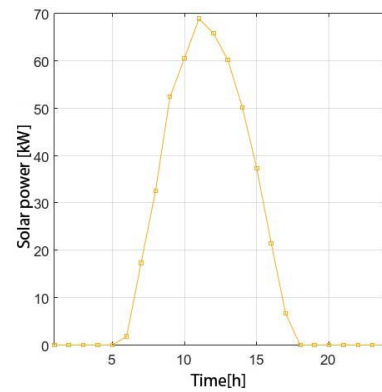


Figure 4. Solar power generation

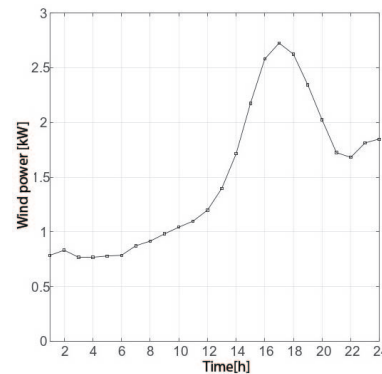


Figure 5. Wind power generation

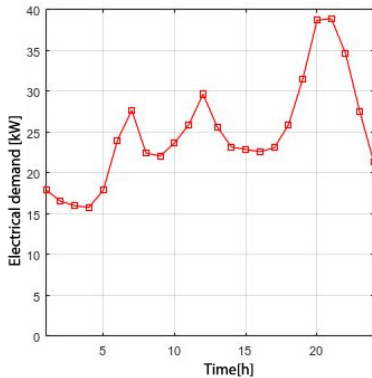
Furthermore, the remaining input units described in Figure 2 correspond to the BESS (Battery Energy Storage System) power, consisting of a total of 165 batteries that will be charged with electrical energy by the solar generation unit. Table 2 displays the technical features of the battery utilized, a RELION lithium-ion battery [29] selected due its deep cycle features, providing a depth of discharge of 42% with a life cycle of 2500 cycles. In addition, based on the battery parameters and specifications, the BESS operating cost and its efficiencies in both charge and discharge modes were obtained.

Table 2. Battery manufacturer's data [29]

Model	RELION BATTERY RB100T		
Nominal voltage	12.8 V	Nominal capacity	100 Ah
Charge voltage	13.5 V	Charge current	5 A - 50 A
Maximum charge current	280 A + 50 A (32+10 ms)	Cut-off voltage	14.2 V - 14.6 V
Operation temperature	Discharge: -20 °C a + 60 °C Charge: -20 °C a + 45 °C		
Life cycle	2500 cycles (42%DOD)		
	3500 cycles (20%DOD)		

The diesel power belongs to the generating set; in this case, this corresponds to a diesel generator that requires a quantity of fossil fuel for its operation. The hourly consumption ratio is limited by the power output of the diesel generator. For this purpose, a quadratic equation has been established, derived from a second-order polynomial nonlinear approximation due to its similarity with the real behavior of the generating set. The amount of fuel as a function of the power delivered by the diesel generator is defined in equation (7); furthermore, equation (4) bounds the diesel power consumption between a maximum and minimum value established by the manufacturer.

On the other hand, the electrical demand has been obtained from a load study of a real household in Santa Cruz Island, part of the Galápagos Province in Ecuador. The electrical demand data used as input for the economic dispatch, is depicted in Figure 6 for a 24-hour interval, where a maximum consumption value of 40 kW can be identified. At last, the outputs of the economic dispatch establish the technological mix for proper system operation based on the BESS power in charge/discharge mode, diesel generator power, power spillage and unsupplied energy.

**Figure 6.** Electric demand

2.2. Mixed-integer nonlinear optimization problem

Building upon the mixed-integer linear programming (MILP) optimization problem demonstrated in [30], a mixed-integer nonlinear programming (MINLP) model has been established, which proposes the use of a quadratic function consistent with the real behavior of

the diesel generator curve. This model aims to minimize the operating costs within the optimization problem, while ensuring the supply of electrical demand for an isolated microgrid. The proposed optimization model is described below.

2.2.1. Objective function

From the optimization problem stated in [30], it may be established the objective function shown in equation (1), which seeks to minimize the operating cost of an isolated microgrid in a time interval of 168 hours (one week).

$$J = \text{Min} \sum_{t=1}^T \left(C_D Q_{dt} + C_{ENS} P_{ENS_t} + C_{SH} P_{SH_t} + (CU_{BESS}) \left(P_{B_t}^C \eta^C + \frac{P_{B_t}^D}{\eta^D} \right) \right) \quad (1)$$

Where C_D represents the diesel generation cost, Q_{dt} quantifies the amount of fuel based on the power established by the diesel generator, C_{ENS} identifies the cost of the unsupplied energy, P_{ENS_t} represents the unsupplied energy, C_{SH} is the cost attributed to power spillage, P_{SH_t} represents the power spillage.

On the other hand, CU_{BESS} is the cost of using the battery bank system (BESS), which is calculated by means of equation (2) from the investment cost of the BESS (CI_{BESS}), the maximum energy that the BESS may deliver (E_{max}) and the number of cycles (N_{cycles}) of the BESS life span. η^C and η^D represent the charge and discharge efficiency of the BESS according to its mode of use. At last, $P_{B_t}^C$ y $P_{B_t}^D$ identify the charge and discharge power, respectively.

$$CU_{BESS} = \frac{CI_{BESS}}{E_{max} \cdot N_{ciclos}} \quad (2)$$

2.2.2. Constraints

The objective function involves various constraints that ensure a proper solution of the optimization problem. For instance, the power balance is depicted in equation (3).

$$P_{D_t} + P_{S_t} + P_{W_t} - P_{SH_t} + P_{B_t}^D = D_t - P_{ENS_t} + P_{B_t}^C \quad (3)$$

The bounds of the objective function are presented in equation (4), which delimits the power of the diesel generator, equation (5), which restricts the unsupplied energy, and equation (6), which constrains the spillage power.

$$P_{D_{min}} \leq P_{D_t} \leq P_{D_{max}} \quad (4)$$

$$0 \leq P_{ENS_t} \leq D_t \quad (5)$$

$$0 \leq P_{SH_t} \leq P_{S_t} + P_{W_t} \quad (6)$$

Equation (7) defines the quadratic function responsible for controlling the diesel generator, where the coefficients (a, b, c) are determined through the analysis of the real behavior of the diesel generator.

$$Q_{D_t} = aP_{D_t}^2 + bP_{D_t} + c \quad (7)$$

Equation (8) establishes the initial conditions of the BESS to obtain preliminary energy information, while equation (9) enables to calculate the BESS energy for $t > 0$. Equation (10) constrains the BESS energy.

$$E_t = E_0 + (P_{B_t}^C * \eta^C) - \left(\frac{P_{B_t}^D}{\eta^D} \right) \quad (8)$$

$$E_t = E_{t-1} + (P_{B_t}^C * \eta^C) - \left(\frac{P_{B_t}^D}{\eta^D} \right) \quad (9)$$

$$E_{min} \leq E_t \leq E_{max} \quad (10)$$

The use of binary variables is represented in equations (11), (12) and (13), which will enable to know the state of the BESS in any of its two modes of use: charge/discharge. It is important to clarify that the BESS can only operate in one mode of use at a time.

$$X_t^C + X_t^D \leq 1 \quad (11)$$

$$E_{min} \geq P_{B_t}^C \geq -E_{max} * X_t^C \quad (12)$$

$$E_{min} \leq P_{B_t}^D \leq E_{max} * X_t^D \quad (13)$$

The state of charge (SOC) of the BESS may be obtained through equation (14), where E_t is the current energy and E_{max} is the maximum energy. This equation is constrained by equation (15), where the range of the SOC has been established as (100-0)%.

$$SOC_t = \frac{E_t}{E_{max}} \quad (14)$$

$$SOC_{min} \leq SOC_t \leq SOC_{max} \quad (15)$$

2.3. Response of the economic dispatch

The methodology used to solve the optimization problem is shown in Figure 7, which depicts the flow diagram for the validation of the economic dispatch. Initially, the input data for the optimization problem must be entered, including electrical demand, solar and wind power, BESS data, and diesel generator power for every hour.

Next, it is sought to solve the mixed-integer non-linear optimization problem (MINLP) using specific software; in this case, the FICO XPRESS OPTIMIZATION SUITE [31] has been used due to its ease for generating and interpreting the results. It is necessary to validate the economic dispatch response under, at least, three usage criteria: achieving the minimization of the objective function costs, ensuring compliance of all constraints, and eliminating the intermitencies produced by the generating set.

If the economic dispatch response is unsatisfactory, the optimization model should be adjusted to correct its functioning. On the other hand, if the economic dispatch response is satisfactory, the results from the specialized software can be exported, interpreted and plotted.

Finally, this procedure has been used for all case studies proposed in this research work. Merely by altering the runtime of the optimization problem, results for the economic dispatch may be obtained for 24, 48, and 168 hours.

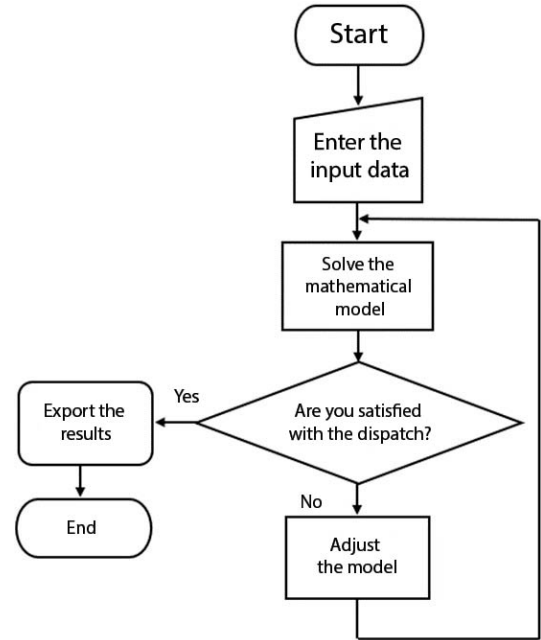


Figure 7. Flow diagram of the economic dispatch

3. Results and discussion

This section presents the parameters of the isolated microgrid used as a case study for the proposed economic dispatch problem. Figure 8 depicts a didactic scheme that illustrates the operation of the microgrid utilized in this research work, considering dispatchable and non-dispatchable generation units aimed at supplying the demand continuously.

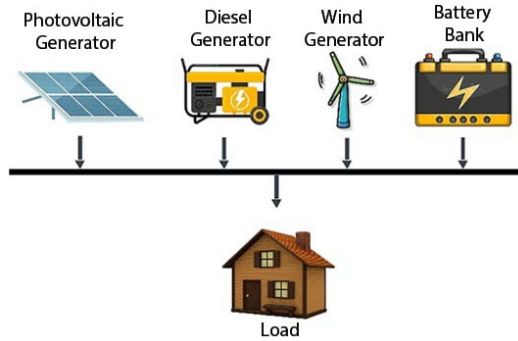


Figure 8. Diagram of the isolated microgrid based on ERNC

Table 3 displays the bounds of the different generation units used in the proposed economic dispatch, including the bounds of the power demanded by the isolated microgrid. Table 4 presents the parameters used to model the Battery Energy Storage System (BESS), highlighting the efficiencies in charge/discharge mode, the degradation percentage, and the state of charge bounds. Table 5 shows the operating costs used in the optimization problem, such as the BESS investment cost obtained from the total cost of the battery bank, the BESS usage cost calculated using equation (2) and the diesel operation cost defined from [32]. Finally, the spillage energy cost corresponds to 10% of the diesel inherent value, and the unsupplied energy cost is set as 5 times the diesel cost.

Table 3. Installed capacity and power demanded by the microgrid

Element	P_min (kW)	P_max (kW)
BESS	0	211
Diesel generator	10	40
Solar generator	0	135
Wind generator	0	1.2
Demand	15.19	41.4

Table 4. BESS parameters

Name	Variable	Valor	Unidad
Maximum nominal energy	E_{max}	211	kWh
Life time	N_{ciclos}	2500	Ciclos
Percentage degradation	% degradación	80	%
Discharge efficiency	η_D	88	%
Charge efficiency	η_C	85	%
Minimum state of charge	SOC_{min}	0	%
Maximum state of charge	SOC_{max}	100	%

Table 5. Operating costs

Name	Variable	Value	Unit
BESS investment cost	CIBESS	189750	USD
BESS usage cost	CUBESS	0.36	USD/ciclo
Diesel operating cost	CD	1.25	USD/litro
Unsupplied energy cost	CENS	6.25	USD/kW
Spillage energy cost	CESH	1.37	USD

3.1. Response of the economic dispatch

Figure 9 illustrates the performance of the different electrical energy sources that entirely supply the energy demand over a 24-hour interval, with a contribution of 56.50% from solar power, 4.23% from wind power, 17.23% from the battery bank, and 21.96% from the diesel generator, fulfilling the entire electrical demand.

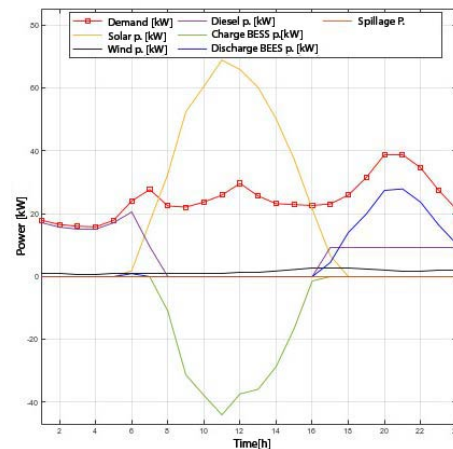


Figure 9. Economic dispatch for 24 hours

Figure 10 depicts the economic dispatch behavior over 48 hours, which exhibits slight differences compared to the economic dispatch response over 24 hours in terms of the technological mix. In this case, the entire electrical demand is also met with 0% unsupplied energy, where solar power contributes 56.88%, wind power 4.81%, the diesel generator 19.20% and the battery bank 19.11%.

Figure 11 displays the results obtained when solving the economic dispatch problem for a time period of 168 hours (one week), highlighting a harmonious interaction across all days of the proposed week. It evidences slight differences compared to the previous two study cases, with solar power contributing 50.40% to the electrical demand, wind power 5.53%, the diesel generator 23.92% and the battery bank 17.14%.

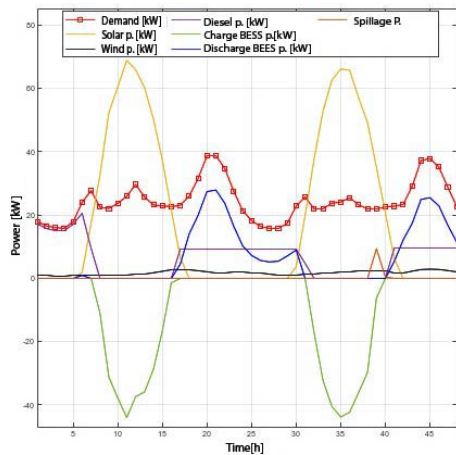


Figure 10. Economic dispatch for 48 hours

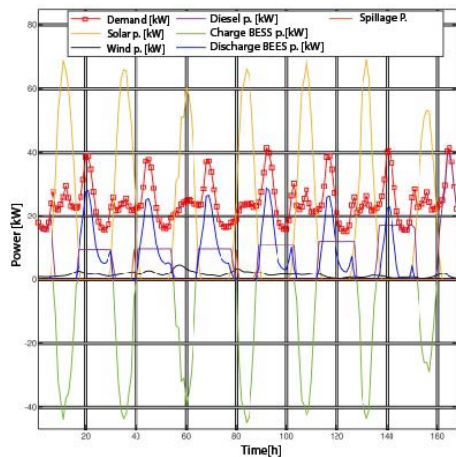


Figure 11. Economic dispatch for 168 hours (1 week)

In addition, the previous graphs show that the diesel generator maintains a continuous ignition point due to the modeling used in the proposed optimization problem. The incorporation of the generator through a quadratic equation eliminates its intermitencies, resulting in continuous on/off moments along time. This occurred for all three proposed study cases of 24, 48 and 168 hours.

3.2. Discussion of the economic dispatch

A discussion of the results obtained for the three case studies shown in Figures 9, 10 and 11 is now presented.

For instance, in response to the 24-hour economic dispatch simulation (Figure 9), it is evident that in the early hours of the day, the electrical demand is entirely supplied by the diesel generator, with minimal contribution from the wind generator. From 6:00 AM, the solar generator begins its operation, gradually taking over the electrical demand until it exceeds the demand value. At this point, the surplus energy is stored by the battery bank, which switches to charging mode.

From 4:00 PM onwards, the diesel generator comes into operation, supported by the battery bank in discharge mode and minimally by the wind generator, successfully supplying the remaining hours of the day until reaching 12:00 AM.

Figure 10 displays a behavior similar to the first day, with slight variations in the hours of interaction among different energy sources due to the unpredictable nature of the Unconventional Renewable Energy (URE) Sources. It is worth noting that the power of the Battery Energy Storage System (BESS) in the charging state represents an electrical energy consumption, thus becoming part of the demand. The batteries store energy when they are discharged and supply energy when they reach their maximum charge; in this case, they achieve 100% state of charge (SOC).

Finally, in Figure 11 a satisfactory supply of electrical demand is analyzed. There is a recurrence in the behavior of energy sources, displaying a pattern especially noticeable in the diesel generator, which maintains intervals of complete shutdown during certain hours of the day, reducing operating costs and continually supporting the Battery Energy Storage System (BESS). It is important to note that the wind power maintains a constant, albeit minimal, continuous energy contribution due to the climatic conditions of the isolated microgrid, with slight fluctuations. Despite these fluctuations, it continues to provide electrical energy 24 hours a day throughout the entire week under analysis.

On the other hand, Figure 12 illustrates the BESS usage cycle, which relates the power in charge/discharge mode with the BESS state of charge, following a positive (charge) and negative (discharge) cycle within a 24-hour interval. The BESS reaches its maximum energy charge around 2:00 PM due to the available solar resources, enabling it to cover the demand and charge the BESS. Meanwhile, from 6:00 PM, it begins to discharge, reaching complete discharge around 12:00 AM.

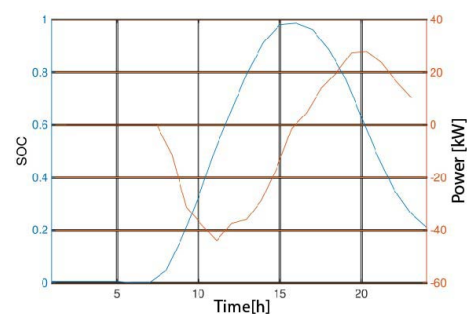


Figure 12. BESS usage cycle in 24 hours

Figure 13 depicts the BESS usage cycle over a 48-hour interval, demonstrating the similarities between the curves. This similarity arises from the energy supplied by the solar generator, which provides different

daily peaks of charge and discharge every day.

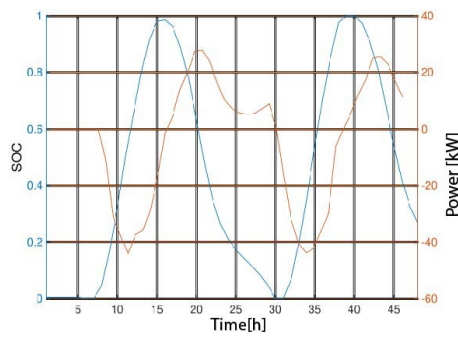


Figure 13. BESS usage cycle in 48 hours

Finally, Figure 14 illustrates the BESS usage cycle over 168 hours, demonstrating a cyclic process throughout the entire week. It is evident that the battery bank achieves maximum charges of 100% SOC and complete discharges to 0% SOC, which validates its operation within the proposed economic dispatch problem. Thus, it may be concluded that the BESS contributes continuously and efficiently to the electrical demand.

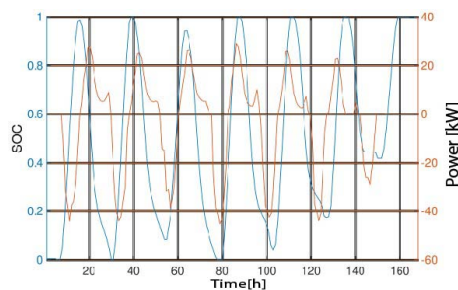


Figure 14. BESS usage cycle in 168 hours

4. Conclusions

The present research work presents the assessment of an economic dispatch problem through a mixed-integer nonlinear programming optimization model, which incorporates the modeling of the actual behavior of the diesel generator as a second-degree polynomial equation.

The input data for the economic dispatch were obtained from Santa Cruz Island in the Galápagos Province, Ecuador. Solar irradiation and wind speed values were identified using the NASA web platform, while the electrical demand data correspond to real data from the actual location. In addition, a battery bank and a diesel generator were dimensioned to meet the demand of the region in case of unconventional renewable energy deficiency.

The economic dispatch results were obtained for 24, 48, and 168 hours at an hourly resolution, showing the contribution of all generation units to meet the

demand proportionally: solar generator 54.40%, BESS 17.14%, diesel generator 23.92% and wind generator 4.43%.

The intermittent behavior of the generating set was effectively controlled, limiting the operation of the diesel generator to a maximum of 8 hours, while simultaneously achieving minimization of operating costs and meeting the entire electrical demand.

Finally, as future work it is proposed to incorporate the uncertainty of the input data into the economic dispatch problem, to obtain a stochastic optimization problem. In addition, it could be also carried out a comparison between the response of the mixed-integer nonlinear economic dispatch and a mixed-integer linear economic dispatch, which includes modeling the generating set using piecewise linearization.

Acknowledgement

The authors thank the “Academic Partner Program” (APP) of the FICO Xpress Optimization Suite, for making available their academic licenses to carry out undergraduate and graduate research works.

References

- [1] J. D. Jiménez, S. M. Vives, E. G. Jiménez, and A. P. Mendoza, “Development of a methodology for planning and design of microgrids for rural electrification,” in *2017 CHILEAN Conference on Electrical, Electronics Engineering, Information and Communication Technologies (CHILECON)*, 2017. [Online]. Available: <https://doi.org/10.1109/CHILECON.2017.8229558>
- [2] X. Liu, X. Li, J. Tian, Y. Wang, G. Xiao, and P. Wang, “Day-ahead economic dispatch of renewable energy system considering wind and photovoltaic predicted output,” *International Transactions on Electrical Energy Systems*, vol. 2022, p. 6082642, Jun 2022. [Online]. Available: <https://doi.org/10.1155/2022/6082642>
- [3] H. Hou, Q. Wang, Z. Xiao, M. Xue, Y. Wu, X. Deng, and C. Xie, “Data-driven economic dispatch for islanded micro-grid considering uncertainty and demand response,” *International Journal of Electrical Power & Energy Systems*, vol. 136, p. 107623, 2022. [Online]. Available: <https://doi.org/10.1016/j.ijepes.2021.107623>
- [4] G. S. Thirunavukkarasu, M. Seyedmahmoudian, E. Jamei, B. Horan, S. Mekhilef, and A. Stojcevski, “Role of optimization techniques in microgrid energy management systems - A review,” *Energy Strategy Reviews*, vol. 43, p. 100899, 2022. [Online]. Available: <https://doi.org/10.1016/j.esr.2022.100899>

- [5] R. Palma-Behnke, C. Benavides, E. Aranda, J. Llanos, and D. Sáez, “Energy management system for a renewable based microgrid with a demand side management mechanism,” in *2011 IEEE Symposium on Computational Intelligence Applications In Smart Grid (CIASG)*, 2011. [Online]. Available: <https://doi.org/10.1109/CIASG.2011.5953338>
- [6] H. Apolo, D. Arcentales, and K. Escobar Segovia, “Santa Cruz, Galapagos Electricity sector towards a zero fossil fuel island,” in *17th LACCEI International Multi-Conference for Engineering, Education, and Technology*, 01 2019. [Online]. Available: <http://dx.doi.org/10.18687/LACCEI2019.1.1.170>
- [7] B. Dey, B. Bhattacharyya, and F. P. G. Márquez, “A hybrid optimization-based approach to solve environment constrained economic dispatch problem on microgrid system,” *Journal of Cleaner Production*, vol. 307, p. 127196, 2021. [Online]. Available: <https://doi.org/10.1016/j.jclepro.2021.127196>
- [8] A. B. Kunya, A. S. Abubakar, and S. S. Yusuf, “Review of economic dispatch in multi-area power system: State-of-the-art and future prospective,” *Electric Power Systems Research*, vol. 217, p. 109089, 2023. [Online]. Available: <https://doi.org/10.1016/j.epsr.2022.109089>
- [9] L. Tipán and O. Vargas, “Despacho económico de sistemas de energía en áreas múltiples usando programación de flujo de red,” *Energía*, vol. 19, no. 2, pp. 42–57, 2023. [Online]. Available: <https://doi.org/10.37116/revistaenergia.v19.n2.2023.540>
- [10] E. M. García Torres, “Estimated cost of electricity with time horizon for micro grids based on the policy response of demand for real price of energy,” *Enfoque UTE*, vol. 11, no. 1, pp. 41–55, Jan. 2020. [Online]. Available: <https://doi.org/10.29019/enfoque.v11n1.579>
- [11] W. Gil-González, O. D. Montoya, L. F. Grisales-Noreña, F. Cruz-Peragón, and G. Alcalá, “Economic dispatch of renewable generators and BESS in DC microgrids using second-order cone optimization,” *Energies*, vol. 13, no. 7, 2020. [Online]. Available: <https://doi.org/10.3390/en13071703>
- [12] B. Xu, Y. Zhang, J. Liu, X. Miao, X. Zhang, Z. Zhu, and Z. Wang, “Economic dispatch of micro-grid based on sequential quadratic programming—model and formulation,” *E3S Web Conf.*, vol. 136, p. 01010, 2019. [Online]. Available: <https://doi.org/10.1051/e3sconf/201913601010>
- [13] H. Minor-Popocatl, O. Aguilar-Mejía, F. D. Santillán-Lemus, A. Valderrabano-González, and R.-I. Samper-Torres, “Economic dispatch in microgrids with alternative energy sources and batteries,” *IEEE Latin America Transactions*, vol. 21, no. 1, pp. 124–132, 2023. [Online]. Available: <https://doi.org/10.1109/TLA.2023.10015134>
- [14] L. Zhu, H. Ren, M. Habibi, K. J. Mohammed, and M. A. Khadimallah, “Predicting the environmental economic dispatch problem for reducing waste nonrenewable materials via an innovative constraint multi-objective chimp optimization algorithm,” *Journal of Cleaner Production*, vol. 365, p. 132697, 2022. [Online]. Available: <https://doi.org/10.1016/j.jclepro.2022.132697>
- [15] Y. Duan, Y. Zhao, and J. Hu, “An initialization-free distributed algorithm for dynamic economic dispatch problems in microgrid: Modeling, optimization and analysis,” *Sustainable Energy, Grids and Networks*, vol. 34, p. 101004, 2023. [Online]. Available: <https://doi.org/10.1016/j.segan.2023.101004>
- [16] P. Arévalo, A. A. Eras-Almeida, A. Cano, F. Jurado, and M. A. Egido-Aguilera, “Planning of electrical energy for the Galapagos Islands using different renewable energy technologies,” *Electric Power Systems Research*, vol. 203, p. 107660, 2022. [Online]. Available: <https://doi.org/10.1016/j.epsr.2021.107660>
- [17] F. D. Santillán-Lemus, H. Minor-Popocatl, O. Aguilar-Mejía, and R. Tapia-Olvera, “Optimal economic dispatch in microgrids with renewable energy sources,” *Energies*, vol. 12, no. 1, 2019. [Online]. Available: <https://doi.org/10.3390/en12010181>
- [18] S. Al-Sakkaf, M. Kassas, M. Khalid, and M. A. Abido, “An energy management system for residential autonomous dc microgrid using optimized fuzzy logic controller considering economic dispatch,” *Energies*, vol. 12, no. 8, 2019. [Online]. Available: <https://doi.org/10.3390/en12081457>
- [19] M. T. Guneser, A. Elbaz, and C. Seker, *Hybrid Optimization Methods Application on Sizing and Solving the Economic Dispatch Problems of Hybrid Renewable Power Systems*, ser. Applications of Nature-Inspired Computing in Renewable Energy Systems. Hershey, PA, USA: IGI Global, 2022, pp. 136–165. [Online]. Available: <https://doi.org/10.4018/978-1-7998-8561-0.ch008>
- [20] E. López-Garza, R. F. Domínguez-Cruz, F. Martell-Chávez, and I. Salgado-Tránsito, “Fuzzy logic and linear programming-based power grid-enhanced economical dispatch for sustainable and stable grid operation in eastern Mexico,”

- Energies*, vol. 15, no. 11, 2022. [Online]. Available: <https://doi.org/10.3390/en15114069>
- [21] H. Xu, Z. Meng, and Y. Wang, “Economic dispatching of microgrid considering renewable energy uncertainty and demand side response,” *Energy Reports*, vol. 6, pp. 196–204, 2020, 2020 The 7th International Conference on Power and Energy Systems Engineering. [Online]. Available: <https://doi.org/10.1016/j.egy.2020.11.261>
- [22] L. Jian, Z. Qian, Z. Liangang, and Y. Mengkai, “Distributed economic dispatch method for power system based on consensus,” *IET Renewable Power Generation*, vol. 14, no. 9, pp. 1424–1432, 2020. [Online]. Available: <https://doi.org/10.1049/iet-rpg.2019.1085>
- [23] K. Chen, Z. Zhu, and J. Wang, “Economic dispatch for smart buildings with load demand of high volatility based on quasi-quadratic online adaptive dynamic programming,” *Mathematics*, vol. 10, no. 24, 2022. [Online]. Available: <https://doi.org/10.3390/math10244701>
- [24] F. Xu, X. Zhang, X. Ma, X. Mao, Z. Lu, L. Wang, and L. Zhu, “Economic dispatch of microgrid based on load prediction of back propagation neural network-local mean decomposition-long short-term memory,” *Electronics*, vol. 11, no. 14, 2022. [Online]. Available: <https://doi.org/10.3390/electronics11142202>
- [25] J. L. Proaño, D. O. Villalba, D. Sáez, and D. O. Quero, “Economic dispatch for optimal management of isolated microgrids,” in *2016 IEEE 36th Central American and Panama Convention (CONCAPAN XXXVI)*, 2016. [Online]. Available: <https://doi.org/10.1109/CONCAPAN.2016.7942382>
- [26] C. Bai, Q. Li, W. Zhou, B. Li, and L. Zhang, “Fast distributed gradient descent method for economic dispatch of microgrids via upper bounds of second derivatives,” *Energy Reports*, vol. 8, pp. 1051–1060, 2022, 2022 The 5th International Conference on Electrical Engineering and Green Energy. [Online]. Available: <https://doi.org/10.1016/j.egy.2022.08.110>
- [27] F. Ordóñez and D. Vaca, *Mapa solar del Ecuador*. Escuela Politécnica Nacional, 2020. [Online]. Available: <https://bit.ly/3RArzjc>
- [28] NASA. (2023) Welcome to the power data access viewer. NASA prediction of worldwide Energy Resources. The Power Project. NASA prediction of worldwide Energy Resources. The Power Project. [Online]. Available: <https://bit.ly/48nVUID>
- [29] RELION. (2023) Find the right LiFePO4 battery for your application. RELiON Batteries. RELiON Batteries. [Online]. Available: <https://bit.ly/3NZqaSz>
- [30] D. Jiménez, A. Jaya, D. Lagla, C. Chasi, R. Salazar, A, and P. Zurita, “An optimization model assessment for the economic dispatch of isolated microgrids,” in *2022 IEEE Sixth Ecuador Technical Chapters Meeting (ETCM)*, 2022. [Online]. Available: <https://doi.org/10.1109/ETCM56276.2022.9935730>
- [31] FICO. (2023) Applied intelligence – powering your customer connections. FICO. FICO.
- [32] GlobalPetrolPrices. (2023) Precios de gasolina internacional. GlobalPetrolPrices. GlobalPetrolPrices. [Online]. Available: <https://bit.ly/3Rps53m>



ELECTRIC SUBSTATION INSPECTION: YOLOv5 IN HOTSPOT DETECTION THROUGH THERMAL IMAGING

INSPECCIÓN DE SUBESTACIONES ELÉCTRICAS: YOLOv5 EN LA IDENTIFICACIÓN DE PUNTOS CALIENTES MEDIANTE IMÁGENES TÉRMICAS

Daniel A. Pérez-Aguilar^{1,*}, Jair M. Pérez-Aguilar¹,
Andy P. Pérez-Aguilar¹, Redy H. Risco-Ramos²,
Manuel E. Malpica-Rodríguez³

Received: 11-10-2023, Received after review: 27-11-2023, Accepted: 30-11-2023, Published: 01-01-2024

Abstract

Substations are key facilities within an electrical system, untimely failures tend to cause low quality and negative effects on the electrical supply. An early indicator of potential electrical equipment failure is the appearance of hot spots; therefore, its detection and subsequent programmed correction avoids incurring in major failures and unnecessary operation stops. In this research, 64 experiments of the YOLOv5 algorithm were carried out, with the purpose of proposing an automated computer vision mechanism for the detection of hot spots in thermal images of electrical substations. The best results show a mAP value of 81.99 %, which were obtained with the YOLOv5m algorithm and the transfer learning application. These results leave a basis to deepen and improve the performance of the algorithm by varying other hyperparameters to those considered in this study.

Keywords: Electrical substations, Hot spots, Object detection, Thermal images, Transfer learning, YOLOv5

Resumen

Las subestaciones son instalaciones clave dentro de un sistema eléctrico; las fallas intempestivas tienden a causar baja calidad y efectos negativos del suministro eléctrico. Un indicador temprano de posibles fallas en los equipos eléctricos es la aparición de puntos calientes; por lo que su detección y posterior corrección programada evita incurrir en fallas mayores y paradas de operación innecesarias. En esta investigación se realizaron 64 experimentos del algoritmo YOLOv5, con la finalidad de proponer un mecanismo automatizado de visión por computadora para la detección de puntos calientes en imágenes térmicas de subestaciones eléctricas. Los mejores resultados muestran un valor mAP de 81,99 %, los cuales se obtuvieron con el algoritmo YOLOv5m y la aplicación de transfer learning. Estos resultados dejan una base para profundizar y mejorar el desempeño del algoritmo, variando otros hiperparámetros a los considerados en el presente estudio.

Palabras clave: aprendizaje por transferencia, detección de objetos, imágenes térmicas, puntos calientes, subestaciones eléctricas, YOLOv5

^{1,*}Facultad de Ingeniería, Universidad Tecnológica del Perú, Perú. Corresponding author ✉: daniel.perez@upn.pe.

²Facultad de Ingeniería, Universidad de Piura, Perú

³Facultad de Ingeniería, Universidad Privada del Norte, Perú

Suggested citation: Pérez-Aguilar, D.A.; Pérez-Aguilar, J.M.; Pérez-Aguilar, A.P.; Risco-Ramos, R. H. and Malpica-Rodríguez, M.E. "Electric substation inspection: YOLOv5 in hotspot detection through thermal imaging," *Ingenius, Revista de Ciencia y Tecnología*, N.º 31, pp. 43-54, 2024, DOI: <https://doi.org/10.17163/ings.n31.2024.04>.

1. Introduction

Electric substations are facilities composed of equipment necessary for voltage, frequency, phase quantity transformations, or circuit connections. This type of equipment is often situated near power generation plants or in non-urban areas [1, 2]. Ensuring the adequate quality of the electrical supply mandates that these pieces of equipment remain operational for most of their lifespan [3, 4]. It is customary for faults in electric substations to be anticipated by the emergence of what specialists refer to as hotspots. These elements exhibit a temperature above their regular operation compared to other equipment with similar characteristics and operating conditions [5].

Hotspots usually arise due to an increase in electrical resistance in a circuit, resulting from various factors such as dirt, false contacts, overcurrents, load imbalances, and insulation loss, among others. These hotspots are not visible to the naked eye, so their detection requires specialized techniques such as infrared thermography. However, the analysis must be carried out manually by an expert or specialist in the field, involving a significant time investment and the risk of human errors in the diagnosis [6].

This non-invasive technique is employed for measuring the temperature of various objects without the need for direct physical contact. To perform this measurement, the infrared radiation from the electromagnetic spectrum is captured using thermal cameras, which generate images in the infrared spectrum [7].

Artificial Intelligence (AI) is a discipline that has had a significant technological impact in recent years and is being applied in various sectors, including the electrical field [8]. The combination of thermography and AI techniques encompasses a wide range of applications, such as predictive maintenance in industrial environments, assessment of built structures, identification of energy losses, detection of thermal bridges, location of gas emissions, identification of areas with elevated temperatures, medical research, weather forecasting, military applications, among others [9].

Object detection is a crucial aspect of artificial intelligence and computer vision, aiming to identify one or multiple objects in images or videos. Within the domain of object detection, algorithms are broadly categorized into two primary groups: (i) Manual extraction (handcrafted features) and (ii) Automatic extraction (based on deep learning). The latter category is subdivided into one-stage and two-stage object detection algorithms, with the former achieving detections in less time (See Figure 1) [10].

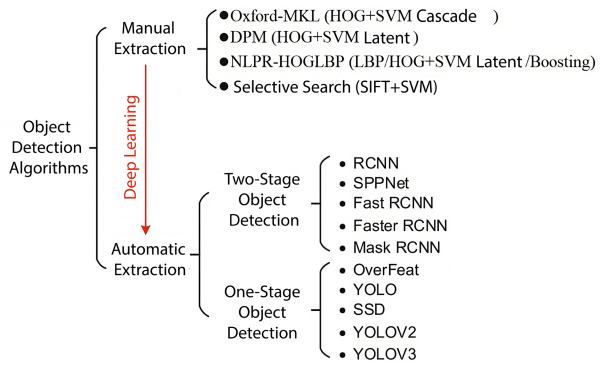


Figure 1. Object detection algorithms [11]

YOLO, an acronym for "You Only Look Once," stands out as a prominent object detection algorithm, particularly notable for its real-time detection and recognition of multiple objects. In contrast to alternative algorithms like SSD or Faster R-CNN, YOLO approaches detection as a regression problem, delivering probabilities linked to each identified class within a single algorithmic execution. The distinctive strengths of YOLO encompass its (i) rapid processing speed, facilitating real-time detection; (ii) exceptional accuracy attributed to a notably low error rate; and (iii) noteworthy learning capacity [12].

YOLOv5, the fifth iteration of the YOLO algorithm, is presented as a one-stage object detector, emerging as one of the most viable options for real-time object detection (FPS) [13]. Figure 2 illustrates the architecture of YOLOv5, unveiling the algorithm's custom layers, predominantly composed of convolutions and max-pooling. Additionally, the pseudocode for YOLOv5 is provided in Figure 3.

Mathematically (see equation (1)), the model predicts the coordinates b_x, b_y, b_w, b_h of bounding boxes and the confidence C , indicating the presence of an object in each cell of an $S \times S$ grid. Each cell is responsible for detecting the objects within it. These predictions are derived by applying a sigmoid function (σ) to the output of a neural network, where W represents the neural network's weights, $f(x)$ is the input, and b is the bias. The model generates these predictions for B boxes, enabling it to detect multiple objects in a single pass, rendering it efficient for real-time detection. YOLOv5 primarily incorporates three techniques: (i) the use of residual blocks, (ii) bounding box regression, and (iii) intersection over union (IOU) [14]. Figure 4 illustrates the results of the combination of these three techniques.

$$B \cdot (b_x, b_y, b_w, b_h, C) = \sigma(W \cdot f(x) + b) \quad (1)$$

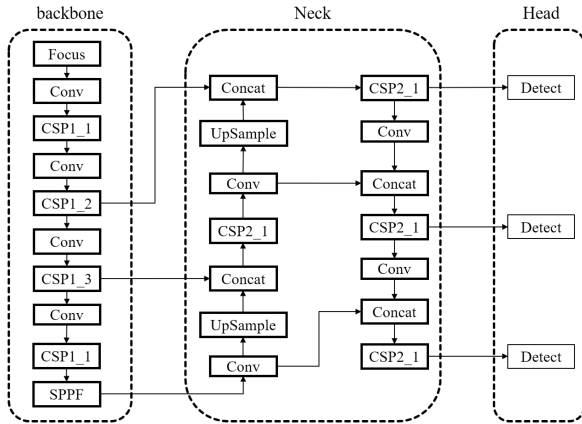


Figure 2. Architecture of YOLOv5 [15]

Pseudocode - YOLOv5	
Input:	Number class; Class name;
1.	Load images and pre-process data
2.	Define the model architecture
3.	- Backbone network (e.g., CSPNet, GAMMAttention, SPPFCSPC)
4.	- Neck network (e.g., YOLOv5Neck)
5.	- Detection head (e.g., YOLOv5Head)
6.	- Loss function (e.g., Focal Loss)
7.	Train the model
8.	- Compute loss on mini-batch of images
9.	- Compute gradients and update weights using optimizer (e.g., Adam)
10.	Prediction
11.	- Apply non-maximum suppression to remove overlapping predictions
12.	- Output final detection results (bounding boxes, class probabilities, confidence scores)

Figure 3. Pseudocode - YOLOv5 [15]

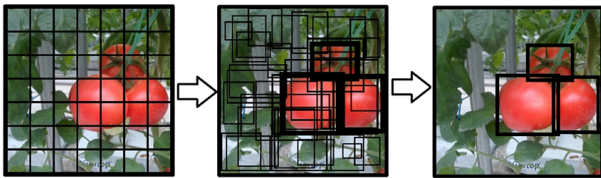


Figure 4. YOLOv5 – Combination of techniques [14]

Here is a compilation of prior research and studies related to this topic.

To ensure the integrity of electrical power systems, an investigation was carried out employing a convolutional neural network (CNN) based on the YOLO object detection algorithm. Predictions were made concerning the coordinates, orientation angle, and classification of each equipment component. Experimental results suggest that this approach is resilient to noise, attaining an accuracy level of 93.7% by using a graphics processing unit (GPU) during the training phase [16].

Power equipment is a crucial energy system component, constituting the focal point of operation and maintenance. According to Li [17], infrared anomaly detection technology is an effective method for identifying faults in electrical equipment due to its safety, simplicity, and intuitiveness. The implementation of YOLOv3 was proposed using a set of infrared images collected in the field, achieving an mAP (Mean Average Precision) value of 34.63% and a recovery rate of 21%.

Greco et al. [18] point out that faults commonly appear as hotspots on the surface of photovoltaic panels. Consequently, they conducted an investigation focused on hotspot detection using YOLO. The study demonstrated that this algorithm can segment panels in an image efficiently. A quantitative evaluation was carried out, including a comparison with previously established approaches for photovoltaic panel detection. The experimental results obtained affirmed the robustness and effectiveness of YOLO.

The use of CNN demands high computational and memory capacity. Nguyen et al. [19] proposed an object detection method based on a CNN and YOLO, considering the PASCAL VOC labeling format. The model achieved an mAP value of 64.16%.

A comparative study of three object detection algorithms in images [12] revealed that (i) Single Shot Detector or SSD [20] performs poorly in detecting small objects compared to Faster R-CNN. SSD has the disadvantage of requiring an extensive dataset and data augmentation techniques for training, which is computationally expensive and increases the execution time. (ii) Faster R-CNN [21] is more accurate, but its algorithmic complexity involves a prolonged training time. Additionally, Faster R-CNN is considerably slower than YOLO and requires analyzing each image multiple times, unlike YOLO. Finally, (iii) YOLO [22] stands out for its optimized and efficient model compared to SSD and Faster R-CNN. The latest versions of the algorithm offer low latency and improvements in training and execution time. YOLO also allows real-time operation and better accuracy, especially when employing transfer learning techniques [23].

Regarding traditional object detection techniques, some of the most commonly used include K-means clustering, support vector machines, fuzzy systems, and Histograms of Oriented Gradients (HOG), among others [24], which have demonstrated precision levels exceeding 80%. However, the primary purpose of this article is not to delve into traditional techniques but to provide alternatives based on modern and specific algorithms for object detection, such as YOLOv5. Nevertheless, Table 1 (compiled from [24–26]) presents a comparison between traditional techniques and YOLOv5, highlighting the superiority of YOLOv5 in key aspects for object detection.

Table 1. Comparison between YOLOv5 and traditional techniques

Characteristic	Traditional techniques	YOLOv5
Precision	Variable and dependent on the quality of manual features or specific parameters.	High precision, especially in real-time detection of multiple objects of different sizes.
Handling object overlap	Challenges may arise when dealing with object overlap.	Effective handling of object overlap due to its ability to predict multiple bounding boxes.
Adaptability to different object sizes	Manual adjustments are required to adapt to different object sizes.	Scalable and can adapt to objects of different sizes.
Generalization capacity	Lower generalization capacity to new situations without manual adjustments.	Ability to generalize patterns and features automatically in different scenarios.
End-to-End training	The training process is more complex, involving multiple stages and adjustments.	End-to-end training facilitates implementation and reduces the need for manual intermediate stages.
Real-time performance	Variable performance. It can be slow, depending on the technique and the number of manual features.	Designed explicitly for achieving real-time detection, making it efficient for practical applications.
Handling large datasets	Some traditional techniques may have limitations when handling large datasets.	Efficient handling of large datasets, leveraging the GPU's capability to accelerate operations.

It is worth mentioning that YOLO has various applications; however, according to the literature analysis, these techniques have not been employed to identify hotspots in thermal images of electrical substations, representing an innovative approach. Therefore, this study is a continuation of an investigation previously published by the authors in this prestigious journal [27]. The aim is to examine the performance of four versions of the YOLOv5 algorithm by conducting 64 experiments applied to hotspot detection. To achieve this, a set of thermal images from electrical substations captured by an energy distribution company in northern Peru is employed.

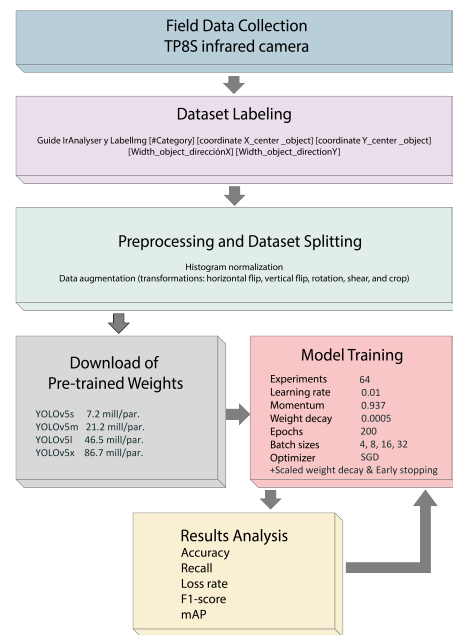
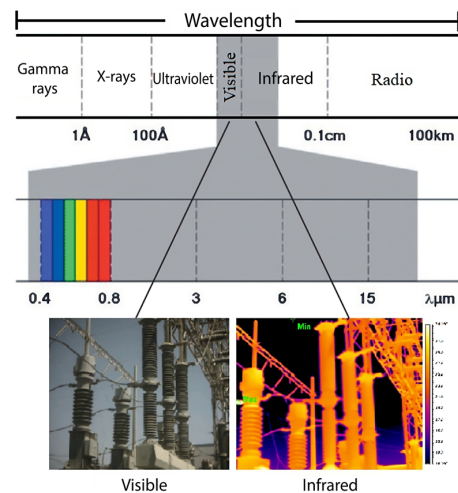
The paper begins with a detailed description of the algorithm and the methodology employed. Subsequently, the results are presented, and the corresponding conclusions are outlined.

2. Materials and methods

The research began with capturing thermal images, followed by the labeling process, preprocessing procedures, and dataset division. Subsequently, the pre-trained weights of YOLOv5 versions YOLOv5s (small), YOLOv5m (medium), YOLOv5l (large), and YOLOv5x (extra-large) were obtained. After this, 64 experiments were conducted and evaluated using various metrics. Figure 5 illustrates the implementation process. The details of the process are outlined in the subsequent sections.

2.1. Field data collection

The methodology began with the collection of field data through thermal image capture. To facilitate this procedure, the TP8S infrared camera was employed, characterized by a spectral range of 8-14 μm , an FPA detector (384x288 pixels, 35 μm), a $22^\circ \times 16^\circ / 35$ mm field of view, automatic electronic focus, thermal sensitivity ranging from 0.08 $^\circ\text{C}$ a 130 $^\circ\text{C}$, and a continuous zoom capability from $\times 1$ to $\times 10$.

**Figure 5.** Steps for the implementation of YOLOv5.**Figure 6.** Electromagnetic spectrum of an electrical substation

The data source employed in this study consists of 815 thermographic images acquired by professionals from an entity dedicated to the distribution of electrical energy in the northern region of Peru. Figure 6 illustrates an example of generating a thermographic image of an electrical substation by capturing radiation in the electromagnetic spectrum.

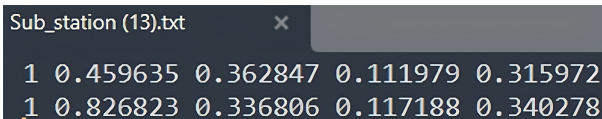
These images displayed a 384×288 pixels resolution and were classified into two main classes: electrical lines and electrical substations (See Table 2).

Table 2. Distribution of the original dataset

Classes	Total
Line	342
Substation	473

2.2. Dataset labeling

This dataset was labeled by a specialist in hotspot detection within thermographic images using the Guide IrAnalyser and LabelImg tools. Each identified hotspot was linked to a corresponding text file for the underlying image, documenting the object class and its coordinates in a specific format: [category number] [X-coordinate of the object’s center] [Y-coordinate of the object’s center] [object width in X direction] [object width in Y direction]. Figure 7 illustrates the format employed to represent two hotspots. This format is reiterated in each row according to the number of identified and labeled hotspots.



```
Sub_station (13).txt
1 0.459635 0.362847 0.111979 0.315972
1 0.826823 0.336806 0.117188 0.340278
```

Figure 7. Text file – 2 hotspots

2.3. Preprocessing and dataset splitting

During the image preprocessing stage, histogram normalization was performed to adjust the pixel intensity distribution in each thermal image, thereby enhancing its inherent characteristics.

At the outset, 815 images were available, comprising 342 images of power lines and 473 of electrical substations, as outlined in Table 2. Nevertheless, after labeling images with hotspots, the number of images was reduced to 138. Out of these, 116 pertained to substations and 22 to power lines. Consequently, this study was exclusively dedicated to the analysis of electrical substations.

Subsequently, the images were uploaded to the Roboflow platform, and using the "hold-out" splitting

technique, three datasets were generated: (i) a set of 81 images designated for training, (ii) a set of 23 images for validation, and (iii) a set of 12 images for testing.

Data augmentation techniques were implemented to increase the number of images and enhance training effectiveness, incorporating transformations such as horizontal inversion, vertical inversion, rotation, shearing, and cropping. This led to an expanded dataset comprising 278 images: (i) 243 images for training, (ii) 23 for validation, and (iii) 12 for testing.

Andrew Yan-Tak Ng, director of the Artificial Intelligence Laboratory at Stanford University, states the following in an article published in Spectrum, a journal edited by IEEE: “In various industries, having millions of data to train artificial intelligence models is challenging; therefore, having a small quantity of truly good or high-quality images can be useful for building defect inspection systems. In addition, accuracy increases when working with the weights of pre-trained models” [28].

2.4. Download of pre-trained weights

The pre-trained weights of the four algorithms belonging to YOLOv5 were downloaded to enhance the solution’s performance. These pre-trained weights were applied to the convolutional layers of the detector, significantly contributing to increased accuracy percentages and reduced training process durations. Table 3 provides detailed information about the pre-training weights associated with each algorithm and the number of parameters contained in each algorithm. It is noteworthy that YOLOv5s stands out as the least complex algorithm, whereas YOLOv5x is the most sophisticated regarding parameters and complexity.

Table 3. Weight and parameters of each algorithm

Algorithm	Trained weights (MB)	Parameters (millions)
YOLOv5s	14.1	7.2
YOLOv5m	40.8	21.2
YOLOv5l	89.3	46.5
YOLOv5x	166	86.7

2.5. Model training

A total of 64 experiments were conducted on the Google Colaboratory (Colab) platform, as detailed in Table 4. The free version of Colab provides an Intel Xeon processor with 2.30 GHz, an NVIDIA Tesla K80 GPU accelerator, 13 GB of RAM, and 40 GB of disk space.

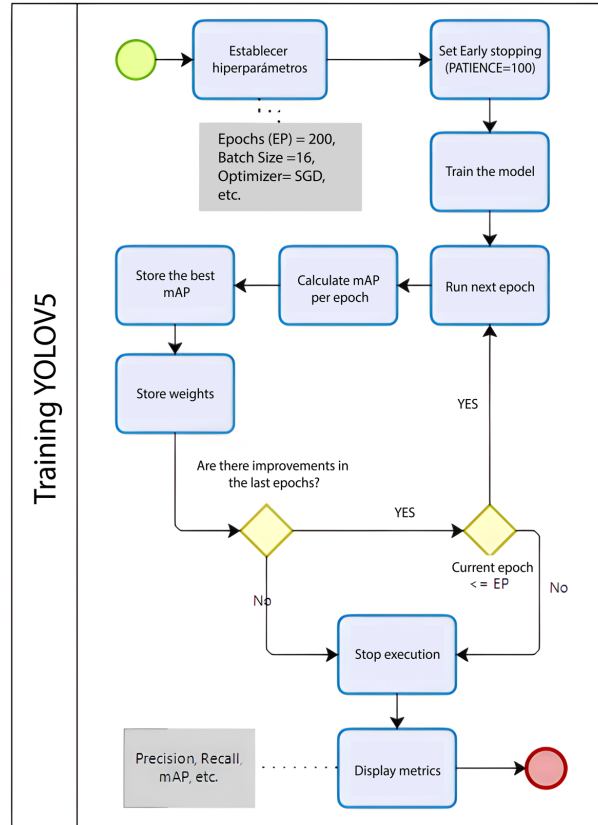
Table 4. Weight and parameters of each algorithm

Exp.	Algorithm	Batch size	Data augmentation	Transfer learning
E1	YOLOv5s	4	No	No
E2	YOLOv5s	8	No	No
E3	YOLOv5s	16	No	No
E4	YOLOv5s	32	No	No
E5	YOLOv5s	4	No	Si
E6	YOLOv5s	8	No	Si
E7	YOLOv5s	16	No	Si
E8	YOLOv5s	32	No	Si
E9	YOLOv5s	4	Si	No
E10	YOLOv5s	8	Si	No
E11	YOLOv5s	16	Si	No
E12	YOLOv5s	32	Si	No
E13	YOLOv5s	4	Si	Si
E14	YOLOv5s	8	Si	Si
E15	YOLOv5s	16	Si	Si
E16	YOLOv5s	32	Si	Si
E17	YOLOv5m	4	No	No
E18	YOLOv5m	8	No	No
E19	YOLOv5m	16	No	No
E20	YOLOv5m	32	No	No
E21	YOLOv5m	4	No	Si
E22	YOLOv5m	8	No	Si
E23	YOLOv5m	16	No	Si
E24	YOLOv5m	32	No	Si
E25	YOLOv5m	4	Si	No
E26	YOLOv5m	8	Si	No
E27	YOLOv5m	16	Si	No
E28	YOLOv5m	32	Si	No
E29	YOLOv5m	4	Si	Si
E30	YOLOv5m	8	Si	Si
E31	YOLOv5m	16	Si	Si
E32	YOLOv5m	32	Si	Si
E33	YOLOv5l	4	No	No
E34	YOLOv5l	8	No	No
E35	YOLOv5l	16	No	No
E36	YOLOv5l	32	No	No
E37	YOLOv5l	4	No	Si
E38	YOLOv5l	8	No	Si
E39	YOLOv5l	16	No	Si
E40	YOLOv5l	32	No	Si
E41	YOLOv5l	4	Si	No
E42	YOLOv5l	8	Si	No
E43	YOLOv5l	16	Si	No
E44	YOLOv5l	32	Si	No
E45	YOLOv5l	4	Si	Si
E46	YOLOv5l	8	Si	Si
E47	YOLOv5l	16	Si	Si
E48	YOLOv5l	32	Si	Si
E49	YOLOv5xl	4	No	No
E50	YOLOv5xl	8	No	No
E51	YOLOv5xl	16	No	No
E52	YOLOv5xl	32	No	No
E53	YOLOv5xl	4	No	Si
E54	YOLOv5xl	8	No	Si
E55	YOLOv5xl	16	No	Si
E56	YOLOv5xl	32	No	Si
E57	YOLOv5xl	4	Si	No
E58	YOLOv5xl	8	Si	No
E59	YOLOv5xl	16	Si	No
E60	YOLOv5xl	32	Si	No
E61	YOLOv5xl	4	Si	Si
E62	YOLOv5xl	8	Si	Si
E63	YOLOv5xl	16	Si	Si
E64	YOLOv5xl	32	Si	Si

The hyperparameters used included a learning rate of 0.01, a momentum of 0.937, a weight decay of 0.0005, 200 epochs, 4 batch sizes, and the SGD optimizer.

To prevent model overfitting, the "Scaled weight de-

cay" regularization and the "Early stopping" technique were incorporated and configured with a patience of 100, meaning the model will halt training if no improvements are observed in the last 100 epochs. Additionally, the weights from the best epochs are stored in each run, and the results of the mAP, Precision, Recall, and Loss curves are analyzed. Figure 8 illustrates the training flow of YOLOv5.

**Figure 8.** YOLOv5 training flowchart

2.6. Analysis of results

After the training of each model, analyses of metrics such as Precision (2), Recall (3), F1-score (4), loss rate, and mAP (5) were conducted, the latter being calculated based on Average Precision (6). TP represents the set of true positives, FP false positives, FN false negatives, and N the number of classes.

Several studies indicate that metrics such as F1-score and mAP (Mean Average Precision) are appropriate for model comparison [12], [29].

$$Precision = \frac{TP}{TP + FP} \quad (2)$$

$$Recall = \frac{TP}{TP + FN} \quad (3)$$

$$F1_{SCORE} = 2 * \frac{precision * recall}{precision + recall} \quad (4)$$

$$mAP = \frac{1}{n} \sum_{k=1}^{k=n} AP_k \quad (5)$$

$$AP = \sum_{k=0}^{k=n-1} [Recalls(k) - Recalls(k+1) * Precisions(k)] \quad (6)$$

3. Results and Discussion

Below, the results obtained by each of the four versions of YOLOv5 are presented.

3.1. YOLOv5s

YOLOv5 small achieved better results (mAP = 69.42% and F1-score = 68.23%) when training the model with experiment 5, i.e., with a batch size of 8, 171 epochs, applying transfer learning, and without incorporating data augmentation (See Table 5).

Table 5. YOLOv5 small – Training Results

Exp.	Precision	Recall	F1-score	mAP
E1	47.16 %	67.57 %	55.55 %	50.26 %
E2	75.97 %	51.35 %	61.28 %	59.77 %
E3	59.97 %	64.86 %	62.32 %	65.08 %
E4	55.95 %	75.68 %	64.34 %	64.70 %
E5	60.40 %	78.38 %	68.23 %	69.42 %
E6	59.17 %	78.33 %	67.42 %	65.44 %
E7	79.98 %	53.99 %	64.47 %	68.99 %
E8	57.57 %	70.27 %	63.29 %	57.24 %
E9	80.00 %	54.05 %	64.51 %	64.65 %
E10	57.43 %	72.97 %	64.27 %	64.96 %
E11	56.39 %	59.46 %	57.89 %	53.07 %
E12	55.26 %	56.76 %	56.00 %	52.85 %
E13	67.72 %	56.70 %	61.72 %	56.30 %
E14	57.12 %	64.80 %	60.72 %	59.94 %
E15	58.31 %	75.68 %	65.87 %	58.82 %
E16	58.47 %	64.86 %	61.50 %	60.52 %

3.2. YOLOv5m

YOLOv5 medium achieved better results than YOLOv5s (mAP = 81.99% and F1-score = 78.57%) when training the model with experiment 22, i.e., with a batch size of 16, 139 epochs, applying transfer learning, and without incorporating data augmentation (See Table 6).

Table 6. YOLOv5 medium – Training Results

Exp.	Precision	Recall	F1-score	mAP
E17	59.01 %	70.27 %	64.15 %	50.26 %
E18	86.13 %	51.35 %	64.34 %	59.77 %
E19	70.27 %	70.26 %	70.27 %	65.08 %
E20	65.71 %	62.16 %	63.89 %	64.70 %
E21	70.72 %	78.38 %	74.35 %	69.42 %
E22	70.21 %	89.18 %	78.57 %	65.44 %
E23	74.34 %	78.31 %	76.28 %	68.99 %
E24	74.28 %	70.24 %	72.20 %	57.24 %
E25	84.05 %	45.95 %	59.41 %	64.65 %
E26	88.62 %	43.24 %	58.12 %	64.96 %
E27	58.95 %	62.16 %	60.51 %	53.07 %
E28	49.97 %	75.68 %	60.19 %	52.85 %
E29	91.60 %	59.46 %	72.11 %	56.30 %
E30	64.82 %	64.86 %	64.84 %	59.94 %
E31	69.42 %	67.50 %	68.45 %	58.82 %
E32	81.42 %	59.46 %	68.73 %	60.52 %

3.3. YOLOv5l

YOLOv5 large achieved results similar to YOLOv5m (mAP = 81.88% and F1-score = 80.51%) when training the model with experiment 37, i.e., with a batch size of 8, 180 epochs, applying transfer learning, and without incorporating data augmentation (See Table 7).

Table 7. YOLOv5 large – resultados del entrenamiento

Exp.	Precision	Recall	F1-score	mAP
E33	80.70 %	45.95 %	58.55 %	55.38 %
E34	60.97 %	67.57 %	64.10 %	62.77 %
E35	55.97 %	75.68 %	64.35 %	68.42 %
E36	61.86 %	70.13 %	65.74 %	63.07 %
E37	89.79 %	72.97 %	80.51 %	81.88 %
E38	73.80 %	83.78 %	78.48 %	79.98 %
E39	68.11 %	81.08 %	74.03 %	78.10 %
E40	89.18 %	67.57 %	76.88 %	80.56 %
E41	57.14 %	64.86 %	60.76 %	61.48 %
E42	73.04 %	51.27 %	60.25 %	59.81 %
E43	52.99 %	70.27 %	60.42 %	63.03 %
E44	49.12 %	75.65 %	59.56 %	65.17 %
E45	73.53 %	67.56 %	70.42 %	71.16 %
E46	80.47 %	78.38 %	79.41 %	77.68 %
E47	82.20 %	64.86 %	72.51 %	71.97 %
E48	69.22 %	72.95 %	71.04 %	70.16 %

3.4. YOLOv5xl

YOLOv5 extra-large achieved slightly lower results than YOLOv5m and YOLOv5l (mAP = 79.25% and F1-score = 76.92%) when training the model with experiment 56, i.e., with a batch size of 32, 178 epochs, applying transfer learning, and without incorporating data augmentation (See Table 8). This was the only case where the best results were achieved with a batch size that was relatively larger compared to the other three algorithms.

Table 8. YOLOv5 extra-large – Training Results

Exp.	Precision	Recall	F1-score	mAP
E49	51.32 %	51.28 %	51.30 %	55.38 %
E50	53.29 %	64.86 %	58.51 %	62.77 %
E51	62.42 %	67.57 %	64.89 %	68.42 %
E52	67.51 %	67.57 %	67.54 %	63.07 %
E53	77.04 %	72.56 %	74.73 %	81.88 %
E54	72.09 %	83.70 %	77.46 %	79.98 %
E55	69.76 %	81.06 %	74.99 %	78.10 %
E56	73.17 %	81.08 %	76.92 %	80.56 %
E57	57.12 %	64.86 %	60.74 %	61.48 %
E58	49.99 %	64.86 %	56.47 %	59.81 %
E59	56.51 %	70.27 %	62.64 %	63.03 %
E60	77.26 %	45.91 %	57.59 %	65.17 %
E61	70.96 %	59.45 %	64.70 %	71.16 %
E62	76.66 %	62.16 %	68.65 %	77.68 %
E63	71.42 %	81.03 %	75.92 %	71.97 %
E64	73.78 %	83.78 %	78.46 %	70.16 %

3.5. YOLOv5 – Best results

A ranking of the 64 experiments was generated, considering the Mean Average Precision (mAP) as the classification factor (See Table 9).

Table 9. Details of the conducted experiments

Exp.	Ranking	Loss	mAP	Mejor época
E1	63	0.05484	50.26 %	157
E2	52	0.05137	59.77 %	153
E3	31	0.04212	65.08 %	167
E4	34	0.04340	64.70 %	143
E5	22	0.04060	69.42 %	171
E6	29	0.03988	65.44 %	190
E7	23	0.04106	68.99 %	146
E8	56	0.04953	57.24 %	193
E9	35	0.04657	64.65 %	115
E10	32	0.03710	64.96 %	168
E11	61	0.03740	53.07 %	134
E12	62	0.03750	52.85 %	185
E13	57	0.03718	56.30 %	76
E14	50	0.03360	59.94 %	74
E15	54	0.02952	58.82 %	127
E16	49	0.03107	60.52 %	200
E17	44	0.05050	62.57 %	160
E18	25	0.05133	68.49 %	139
E19	33	0.04590	64.73 %	194
E20	60	0.05628	53.40 %	175
E21	17	0.04042	72.87 %	107
E22	1	0.04541	81.99 %	139
E23	12	0.04426	75.69 %	182
E24	11	0.04362	75.97 %	154
E25	45	0.05280	61.87 %	86
E26	46	0.04952	61.65 %	86
E27	42	0.05051	62.80 %	88
E28	39	0.04908	63.09 %	63
E29	16	0.05071	73.20 %	108
E30	28	0.04914	66.17 %	69
E31	27	0.04743	68.35 %	37
E32	20	0.04665	70.96 %	63
E33	58	0.05487	55.38 %	154
E34	43	0.04841	62.77 %	153
E35	26	0.04331	68.42 %	182
E36	40	0.03910	63.07 %	123
E37	2	0.01974	81.88 %	180
E38	4	0.01602	79.98 %	128
E39	7	0.01615	78.10 %	125
E40	3	0.01396	80.56 %	160
E41	47	0.04325	61.48 %	136
E42	51	0.03757	59.81 %	162
E43	41	0.03571	63.03 %	60

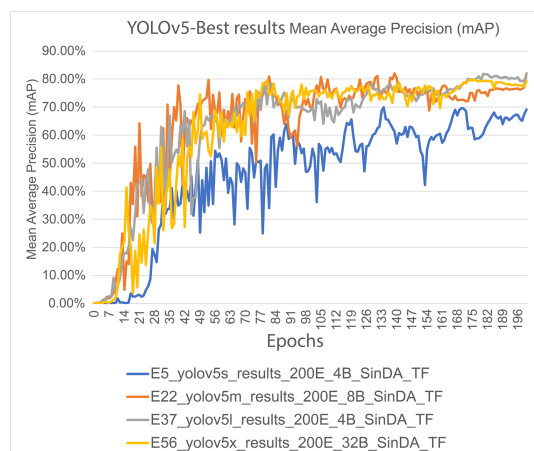
Exp.	Ranking	Loss	mAP	Mejor época
E44	30	0.03288	65.17 %	126
E45	19	0.01628	71.16 %	182
E46	8	0.01431	77.68 %	124
E47	18	0.01702	71.97 %	43
E48	21	0.01196	70.16 %	165
E49	64	0.06242	44.01 %	184
E50	53	0.04919	58.92 %	198
E51	37	0.04517	63.48 %	198
E52	14	0.04052	74.29 %	196
E53	9	0.02470	77.62 %	50
E54	6	0.01478	78.78 %	178
E55	13	0.01468	75.57 %	87
E56	5	0.01247	79.25 %	178
E57	48	0.04357	61.42 %	101
E58	59	0.04474	54.13 %	181
E59	36	0.03493	64.20 %	156
E60	55	0.03677	58.66 %	98
E61	38	0.01463	63.36 %	165
E62	24	0.01390	68.92 %	89
E63	15	0.01015	73.42 %	109
E64	10	0.01134	77.01 %	92

The most outstanding results for each algorithm are documented in Table 10 and presented graphically in Figure 9 (mAP), Figure 10 (precision), Figure 11 (recall), Figure 12 (training loss rate) and Figure 13 (validation loss rate). In the four evaluated scenarios, it is observed that the most remarkable performance was achieved by employing transfer learning without incorporating data augmentation.

From the 64 experiments conducted, the most outstanding model was developed by employing YOLOv5m and training it for 139 epochs, with a batch size of 8, without incorporating data augmentation and applying the transfer learning technique.

Table 10. Top performances for each algorithm

Algorithm	Experiment	mAP	Best epoch	Ranking
YOLOv5s	E5	69.42 %	171	22
YOLOv5m	E22	81.99 %	139	1
YOLOv5l	E37	81.88 %	180	2
YOLOv5xl	E56	79.25 %	178	5

**Figure 9.** YOLOv5 – Best results: mAP – Model training

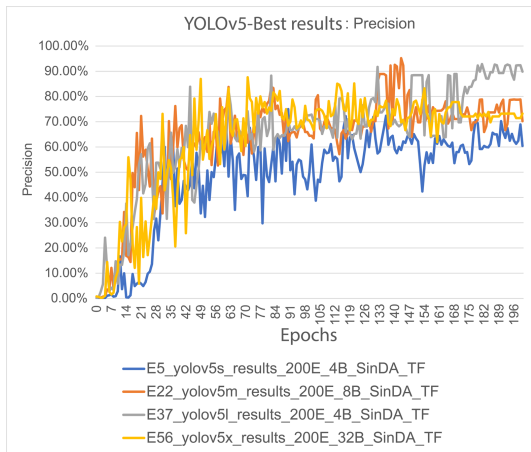


Figure 10. YOLOv5 – Best results: Precision – Model training

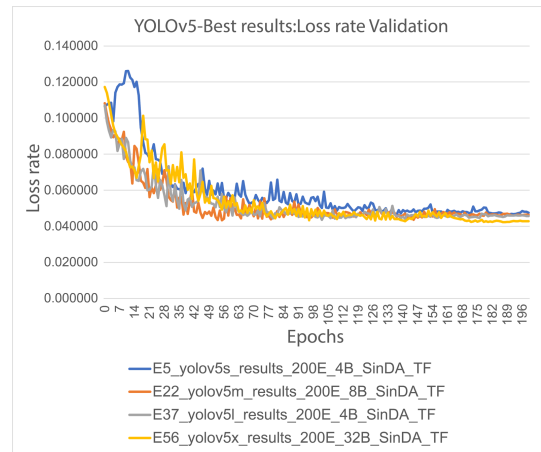


Figure 13. YOLOv5 – Best results: Loss rate – Model validation

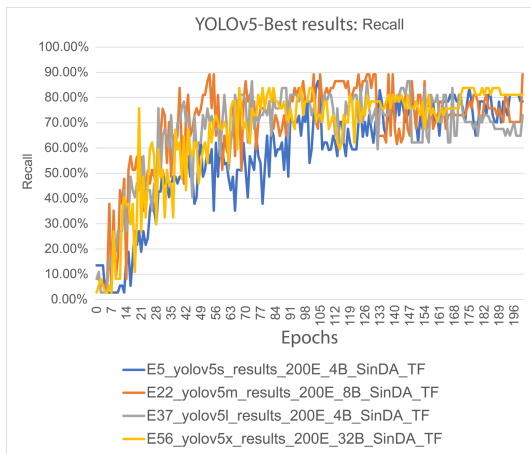


Figure 11. YOLOv5 – Best results: Recall – Model training

Figure 14 illustrates the graphical representation of the proposal derived from this research. The first step in the process is to incorporate the thermographic image database; then, the model is trained using the YOLOv5m algorithm, and finally, hotspots are detected in images of electrical substations.

Figure 15 displays various predictions made by the model, along with their respective percentages. These results were obtained using images from the test dataset, which were not previously included in the training and validation phases of the model.

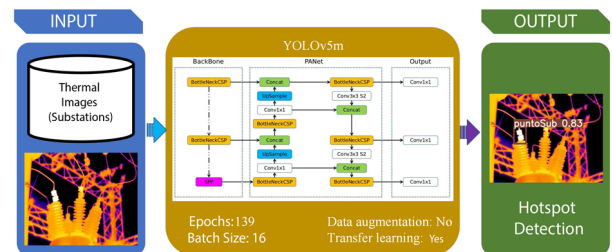


Figure 14. Proposed model

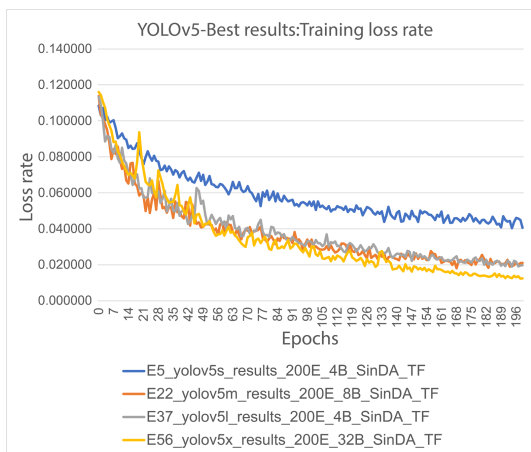


Figure 12. YOLOv5 – Best results: Loss rate – Model training

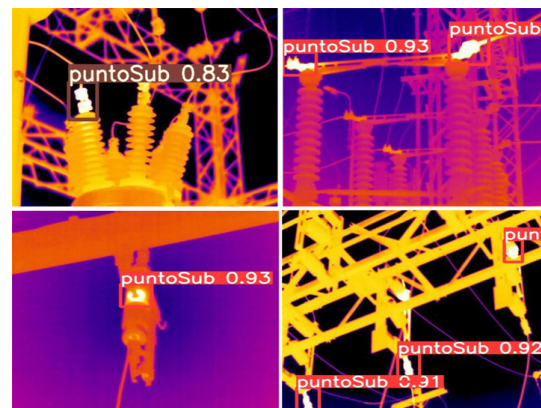


Figure 15. YOLOv5 medium – Hotspot detection

4. Conclusions

The primary aim of this study was to delve into innovative perspectives diverging from conventional artificial intelligence techniques. Special attention was directed towards the YOLOv5 object detection algorithm, acknowledging its remarkable efficiency in training processes.

Four iterations of the YOLOv5 algorithm underwent evaluation across 64 experiments, trained with a dataset of thermal images sourced from electrical substations. The findings reveal a discernible trend towards enhanced precision with an escalation in the number of training epochs, coupled with exploring alternative values beyond those employed in this study, encompassing optimizers, hyperparameters, and others.

Integrating data augmentation techniques has a negative impact on the precision of the models across all evaluated scenarios. Conversely, the transfer learning strategy, incorporating pre-trained weights for convolutional layers, enhances performance. Regarding the batch size, optimal results were attained within the range of 4 to 32, justified by the inherent size constraints of the current dataset. Nevertheless, it is crucial to note that this parameter may vary in future research involving more extensive datasets of thermographic images.

Scaled weight decay and Early stopping techniques were crucial in preventing overfitting. In this context, early termination of training was implemented when there was no improvement in performance over a specific number of epochs.

The findings of this research establish a valuable foundation for future investigations exploring the application of similar algorithms in the domain of hotspot detection in the electrical sector. As a recommendation for subsequent studies, it is advised to consider incorporating models with additional variants of the YOLOv5 algorithm, such as YOLOv5n6, YOLOv5s6, YOLOv5m6, YOLOv5l6, YOLOv5x6, or exploring alternative approaches like R-CNN and Faster R-CNN, among others. Based on the outcomes of this study, it could be anticipated that these explorations could result in enhanced performance.

Ultimately, exploring the possibility of integrating the developed model into a thermographic camera is highly recommended, thus facilitating real-time alert generation during image capture in the field.

References

- [1] S. Hussain, J. Hernandez Fernandez, A. K. Al-Ali, and A. Shikfa, "Vulnerabilities and countermeasures in electrical substations," *International Journal of Critical Infrastructure Protection*, vol. 33, p. 100406, 2021. [Online]. Available: <https://doi.org/10.1016/J.IJCIP.2020.100406>
- [2] Y.-E. Bouffard-Vercelli and B. André, "Future architectures of electrical substations," in *2021 Petroleum and Chemical Industry Conference Europe (PCIC Europe)*, 2021. [Online]. Available: <https://doi.org/10.23919/PCICEurope50407.2021.9805424>
- [3] W. Pavon, E. Inga, S. Simani, and M. Nonato, "A review on optimal control for the smart grid electrical substation enhancing transition stability," *Energies*, vol. 14, no. 24, 2021. [Online]. Available: <https://doi.org/10.3390/en14248451>
- [4] M. Lin, L. Fu, F. Zeng, G. Yang, and M. Sun, "Design of distributed substation high voltage electrical equipment online monitoring system based on image segmentation technology," *Journal of Physics: Conference Series*, vol. 2143, no. 1, p. 012001, dec 2021. [Online]. Available: <https://dx.doi.org/10.1088/1742-6596/2143/1/012001>
- [5] M. A. Haq, D. Kurniawan Danu, Syafii, and Muhardika, "Mitigation of the potential for sudden high-temperature hotspots on substation equipment," in *2023 4th International Conference on High Voltage Engineering and Power Systems (ICHVEPS)*, 2023, pp. 194–198. [Online]. Available: <https://doi.org/10.1109/ICHVEPS58902.2023.10257349>
- [6] S. Y. Lee and S. S. Teoh, "A survey on infrared thermography based automatic electrical fault diagnosis techniques," in *10th International Conference on Robotics, Vision, Signal Processing and Power Applications*, M. A. M. Zawawi, S. S. Teoh, N. B. Abdullah, and M. I. S. Mohd Sazali, Eds. Singapore: Springer Singapore, 2019, pp. 537–542. [Online]. Available: https://doi.org/10.1007/978-981-13-6447-1_68
- [7] F. Ciampa, P. Mahmoodi, F. Pinto, and M. Meo, "Recent advances in active infrared thermography for non-destructive testing of aerospace components," *Sensors*, vol. 18, no. 2, 2018. [Online]. Available: <https://doi.org/10.3390/s18020609>
- [8] M. Haenlein and A. Kaplan, "A brief history of artificial intelligence: On the past, present, and future of artificial intelligence," *California Management Review*, vol. 61, no. 4, pp. 5–14, 2019. [Online]. Available: <https://doi.org/10.1177/0008125619864925>
- [9] A. Ghahramani, G. Castro, S. A. Karvigh, and B. Becerik-Gerber, "Towards unsupervised learning of thermal comfort using infrared thermography," *Applied Energy*, vol.

- 211, pp. 41–49, 2018. [Online]. Available: <https://doi.org/10.1016/j.apenergy.2017.11.021>
- [10] Y. J. Wai, Z. bin Mohd Yussof, S. I. bin Salim, and L. K. Chuan, “Fixed point implementation of Tiny-Yolo-v2 using OpenCL on FPGA,” *International Journal of Advanced Computer Science and Applications*, vol. 9, no. 10, 2018. [Online]. Available: <http://dx.doi.org/10.14569/IJACSA.2018.091062>
- [11] Y. Xiao, Z. Tian, J. Yu, Y. Zhang, S. Liu, S. Du, and X. Lan, “A review of object detection based on deep learning,” *Multimedia Tools and Applications*, vol. 79, no. 33, pp. 23 729–23 791, Sep 2020. [Online]. Available: <https://doi.org/10.1007/s11042-020-08976-6>
- [12] S. Srivastava, A. V. Divekar, C. Anilkumar, I. Naik, V. Kulkarni, and V. Pattabiraman, “Comparative analysis of deep learning image detection algorithms,” *Journal of Big Data*, vol. 8, no. 1, p. 66, May 2021. [Online]. Available: <https://doi.org/10.1186/s40537-021-00434-w>
- [13] D. Dlužnevskij, P. Stefanovic, and S. Ramanauskaite, “Investigation of yolov5 efficiency in iphone supported systems,” *Baltic Journal of Modern Computing*, vol. 9, no. 3, pp. 333–344, 2021. [Online]. Available: <https://doi.org/10.22364/bjmc.2021.9.3.07>
- [14] G. Liu, J. C. Nouaze, P. L. Touko Mbouembe, and J. H. Kim, “Yolo-tomato: A robust algorithm for tomato detection based on yolov3,” *Sensors*, vol. 20, no. 7, 2020. [Online]. Available: <https://doi.org/10.3390/s20072145>
- [15] Z. Ma, Y. Wan, J. Liu, R. An, and L. Wu, “A kind of water surface multi-scale object detection method based on improved yolov5 network,” *Mathematics*, vol. 11, no. 13, 2023. [Online]. Available: <https://doi.org/10.3390/math11132936>
- [16] X. Gong, Q. Yao, M. Wang, and Y. Lin, “A deep learning approach for oriented electrical equipment detection in thermal images,” *IEEE Access*, vol. 6, pp. 41 590–41 597, 2018. [Online]. Available: <https://doi.org/10.1109/ACCESS.2018.2859048>
- [17] X. Li, “Design of infrared anomaly detection for power equipment based on yolov3,” in *2019 IEEE 3rd Conference on Energy Internet and Energy System Integration (EI2)*, 2019, pp. 2291–2294. [Online]. Available: <https://doi.org/10.1109/EI247390.2019.9061852>
- [18] A. Greco, C. Pironti, A. Saggese, M. Vento, and V. Vigilante, “A deep learning based approach for detecting panels in photovoltaic plants,” in *Proceedings of the 3rd International Conference on Applications of Intelligent Systems*, ser. APPIS 2020. New York, NY, USA: Association for Computing Machinery, 2020. [Online]. Available: <https://doi.org/10.1145/3378184.3378185>
- [19] D. T. Nguyen, T. N. Nguyen, H. Kim, and H.-J. Lee, “A high-throughput and power-efficient FPGA implementation of YOLO CNN for object detection,” *IEEE Transactions on Very Large Scale Integration (VLSI) Systems*, vol. 27, no. 8, pp. 1861–1873, 2019. [Online]. Available: <https://doi.org/10.1109/TVLSI.2019.2905242>
- [20] D. Fan, D. Liu, W. Chi, X. Liu, and Y. Li, “Improved ssd-based multi-scale pedestrian detection algorithm,” in *Advances in 3D Image and Graphics Representation, Analysis, Computing and Information Technology*, R. Kountchev, S. Patnaik, J. Shi, and M. N. Favorskaya, Eds. Singapore: Springer Singapore, 2020, pp. 109–118. [Online]. Available: https://doi.org/10.1007/978-981-15-3867-4_14
- [21] S. Ren, K. He, R. Girshick, and J. Sun, “Faster R-CNN: Towards real-time object detection with region proposal networks,” *IEEE Transactions on Pattern Analysis and Machine Intelligence*, vol. 39, no. 6, pp. 1137–1149, 2017. [Online]. Available: <https://doi.org/10.1109/TPAMI.2016.2577031>
- [22] W. Chen, H. Huang, S. Peng, C. Zhou, and C. Zhang, “Yolo-face: a real-time face detector,” *The Visual Computer*, vol. 37, no. 4, pp. 805–813, Apr 2021. [Online]. Available: <https://doi.org/10.1007/s00371-020-01831-7>
- [23] S. A. Sanchez, H. J. Romero, and A. D. Morales, “A review: Comparison of performance metrics of pretrained models for object detection using the tensorflow framework,” *IOP Conference Series: Materials Science and Engineering*, vol. 844, no. 1, p. 012024, may 2020. [Online]. Available: <https://dx.doi.org/10.1088/1757-899X/844/1/012024>
- [24] J. Xue, F. Cheng, Y. Li, Y. Song, and T. Mao, “Detection of farmland obstacles based on an improved YOLOv5s algorithm by using Clou and anchor box scale clustering,” *Sensors*, vol. 22, no. 5, 2022. [Online]. Available: <https://doi.org/10.3390/s22051790>
- [25] A. Li, S. Sun, Z. Zhang, M. Feng, C. Wu, and W. Li, “A multi-scale traffic object detection algorithm for road scenes based on improved YOLOv5,” *Electronics*, vol. 12, no. 4, 2023. [Online]. Available: <https://doi.org/10.3390/electronics12040878>

- [26] J. Shi, J. Yang, and Y. Zhang, “Research on steel surface defect detection based on YOLOv5 with attention mechanism,” *Electronics*, vol. 11, no. 22, 2022. [Online]. Available: <https://doi.org/10.3390/electronics11223735>
- [27] D. A. Pérez-Aguilar, R. H. Risco-Ramos, and L. Casaverde-Pacherrez, “Transfer learning en la clasificación binaria de imágenes térmicas,” *INGENIUS*, no. 26, pp. 71–86, 2021. [Online]. Available: <https://doi.org/10.17163/ings.n26.2021.07>
- [28] A. Yan-Tak Ng. (2022) Unbiggen ai. IEEE Spectrum. IEEE Spectrum. [Online]. Available: <https://bit.ly/3RNNvsvr>
- [29] R. Padilla, W. L. Passos, T. L. B. Dias, S. L. Netto, and E. A. B. da Silva, “A comparative analysis of object detection metrics with a companion open-source toolkit,” *Electronics*, vol. 10, no. 3, 2021. [Online]. Available: <https://doi.org/10.3390/electronics10030279>



NETWORK CENTRALITY MEASURES FOR CLASSIFYING IMPORTANT COMPONENTS IN ELECTRICAL POWER SYSTEMS BASED ON LINEGRAPH TRANSFORMATION

CLASIFICACIÓN DE ELEMENTOS IMPORTANTES EN SISTEMAS ELÉCTRICOS DE POTENCIA SEGÚN MEDIDAS DE CENTRALIDAD EN REDES Y TRANSFORMACIÓN LINEGRAPH

José A. Moronta R.^{1,*} , Claudio M. Rocco S.² 

Received: 30-06-2023, Received after review: 27-11-2023, Accepted: 30-11-2023, Published: 01-01-2024

Abstract

Network theory techniques have recently contributed to the analysis of electrical power systems, enabling faster computational solutions. Taking advantage of the topological information of a network, it becomes possible to characterize its elements both locally (individual network components) and globally (interactions and behavior of the components). Identifying the crucial elements within an electrical system involves classifying each component based on its interaction with the entire network, considering, possibly, various operating conditions. Current network centrality measures predominantly focus on nodes, which represent connection buses in the system, to quantify the significance of individual elements. In this study, we employ the linegraph technique to transform links into nodes. Subsequently, we calculate and categorize the links (representing lines and transformers) of different electrical networks found in the literature using three centrality measures. Moreover, our methodology allows for the aggregation or combination of the indices from each measure, leading to a unified classification based on the importance of links in the considered electrical power systems. Analyzing diverse networks reveals a consistent empirical distribution of centrality indices, resulting in similar classifications of significant elements regardless of network size.

Keywords: Centrality measures, electrical networks, linegraph, link classification

Resumen

El análisis de sistemas eléctricos de potencia se ha apoyado, recientemente, en la aplicación de técnicas de la teoría de redes, con la finalidad de obtener soluciones computacionalmente más rápidas. A partir de la información topológica de una red, es posible definir características desde lo local (elementos de la red) hasta lo global (comportamiento e interacción de los elementos). La identificación de elementos importantes de un sistema eléctrico, consiste en clasificar cada uno de los elementos desde su interacción con toda la red, y, posiblemente, tomando en cuenta diversas condiciones de operación del sistema. Las medidas de centralidad en redes, que permiten asignar importancia cuantitativa a los elementos de un sistema, están definidas en su mayoría para los nodos (representan buses de conexión) de las mismas. En este trabajo, a partir de la transformación de enlaces a nodos, según la técnica linegraph, se calculan y clasifican los enlaces (representan líneas y transformadores) de diversas redes eléctricas de la literatura, de acuerdo con tres medidas de centralidad. Adicionalmente, el procedimiento presentado permite agregar o combinar los índices de cada medida, y obtener una única clasificación según su importancia para los enlaces de los sistemas eléctricos de potencia considerados. La diversidad de redes analizadas permite concluir que la distribución empírica de los índices de centralidad es similar, y origina una clasificación de elementos importantes semejantes, independiente de la dimensión de la red.

Palabras clave: clasificación de enlaces, linegraph, medidas de centralidad, redes eléctricas

^{1,*}Departamento de Tecnología Industrial, Universidad Simón Bolívar, Venezuela.

Corresponding author ✉: jmoronta@usb.ve.

²Facultad de Ingeniería, Universidad Central de Venezuela, Venezuela.

Suggested citation: Moronta R., J.A. and Rocco S., C.M. "Network centrality measures for classifying important components in electrical power systems based on linegraph transformation," *Ingenius, Revista de Ciencia y Tecnología*, N.º 31, pp. 55-63, 2024, DOI: <https://doi.org/10.17163/ings.n31.2024.05>.

1. Introduction

Identifying important electrical power systems (EPS) elements involves determining the most relevant components under one or several specific operating conditions. In this regard, the works of various authors [1–3] can be cited. Based on the evaluation of power flows in the EPS, they select elements whose deactivation results in the greatest load rationing.

Other researchers have focused on identifying the elements that most affect the vulnerability of EPS [4,5], the elements with the most significant potential to trigger cascading failures in the EPS [6], and the elements that impact the reliability of the EPS [7].

Recently, research on the analysis of power systems has focused on network theory to achieve faster computational solutions. This approach does not involve evaluating the physical equations governing the system's behavior but relies solely on the topological characteristics of the network [8].

The approach based on centrality measures is widely used to assess the importance of elements in a network, considering exclusively the topology. According to Newman [9], researchers aim to answer the following question: What are the most important or central nodes in a network? Although most centrality measures are defined for nodes in the system, some scientists have extended node centrality [10] to links. Considering this, the previous question can be answered from the perspective of network links.

In the case of electrical power systems, the links (representing energy transmission lines or electrical transformers) are more important than in other types of systems. As pointed out by Ortiz et al. [11], centrality measures (considered on the links) are helpful because they enable an understanding of the importance of a link that connects with other links to facilitate the flow of electrical energy between sources and loads.

Some authors [11,12] focus on transforming the original network into an equivalent one, converting the links from the original network into nodes in the equivalent network. In this equivalent network, node centrality metrics can be assessed, allowing for an indirect determination of the importance of the links in the original network. This transformation is based on the mathematical concept known as linegraph [13], which involves creating a new equivalent graph $L(G)$ from a graph G , where the nodes of $L(G)$ represent the links of G .

This work aims to classify the links (transmission lines and/or transformers) of network G according to their level of importance by transforming network G , representing the topology of an EPS, into a new network $L(G)$ using the linegraph [13] and evaluating centrality measures in networks. To achieve this, the technique of ordered list aggregation is employed, which allows combining multiple lists into a single en-

tity. Aggregation poses a common challenge in social sciences, statistics, and other fields, where it is necessary to merge different ordered lists according to a specific criterion [14].

1.1. Previous studies

The authors cited in [15] and [8] analyze the Italian electrical system (hviet) and the Venezuelan electrical system (SENTRONCAL), respectively, from the perspective of complex networks. The importance of topology in characterizing the network is determined, although evaluations and classifications of elements mainly focus on the nodes of the electrical system.

On the other hand, Hines and Blumsack [16] point out a clear connection between the network's topology and its vulnerability. This work [16] defines a measure called "equivalent electrical distance between pairs of nodes" based on information centrality measures [17,18].

Some researchers [19] assess various electrical systems from the literature (IEEE30, IEEE57 and IEEE 118) using centrality measures modified to incorporate electrical parameters. The considered measures are Degree centrality, Closeness centrality, and Betweenness centrality, all evaluated at the network nodes. Subsequently, Nasiruzzaman and Pota [6] propose a method to assess the stability of power systems based on network theory. They employ, as a centrality measure, an extension of the concept of Betweenness centrality called Edgebetweenness centrality; in other words, a centrality measure applied to network links.

Article [19] proposes an enhanced model of the closeness centrality index to identify critical nodes in cascading failure processes within networks. Chen et al. [5] suggest an index called "weighted line betweenness" to pinpoint essential transmission lines (network links). This identification is not solely based on their electrical power capacity but also on their topological arrangement in the network. Amani and Jalili [4] provide a review of vulnerability and resilience analysis in power systems from the perspective of complex network theory. They identify a set of measures and indices, emphasizing a summary where specific measures for nodes and links are mentioned, including some that are centrality measures or centrality measures adapted to electrical networks.

Nakarmi et al. [7] conduct a classification of reliability analysis in power systems using graphs and the interaction of their elements. A significant subclassification they perform is the "identification of critical components". This reliability analysis focuses on finding critical nodes/transmission lines (links) by analyzing the structural properties of the graphs. They use standard centrality measures or define new graph-based metrics, which typically incorporate electrical characteristics into the standard measure [20–22].

Bröhl and Klaus [10] point out that while there are many methods for measuring the centrality of individual nodes, there are few metrics for measuring the centrality of individual links. Consequently, they propose modifications to widely used centrality concepts for nodes to be applied to network links, thereby identifying important links or sets of links. They specifically focus on three indices:

- Betweenness centrality
- Closeness centrality
- Eigenvector centrality

Ortiz et al. [11] utilize the mathematical concept called linegraph [13], wherein, from an original graph G , a new graph $L(G)$ can be created, with its nodes representing the links of G . This facilitates the application of traditional centrality measures for nodes to the links in the network, based on this new graph $L(G)$. This proposal enables the identification of important links in the network, applying centrality indices to links in social networks such as Facebook. They also suggest that this could provide information about the importance of a link interconnected with others to facilitate the flow of information between sources and destinations.

Built upon the concept of linegraph $L(G)$ [13], this work aims to classify important links in electrical networks, quantifying their centrality values. An aggregation of the previously ordered lists is carried out to generate a unique classification of the importance of elements, considering and integrating various centrality measures employed. A comparison of the distribution of centrality values in different electrical networks analyzed in the literature is conducted.

2. Materials and methods

2.1. Preliminary definitions

2.1.1. Graph

A network, including power systems, can be modeled as a graph $G = (V, E)$ where $V = \{v_1, \dots, v_n\}$ represents the set of nodes (system connection buses) and $E = \{e_1, \dots, e_m\}$ represents the set of links connecting the nodes of the graph (transmission lines and transformers). The number of nodes is $n = |V|$, and the number of links is $m = |E|$.

Then, $A(G) = (a_{ij})$ represents the adjacency matrix of the graph G with order $n \times n$, where a_{ij} indicates a connection between nodes v_i and v_j , $a_{ij} = 1$ if v_i and v_j are connected, and $a_{ij} = 0$ if they are not.

On the other hand, $B(G) = (b_{ij})$ represents the incidence matrix of G with order $n \times m$, where $b_{ij} = 1$ if v_i and v_j are incident, and $b_{ij} = 0$ when they are not.

2.1.2. Linegraph

The Line Graph $L(G)$ is a graph whose nodes represent the links of the original graph G and $A(L(G))$ denotes its adjacency matrix. Equation (1) represents the adjacency matrix of $L(G)$ with order $m \times m$.

Then:

$$A(L(G)) = (B^t B) - 2 * I_m \tag{1}$$

Where I_m is the identity matrix of dimension $m \times m$.

Figure 1 shows examples of simple graphs (left) with their corresponding $L(G)$ (right). The original nodes are not considered in the $L(G)$ graphs, resulting in a graph where nodes correspond to links. For instance, in the graph shown in the top left of Figure 1, with nodes $\{1, 2, 3\}$ and links $a = (1, 2)$ and $b = (2, 3)$, it transforms into another graph with only two nodes $\{a, b\}$ and a single link $\{2\}$.

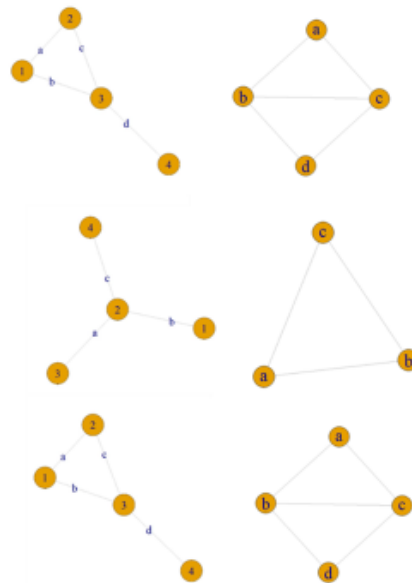


Figure 1. Graphs G on the left with their corresponding $L(G)$ on the right. The nodes in $L(G)$ represent the links in G .

2.1.3. Measures or centrality indices Betweenness centrality (Betweenness centrality [23])

According to [24], the betweenness centrality of a node k can be defined according to Equation (2):

$$C_V^B(k) = \frac{2}{(V-1)(V-2)} \sum_{k \neq i \neq j} \frac{q_{ij}(k)}{G_{ij}} \tag{2}$$

Where $\{k, i, j\} \in V$ and q_{ij} is the number of shortest paths between nodes i and j passing through node

k . G_{ij} is the total number of shortest paths between vertices i and j .

Closeness centrality (Closeness centrality [23]). The closeness centrality of the node (for a node k) is defined according to Equation (3):

$$C_V^B(k) = \frac{(V-1)}{\sum_l d_{kl}} \quad (3)$$

With $\{k, l\} \in V$, where d_{kl} denotes the shortest path length from node k to node l .

Eigenvector centrality (Eigenvector centrality [23]). The eigenvector centrality of the node (node k) is defined as the k -th entry of the eigenvector \vec{v} corresponding to the dominant eigenvalue λ_{max} of the matrix M , derived from the eigenvector equation $M\vec{v} = \lambda\vec{v}$, equation (4), with $\{k, l\} \in V$. Where M denotes the adjacency matrix $A^{(v)} \in \{0, 1\}^{V \times V}$ of a network, with $A_{ij}^{(v)} = 1$ indicating a link between nodes i and j , and 0 indicating no link.

$$C_V^E(k) = \frac{1}{\lambda_{max}} \sum_l M_{kl} C_V^E(l) \quad (4)$$

2.2. Procedure for classifying links according to their importance

In an EPS, considering its topology exclusively, the graph $G = (V, E)$. Then, $L(G)$ can be determined, where its nodes represent the links of the original graph G . Subsequently, the following is determined based on this equivalent graph $L(G)$:

- Betweenness centrality (EB)
- Closeness centrality (EC)
- Eigenvector centrality (EE)

The three mentioned centrality measures are determined for each link of the electrical power system represented as nodes in the equivalent graph $L(G)$. These measures are normalized and arranged from highest to lowest, allowing for the classification of the link's importance according to the provided index.

Afterwards, the links can be classified as important based on a pre-established index value. For instance, it can be stipulated that links with values exceeding 0.9 are deemed the most important in the network or according to any other criterion established by the decision-maker.

After obtaining each list or ranking for the considered centrality indices, a general classification of the elements combining the characteristics measured by each index separately can be generated. This allows determining a unique order of importance for each element.

This work employs a method to combine ordered lists based on their importance, determining a compromise order in which the differences or distances from the ordered lists are minimal. Naturally, other techniques, such as multicriteria decision methods [25], can be considered to determine the combined order. The list combination method used in this work is found in the RankAgregg library [14] of the R software [26]. The distances between the sought compromise order and each ordered list are calculated using the Spearman similarity index, and optimization (minimization of the sum of distances) is achieved using a heuristic based on the Cross-Entropy Monte Carlo algorithm [27]. As with any heuristic, an optimal solution is not guaranteed for large-scale problems.

Figure 2 illustrates the complete aggregation process for selecting link groups in the considered EPS.

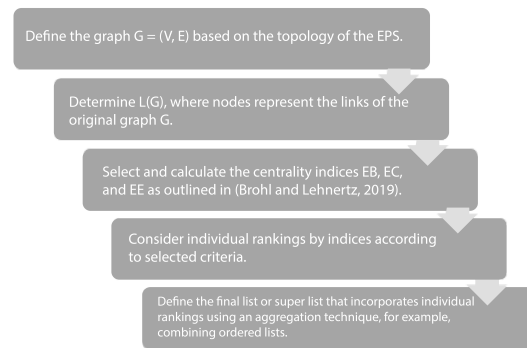


Figure 2. Classification process of important elements in an EPS considering centrality measures.

2.3. Illustrative example of the procedure

To illustrate the procedure described in Figure 2, an EPS represented by the graph in Figure 3 (left) is considered. Using the linegraph technique (available in the igrph library [28]), the equivalent graph, where links are now presented as nodes, is obtained, as shown in Figure 3 (right). For example, the link h connecting nodes 5 and 6 in the graph of Figure 3 (left) corresponds to node h in the graph of Figure 3 (right).

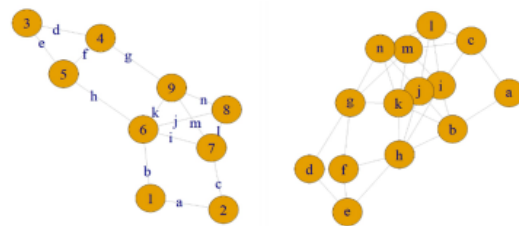


Figure 3. Representative graph of a 9-node EPS (left) -Equivalent graph (line-graph) of a 9-node EPS using line-graph (right)

For the equivalent graph shown in Figure 3 (right), the centrality indices (EB, EC, and EE) are calculated using functions coded in the igraph library [28] of the R v4.2.2 statistical software [26]. Table 1 displays the centrality index values of the considered links, ordered from most important to least important. It is observed that no single link emerges as the most important when all three centrality indices are simultaneously considered. Consequently, there is a need to establish a compromise ranking. Table 1 provides details of the elements (from-to) corresponding to the graph in Figure 3 (left).

Table 1. Rankings for each index of the links of the representative graph of a 9-node EPS.

EB	from	to	EC	from	to	EE	from	to
1	5	6	1	6	9	1	6	9
0.71	1	6	0.86	5	6	0.98	6	7
0.71	4	9	0.86	6	7	0.87	6	8
0.51	2	7	0.74	7	9	0.77	7	9
0.34	7	9	0.74	6	8	0.69	5	6
0.32	3	5	0.62	1	6	0.66	8	9
0.28	6	7	0.62	4	9	0.65	7	8
0.18	6	8	0.52	8	9	0.63	1	6
0.18	6	9	0.43	7	8	0.45	4	9
0.16	3	4	0.34	2	7	0.37	2	7
0.1	1	2	0.34	4	5	0.14	4	5
0.06	4	5	0.12	3	5	0.03	3	5
0.06	8	9	0	3	4	0.02	1	2
0	7	8	0	1	2	0	3	4

Ultimately, the five most significant elements of the combined ordered list, also known as the superlist of links, are presented in Table 2. This list simultaneously incorporates all three indices using the RankAggreg package in the statistical software R v4.2.2 [26]. To achieve this, the RankAggreg method [14] is iteratively implemented a thousand times on the network, and positions in the list are determined based on the highest frequency of element occurrence at each position.

Table 2. Ordered list of the 5 most important elements of the links in the representative graph of a 9-node EPS, sorted from highest to lowest.

from	to	Link
6	9	k
5	6	h
6	7	i
6	8	j
7	9	m

It is worth emphasising that this ordering is robust, as it persists even after running the selected

aggregation algorithm a thousand times based on an optimization heuristic.

3. Results and discussion

The procedure for identifying important elements in an electrical power system is implemented in a set of 16 EPS [29], where only the topology associated with each system is utilized. Table 3 displays the number of nodes and links corresponding to each analyzed network.

Table 3. Topology of the electrical power systems considered [29]

#	Name	Nodes	Links	Note
1	IEEE24	24	34	IEEE24 test case
2	IEEE30	30	41	IEEE30 test case
3	IEEE57	57	80	IEEE57 test case
4	IEEE118	118	186	IEEE118 test case
5	Germany	438	662	German power
6	SETRONCAL	80	107	Venezuelan power
7	hviet	310	347	Italian power
8	power494	494	586	-
9	power685	685	1282	-
10	power1138	1138	1458	-
11	powerbcspwr	5300	8271	Western US power
12	powerUS	4941	6594	US power
13	Texas	2007	2607	Texas power
14	CentralChilean PG	318	409	Chilean power
15	Spain	1104	1416	Iberian Peninsula
16	France	904	1163	Frenchpower

Figure 4 illustrates the distribution of centrality measures for each network mentioned in Table 3. To achieve this, the value of each considered centrality measure (EB, EC, and EE) is determined and normalized to compare the networks of the 16 power systems. In the case of the EB and EE indices, the distributions are primarily concentrated at low values (to the left), except for networks with few nodes (IEEE24 and IEEE30) exhibiting greater dispersion. Meanwhile, the EC index demonstrates a more equitable distribution.

A specific network is considered, such as the IEEE57 network, composed of 80 links. In Figure 5, the normalized values of centrality measures for each of the 80 links in the network are displayed, highlighting links 17, 21, and 33 with the highest values in all three evaluated indices. It is noteworthy that there is not a single, more important link (technically, a link that dominates over the rest of the links simultaneously), and there are indices that assess the importance of each link differently. Thus, it is necessary to determine a

unique ranking that combines the relative importance of each index.

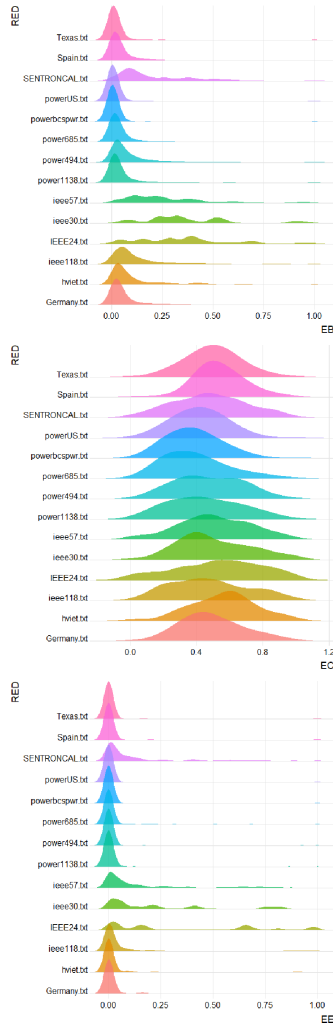


Figure 4. Probability density of centrality values (EB, EE, and EC) in electrical power systems from the literature in Table 2

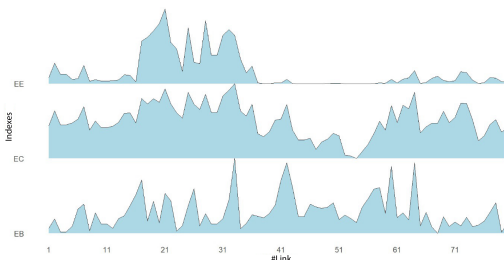


Figure 5. Values of each considered index (top: Betweenness centrality (EB); middle: Closeness centrality (EC); bottom: Eigenvector centrality (EE)) for the links of the IEEE57 network.

For the same IEEE57 network, it is determined that the decision-maker sets a minimum value of 0.70

for normalized centrality indices to classify a link as important in the network. On the left side of Figure 6, the ordered list of important links (index values exceeding 0.70) is displayed for each specific index. The network's topology is presented on the right, highlighting the important links (blue line) following the aforementioned criterion.

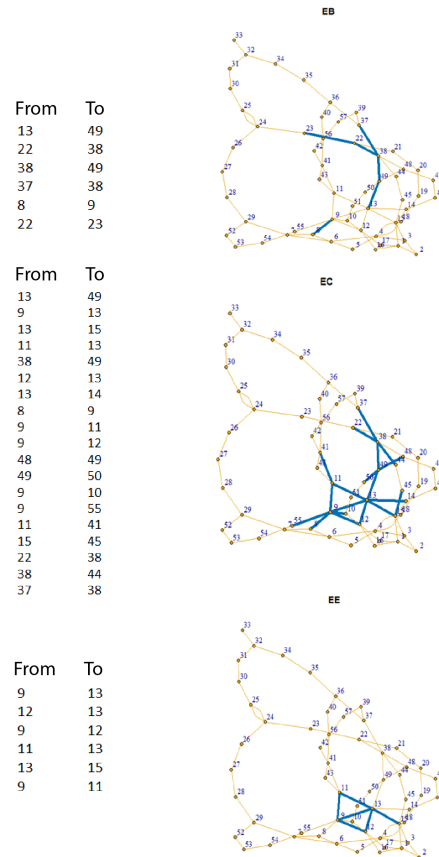


Figure 6. Important links according to specific centrality indices (top: Betweenness centrality (EB); middle: Closeness centrality (EC); bottom: Eigenvector centrality (EE)), with their associated graphs (important links are highlighted in blue).

Each index orders the links differently. For instance, the link connecting nodes 13-49 (link 33) is classified as the most important according to centrality indices: Betweenness centrality (EB) and Closeness centrality (EC); however, it does not appear in the list of important links according to Eigenvector centrality (EE).

The algorithm for aggregating ordered lists mentioned earlier [14] is used to obtain a ranking that considers all indices simultaneously. Figure 7 displays the network $L(G)$ corresponding to IEEE57 and the first ten elements of the ordered list corresponding to links 33, 21, 32, 25, 64, 28, 31, 17, 19 and 20 (arranged from most important to least important).

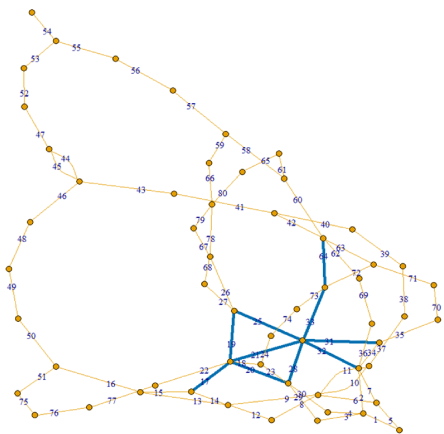


Figure 7. Network corresponding to the IEEE57 system with the first ten links ranked according to their importance and highlighted in blue.

Considering the original graph representing the IEEE57 network, the ten most important links are those shown in Table 4.

Table 4. Ordered list of importance of links in the graph representing the IEEE57 EPS.

#Link	from	to
33	13	49
21	9	13
32	13	15
25	11	13
64	38	49
28	12	13
31	13	14
17	8	9
19	9	11
20	9	12

Figure 7 shows that the most important elements result from the individual lists of centrality indices. For instance, the element connecting node 13 to node 49 is the most important in the aggregated list, exhibiting the highest values in the EB and EC indices. However, it is positioned seventh in the EE index (with a value of $0.65 < 0.7$).

The number of links to be considered important can be previously defined by the decision-maker. On the other hand, the combined list of links considered important can be used as a baseline for additional analyses of the electrical system (e.g., protection, vulnerability, or resilience studies), thereby reducing the analysis space to the set of important elements. In the case of the IEEE57 network, the first ten elements considered important represent less than 15% of the total links in the network, which can decrease the number of potential assessments requiring high computational demand, especially in networks with a more significant number of elements.

4. Conclusions

This study proposes a framework that facilitates the determination of a ranked list based on the importance of links in an electrical network, utilizing a set of centrality indices. To achieve this, the original network is transformed into an equivalent one, where links are represented as nodes. In this equivalent network, a set of centrality indices is assessed (typically, these indices are designed for nodes and not for links). Three specific centrality indices are employed in this study, although any set of centrality indices could be utilized.

Subsequently, a unique ranking is derived from these lists, integrating the individually considered properties and establishing an order of importance for the network elements.

This procedure was evaluated on a set of networks that share the characteristic of representing the topology of electrical power systems, varying in scale, originating from different regions of the world, and possibly following different design criteria. The results suggest that the estimated statistical distribution of centrality index values exhibits similar behavior.

The indices evaluated in this study consistently suggest that the most important links are located in the "center" of the network, enabling connections with more peripheral links. It is worth noting that for the classification of elements in the network, no evaluation of the specific dynamics of the network is required; in fact, no additional information beyond the network's topology (connections from-to) is needed. Therefore, the proposed procedure could be applied for faster assessments than conventional ones in power systems with incomplete information or simply as input that narrows down possible solutions in a comprehensive evaluation considering the equations modeling the electrical phenomenon.

On the other hand, the omission of the specific electrical phenomenon that enables the evaluation and classification of elements in the power system constitutes a limitation for this procedure. This is because important elements, which would only be correctly classified by the inherent nature of the problem, could be overlooked.

The future extension of this procedure is proposed in two fundamental directions. Firstly, it is suggested to consider centrality measures specifically designed for electrical systems, incorporating properties of links such as capacities, impedances, and other relevant characteristics. Secondly, comparing the results obtained with different schemes for evaluating important components based on functional analyses of electrical systems, such as stability, power flows, or other relevant parameters, is recommended.

References

- [1] V. Donde, V. López, B. Lesieutre, A. Pinar, C. Yang, and J. Meza, “Identification of severe multiple contingencies in electric power networks,” in *Proceedings of the 37th Annual North American Power Symposium, 2005.*, 2005, pp. 59–66. [Online]. Available: <https://doi.org/10.1109/NAPS.2005.1560502><https://doi.org/10.1109/NAPS.2005.1560502>
- [2] J. Arroyo and F. Galiana, “On the solution of the bilevel programming formulation of the terrorist threat problem,” *IEEE Transactions on Power Systems*, vol. 20, no. 2, pp. 789–797, 2005. [Online]. Available: <https://doi.org/10.1109/TPWRS.2005.846198>
- [3] C. Rocco, J. Ramírez-Márquez, D. Salazar, and C. Yajure, “Análisis preliminar de la vulnerabilidad de un sistema de potencia mediante interdicción determinista multiobjetivo,” *Revista de la Facultad de Ingeniería Universidad Central de Venezuela*, vol. 25, pp. 61–69, 03 2010. [Online]. Available: <https://bit.ly/46JapWe>
- [4] A. M. Amani and M. Jalili, “Power grids as complex networks: Resilience and reliability analysis,” *IEEE Access*, vol. 9, pp. 119 010–119 031, 2021. [Online]. Available: <https://doi.org/10.1109/ACCESS.2021.3107492>
- [5] X. Chen, K. Sun, Y. Cao, and S. Wang, “Identification of vulnerable lines in power grid based on complex network theory,” in *2007 IEEE Power Engineering Society General Meeting*, 2007. [Online]. Available: <https://doi.org/10.1109/PES.2007.385733>
- [6] A. B. M. Nasiruzzaman and H. R. Pota, “Transient stability assessment of smart power system using complex networks framework,” in *2011 IEEE Power and Energy Society General Meeting*, 2011. [Online]. Available: <https://doi.org/10.1109/PES.2011.6038970>
- [7] U. Nakarmi, M. Rahnamay Naeini, M. J. Hossain, and M. A. Hasnat, “Interaction graphs for cascading failure analysis in power grids: A survey,” *Energies*, vol. 13, no. 9, 2020. [Online]. Available: <https://doi.org/10.3390/en13092219>
- [8] C. M and R. S, “Análisis del sistema eléctrico venezolano desde la perspectiva de la teoría de redes complejas,” *Revista de la Facultad de Ingeniería Universidad Central de Venezuela*, vol. 23, pp. 103–109, 03 2008. [Online]. Available: <https://bit.ly/3t2BIgk>
- [9] M. Newman, *Networks: An Introduction (1st edn)*. Oxford Academic, 2010. [Online]. Available: <https://doi.org/10.1093/acprof:oso/9780199206650.001.0001>
- [10] T. Bröhl and K. Lehnertz, “Centrality-based identification of important edges in complex networks,” *Chaos: An Interdisciplinary Journal of Nonlinear Science*, vol. 29, no. 3, Mar. 2019. [Online]. Available: <http://dx.doi.org/10.1063/1.5081098>
- [11] R. Ortiz-Gaona, M. Postigo-Boix, and J. L. Melus-Moreno, “Centrality metrics and line-graph to measure the importance of links in online social networks,” *International Journal of New Technology and Research*, vol. 2, no. 12, 12 2016. [Online]. Available: <https://bit.ly/3Ru4rnR>
- [12] O. de la Cruz Cabrera, M. Matar, and L. Reichel, “Edge importance in a network via line graphs and the matrix exponential,” *Numerical Algorithms*, vol. 83, no. 2, pp. 807–832, Feb 2020. [Online]. Available: <https://doi.org/10.1007/s11075-019-00704-y>
- [13] F. Harary, *Graph Theory*. Addison-Wesley Publishing Company. University of Minnesota, 1969. [Online]. Available: <https://bit.ly/4a9HYDV>
- [14] V. Pihur, S. Datta, and S. Datta, “Rank-aggreg, an R package for weighted rank aggregation,” *BMC Bioinformatics*, vol. 10, no. 1, p. 62, Feb 2009. [Online]. Available: <https://doi.org/10.1186/1471-2105-10-62>
- [15] P. Crucitti, V. Latora, and M. Marchiori, “A topological analysis of the italian electric power grid,” *Physica A: Statistical Mechanics and its Applications*, vol. 338, no. 1, pp. 92–97, 2004, proceedings of the conference A Nonlinear World: the Real World, 2nd International Conference on Frontier Science. [Online]. Available: <https://doi.org/10.1016/j.physa.2004.02.029>
- [16] P. Hines and S. Blumsack, “A centrality measure for electrical networks,” in *Proceedings of the 41st Annual Hawaii International Conference on System Sciences (HICSS 2008)*, 2008, pp. 185–185. [Online]. Available: <https://doi.org/10.1109/HICSS.2008.5>
- [17] K. Stephenson and M. Zelen, “Rethinking centrality: Methods and examples,” *Social Networks*, vol. 11, no. 1, pp. 1–37, 1989. [Online]. Available: [https://doi.org/10.1016/0378-8733\(89\)90016-6](https://doi.org/10.1016/0378-8733(89)90016-6)
- [18] S. Wasserman and K. Faust, *Social Network Analysis: Methods and Applications*, ser. Structural Analysis in the Social Sciences. Cambridge University Press, 1994. [Online]. Available: <https://doi.org/10.1017/CBO9780511815478>

- [19] A. B. M. Nasiruzzaman, H. R. Pota, and M. A. Mahmud, "Application of centrality measures of complex network framework in power grid," in *IECON 2011 - 37th Annual Conference of the IEEE Industrial Electronics Society*, 2011, pp. 4660–4665. [Online]. Available: <https://doi.org/10.1109/IECON.2011.6120079>
- [20] S. Arianos, E. Bompard, A. Carbone, and F. Xue, "Power grid vulnerability: A complex network approach," *Chaos: An Interdisciplinary Journal of Nonlinear Science*, vol. 19, no. 1, p. 013119, Feb 2009. [Online]. Available: <https://doi.org/10.1063/1.3077229>
- [21] K. Wang, B. Zhang, Z. Zhang, X. Yin, and B. Wang, "An electrical betweenness approach for vulnerability assessment of power grids considering the capacity of generators and load," *Physica A: Statistical Mechanics and its Applications*, vol. 390, no. 23, pp. 4692–4701, 2011. [Online]. Available: <https://doi.org/10.1016/j.physa.2011.07.031>
- [22] E. Bompard, R. Napoli, and F. Xue, "Analysis of structural vulnerabilities in power transmission grids," *International Journal of Critical Infrastructure Protection*, vol. 2, no. 1, pp. 5–12, 2009. [Online]. Available: <https://doi.org/10.1016/j.ijcip.2009.02.002>
- [23] R. Herrero and M. Herrero, "La terminología del análisis de redes. Problemas de definición y de traducción," *Política y sociedad, 2000*, vol. 33, 01 2000. [Online]. Available: <https://bit.ly/46P6IOK>
- [24] M. E. J. Newman, "Scientific collaboration networks. II. Shortest paths, weighted networks, and centrality," *Phys. Rev. E*, vol. 64, p. 016132, Jun 2001. [Online]. Available: <https://doi.org/10.1103/PhysRevE.64.016132>
- [25] M. Aruldoss, M. Lakshmi, and V. P. Venkatesan, "A survey on multi criteria decision making methods and its applications," *Science and Education Publishing*, vol. 11, pp. 31–43, 2013. [Online]. Available: <https://bit.ly/3GO3wbP>
- [26] R. Core Team, *R: A language and environment for statistical computing*. Foundation for Statistical Computing, Vienna, Austria, 2022. [Online]. Available: <https://bit.ly/484HuNg>
- [27] V. Pihur, S. Datta, and S. Datta, "Weighted rank aggregation of cluster validation measures: a Monte Carlo cross-entropy approach," *Bioinformatics*, vol. 23, no. 13, pp. 1607–1615, 2007. [Online]. Available: <https://doi.org/10.1093/bioinformatics/btm158>
- [28] G. Csardi and T. Nepusz, "The igraph software package for complex network research," *InterJournal*, vol. Complex Systems, p. 1695, 11 2005. [Online]. Available: <https://bit.ly/3TdyNfs>
- [29] C. M. Rocco, K. Barker, and J. Moronta, "Determining the best algorithm to detect community structures in networks: application to power systems," *Environment Systems and Decisions*, vol. 42, pp. 251–264, 2022. [Online]. Available: <https://doi.org/10.1007/s10669-021-09833-z>



OPTIMIZATION ALGORITHMS FOR ADAPTATIVE ROUTE SEQUENCING ON REAL-WORLD LAST-MILE DELIVERIES

ALGORITMOS DE OPTIMIZACIÓN PARA SECUENCIACIÓN ADAPTATIVA DE RUTAS REALES EN ENTREGAS DE ÚLTIMA MILLA

Fernando Hernández Gobertti^{1,*} , Rafael Sotelo¹ , Marcelo Forets² 

Received: 06-06-2023, Received after review: 14-09-2023, Accepted: 06-10-2023, Published: 01-01-2024

Abstract

This article explores the design and application of machine learning techniques to enhance traditional approaches for solving NP-hard optimization problems. Specifically, it focuses on the Last-Mile Routing Research Challenge (LMRRC), supported by Amazon and MIT, which sought innovative solutions for cargo routing optimization. While the challenge provided travel times and zone identifiers, the dependency on these factors raises concerns about the algorithms' generalizability to different contexts and regions with standard delivery services registries. To address these concerns, this study proposes personalized cost matrices that incorporate both distance and time models, along with the relationships between delivery stops. Additionally, it presents an improved approach to sequencing stops by combining exact and approximate algorithms, utilizing a customized regression technique alongside fine-tuned metaheuristics and heuristics refinements. The resulting methodology achieves competitive scores on the LMRRC validation dataset, which comprises routes from the USA. By carefully delineating route characteristics, the study enables the selection of specific technique combinations for each route, considering its geometrical and geographical attributes. Furthermore, the proposed methodologies are successfully applied to real-case scenarios of last-mile deliveries in Montevideo (Uruguay), demonstrating similar average scores and accuracy on new testing routes. This research contributes to the advancement of last-mile delivery optimization by leveraging personalized cost matrices and algorithmic refinements. The findings highlight the potential for improving existing approaches and their adaptability to diverse geographic contexts, paving the way for more efficient and effective delivery services in the future.

Keywords: Optimization, Routing, Operations, Logistics, International Competition

Resumen

Este artículo explora el diseño y aplicación de técnicas de aprendizaje automático para mejorar los enfoques tradicionales y así resolver problemas de optimización NP-hard. En particular, se enfoca en el Last-Mile Routing Research Challenge (LMRRC), apoyado por Amazon y MIT, que buscaba soluciones innovadoras para la optimización de rutas de carga. Si bien el desafío proporcionó tiempos de viaje e identificadores de zona, la dependencia de estos factores plantea preocupaciones sobre la generalización de los algoritmos a diferentes contextos y regiones con registros de servicios de entrega estándar. Para abordar estas interrogantes, este estudio propone matrices de costos personalizadas que incorporan modelos de distancia y tiempo, junto con las relaciones entre las paradas de entrega. Además, presenta enfoques mejorados para la secuenciación de paradas mediante la combinación de algoritmos exactos y aproximados, utilizando técnicas de regresión personalizada junto con metaheurísticas y refinamientos heurísticos ajustados. La metodología resultante logra puntajes competitivos en el conjunto de datos de validación LMRRC, que usa rutas de EE. UU. Al delinear cuidadosamente las características de la ruta, el estudio permite la selección de combinaciones de técnicas específicas para cada ruta, considerando sus atributos geométricos y geográficos. Además, las metodologías propuestas se aplican con éxito a escenarios de casos reales de entregas en Montevideo (Uruguay), demostrando puntajes promedio y precisión similares en nuevas rutas de prueba. Esta investigación contribuye al avance de la optimización de la entrega de última milla al aprovechar matrices de costos personalizadas y refinamientos algorítmicos. Los hallazgos resaltan el potencial para mejorar los enfoques existentes y su adaptabilidad a diversos contextos geográficos, allanando el camino para servicios de entrega más eficientes y efectivos en el futuro.

Palabras clave: Optimización, enrutamiento, operaciones, logística, competencia internacional

^{1,*}Facultad de Ingeniería, Universidad de Montevideo, Uruguay.

Corresponding author ✉: fhernandez@correo.um.edu.uy.

²Centro Universitario Regional del Este, Universidad de la República, Uruguay.

Suggested citation: Hernández, F.; Sotelo, R.; Forets, M. "Optimization algorithms for adaptative route sequencing on real-world last-mile deliveries," *Ingenius, Revista de Ciencia y Tecnología*, N.º 31, pp. 64-80, 2024, DOI: <https://doi.org/10.17163/ings.n31.2024.06>.

1. Introduction

The proper definition and sequencing of multiple stops on cargo routes has a direct practical impact on the transports' efficacy, logistics and fuel consumption [1]. These factors encourage the search of time-efficient and optimal solutions capable of performing acceptably under real and scalable use cases on every day and ever-growing demands of deliveries [2]. This section includes information with regard to the project genesis over an Amazon's and MIT's recent contest and continues to define the main problems subdivided as both supervised and unsupervised learning treated on this document. Finally, once these topics are considered, a consequent thematic flow is proposed, specifying basis and original contributions of this work.

1.1. Amazon's Last-Mile Routing Research Challenge, supported by MIT

During the course of March to June 2021, the competition known as LMRRC [3] took place, promoting the participants to group and solve a terrestrial cargo routing optimization problem with real routes data from cities of USA with great demand of last-mile deliveries (i.e. transportation from the initial deposit or station to several dropoff sites), seeking innovative original solutions for sequencing geographical nodes. These data corresponded to stops, packages and travel times information for each of the 6125 training and validation routes whose segmentation was already defined. There was a total of 1,457,175 packages and 898,415 stops, where several packages were linked to each stop, which at the same time were associated to a zone identifier specific to the city. Each of these routes also had an actual sequence with which to compare the results according to an 'order-differential' score that became smaller the best the algorithms performed and later generalized on testing set. The authors' team, named AlphaCentauri, classified as one of the top-performing team of the competition.

1.2. Problem Statement

With focus on expanding the LMRRC initiative, the global difficulties range from certain supervised learning aspects through prediction and routing algorithms with objectives of reaching the best possible results with respect to predefined solutions.

The current cargo routing problem requests to approximate a stops sequence solution diagrammed by experienced drivers based on previous package transports and route state knowledge. All packages are weightless but dimensioned, as well as the single transport units per route, which may involve a necessity to resupply at station. Also, some packages are subject to fairly loose time windows that limit the packages

provisioning hours. Then, most stops are linked to geographically distributed zones, with variable dependencies $1:n_i$ for packages and stops as well as stops and zones. All possible travel times combinations between stops are known in addition to their coordinates and the planned service time needed for each package. The problem is framed as a type of Asymmetric Traveling Salesman Problem with no return or a weighted Hamiltonian Path Problem with Time Windows and Capacity constraints.

This article follows a logical disposition in order to handle the full process of data preparation, structures organization, algorithms experimentation and results observation.

Figure 1 shows the global proposed thematic sequence. This article will primarily focus on the personalized cost matrices formulations and the adaptive stops routing through extremely diverse routes while examining main applications, limitations and errors of the methodologies.

1.3. Literature Review

Large-scale logistics clustering and routing optimization problems have been research topics since mid-20th century, even before the terminology and practices for unsupervised and supervised learning and contemporary applications premiered. Documents such as [4] sought using clustering among other techniques for production scheduling and mobilization optimal estimations, while [5] remains one of the first records of large routing problem solution approximation. Generalities of recent investigations on these topics are mentioned in this section, focusing on contents related to the current research.

1.3.1. Research on Cargo Routing

The general case of cargo routing involves searching for the optimal sequence of nodes (known as stops) on a set of routes for a fleet of vehicles that must satisfy some customer demands such as the roads' state, the vehicles' load capacity, the travel times between each stop, the processing times per package delivered, the time windows when some package needs to be dispatched and the drivers' working hours. In the following subsections, an overview of usual routing approaches is undertaken and an exposition through examples of recent routing investigation topics is presented.

1.3.2. Overview of Routing Approaches.

Certain cargo routing optimization are NP-hard problems [6] that involve ordering stops to fulfill constraints for a physical unit carrying dimensioned and weighted packages [7].

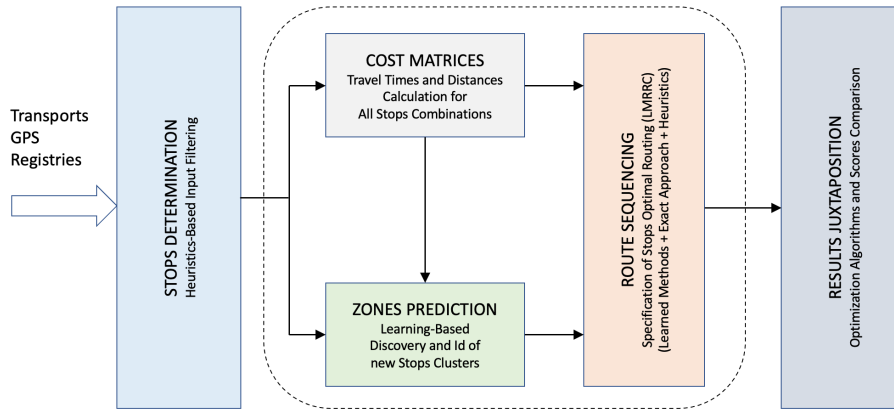


Figure 1. Diagram of the document’s entire flow consisting of grouped and ordered inter-dependable blocks. Delineated central block illustrates required validation over provided LMRRC’s datasets.

The initial problem formulation can vary, considering revisiting the starting stop and the use of single or multiple transport units. Figure 2 illustrates typical interrelated problems, including the NP-complete and NP-hard Vehicle Routing Problem (VRP) [8], that seeks minimum-length and minimum-time routes for a fleet. The Quadratic Assignment Problem (QAP) [9], assigns facilities to different locations to minimize distances multiplied by flows. The Travelling Salesman Problem (TSP) [10], finds the shortest sequence visiting each stop exactly once before returning to the

starting station. This problem has applications in logistics, microchip manufacturing [11], and DNA sequencing [12]. The Hamiltonian Path Problem (HPP) [13], a subproblem of TSP, searches for a global optimal sequence without returning to the station, aiming for a Hamiltonian-connected graph with unique paths between all vertices. Exhaustive search is not feasible due to the number of different Hamiltonian cycles: $\frac{(n-1)!}{2}$ a complete undirected graph with n stops and $(n-1)!$ in a complete directed graph.

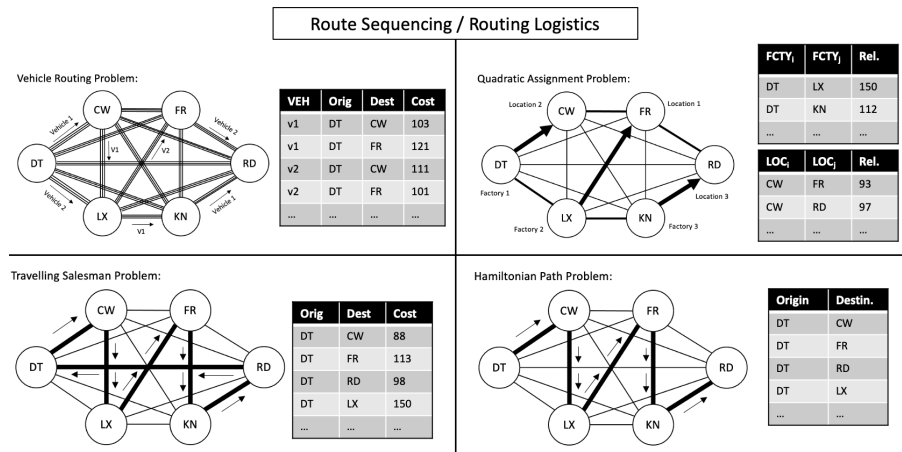


Figure 2. Different standard types of cargo routing problems. Nodes are labelled using stop names.

1.3.3. Related Routing Applications.

Globally, the routing scenarios tend to seek innovative and particular procedures through time-efficient algorithms that facilitate the enterprise’s effort for providing effective service as well as reduce transportation’s costs. This can be seen on documents such as [14], with recent Quantum Computing approaches to VRP using Quantum and Simulated Annealers. Similarly, possible

QAP resolutions are analyzed in [15–17], using QUBO and Ising formulations. In any case, although problem-specific in nature, the pursue for finding general use routing optimization protocols for air, sea and land transportation remains an active research area [18, 19].

Regarding TSP, multiple approaches have been developed, including standard logic algorithms such as greedy (e.g. nearest neighbour) and/or with dynamic programming, as well as with constructive heuristics

based approximations like multi-fragment [20] and different variable-opt techniques [21]. However, none of these possibilities reaches a global solution in polynomial time, and are deemed not applicable to the current problem, given the extended amount of stops in each route and their interrelationships.

With regards to the specific routing problem, the MIT’s LMRRC Technical Proceedings illustrate the proposals of several competitors that faced the challenge with a wide range of perspectives. Analyzing the finalists’ documents and algorithms, CHH [22] suggests doing local searches by travel time on which to apply precedence, path and neighbor restrictions for sequencing learned areas based on penalties. Then, GMW [23] presents an untrained approach by zones in three levels, together with a linear modification of the travel times cost matrix and a later stage of post-processing of the final sequence for possible sequence inversion. Similarly, ArsAb [24] brings a greedy procedure along with an already trained genetic algorithm with a TSP subroutine also based on penalizations. Finally, HSFv1 [25] puts forward a combination of exact and heuristic approaches that conciliates multiple possible perspectives and generalize appropriately to the LMRRC’s testing dataset (thus improving the resulting score with regards to validation routes).

1.3.4. Research on Multimethodologies

Multimethodologies for routing logistics have evolved over time to address the complex challenges associated with optimizing transportation routes together with improving e-commerce [26] and collaborative approaches [27] in order to improve efficiency as well as reduce delivery costs. Related recent studies [28,29] suggest diverse multistage hierarchical methods to solve

the vehicle routing problem for a heterogeneous fleet with various constraints, and its unique feature is the close proximity to real logistics practice. Other proposals [30,31] help to reduce post-harvest wastage during the collection process by using both internal and hired fleets with heterogeneous capacities and employing a Greedy algorithm-based heuristic and several local search methods to obtain near-optimal solutions.

Apart from interesting simultaneous methodologies for supply chain pickup and delivery for e-commerce [32] when being trained with a great deal of routes [33], there has been an increasing demand of efficient real-world mixed approaches due to the recent COVID epidemic [34]. The provided experimental results enrich the research related to vehicle routing problem models and algorithms under major public health emergencies and provide optimized relief distribution solutions for decision-makers of emergency logistics [35]. Similar articles [36] investigate a collaborative truck-drone routing problem for contactless parcel delivery in epidemic areas, which combines the Metropolis acceptance criterion [37] of Simulated Annealing and Tabu Search for urban logistics in smart cities [38].

2. Materials and methods

2.1. Cost Matrices Formulation

Defining cost matrices is crucial for sequencing procedures, enabling problem structuring and resolution. Even slight variations in these matrices can lead to significant changes in results for routing optimization. Figure 3 illustrates two approaches for defining cost matrices, each with their own variations for parameter combination and tuning.

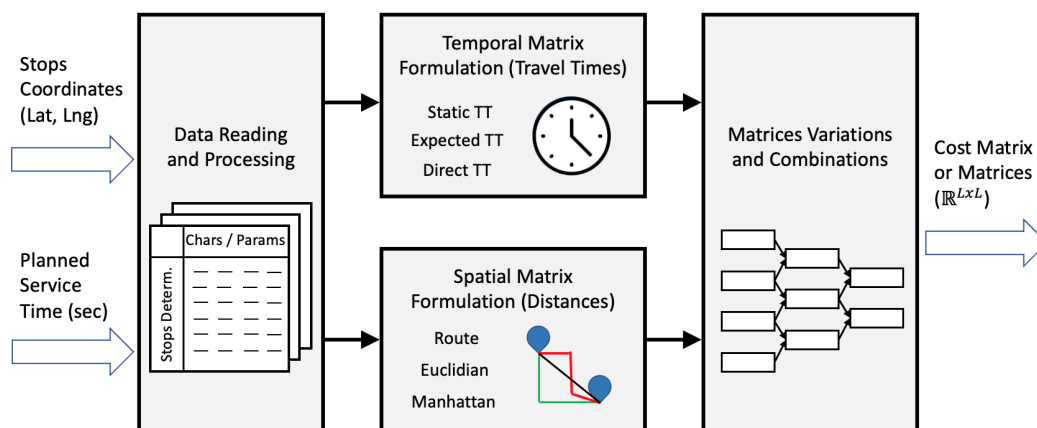


Figure 3. Cost prospects analysis considering temporal and distance information.

2.2. Temporal Information through Travel Times

Time-related data used as cost matrix is useful for abstract distance-independent approaches. The traditional parameter for general routing scenarios is using an asymmetrical squared travel times matrix where each element contains the value in seconds needed for unidirectional movement from one stop to another. For a given set of l stops, a general temporal matrix is defined in Equation (1).

$$StaticTT = \begin{bmatrix} 0 & tt_{1,2} & \dots & tt_{1,l-1} & tt_{1,l} \\ tt_{2,1} & 0 & \dots & tt_{2,l-1} & tt_{2,l} \\ \vdots & \vdots & \ddots & \vdots & \vdots \\ tt_{l-1,1} & tt_{l-1,2} & \dots & 0 & tt_{l-1,l} \\ tt_{l,1} & tt_{l,2} & \dots & tt_{l,l-1} & 0 \end{bmatrix} \quad (1)$$

$$\forall tt_{i,j} \in \mathbb{R}^+ : stop_i \rightarrow stop_j$$

This expression is known as the static travel times matrix, where usual transport characteristics (e.g. vehicle speed, acceleration) are considered.

A relevant alternative consists of the expected travel times matrix (Equation (2)), where an individual perturbation is associated to each element as transit properties for a given time and date (e.g. traffic jams, no signaling) are reported.

$$ExpectedTT(x, y) = tt_{x,y} + \epsilon_{x,y} \quad (2)$$

$$\forall tt_{x,y} \in StaticTT : stop_x \rightarrow stop_y$$

Thus, defining P as the set of packages associated to a given route, the current time trace (Equation (3)) counted for a sequence interval i is calculated as the sum of the starting route time with the planned service time per package and the travel times duration up to that point.

$$serviceTime_i = plannedService_{p_i}, \forall p \in P \quad (3a)$$

$$travelTime_i = tt_{a,b} \quad (3b)$$

$$\forall tt \in TT : stop_i = stop_a \rightarrow stop_b$$

$$time_i = time_0 + \sum_{j=1}^i serviceTime_j + travelTime_j \quad (3c)$$

Time considerations are important for travel times, including time windows, restrictions, and package-specific constraints. Simpler approaches use a constant vehicle speed, while more complex options consider distributed speeds based on street configurations.

2.3. Spatial Information through Distances

Distance-based data wielded as cost matrix is advantageous for geographical time-independent perspectives. Similar to previous temporal case, the general instance depicts a mainly asymmetric square matrix with distance values that unidirectionally links one stops with another. Analogous to time-dependent expression, all possible combinations are examined as in Equation (4).

$$D = \begin{bmatrix} 0 & d_{1,2} & \dots & d_{1,l-1} & d_{1,l} \\ d_{2,1} & 0 & \dots & d_{2,l-1} & d_{2,l} \\ \vdots & \vdots & \ddots & \vdots & \vdots \\ d_{l-1,1} & d_{l-1,2} & \dots & 0 & d_{l-1,l} \\ d_{l,1} & d_{l,2} & \dots & d_{l,l-1} & 0 \end{bmatrix} \quad (4)$$

$$\forall d_{i,j} \in \mathbb{R}^+ : stop_i \rightarrow stop_j$$

The mentioned distance element is considered to be indirect (i.e. Route distances, where street directions and silhouettes are respected) or direct (e.g. Euclidean or Manhattan distances, where street-related examinations are not needed). Formulations regarding these distances are:

$$d_{i,j} = \{d_{i,j}^R, d_{i,j}^2, d_{i,j}^\infty\}, \forall d \in D \text{ where } stop_i \rightarrow stop_j$$

$$d^{(R)}(x, y) = MapDirections(x, y) \Rightarrow (RouteD) \subset D \text{ with } d_{i,j} = d^{(R)}(i, j)$$

$$d^{(2)}(x, y) = \sqrt{(lat_x - lat_y)^2 + (lng_x - lng_y)^2} \Rightarrow (EuclideanD) \subset D, d_{i,j} = d^{(2)}(i, j)$$

$$d^{(\infty)}(x, y) = |lat_x - lat_y| + |lng_x - lng_y| \Rightarrow (ManhattanD) \subset D, d_{i,j} = d^{(\infty)}(i, j)$$

Then, the current distance trace (Equation (5)) with respect to a sequence interval i is calculated as the sum of all previous distances following the stops ordering.

$$dist_i = d_{a,b}, \forall d \in D : stop_i = stop_a \rightarrow stop_b$$

$$distance_i = \sum_{j=1}^i dist_j \quad (5)$$

Contrasting with current time calculation, the current distance expression is computationally easier to manage and dependable of fewer parameters once the spatial cost matrix is determined.

2.4. Mixed Information through Matrix Combinations

Matrix variations in time and space costs offer a different perspective on the problem, considering seemingly independent attributes. However, it is necessary to examine and tune combinations of standard parameters to achieve simplicity and generality.

The formulation of the mixed information matrix CCM is expressed in Equation (6), considering temporal and spatial matrices. Empirical observations show the similarity and redundancy of StaticTT and ExpectedTT for last-mile trajectories. DirectTT is deemed too general and imprecise, while the RoutedD cost matrix varies based on coordinates and local transportation updates.

$$ccm_{i,j} = ccm_{i,j}^t + ccm_{i,j}^d \quad (6)$$

$$\forall ccm \in CCM(\{\lambda^{(k)}\})$$

$$\text{where } ccm_{i,j}^t = \lambda_{i,j}^{(1)} stt + \lambda_{i,j}^{(2)} ett + \lambda_{i,j}^{(3)} dtt$$

$$\forall stt \in StaticTT, \forall ett \in ExpectedTT, \forall dtt \in DirectTT$$

$$\text{and } ccm_{i,j}^d = \lambda_{i,j}^{(4)} rd + \lambda_{i,j}^{(5)} ed + \lambda_{i,j}^{(6)} md$$

$$\forall rd \in RouteD, \forall ed \in EuclideanD, \forall md \in ManhattanD$$

2.5. Route Sequencing Algorithms

Route planning is vital for efficient transportation sequencing, determining the order of stops to optimize delivery. The LMRRC proposal considers various factors, such as time-expanded variations, metric and distance-based algorithms, and symmetric/asymmetric alternatives [39]. To address the challenge of multiple perspectives, a multi-approach method combining learning, exact, and heuristics methodologies is proposed.

Figure 4 depicts the procedural flow, including stop sequence generation, attribute, and cost matrix determination. The global section analyzes route features, employs regression for cluster ordering, and presents exact/heuristics approaches for individual stops. Validation results are compared using a variation score. This sequencing challenge was central in the LMRRC competition.

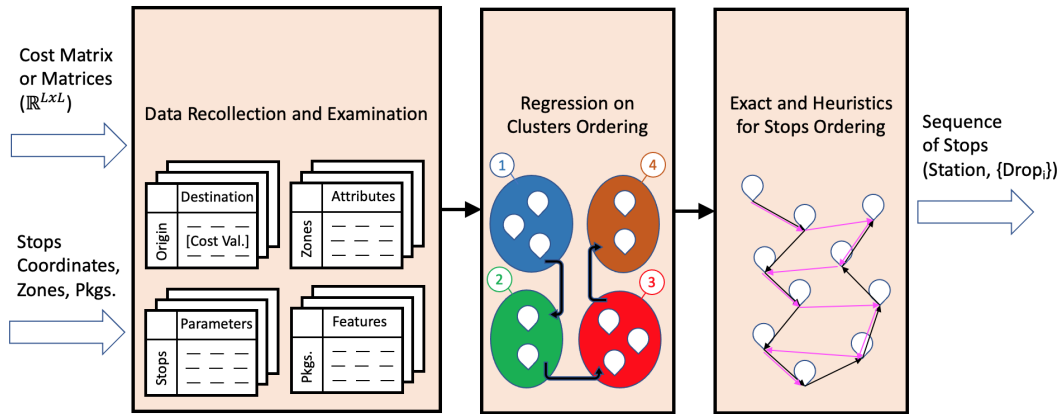


Figure 4. General routing sequencing flow treated in the section.

2.6. General Analysis

The proposed methodology adopts a systematic process that incorporates regression, exact, and heuristic approaches to provide a direct and comprehensive solution. Regression approaches utilize specific learning algorithms and past experimentation to make predictions. However, relying solely on regression can lead to predictions that are too dependent on the training data, especially when considering multiple cities and contexts. Exact approaches aim to find precise solutions

for constrained problems but can be computationally intensive for practical scenarios. Heuristic approaches, on the other hand, offer approximate solutions within reasonable time frames, albeit with reduced accuracy and precision. The proposed procedure strategically combines these approaches to maximize their utility.

Figure 5 illustrates the overall procedure that encompasses all the considered approaches, ensuring relevant results within a realistic timeframe. This noniterative nature of the methodology facilitates efficient execution.

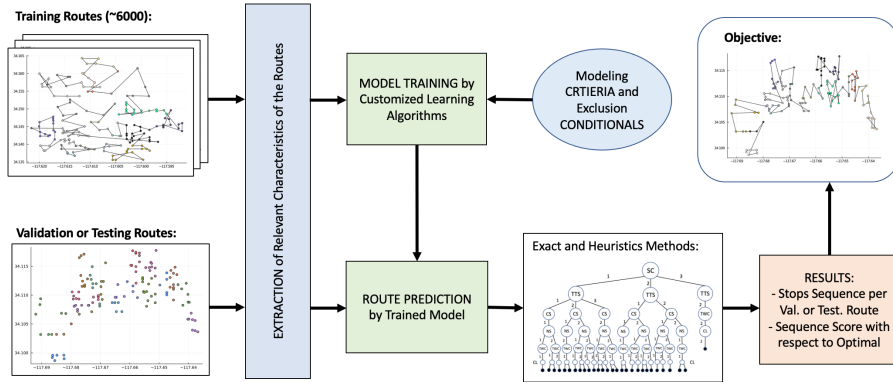


Figure 5. General routing process including a learning phase as well as exact and heuristics approaches.

Additionally, to enhance the initial analysis and facilitate comparison of final results, certain route features of interest are studied as part of the characteristics extraction step:

- **Route Extension Ratio (RER):** Spatial relation per route, considering its entire set of zones.
- **Zone Extension Ratio (ZER):** Spatial relation per zone, considering its entire set of stops.
- **Zone Extension Variation (ZEV):** Difference between maximum and minimum spatial dimensions of zones included in the route (averaging in longitude and latitude).
- **Stops Amount per Zone (SAZ):** Quantity of stops in a given zone from the data of a route.
- **Stops Variation per Zone (SVZ):** Difference between the maximum and minimum number of stops of the total set of zones belonging to the route of interest.
- **Zones Amount per Route (ZAR):** Quantity of zones in a given route.

The learning step estimates zone sequencing using LMRRC's training data and the observation that cluster order is generally preserved regardless of the city, aiming to minimize Unicode variation between contiguous stop groups. However, to account for cases where learned cluster sequences are not faithfully continued in subsequent routes, exclusion conditionals are defined. Global exact and heuristic perspectives with specific parameters are then employed to complete cluster ordering not covered by the learning step and arrange remaining stops.

2.7. Learning Methodology

The presented regression seeks to find relationships between contiguous stops clusters, based on the hypothesis that previously learned zone sequence is mostly

maintained and reiterated on further routes. Clusters are divided in four layers and identified with alphanumeric characters with an heterogeneous spatial distribution and dynamic silhouettes. This necessity for a learning methodology is rooted on routes visualization and examination of historical sequences, thus determining a correlation and dependency towards initially independent stops orderings which stem from clustering definition and identification consistencies.

2.7.1. Empirical Motivation.

Observed stop sequences follow a pattern of visiting all stops within a zone before proceeding, prioritizing contiguous clusters and accounting for zone and package structure. This suggests a layered approach, simplifying routing with an average of 8 stops per cluster and emphasizing accurate zone sequencing. Figure 6 illustrates this layered perspective, completing stops within zones before advancing, regardless of proximity. The learning approach focuses on major and minor zones, aiming for simplicity and variable results, as major layers remain stable within a route.

2.7.2. Algorithm for Cluster Ordering.

The training step of the regression algorithm builds a model from a training dataset, counting the repetitions of cluster sequences for major and minor zones independently, grouped in sets of 7. Major and minor zones consist of alphabetic and numeric layers, with the numeric layer being the most variable (e.g., 'A-F' and '1-25' character ranges). Relevant exclusion conditions include unequal first layers for major zones (i.e., $\text{dif}(M_1^{(j)}, M_1^{(j+1)}) \geq 1$), a difference of 3 or more points in the first layer of minor zones (i.e., $\text{dif}(m_1^{(j)}, m_1^{(j+1)}) \geq 3$), and a Unicode variation of 6 or more points across all zone layers (i.e., $\sum_i \text{dif}(z_i^{(j)}, z_i^{(j+1)}) \geq 6$). The model's depth is shallow for major zones but grows in specificity for minor

zones. Considering consistent repeatability of identifiers and an average of 21 clusters per route, the training algorithm has a complexity of $O(m)$ for routes with m zones and takes approximately 0.15 seconds on a 2.3 GHz Quad-Core i7 processor.

In the evaluation step, zones are initially ordered using the model sequences with the highest repetitions.

Unused clusters are then checked against sequences with progressively lower repetitions and incorporated into the initial ordering if found. If there are any remaining unused zones, they are ordered using exact and approximate designs explained in the next section. This process also has a complexity of $O(m)$ and takes around 0.4 seconds per route.

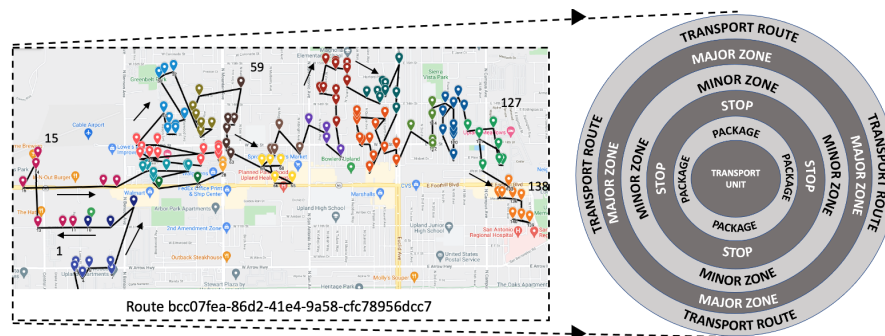


Figure 6. Layered approach to routing problem visualized through a route of California on Google Maps.

2.8. Exact and Approximate Approaches

In order to determine each cluster' stops sequence as well as to consider outliers and particularities from previous learning step, a set of rules exact and heuristics possibilities are defined. The suggested approaches, realized empirically through observation and parameter determinations, seek to provide solutions with realistic time complexities that approximate the given optimal results.

2.8.1. Procedure Design.

The process of defining rules begins by understanding the problem and classifying each input route based on RER, ZER, SAZ, and ZAR characteristics. Relevant

attributes are then determined, forming a hierarchy that mirrors the decisions made by actual sequences. The defined approaches and configurations are tested using a scheduling procedure with new routes. Finally, the results obtained from these formulations and executions are compared to optimize the output.

Figure 7 outlines the chronological guidelines for defining and testing exact and heuristic parameters. The scheduling involves three steps based on the attributes hierarchies mentioned earlier. The capacity approach has the least influence on the overall route structuring, making variables such as package dimensions auxiliary. The temporal approach, which involves calculations based on the current time and time window specifications, is also considered secondary compared to typical global route characteristics.

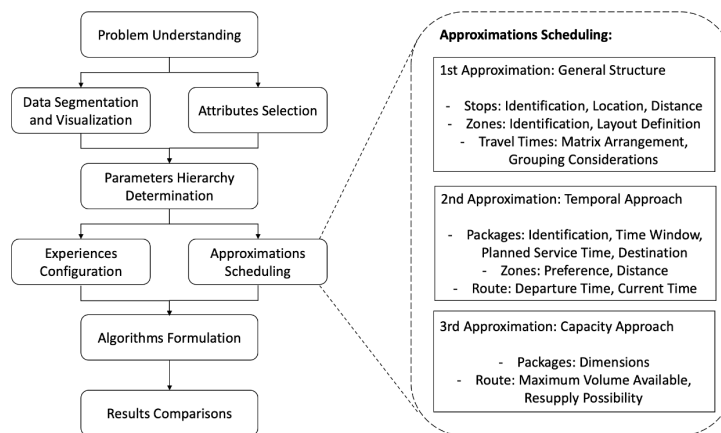


Figure 7. General design for exact and heuristics parameters' process definition.

2.8.2. Parameters Definition.

The following attributes are thus observed useful for routing designation, focusing on empirically relevant cases and approaches:

- **Clusters Sequencing (CS):** Order of zones that remain unused from learning approach.
 - **Metric distance (CS1):** Exact minimum euclidean separation from contiguous zones' baricenters determined as the geographical middle point of each cluster polygon.
 - **Set distance (CS2):** Heuristic minimum Hausdorff interval between contiguous zones.
- **Stops Ordering (SO):** Sequence of stops inside a given cluster.
 - **Global approach (SO1):** Exact reduced or exhaustive search for global minimum cost.
 - **Local approach (SO2):** Heuristic search for local minimum cost on contiguous stops.
- **Transition Stop Definition (TSD):** Determination of stops inbetween clusters.
 - **Last Inner Stop (TSD1):** Last stop of current cluster is first stop of following cluster.
 - **First Outer Stop (TSD2):** Local approach between clusters for first stop of next cluster.
- **Time Window Conditional (TWC):** Stops boost or delay in sequence based on time occurrence.
 - **Cluster perspective (TWC1):** Order modification based on exact time windows per cluster.
 - **Route perspective (TWC2):** Order modification based on heuristic global time windows.
- **Capacity Limitations (CL):** Necessity to resupply transport at deposit based on load excess.
 - **At cluster division (CL1):** Resupply before entering following cluster if needed.
 - **Maximum saturation (CL2):** Resupply when the unit locally reached maximum capacity.

The utilization of these tasks or parameters does not rely on a training step as each scenario is evaluated directly through each route examination. The mentioned cost matrix for this routing optimization problem is defined as mostly time dependent as in Equation (7).

$$CombinedCM = \alpha_1 ExpectedTT + \alpha_2 EuclideanD \quad (7)$$

where $(\alpha_1, \alpha_2) = (0.9, 0.2)$

The complexity needed for the evaluated cases using these approaches consists of $O(n + m)$ per route with n stops and m clusters, demanding for each route an average of 0.22 seconds on a 2.3 GHz Quad-Core i7 processor.

3. Results and discussion

3.1. Sequencing Examination

This section analyzes the validation sequences using qualitative and quantitative methods. LMRRRC provides a score metric to observe the ordering results, including Sequence Deviation (SD) and Edit Distance with Real Penalty (ERPe and ERPnorm).

$$score_{LMRRRC} = \frac{SD(A, B) \times ERP_{norm}(A, B)}{ERP_e(A, B)}$$

where $score_{LMRRRC} \in \mathbb{R}^+$

The metric yields positive values, where lower scores indicate better routing matching the optimal sequence. A score between 0.8 and 1.2 represents a uniformly random order, and the sequence must start at a station without repetition. Scores below 0.1 are considered competitive based on the LMRRRC criteria.

3.2. Validation Results for Regression.

The regression-based zones ordering had an average score variation of 0.06 between correct and incorrect cluster sequencing. Major zones order accounted for approximately 0.02 of the variation, while minor zones order contributed to a 0.04 variation due to increased variability.

The proposed segmentation of 7 clusters facilitated the identification of coherent repetitions during the training step, disregarding transition sequences between segments. However, this clustering error affected less than 5% of observed scenarios, ensuring efficient data management. The error arose from a maximum repetition of 3 contiguous clusters per segment, resulting in a significant number of interleaving clusters.

Figure 8 presents example results and route sequences illustrating the aforementioned considerations. The main cause of error during the evaluation step was the secondary checks of model sequences with fewer repetitions and cluster orders that had the same repetition quantity. An improvement could involve weighted repetitions counts based on Unicode variations or additional empirical observations.

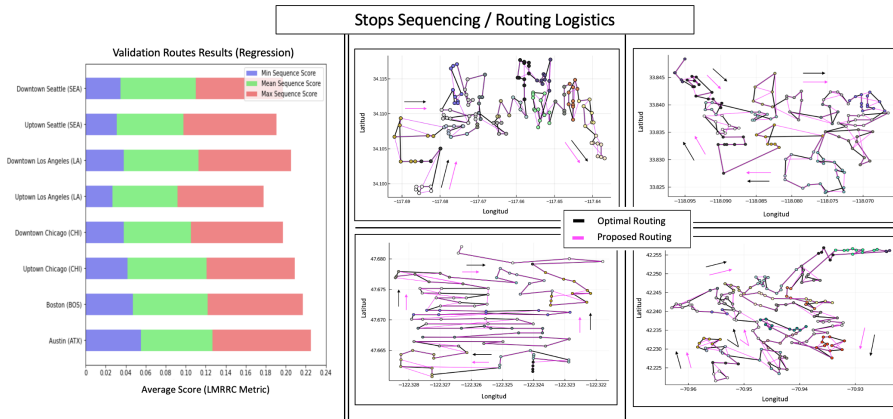


Figure 8. Results of approaches combinations on validation dataset, joined by sequencing layout of example routes with actual and proposed routing.

3.3. Multimethodologies Considerations.

Utilizing metaheuristic, exact, and heuristic methods enhances the precision of the global stop routing system, especially when combined with the initial regression-based approach. Combinations of these methods, as shown in Figure 9, adapt to different route attributes. By modifying routing parameters, the combinations exchange global and local analysis functionalities, assessing their impact on validation paths and identifying the most suitable permutations.

The combined exact and heuristic approaches yield superior results for routes with higher RER and ZAR, particularly in cities like Chicago, Los Angeles, and Seattle. CS2 outperforms CS1 with a score variance of

0.013, as seen in Figure 9 and Table 1. SO1 achieves the best mean score of approximately 0.006 for small SAZ and larger ZER, while TSD1 generally outperforms TSD2. TWC and CL have minimal effects, but TWC1 and CL2 yield slightly better results. CS1 and SO1 are more suitable for low ZEVs and high SVRs, while TSD2 and TWC1 also provide improvements with minimal variation in the CL attribute.

Figure 9 illustrates the method combinations based on route characteristics and their associated validation scores. The dominant source of error is the CS analysis, which significantly impacts results. Potential improvements involve defining new parameters and exploring additional variants within the proposed approaches.

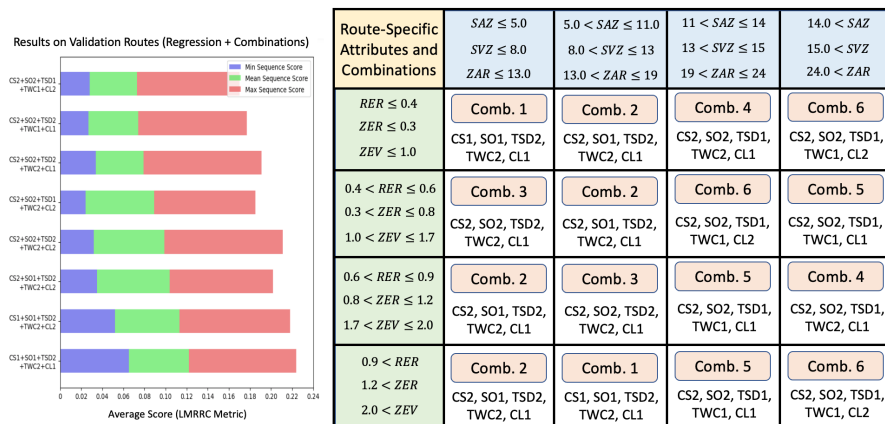


Figure 9. Average results and distributions of particular combinations of exact and approximate stop routing techniques, using characteristic route attributes.

Table 1. Evaluation of average results of combinations of methodologies of interest using the validation routes in different cities from USA provided by LMRRC.

Permutations	Austin	Boston	Chicago	Los Angeles	Seattle	Average Scores
Combination 1	0.0935	0.0930	0.0912	0.0905	0.0890	0.0914
Combination 2	0.0944	0.0941	0.0901	0.0883	0.0875	0.0909
Combination 3	0.0923	0.0914	0.0845	0.0836	0.0824	0.0868
Combination 4	0.0867	0.0884	0.0825	0.0817	0.0797	0.0838
Combination 5	0.0836	0.0861	0.0763	0.0792	0.0754	0.0801
Combination 6	0.0812	0.0794	0.0723	0.0665	0.0692	0.0737

3.4. Application to General Case

This section analyzes the testing results of the entire process, including stop differentiations, zone predictions, and customized routing mechanisms. The main observations pertain to the custom cost functions and adaptable routing techniques discussed in Sections 3 and 4. It concludes with observations on sequencing, clustering applications, and generalizations to routes outside of the United States. These route features have varying effects when combined with optimization algorithms derived from LMRRC competition.

3.5. Routes Characteristics

Obtained real datasets consists of 66 routes from the country Uruguay located in the Southern Cone of South America. Its cities are considerably smaller than those LMRRC selected, which usually translates to shorter distances and travel times between stops. They also have a centralized and populous downtown where businesses abound while bidirectional streets meager, and a peripheral and extended uptown where most markets and residential homes are localized. Given that transports travel daily to both city sections, their stations remain separated from about 20 kilometers of the nearest urban stop. Moreover, its cities' structures are not uniformly diagrammed, laying globally an average of 85 metres per block and a maximum of 145 metres which also impacts considered costs. Finally, the whole extension is fairly plain (i.e. with no stepped mountain nor valley) and lacking of bridges, tunnels or subways, which complicates long-distanced travel times.

3.6. Optimization Algorithms Selection

The decision over four routing methodologies derives from their LMRRC's ranking, availability and variability, being all defined using Julia and Python programming languages [40]. In particular, GMW is used given its focus and baseline on zone identifiers and its relationships. Then, ArsAb is selected due to its original genetic training phase and greater results on routes with more than 100 stops. Finally, the initial

HSFv1perspective, which declares a non-trained procedure as in GMWcase, provides better results with extremes latitude over longitude route ratio.

These algorithms are all extracted from the MIT's LMRRC Technical Proceedings [41], discussed on Section 1.3.3. Also, in addition to juxtapose results over mentioned algorithms, the current proposition HSFv2with a previous training phase and improved evaluative approaches is compared, reaching satisfactory and competitive results with more direct approaches that successfully determines and makes use of the characteristics of each location. Indeed, the proposed procedure empirically benefit from the diversity of selected multimethodologies and the simplicity of its combinations. Preceding stops and zones determination are used as preliminary steps for all algorithms.

3.7. Optimization Algorithms Results

The selected routes had square spatial extensions and clustered stops with minimal intersections, aiding zone identification and stop classification. Increased stops per zone led to non-square spatial extensions, introducing higher complexity favoring local heuristics over global approaches. Multiple nexus zones had distinct identifiers in different route analyses, but tuned parameters remained useful for new routes with minimal score variation.

Figure 10 shows a test route with concentrated stops in downtown areas and scattered stops elsewhere, with zone prediction not prioritizing cluster characteristics.

Table 2 displays quantitative results for the four routing algorithms. GMW consistently achieved better metrics with lower variance as the number of stops increased. ArsAb performed similarly for routes with many stops. HSFv2 improved over HSFv1, especially for intermediate route lengths. Zone sequencing was the main source of error, as learning was based on non-local training routes.

The proposed algorithms perform and escalates adequately in terms of time and spatial complexity when applied to last-mile routes with lengths of at most 155 stops on a 2.3 GHz Quad-Core i7 proces-

sor, with comparable and lower complexities than the aforementioned competition algorithms. This is considered acceptable, given the demands considerations of current real-world last-mile routes.

The selected procedures also remain flexible to further customization by modifying the cost matrices parameters as well as by enabling a different combination of sequencing attributes, aiming at supporting

multiple transportation modes and constraints. Indeed, filtering sequencing attributes, particularly CS considerations, allow for more operative resource availability which translates to faster processing times and a greater scalability of the sequencing process.

Despite additional error sources from customized stops and zone predictions, the scores generally outperformed LMRRC's sequences with similar averages.

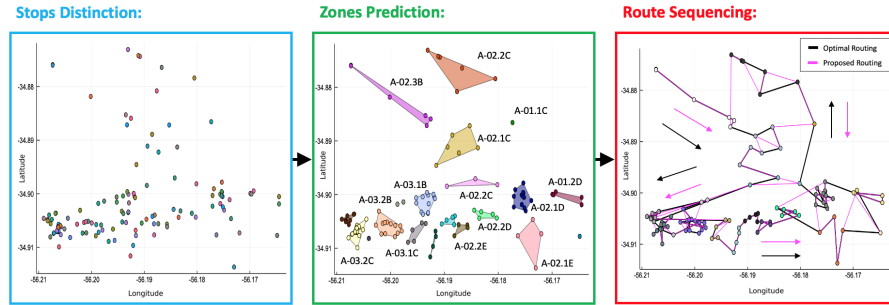


Figure 10. Visualization over key flow steps using an example testing route of Montevideo (Uruguay).

Table 2. Applied algorithms result scores on testing routes, displayed with format (Min, Average, Max).

Route length	GMW [e-04]	ArsAb [e-04]	HSFv1 [e-04]	HSFv2 [e-04]
< 50 stops	(279, 494, 656)	(298, 536, 731)	(432, 1077, 2322)	(387, 839, 1098)
50-79 stops	(263,482,647)	(286, 525, 758)	(428, 1066, 2291)	(368, 790,1077)
80-100 stops	(255, 474, 632)	(283, 522, 783)	(425, 1059, 2267)	(352, 769, 1052)
> 100 stops	(237, 461, 625)	(251, 507, 793)	(391, 1045, 2254)	(324, 721, 1042)

4. Conclusions

This section summarizes and describes the main accomplishments of this project with focus on processes generalization, including observations on future related research possibilities and considerations aimed at corroborating and improving obtained results.

4.1. Global Summary

To summarize, this document provides a review of important project components, followed by key principles and methodologies employed. Limitations and sources of error related to the problems of interest are also discussed. The proposed methodology expands the LMRRC contest initiative by sequencing and planning geographically diverse routes using raw GPS records and datasets from the US and Uruguay. The process includes record filtering, prediction of new stop groups, and a combination of regression, exact, and heuristic approaches for routing. Applying this procedure to the provided data yields competitive scores in validation routes (US) and demonstrates acceptable adaptation

and generalization in test routes (Uruguay) from both LMRRC and OTUC.

4.1.1. Relevant Limitations

The designs and applications of problem models in transport logistics aim to achieve efficient objectives. However, there are practical limitations that hinder their adaptability:

- Limited availability of routes and real routes from specific cities at an international level, provided by official entities, restricts the ability to conduct extensive and comprehensive studies on various structural possibilities.
- Fixed precision of coordinate and numerical data from GPS for waypoint detection, as well as numerical values related to temporal and spatial attributes for cost matrix formulations, impose constraints on the accuracy of the models.
- Customized cost matrices can be complex to create and maintain, especially for large and complex routing problems.

- Euclidean distance is not scaling invariant, meaning that multiplying the data by a common factor will change the distance. Manhattan distance does not take into account the curvature of the Earth, which can lead to inaccurate distance calculations for long distances.
- Expected travel time can be difficult to estimate accurately, especially in dynamic traffic conditions.
- Finite number of proposed combinations of exact and heuristic approaches for stop sequencing balances the need for precise results while avoiding overfitting the global model for additional traversal cases.

Considering limitations helps analyze the proposal, suggest improvements, and guide future works.

4.1.2. Main Error Sources

The main errors identified in the proposal's global procedure are as follows:

- Loss of sequences of zones of interest in the regression model due to the grouping of 7 zones and limited repetition of zones across routes within the same city.
- The accuracy of a customized cost matrix depends on the quality of the data used to create it. If the data is inaccurate or incomplete, then the cost matrix will not be accurate.
- Increased variance of temporal information in comparison to relatively static distance measurements.
- In contrast to time measurements, different distances may be measured in different units (e.g., miles and kilometers) depending on the source.
- High variability of path attributes, posing challenges in determining combinations of meta-heuristic and heuristic approaches while maintaining a balance between performance and score differences.

These errors significantly impact the final results and hinder achieving optimal resolutions. However, despite these limitations, the project still meets the satisfactory accuracy target within its scope.

4.2. Future Research Possibilities

Logistics and optimization techniques are constantly evolving with technology, aiming to provide better services. This project can be expanded within the same

research area and complementary themes to offer original contributions for complex issues in academic and commercial environments.

Future possibilities include extending the proposed algorithms to similar contexts and sharing tools with relevant entities. Emphasis would be placed on disseminating and increasing the project's visibility, ensuring functional compatibility with applications and developing user-friendly software.

Another possibility is exploring the cargo routing problem using quantum perspectives, such as adiabatic annealers, variational methods, and quantum learning. These approaches address combinatorial complexity and utilize quantum computing's potential for massive data management, analysis, and processing. They align with the growing demand for optimization in transport logistics and attract scientists and engineers worldwide to collaborate on routing optimization strategies.

Acknowledgment

We would like to share our appreciation with Universidad de Montevideo for their initiative and support, together with Amazon.com, MIT (Massachusetts Institute of Technology) as well as CINOI (Industrial Organization's Innovation Center) and OTUC (Urban Cargo Transport Observatory) for the fundamental real route data provisioning.

References

- [1] S. Pratap, M. Zhang, C. Shen, and G. Q. Huang, "A multi-objective approach to analyse the effect of fuel consumption on ship routing and scheduling problem," *International Journal of Shipping and Transport Logistics*, vol. 11, p. 161, 01 2019. [Online]. Available: <http://dx.doi.org/10.1504/IJSTL.2019.099270>
- [2] O. Turbaningsih, "The study of project cargo logistics operation: a general overview," *Journal of Shipping and Trade*, vol. 7, no. 1, p. 24, Nov 2022. [Online]. Available: <https://doi.org/10.1186/s41072-022-00125-6>
- [3] MIT, *Amazon last-mile routing research challenge. Supported by the MIT center for transportation logistics*. MIT center for transportation logistics, 2023. [Online]. Available: <https://bit.ly/47N0Q9O>
- [4] A. Charnes, W. W. Cooper, and R. O. Ferguson, "Optimal estimation of executive compensation by linear programming," *Management Science*, vol. 1, no. 2, pp. 138–151, 1955. [Online]. Available: <https://doi.org/10.1287/mnsc.1.2.138>
- [5] G. B. Dantzig, D. R. Fulkerson, and S. M. Johnson, *Solution of a Large-Scale Traveling-Salesman*

- Problem*. Santa Monica, CA: RAND Corporation, 1954. [Online]. Available: <https://bit.ly/3GqKp7p>
- [6] Z. Wang, M. Zhang, R. Chu, and L. Zhao, “Modeling and planning multimodal transport paths for risk and energy efficiency using and/or graphs and discrete ant colony optimization,” *IEEE Access*, vol. 8, pp. 132 642–132 654, 2020. [Online]. Available: <https://doi.org/10.1109/ACCESS.2020.3010376>
- [7] Y. Niu, Z. Yang, P. Chen, and J. Xiao, “A hybrid tabu search algorithm for a real-world open vehicle routing problem involving fuel consumption constraints,” *Complexity*, vol. 2018, pp. 1–12, 02 2018. [Online]. Available: <https://doi.org/10.1155/2018/5754908>
- [8] M. Asghari and S. M. J. Mirzapour Al-e-hashem, “Green vehicle routing problem: A state-of-the-art review,” *International Journal of Production Economics*, vol. 231, p. 107899, 2021. [Online]. Available: <https://doi.org/10.1016/j.ijpe.2020.107899>
- [9] H. Zhang, F. Liu, Y. Zhou, and Z. Zhang, “A hybrid method integrating an elite genetic algorithm with tabu search for the quadratic assignment problem,” *Information Sciences*, vol. 539, pp. 347–374, 2020. [Online]. Available: <https://doi.org/10.1016/j.ins.2020.06.036>
- [10] M. M. Flood, “The traveling-salesman problem,” *Operations Research*, vol. 4, no. 1, pp. 61–75, 1956. [Online]. Available: <https://bit.ly/47K2OHY>
- [11] K. Saito, M. Aono, and S. Kasai, “Amoeba-inspired analog electronic computing system integrating resistance crossbar for solving the traveling salesman problem,” *Scientific Reports*, vol. 10, no. 1, p. 20772, Nov 2020. [Online]. Available: <https://doi.org/10.1038/s41598-020-77617-7>
- [12] H. Bennaceur and E. Alanzi, “Genetic algorithm for the travelling salesman problem using enhanced sequential constructive crossover operator,” *International Journal of Computer Science and Security (IJCSS)*, vol. 11, p. 42, 01 2017.
- [13] A. Sergeenko, O. Granichin, and M. Yakunina, “Hamiltonian path problem: the performance comparison deoxyribonucleic acid computing and the branch-and-bound method,” *Journal of Physics: Conference Series*, vol. 1536, no. 1, p. 012003, may 2020. [Online]. Available: <https://dx.doi.org/10.1088/1742-6596/1536/1/012003>
- [14] M. Borowski, P. Gora, K. Karnas, M. Błajda, K. Król, A. Matyjasek, D. Burczyk, M. Szewczyk, and M. Kutwin, “New hybrid quantum annealing algorithms for solving vehicle routing problem,” in *Computational Science – ICCS 2020*, V. V. Krzhizhanovskaya, G. Závodszy, M. H. Lees, J. J. Dongarra, P. M. A. Sloot, S. Brissos, and J. Teixeira, Eds. Cham: Springer International Publishing, 2020, pp. 546–561. [Online]. Available: https://doi.org/10.1007/978-3-030-50433-5_42
- [15] F. Hernández, K. Díaz, M. Forets, and R. Sotelo, “Application of quantum optimization techniques (QUBO method) to cargo logistics on ships and airplanes,” in *2020 IEEE Congreso Biental de Argentina (ARGENCON)*, 2020. [Online]. Available: <https://doi.org/10.1109/ARGENCON49523.2020.9505401>
- [16] S. J. Weinberg, F. Sanches, T. Ide, K. Kamiya, and R. Correll, “Supply chain logistics with quantum and classical annealing algorithms,” *Scientific Reports*, vol. 13, no. 1, p. 4770, Mar 2023. [Online]. Available: <https://doi.org/10.1038/s41598-023-31765-8>
- [17] R. Haba, M. Ohzeki, and K. Tanaka, “Travel time optimization on multi-agv routing by reverse annealing,” *Scientific Reports*, vol. 12, no. 1, p. 17753, Oct 2022. [Online]. Available: <https://doi.org/10.1038/s41598-022-22704-0>
- [18] P. T. G. dos Santos and D. Borenstein, “Multi-objective optimization of the maritime cargo routing and scheduling problem,” *International Transactions in Operational Research*, vol. 31, no. 1, pp. 221–245, 2024. [Online]. Available: <https://doi.org/10.1111/itor.13147>
- [19] M. Olskevych, V. Danchuk, and O. Mastyash, “Cross-docking cargo delivery routing for guaranteed minimum period,” *Transport Technologies*, vol. 3, no. 1, 2022. [Online]. Available: <https://doi.org/10.23939/tt2022.01.038>
- [20] M. El Krari, B. Ahiod, and B. El Benani, “An empirical study of the multi-fragment tour construction algorithm for the travelling salesman problem,” in *Proceedings of the 16th International Conference on Hybrid Intelligent Systems (HIS 2016)*, A. Abraham, A. Haqiq, A. M. Alimi, G. Mezzour, N. Rokbani, and A. K. Muda, Eds. Cham: Springer International Publishing, 2017, pp. 278–287.
- [21] Punnen, Margot, and Kabadi, “TSP heuristics: Domination analysis and complexity,” *Algorithmica*, vol. 35, no. 2, pp. 111–127, Feb 2003. [Online]. Available: <https://doi.org/10.1007/s00453-002-0986-1>
- [22] W. Cook, S. Held, and K. Helsgaun, “Constrained local search for last-mile routing,” in *Technical Proceedings of the Amazon Last Mile Routing*

- Research Challenge*, 12 2021. [Online]. Available: <https://bit.ly/3sZsS35>
- [23] X. Guo, B. Mo, and Q. Wang, “Amazon last-mile delivery trajectory prediction using hierarchical TSP with customized cost matrix,” *Technical Proceedings of the Amazon Last Mile Routing Research Challenge*, 2023. [Online]. Available: <https://bit.ly/46E0QrC>
- [24] O. Arsian and R. Abay, *Data-driven vehicle routing in last-mile delivery*. Cirrelt, 2021. [Online]. Available: <https://bit.ly/47GLXpg>
- [25] F. Hernández, R. Sotelo, and M. Forets, “Combined exact and heuristicsbased approach to hamiltonian path problem optimization for routeplanning,” *Technical Proceedings of the Amazon Last Mile Routing Research Challenge*, 2021. [Online]. Available: <https://bit.ly/4a3joVh>
- [26] A. Escudero-Santana, J. Muñuzuri, A. Lorenzo-Espejo, and M.-L. Muñoz-Díaz, “Improving e-commerce distribution through last-mile logistics with multiple possibilities of deliveries based on time and location,” *Journal of Theoretical and Applied Electronic Commerce Research*, vol. 17, no. 2, pp. 507–521, 2022. [Online]. Available: <https://doi.org/10.3390/jtaer17020027>
- [27] H. Wen, Y. Lin, H. Wan, S. Guo, F. Wu, L. Wu, C. Song, and Y. Xu, “Deeproute+: Modeling couriers’ spatial-temporal behaviors and decision preferences for package pick-up route prediction,” *ACM Trans. Intell. Syst. Technol.*, vol. 13, no. 2, jan 2022. [Online]. Available: <https://doi.org/10.1145/3481006>
- [28] M. Bilgin and N. Bulut, “Compatibility themed solution of the vehicle routing problem on the heterogeneous fleet,” *The International Arab Journal of Information Technology*, vol. 19, 01 2022. [Online]. Available: <http://dx.doi.org/10.34028/iajit/19/5/9>
- [29] X. Xu, W. Liu, M. Jiang, and Z. Lin, “A multi-cycle and multi-echelon location-routing problem for integrated reverse logistics,” *Industrial Management & Data Systems*, vol. 122, no. 10, pp. 2237–2260, Jan 2022. [Online]. Available: <https://doi.org/10.1108/IMDS-01-2022-0015>
- [30] M. Fernando, A. Thibbotuwawa, H. N. Perera, and R. C. Ratnayake, “Close-open mixed vehicle routing optimization model with multiple collecting centers to collect farmers’ perishable produce,” in *2022 International Conference for Advancement in Technology (ICONAT)*, 2022. [Online]. Available: <https://doi.org/10.1109/ICONAT53423.2022.9725977>
- [31] R. Ivut and I. Tsarenkova, “Formation of logistics approach to economic development of road sector of the republic of belarus,” *Science & Technique*, vol. 21, no. 1, pp. 73–81, 2022. [Online]. Available: <https://doi.org/10.21122/2227-1031-2022-21-1-73-81>
- [32] M. I. D. Ranathunga, A. N. Wijayanayake, and D. H. H. Niwunhella, “Simulation-based efficiency assessment of integrated first-mile pickup and last-mile delivery in an e-commerce logistics network,” in *2022 International Research Conference on Smart Computing and Systems Engineering (SCSE)*, vol. 5, 2022, pp. 246–253. [Online]. Available: <https://doi.org/10.1109/SCSE56529.2022.9905083>
- [33] Y. Zhang, “Research on electronic commerce logistics dispatching routing optimization method under the background of big data,” in *Proceedings of the 7th International Conference on Intelligent Information Processing*, ser. ICIP ’22. New York, NY, USA: Association for Computing Machinery, 2023. [Online]. Available: <https://doi.org/10.1145/3570236.3570272>
- [34] F. Baig, K. Kirytopoulos, J. Lee, E. Tsamilis, R. Mao, and P. Ntzeremes, “Changes in People’s Mobility Behavior in Greece after the COVID-19 Outbreak,” *Sustainability*, vol. 14, no. 6, March 2022. [Online]. Available: <https://bit.ly/3uKuTAz>
- [35] L. Du, X. Li, Y. Gan, and K. Leng, “Optimal model and algorithm of medical materials delivery drone routing problem under major public health emergencies,” *Sustainability*, vol. 14, no. 8, 2022. [Online]. Available: <https://doi.org/10.3390/su14084651>
- [36] G. Wu, N. Mao, Q. Luo, B. Xu, J. Shi, and P. N. Suganthan, “Collaborative truck-drone routing for contactless parcel delivery during the epidemic,” *IEEE Transactions on Intelligent Transportation Systems*, vol. 23, no. 12, pp. 25 077–25 091, 2022. [Online]. Available: <https://doi.org/10.1109/TITS.2022.3181282>
- [37] J. Chang, C. Y. Tang, and Y. Zhu, “Efficiently handling constraints with metropolis-adjusted langevin algorithm,” *ArXiv*, 2023. [Online]. Available: <https://bit.ly/3Rs0Fv7>
- [38] M.-Y. Wu, C.-K. Ke, and S.-C. Lai, “Optimizing the routing of urban logistics by context-based social network and multi-criteria decision analysis,” *Symmetry*, vol. 14, no. 9, 2022. [Online]. Available: <https://doi.org/10.3390/sym14091811>

- [39] A. Arigliano, G. Ghiani, A. Grieco, E. Guerriero, and I. Plana, “Time-dependent asymmetric traveling salesman problem with time windows: Properties and an exact algorithm,” *Discrete Applied Mathematics*, vol. 261, pp. 28–39, 2019, GO X Meeting, Rigi Kaltbad (CH), July 10–14, 2016. [Online]. Available: <https://doi.org/10.1016/j.dam.2018.09.017>
- [40] F. Hernandez. (2021) *Smarrouting*. Github. [Online]. Available: <https://bit.ly/3sEdSaJ>
- [41] M. Winkenbach, S. Parks, and J. Noszek, *Technical Proceedings of the Amazon Last Mile Routing Research Challenge*. MIT Libraries, 2021. [Online]. Available: <https://bit.ly/4a3joVh>



LIQUEFIED PETROLEUM GAS SYSTEMS: A REVIEW ON DESING AND SIZING GUIDELINES

SISTEMAS DE GAS LICUADO DE PETRÓLEO: UNA REVISIÓN SOBRE LINEAMIENTOS DE DISEÑO Y DIMENSIONAMIENTO

Diego Venegas-Vásquez^{1,*} , César Ayabaca-Sarria² ,
 Salvatore Reina-Guzmán² , Luis Tipanluisa-Sarchi³ , Óscar Farías-Fuentes⁴ 

Received: 15-05-2023, Received after review: 26-06-2023, Accepted: 17-07-2023, Published: 01-01-2024

Abstract

Liquefied Petroleum Gas (LPG) is a fossil fuel widely used in residential, commercial, and industrial applications. LPG systems must be designed and sized considering minimum safety standards established in national and international regulations. An LPG system comprises fuel storage containers, pipelines, valves, meters, consumption equipment, and safety and protection elements. These must be sized and selected to withstand the action of the fuel gas and the working conditions to which they will be subjected. This article presents a review of the most important points to consider in the design and sizing of an LPG system based on the most representative international regulations.

Keywords: Liquefied Petroleum Gas, sizing, installations, safety, normative, criteria

Resumen

El gas licuado de petróleo (GLP) es un combustible de origen fósil ampliamente utilizado en aplicaciones residenciales, comerciales e industriales. Los sistemas de GLP deben diseñarse y dimensionarse bajo estándares mínimos de seguridad, los cuales son establecidos en normativas nacionales e internacionales. Un sistema de GLP está conformado por recipientes de almacenamiento del combustible, tuberías, válvulas, medidores, equipos de consumo y elementos de protección y seguridad. Estos deben ser dimensionados y seleccionados para soportar la acción del gas combustible y las condiciones de trabajo a las que serán sometidos. En este documento se presenta una revisión de los puntos más importantes a tener en cuenta en el diseño y dimensionamientos de un sistema de GLP a partir de las normativas más representativas a nivel internacional.

Palabras clave: gas licuado de petróleo, dimensionamiento, instalaciones, seguridad, normativas, criterios

^{1,*}Doctorado en Ingeniería de Materiales y Procesos Sustentables, Universidad del Bio-Bio, Chile.
 Corresponding author ✉: dvenegas@ubiobio.cl.

²Facultad de Ingeniería, Escuela Politécnica Nacional, Quito, Ecuador.

³Facultad de Mecánica, Escuela Superior Politécnica de Chimborazo, Riobamba, Ecuador.

⁴Departamento de Ingeniería Mecánica, Universidad de Concepción, Chile

Suggested citation: Venegas-Vásquez, D.; Ayabaca-Sarria, C.; Reina-Guzmán, S.; Tipanluisa-Sarchi, L. and Farías-Fuentes, O. "Liquefied Petroleum Gas Systems: A Review On Desing And Sizing Guidelines," *Ingenius, Revista de Ciencia y Tecnología*, N.º 30, pp. 81-94, 2024, DOI: <https://doi.org/10.17163/ings.n31.2024.07>.

1. Introduction

Energy demand worldwide is experiencing an annual increase due to rapid population growth, lifestyle changes, and industrialization [1]. In 2019, global energy consumption reached 418 EJ, and a 23% increase is expected by 2040, reaching 516 EJ. Currently, over 80% of the energy comes from fossil fuels, with oil, coal, and natural gas accounting for 30.9%, 26.8%, and 23.2%, respectively [2]. Regarding petroleum derivatives, liquefied petroleum gas (LPG) is one of the most widely used fuels globally due to its versatility as an energy source in domestic, commercial, and industrial services [3]. Despite its fossil origin, it is considered a clean fuel in terms of emissions to the environment since it does not contain sulfur. Therefore, during combustion, it does not emit SO_X [4], making it an attractive energy source.

To use LPG systems, storage, distribution, regulation, and control elements are required, which must be installed considering safety standards established in international technical norms such as NFPA 58 [5]. In Ecuador, compliance with the Ecuadorian Technical Standard INEN 2260:2010 [6] is followed to minimise risks associated with fuel handling. These technical norms outline the minimum safety requirements to be considered by those responsible for LPG installations, fuel distributors, and authorities tasked with overseeing compliance. The NFPA 58 standard has been in effect since 1930, serving as the foundation for LPG systems regulations in most countries worldwide [7–9]. In Ecuador, the first version of the INEN 2260 technical standard was developed in 2001 and has undergone two revisions to the current version, in force since 2010.

The technical standards in force in each country establish the minimum conditions for implementing LPG system projects. These regulations cover aspects such as the acceptance of types, materials and manufacturing standards for pipelines, safety distances between containers and third parties, and physical and human safety and protection. Compliance with these standards is usually mandatory within the corresponding territorial jurisdiction. However, these documents do not provide specific design parameters or technical criteria to ensure the feasibility of projects involving liquefied petroleum gas systems. They also do not include information about brands and manufacturers of different components or mention elements with higher safety standards. This information is typically found in manufacturer catalogs and specialized journals.

This article reviews the minimum safety guidelines established in international technical standards for handling liquefied petroleum gas (LPG) systems and their surroundings. Additionally, it examines details related to the design, selection, location, and maintenance of elements and parts of LPG systems. It also addresses important aspects that must be considered

by the technical authorities responsible for the systems during the approval process by the competent authority. The article presents advantages and recommendations provided by manufacturers of equipment and materials used in LPG systems. Finally, it highlights some poor practices observed in LPG systems to alert users unfamiliar with handling combustible gas like LPG.

1.1. LPG properties

- LPG is typically pressurized, stored, and transported above its boiling point. Upon release, it evaporates rapidly and, being denser than air (with a relative specific gravity of 1.53 with respect to air [5]), tends to accumulate in low-lying areas near the ground. In the presence of an ignition source, this can lead to an explosion and fire.
- LPG vapor forms an explosive compound at concentrations between 2% and 10 % [10].
- LPG is mainly composed of butane (C_4H_{10}) and propane (C_3H_8), with a small amount of lighter and heavier compounds, such as ethane and pentane. It is produced as a byproduct of natural gas and crude oil refining and production processes [11].
- LPG has a higher calorific value than other energy sources (the maximum calorific value of LPG is approximately 50.3 MJ/m^3 or $12\ 000 \text{ kcal/m}^3$ [8]).
- LPG is gaseous under ambient conditions (1 atm and $25 \text{ }^\circ\text{C}$).
- The specific gravity of LPG in liquid state is 0.55 kg/m^3 [5].

1.2. Advantages of using LPG

In comparison with other energy sources such as diesel, gasoline, coal, and wood, LPG offers several advantages, such as:

- LPG is clean regarding polluting gas emissions to the environment, as its combustion does not generate SO_X since it does not contain sulfur [4].
- LPG is neither toxic nor poisonous to humans, although it could cause death by displacing oxygen and causing anoxia [12].
- LPG is a highly versatile fuel. It can be used for cooking, heating water, drying agricultural products, and raising poultry. It is also used in forklifts, industrial ovens, boilers, and as a vehicle fuel [13].

- LPG is a fuel used in residential, commercial, and industrial applications [14].
- When LPG acts as a fuel, it burns completely, leaving no carbon residues and producing no soot [15].
- Its low cost, high accessibility, and environmental advantages have led several governments, such as India [16], Indonesia [17, 18], Burkina Faso [19], Ghana [20], South Africa [21], México [22], Brazil [23], Ecuador [24], Peru [25] among others, to implement compensatory measures such as subsidies to encourage the widespread use of LPG among their citizens.
- Failure to comply with national requirements and regulations, especially in countries with targeted subsidies for residential installations, causing the fuel to be used in commercial and industrial applications [30].
- Being classified as a safe fuel creates an excess of confidence in users of the systems regarding its handling. This has led to accidents with severe physical and human consequences [30].

1.4. Elements of an LPG System

Figure 1 shows the elements of an LPG system, which include:

1.3. Errors identified when using LPG

Despite the advantages mentioned above, several problems have been detected regarding the management of installations, such as:

- **Lack of awareness of the technical standards in force** when designing, installing, and maintaining LPG systems, resulting in poor applications [26].
- **Lack of foresight in the original design of new installations** considering the space allocated for storage, causing tanks to be installed in unsafe locations [27].
- **Lack of protection for the containers storing the fuel and the systems in general**, causing severe accidents worldwide [28].
- **Neglect by users to provide preventive maintenance to equipment and components**, resulting in them being used beyond the recommended service life by manufacturers [29].
- **Storage:** It refers to the containers used to package LPG fuel. These containers can be cylinders, which, due to their weight, are easily transportable by a human and are used through the exchange system. Also included are installed fixed tanks that must be supplied from tanker tanks through hoses for proper operation.
- **Transportation:** It refers to distribution pipelines or pipes and control elements such as valves, regulation devices like pressure regulators, and measurement devices like meters.
- **Consumer appliances:** It refers to devices that use LPG to meet human needs. Due to their ability to generate energy or their specific application, these devices can be used in residential, commercial, and industrial settings.
- **Protection or prevention systems:** It refers to systems designed to protect containers, pipelines, and consumer equipment installed to prevent accidents and reduce the risks associated with fuel handling.

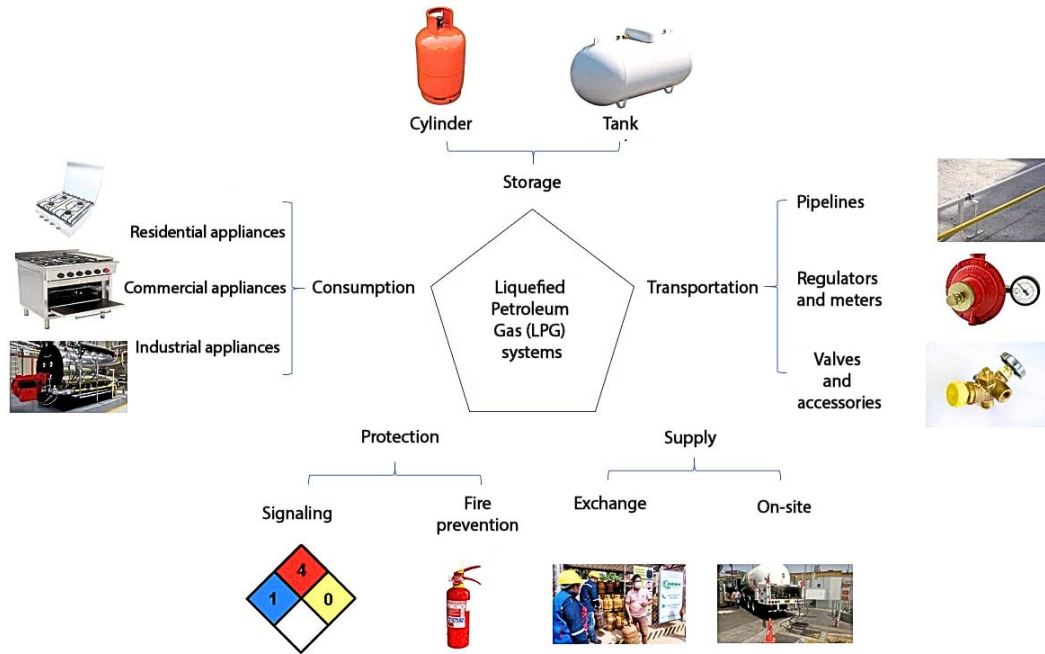


Figure 1. General diagram of an LPG system. Adapted from [31]

2. LPG storage

As mentioned in the previous section, containers store the fuel in a liquid state. LPG is typically used in a gaseous state, so a natural vaporization phenomenon occurs inside the containers before consumption.

2.1. Types of containers

Containers can be classified considering size into portable containers (cylinders) or stationary containers (tanks). Each container has various characteristics that differentiate them in terms of use and application, as shown in Figure 2.

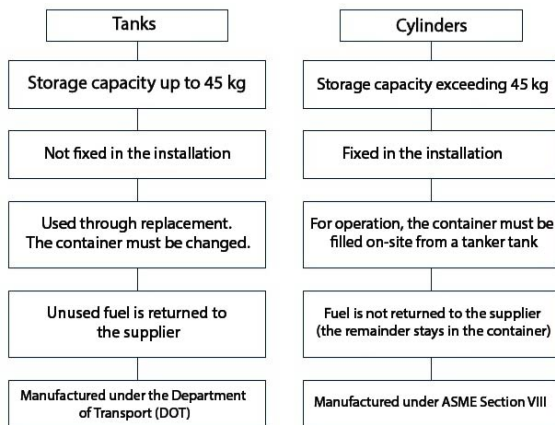


Figure 2. Differences between cylinders and tanks. Adapted from [32, 33]

2.2. Container sizing

To determine the necessary storage capacity in an LPG system, it is crucial to consider the required demand for fuel in consumer appliances and the peak demand hours [34].

2.2.1. Cylinder sizing

There are cylinders with standard storage capacities of 15 kg and 45 kg for residential and commercial use, respectively. There are also cylinders of 5 and 11 kg. One way to determine the number of cylinders is through the vaporization ratio, as illustrated in equation (1), [35]:

$$N = \frac{P_{it}}{R_v} \quad (1)$$

Where: N represents the number of cylinders (in case it is a fractional number, it is approximated to the nearest whole number), P_{it} is the total installed power [kW/h], and R_v is the vaporization ratio, as shown in Table 1.

Table 1. Vaporization ratio for 15 kg and 45 kg cylinders [35]

T [°C]	Cylinder 45 [kW/h]		Cylinder 15 [kW/h]	
	Intermittent consumption	Continuous consumption	Intermittent consumption	Continuous consumption
10	41	35	19	16
5	37	31	17	14
0	34	28	16	13
-5	30	24	15	12
-10	28	21	14	10

The $T[^\circ\text{C}]$ values presented in Table 1 correspond to the minimum temperature of the area where the cylinders will be located. Intermittent consumption refers to less than 4 consecutive hours of operation of consumer equipment daily, while continuous consumption implies more than 4 consecutive hours per day.

2.2.2. Sizing of stationary tanks

Equation (2), [36] indicates the natural vaporization capacity of LPG from a stationary storage container.

$$Q = p \cdot S \cdot K \cdot \frac{(T - T_g)}{CLV} \quad (2)$$

Where: Q is the natural vaporization capacity in kW, p is the percentage of liquid fuel in the container in %, S is the surface area of the container in m^2 , K is the heat transmission coefficient through the walls of the container in $kW/m^2 \text{ } ^\circ\text{C}$, T is the minimum external ambient temperature of the area where the container will be installed in $^\circ\text{C}$, T_g is the liquid-gas equilibrium temperature in $^\circ\text{C}$, and CLV is the latent heat of vaporization of LPG in kWh/kg.

The so-called simultaneity factor is applied in residential applications with multiple users, such as in buildings, as presented in Table 2. This factor allows for a reduction in the maximum demand during the peak consumption hour, assuming that not all users are using the fuel service at that moment.

Table 2. Simultaneity factor in buildings [36]

Number of houses	S_1	Number of houses	S_2
1	1	1	1
2	0.50	2	0.70
3 a 5	0.40	3 a 5	0.60
6 a 8	0.30	6 a 8	0.55
9 a 14	0.25	9 a 14	0.45
15 a 39	0.20	15 a 39	0.40
40 a 50	0.15	40 a 50	0.35

Where: S_1 is the simultaneity factor without heating boilers in the installation, and S_2 is the simultaneity factor with heating boilers.

2.2.3. Vaporizers

When the gaseous phase flow supplied by the natural vaporization of the containers is insufficient to meet the demand of the installation, it is necessary to resort to forced vaporization through a vaporizer. This equipment has an inlet for liquid LPG from the container and an outlet in the gaseous phase towards the service [37].

Equation (3) is used to select the appropriate vaporizer:

$$Q = \frac{E_T \cdot F_d}{PC} \quad (3)$$

Where: Q is the required vaporization capacity in gal/h, E_t is the total energy needed for the system in BTU/h, F_d is the load variation factor (usually considered as 1.10 for gradual loads), and PC is the calorific value of LPG, considered as 94 450 BTU/gal.

2.3. Container location

LPG storage containers must be placed outside buildings, whether installed on the surface or buried. When installed on the surface, they should be in open, well-ventilated areas and equipped with protective elements and signaling [38].

2.3.1. Location of containers on terraces

A particular case regarding the location of containers on the surface is the installation on terraces. To do this, the following requirements must be met [39]:

- Verify beforehand that the rooftop structure is resistant to the load of the container filled with water. Additionally, periodic preventive maintenance tests, including conducting a hydrostatic test, must be carried out on the container.
- Consider installing a lightning rod covering the LPG storage area.
- Consider that the grounding connection for the container should be independent of the building's grounding.
- Consider installing an equipped fire hydrant (EFH) at an accessible point on the terrace.
- Keep a water supply operational to conduct the hydrostatic test of the container.

2.3.2. Location of buried containers

The location of buried containers involves considering various aspects, such as:

- Consider the characteristics of the terrain where the container will be located to implement electrical protections through sacrificial anodes or cathodes.
- Consider that the containers must be anchored on firm and level bases to prevent them from coming out or floating to the surface in case of floods.
- Consider that the containers must come prepared from the factory for burial, including protective paint, space for control and filling elements, and access from the exterior.

2.3.3. Incorrect container locations

LPG storage containers should not be placed under the following conditions [27]:

- Confined spaces without ventilation.
- Basements or subfloors of buildings.
- Under buildings.
- Parking areas and locations with elements that may increase the likelihood of disasters, such as BLEVE, which stands for Boiling Liquid Expanding Vapor Explosion, meaning a sudden explosion of the fuel as it transitions from liquid to gas state [40].
- Areas where garbage accumulates or where there are materials around the containers that could increase the likelihood of fire, as well as areas with storage facilities for fats and oils.

2.4. Safety distances from containers

The technical regulations for LPG installations establish minimum distances from containers to third parties that must be considered. These distances are determined based on the stored volume and the container's location (above or below the surface). Although there may be variations in safety distances, the criteria used to calculate these distances follow the guidelines outlined in Figure 3. This figure refers to the distances considered for stationary containers that can be placed either above or below the surface and filled on-site or through displaced intakes; these containers must have safety devices for pressure relief and venting in case of overpressure.

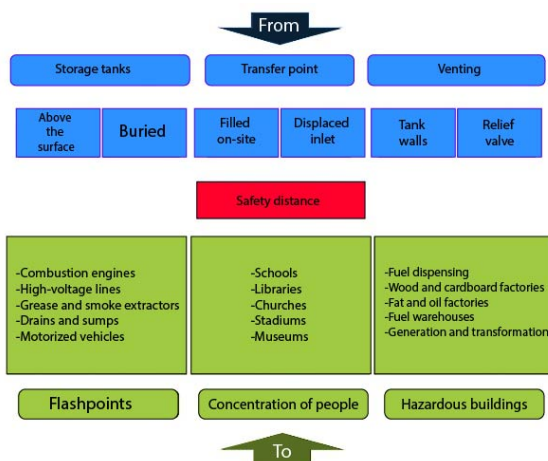


Figure 3. Criteria for locating stationary containers based on safety distance [27]

3. LPG transportation

This section refers to the fuel distribution pipes connecting the storage containers to the consumption points.

3.1. Minimum conditions for selecting pipes

La NTE INEN 2260:2010 [6] establishes minimum criteria for pipe installation, such as:

- Pipes can be metallic or plastic and must withstand the action of the fuel gas and the external environment. They must be protected by an effective system depending on the type of pipe.
- The thickness of the pipe walls must meet at least the pressure test conditions established for these installations. Additionally, they must have a mechanical strength that complies with the manufacturing standards' requirements for each type of pipe.
- Visible pipes must be marked and identified with colors following the ASME A13.1 [41] standard (ochre yellow for gas phase conduction pipes and white for liquid phase conduction pipes); concealed pipes (embedded, buried or in ducts) must also be marked [42].
- Pipes must convey the necessary flow for the operation of consumer appliances.

3.2. Location of pipes

To facilitate inspection, maintenance, and repair in case of leaks, installing the pipes that transport LPG visibly is recommended. However, for aesthetic reasons, users prefer the pipes to be concealed. Figure 4 shows the accepted ways to install pipes for LPG:

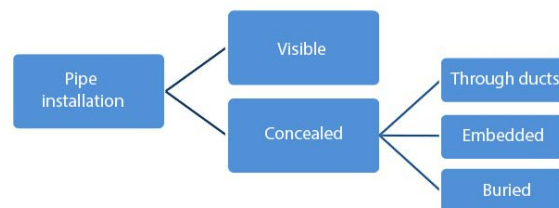


Figure 4. LPG pipe location [26]

It is important to note that embedded pipes, that is, those that are part of the building's structure, are not accepted for LPG transportation [6].

3.3. Pipe sizing

Dependiendo de la ubicación de las tuberías con respecto a los reguladores de presión, estas se clasifican en de media presión de baja presión.

3.3.1. Medium-pressure pipes

These pipes are located at the outlet of the storage containers, between the regulator of the first stage and that of the second stage.

Various publications that present criteria for LPG pipe sizing [43], can be found in the literature. Equation (4), [44] illustrates one of the most used methods, according to Renouard:

$$p_1^2 - p_2^2 = 4810.L.d.Q_s^{1.82}.D^{-4.82} \quad (4)$$

Where: Q_s represents the volumetric flow at standard conditions in m^3/s , D is the internal diameter of the pipe in m, p_1 is the absolute pressure at the pipe's inlet in Pa, p_2 is the absolute pressure at the pipe's outlet in Pa, d is the relative density of the gas $d = 1.5$ [5], and L is the equivalent length of the pipe in m.

The length in equation (3) corresponds to the equivalent pipe length, representing the losses experienced by the fuel passing through the pipes. This equivalent length is expressed in equation (5), [37]:

$$L_{eq} = 1, 2.L \quad (5)$$

Where: L is the pipe length in meters, and L_{eq} is the equivalent length in m.

In equation (3), p_1 is the absolute pressure at the outlet of the first stage regulator, which depends on the atmospheric pressure. It is known that atmospheric pressure varies with the altitude above sea level of the location where the system is installed. Equation (6) shows the atmospheric pressure correction considering a city's height above sea level [37].

$$p = 1, 013.(1 - 0, 0000225577.H) \quad (6)$$

Where: p is the pressure as a function of altitude in bar, and H is the city's height above sea level in m.

3.3.2. Low-pressure pipes

These pipes are located after the second stage regulator [45]. Among the established criteria for sizing low-pressure pipes, one of the most widely used is the equation proposed by Pole, presented in equation (7), [44]:

$$Q_s = C. \left(\frac{D^5(p_1 - p_2)}{L.d} \right)^{0.5} \quad (7)$$

Where: Q_s is the volumetric flow at standard conditions in m^3/s , $C = 4.635$ [44], D is the internal pipe diameter in m, p_1 is the absolute pressure at the pipe's inlet in Pa, p_2 is the absolute pressure at the pipe's outlet in Pa, d is the relative density of the gas $d = 1.5$ [5], and L is the equivalent pipe length in m.

Considering what is expressed in equation (7), the pressure difference between the initial and final points of the pipe section (the section between the second

stage regulator and the inlet of the consumer equipment) is used. Therefore, the pressure expressed in these criteria is gauge, not absolute, as in the medium-pressure criteria. Consequently, the altitude above sea level of the city location is irrelevant [43]. An accepted value for pressure difference in low-pressure sections is 150 Pa [35].

3.3.3. Gas velocity in pipes

The gas velocity is the value obtained by dividing the flow rate by the duct section [36], and it can be a determining factor in optimizing pipe diameters due to the excessive noise generated by the fluid flow through them.

Equation (8) is used to calculate the velocity [46]:

$$v = 360. \frac{Q}{D^2} \quad (8)$$

Where: v is the gas velocity in m/s, Q is the flow rate in m^3/h , and D is the diameter in mm.

Table 3 shows the established maximum values of permissible gas velocities, considering the area through which the conduits pass, to prevent any potential noise generated from becoming bothersome.

Table 3. Gas velocity in pipelines [36]

Velocity	Pipe location
30	General distribution network and service connections, buried conduits.
20	General distribution network and service connections, overhead conduits.
10	Standard building installation and individual installation

3.4. Pipe materials

Various pipe materials are accepted for LPG piping. Table 4 displays the materials allowed by NFPA 58 [47] for LPG pipes, along with commonly employed joining methods. Additionally, some regulations support using polyethylene-aluminum-polyethylene (P-Al-P) pipes in gas system installations [6].

Table 4. Materials accepted by NFPA 58 for LPG transportation [26]

Material	Manufacturing standard	Joining procedure
Steel	ASTM A 53 ASTM A106	SMAW
Stainless steel	ANSI/CSA 6.26	Pressing fit
Copper	ASTM B 88 ASTM B 280	Oxy-acetylene
Polyethylene	ASTM D 2513-09	Thermofusion Electrofusion

The pipes that are not accepted for LPG conveyance are:

- Cast iron pipe [33].
- Lead pipe [35].

3.5. Pipe selection criteria

It is essential to consider various aspects when choosing a pipeline for LPG service, as these can significantly impact the system's total cost or even make the installation unfeasible. Figure 5 illustrates two of the criteria used for selecting LPG pipes.

The weight per unit length of the pipe is crucial, especially in tall installations (buildings) or when covering extensive distances. Tensile strength must be considered essential when the pipeline is installed in areas with a high impact probability.

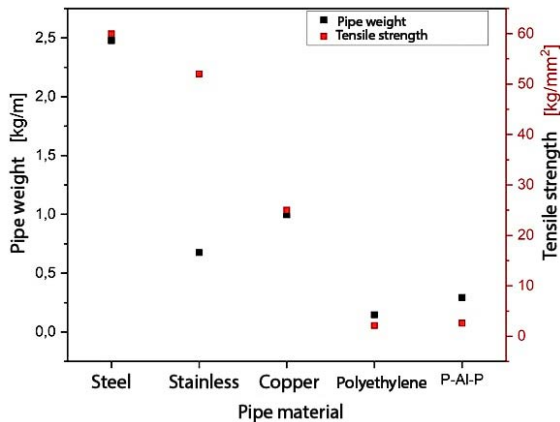


Figure 5. Factors for selecting LPG pipes. Adapted from [48]

Other additional factors are also crucial when selecting pipes, such as:

- Having a sufficient stock of materials to meet the needs of a project.
- Having skilled personnel to join pipes using fittings.
- Having the required energy for the pipe joining equipment with fittings.

4. Pressure regulation

It is a device that automatically reduces the gas inlet pressure, resulting in a lower (outlet or "regulated") but constant pressure downstream from where it is installed, keeping it within established limits for a specified flow range [36]. Pressure regulators can be fixed or adjustable (referring to the outlet pressure). In regulation systems, there are single-stage systems

(a single pressure regulator) and dual-stage regulation systems (medium-pressure regulator and low-pressure regulator) [49]. The pressure regulator is the heart of an LPG installation as it compensates for upstream pressure variations and delivers the required pressure and flow downstream.

4.1. Location of pressure regulators

Medium-pressure regulators should preferably be placed in outdoor areas of buildings. They must be accessible from the common areas of the building or the exterior in the case of single-family homes [50].

They can be installed inside spaces designated for the placement of meters as long as these spaces are located in ventilated areas. If the meters are placed in cabinets inside the building, these cabinets must be sealed, and the interior must be ventilated directly to the outside [51].

A single-stage pressure regulator must be installed outside buildings, and exceptionally, it may be located inside buildings as long as it has an integrated relief valve, with the outlet directed towards the exterior [50].

4.2. Selection of pressure regulators

Figure 6 shows the curves for selecting the first-stage pressure regulator based on energy demand. To use the graph, a specified consumption and service pressure must be considered as a starting point. With these data, a minimum pressure in the container should be considered, and according to the manufacturer's catalog, the model that meets these conditions is selected.

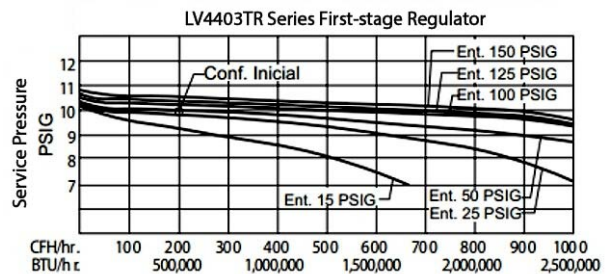


Figure 6. Selection of the first-stage regulator [52]

Figure 7 shows the curves for selecting the second-stage regulator. Reading and selecting these regulators is similar to what has been indicated for selecting first-stage regulators.

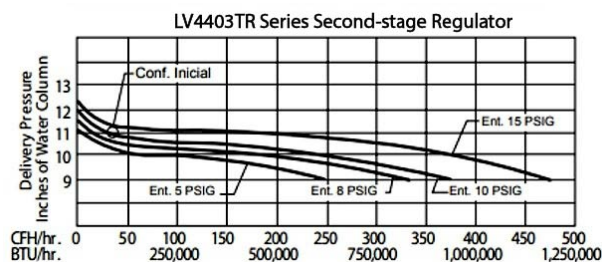


Figure 7. Selection of the second-stage regulator [52]

5. Consumer equipment

These are the elements that require fuel to meet the needs of a user. These devices must have specific characteristics, including [31]:

- Withstand the action of the fuel gas (GLP).
- Be designed to operate with the fuel gas.
- Withstand the action of the external environment in which they must be located.

5.1. Accessibility of consumer equipment

Accessibility to GLP consumption equipment is an essential requirement. This implies that they must be within reach of users for manipulation and control. Three levels of accessibility are established, as shown in Table 5.

Table 5. Accessibility to gas appliances [53]

Level of accessibility	Characteristic
1	They can be manipulated without opening locks, and no stairs or mechanical means are required to access them.
2	They are protected by a cabinet, accessible register, or door with a standard lock, and no stairs or mechanical means are required to access them.
3	Stairs or special mechanical means are needed for manipulation. Access to them is through private areas, which, even if they are common areas, are for personal use.

5.2. Consumer equipment power

The basis for the sizing of an LPG system is linked to the power required by consumer equipment, which must be satisfied through the natural vaporization of the containers. Appliances can be categorized as domestic or industrial. Table 6 shows typical power ratings for LPG consumer equipment.

Table 6. Potencias típicas de equipos de GLP [53]

Appliance	Power [kcal/h]	Appliance	Power [kcal/h]
Water heater		Heater	
80 l	6000	5 l/min	10000
150 l	8000	10 l/min	20000
200 l	8200	13 l/min	26400
260 l	8200	16 l/min	31400
Domestic stove	8000	Cooktop	8000
Semi-industrial stove	24000	Fryer	9300
Clothes dryer	12700	Heater	3000

The power consumption of each system device must be added to determine the total power. In the case of multifamily residential networks (buildings), this power must be adjusted by the simultaneity factor.

Equation (9) shows the power consumption ratio affected by the simultaneity factor for multifamily residential systems (buildings) [50].

$$Q_{sc} = \sum Q_{si} \cdot S_{1-2} \quad (9)$$

Where: Q_{SC} is the maximum probable flow rate, Q_{Si} is the maximum flow rate of each consumer equipment, and S_{1-2} is the simultaneity factor according to the number of users, as established in Table 2.

6. Start-up of systems

To ensure the optimal operation of the LPG system, it is necessary to conduct various tests and verifications before supplying the fuel and igniting the consumption equipment.

6.1. Tightness test

It is necessary to carry out the tightness test on all piping systems before putting them into operation [54]. This test must be conducted at a pressure higher than the system's maximum operating pressure (MOP), as established in Table 7.

Table 7. Pressure and test times according to MOP [6]

Operating pressure [kPa]	Test pressure [kPa]	Test time [min]
$200 < \text{MOP} < 500$	$> 1.50 \cdot \text{MOP}$	60
$10 < \text{MOP} < 200$	$> 1.75 \cdot \text{MOP}$	30
$\text{MOP} < 10$	$> 2.50 \cdot \text{MOP}$	15

This tightness test must be performed on all pipeline sections and can be conducted in segments. The test result must be satisfactory, meaning there should be no pressure drop in the pipeline network during the minimum established time. Additionally, a record must be completed with all the data collected during the test and must bear the signature of the professional in charge of the work and a representative of the building's user [54]. If the test result is not

satisfactory, the location of the possible leak must be verified, and the corresponding repair must be carried out.

6.2. Purge

It is necessary to carry out a network sweep or purge before start-up to eliminate debris and residues that may enter the pipeline during the assembly phase, including welding slag. This helps eliminate such residues and prevents the risk of obstruction or blockage in the regulators or burners of consumer equipment [49].

6.3. Signaling

To alert individuals unfamiliar with the LPG system (storage, pipelines, equipment), safety signs must be installed warning of the danger associated with handling fuel gas. These signs should be placed in visible locations and have appropriate dimensions to be easily identified by users.

6.4. Protections

LPG systems must be protected from third-party interference. The worst-case scenario in storing an LPG system is the formation of a BLEVE (Boiling Liquid Expanding Vapor Explosion) [40]. This phenomenon represents a particular case of a catastrophic explosion of a pressure container, in which there is a sudden release of a large mass of pressurized and superheated liquid or liquefied gas into the atmosphere.

It is necessary to install water-based cooling systems in storage. In the event of a fire around the containers, these systems can delay the formation of this phenomenon until the competent authority can control the fire.

6.5. Required technical documentation

LPG system installation projects must have the necessary documentation. This documentation must be submitted to the competent authority [7] to verify compliance with the technical and legal regulations in force in each territory. The technical documentation must include [30]:

- Technical report of the project, including all aspects considered during the design, construction, assembly, and suitability verification phases of the LPG system.
- Installation drawings, including all the construction details used during the assembly phase.
- Signed records of tightness tests and other verifications on the system to ensure compliance with regulatory and safety standards.

- Certifications of the elements used in the system to verify compliance with the required quality standards.

7. Conclusions and recommendations

LPG is one of the most widely used fossil fuels in residential, commercial, and industrial settings. Its utilization, however, poses risks to both individuals and buildings. This review outlines the minimum safety criteria that should be incorporated into an LPG installation.

It is crucial to emphasize that these systems must be designed by professional engineers with expertise in regulatory compliance to provide users with safe and efficient systems.

Each system has characteristics and peculiarities that set it apart from others. For this reason, the technical designer in charge of the design must be familiar with all the material and accessory options approved by regulations to provide users with high-quality systems.

Acknowledgments

To the Escuela Politécnica Nacional EPN-Ecuador, with its research lines: Sustainable Manufacturing in Manufacturing Processes and Mitigation of Vibrations, and Energy Efficiency in Automotive and Aeronautical Transportation Systems, for the support provided in the development of this work.

References

- [1] S. Singh, J. Prasad Chakraborty, and M. Kumar Mondal, "Intrinsic kinetics, thermodynamic parameters and reaction mechanism of non-isothermal degradation of torrefied acacia nilotica using isoconversional methods," *Fuel*, vol. 259, p. 116263, 2020. [Online]. Available: <https://doi.org/10.1016/j.fuel.2019.116263>
- [2] IEA, *Key World Energy Statistics 2021*. International Energy Agency, 2021. [Online]. Available: <https://bit.ly/3rdeLX5>
- [3] K. J. Morganti, T. M. Foong, M. J. Brear, G. da Silva, Y. Yang, and F. L. Dryer, "The research and motor octane numbers of liquefied petroleum gas (LPG)," *Fuel*, vol. 108, pp. 797–811, 2013. [Online]. Available: <https://doi.org/10.1016/j.fuel.2013.01.072>
- [4] L. Raslavičius, A. Keršys, S. Mockus, N. Keršiene, and M. Starevičius, "Liquefied petroleum gas (LPG) as a medium-term option in the transition to sustainable fuels and transport," *Renewable and Sustainable Energy Reviews*,

- vol. 32, pp. 513–525, 2014. [Online]. Available: <https://doi.org/10.1016/j.rser.2014.01.052>
- [5] NFPA, *Liquefied Petroleum Gas Code*. National Fire Protection Association, 2020. [Online]. Available: <https://bit.ly/45WTobz>
- [6] INEN, *NTE INEN 2 260:2010 Instalaciones de gases combustibles para uso residencial, comercial e industrial. Requisitos*. Instituto Ecuatoriano de Normalización, 2010. [Online]. Available: <https://bit.ly/45YRSFG>
- [7] A. Macías, “Primer foro latinoamericano de adopción e inspección de la normativa NFPA,” *NFPA Journal Latinoamericano*, vol. 3, no. 2, pp. 8–9, 2016.
- [8] —, “La adopción de códigos y normas de seguridad ayuda al desarrollo de nuestros países,” *NFPA Journal Latinoamericano*, vol. 3, no. 2, pp. 4–5, 2014.
- [9] —, “Adoptando NFPA en América Latina,” *NFPA Journal Latinoamericano*, vol. 4, no. 1, p. 6, 2013.
- [10] Naciones Unidas, *Manual de seguridad: Aspectos de inflamabilidad de los gases hidrocarburos*. Programa de las Naciones Unidas para el Medio Ambiente, 2005. [Online]. Available: <https://bit.ly/45XBVQg>
- [11] K. Sarvestani, O. Ahmadi, S. B. Mortazavi, and H. A. Mahabadi, “Development of a predictive accident model for dynamic risk assessment of propane storage tanks,” *Process Safety and Environmental Protection*, vol. 148, pp. 1217–1232, 2021. [Online]. Available: <https://doi.org/10.1016/j.psep.2021.02.018>
- [12] F. Chica Segovia, F. Espinoza Molina, and N. Rivera Campoverde, “Gas licuado de petróleo como combustible alternativo para motores diésel con la finalidad de reducir la contaminación del aire,” *Ingenius, Revista de Ciencia y Tecnología*, no. 4, pp. 73–81, 2010. [Online]. Available: <https://doi.org/10.17163/ings.n4.2010.08>
- [13] R. K. Andadari, P. Mulder, and P. Ritveld, “Energy poverty reduction by fuel switching. impact evaluation of the LPG conversion program in Indonesia,” *Energy Policy*, vol. 66, pp. 436–449, 2014. [Online]. Available: <https://doi.org/10.1016/j.enpol.2013.11.021>
- [14] P. Boggavarapu, B. Ray, and R. Ravikrishna, “Thermal efficiency of LPG and PNG-fired burners: Experimental and numerical studies,” *Fuel*, vol. 116, pp. 709–715, 2014. [Online]. Available: <https://doi.org/10.1016/j.fuel.2013.08.054>
- [15] J. Kim, K. Kim, and S. Oh, “An assessment of the ultra-lean combustion direct-injection LPG (liquefied petroleum gas) engine for passenger-car applications under the FTP-75 mode,” *Fuel Processing Technology*, vol. 154, pp. 219–226, 2016. [Online]. Available: <https://doi.org/10.1016/j.fuproc.2016.08.036>
- [16] P. Kumar, R. Kaushalendra Rao, and N. H. Reddy, “Sustained uptake of LPG as cleaner cooking fuel in rural India: Role of affordability, accessibility, and awareness,” *World Development Perspectives*, vol. 4, pp. 33–37, 2016. [Online]. Available: <https://doi.org/10.1016/j.wdp.2016.12.001>
- [17] K. Thoday, P. Benjamin, M. Gan, and E. Puzzolo, “The mega conversion program from kerosene to LPG in Indonesia: Lessons learned and recommendations for future clean cooking energy expansion,” *Energy for Sustainable Development*, vol. 46, pp. 71–81, 2018, Scaling Up Clean Fuel Cooking Programs. [Online]. Available: <https://doi.org/10.1016/j.esd.2018.05.011>
- [18] M. I. al Irsyad, T. Anggono, C. Anditya, I. Ruslan, D. G. Cendrawati, and R. Nepal, “Assessing the feasibility of a migration policy from LPG cookers to induction cookers to reduce LPG subsidies,” *Energy for Sustainable Development*, vol. 70, pp. 239–246, 2022. [Online]. Available: <https://doi.org/10.1016/j.esd.2022.08.003>
- [19] B. Ouedraogo, “Household energy preferences for cooking in urban Ouagadougou, Burkina Faso,” *Energy Policy*, vol. 34, no. 18, pp. 3787–3795, 2006. [Online]. Available: <https://doi.org/10.1016/j.enpol.2005.09.006>
- [20] K. Adjei-Mantey and K. Takeuchi, “Supply-side factors of LPG adoption and usage frequency in Ghana: Assessing the validity of subjective distance to refill,” *Energy for Sustainable Development*, vol. 70, pp. 475–481, 2022. [Online]. Available: <https://doi.org/10.1016/j.esd.2022.08.021>
- [21] D. Kimemia and H. Annegarn, “Domestic LPG interventions in South Africa: Challenges and Lessons,” *Energy Policy*, vol. 93, pp. 150–156, 2016. [Online]. Available: <https://doi.org/10.1016/j.enpol.2016.03.005>
- [22] K. Troncoso, P. Segurado, M. Aguilar, and A. Soares da Silva, “Adoption of LPG for cooking in two rural communities of Chiapas, Mexico,” *Energy Policy*, vol. 133, p. 110925, 2019. [Online]. Available: <https://doi.org/10.1016/j.enpol.2019.110925>

- [23] G. M. Jannuzzi and G. A. Sanga, “LPG subsidies in Brazil: an estimate,” *Energy for Sustainable Development*, vol. 8, no. 3, pp. 127–129, 2004. [Online]. Available: [https://doi.org/10.1016/S0973-0826\(08\)60474-3](https://doi.org/10.1016/S0973-0826(08)60474-3)
- [24] C. F. Gould, S. B. Schlesinger, E. Molina, M. L. Bejarano, A. Valarezo, and D. W. Jack, “Household fuel mixes in peri-urban and rural Ecuador: Explaining the context of LPG, patterns of continued firewood use, and the challenges of induction cooking,” *Energy Policy*, vol. 136, p. 111053, 2020. [Online]. Available: <https://doi.org/10.1016/j.enpol.2019.111053>
- [25] S. L. Pollard, K. N. Williams, C. J. O’Brien, A. Winiker, E. Puzzolo, J. L. Kephart, M. Fandiño-Del-Río, C. Tarazona-Meza, M. R. Grigsby, M. Chiang, and W. Checkley, “An evaluation of the Fondo de Inclusión Social Energético program to promote access to liquefied petroleum gas in Peru,” *Energy for Sustainable Development*, vol. 46, pp. 82–93, 2018, Scaling Up Clean Fuel Cooking Programs. [Online]. Available: <https://doi.org/10.1016/j.esd.2018.06.001>
- [26] D. Venegas, J. Yáñez, S. Celi, C. Ayabaca, L. Tipanluisa, D. Bastidas, and M. Arrocha, “Materiales recomendados por las normas internacionales para utilizar en una instalación de GLP,” *Asociación Española de Ingeniería Mecánica*, pp. 599–606, 2016. [Online]. Available: <https://bit.ly/3PLhCji>
- [27] D. Venegas Vásconez and O. Farías, “La BLEVE, un motivo para la seguridad en las instalaciones de GLP,” in *13 Congreso Iberoamericano de Ingeniería Mecánica*, 10 2017. [Online]. Available: <https://bit.ly/45WAPUF>
- [28] J. I. Chang and C.-C. Lin, “A study of storage tank accidents,” *Journal of Loss Prevention in the Process Industries*, vol. 19, no. 1, pp. 51–59, 2006. [Online]. Available: <https://doi.org/10.1016/j.jlp.2005.05.015>
- [29] D. Venegas Vásconez, J. Yáñez, S. Celi, C. Ayabaca Sarria, L. Tipanluisa, D. Bastidas, and M. Carrera, “Mantenimiento necesario en instalaciones de GLP,” in *XXI Congreso Nacional de Ingeniería Mecánica*, 11 2016, pp. 353–360. [Online]. Available: <https://bit.ly/2LeqSf0>
- [30] D. Venegas Vásconez, C. Ayabaca Sarria, S. Celi Ortega, and J. Rocha Hoyos, “El riesgo en el almacenamiento de GLP en el Ecuador,” *INNOVA Research Journal*, vol. 3, no. 1, pp. 19–29, 2018. [Online]. Available: <https://doi.org/10.33890/innova.v3.n1.2018.331>
- [31] D. Venegas Vásconez, “Sistemas de gas licuado de petróleo: Ingeniería y normas técnicas en pro de la seguridad,” *Construcción y Servicios*, 2022. [Online]. Available: <https://bit.ly/46dvNms>
- [32] D. Venegas Vásconez and C. Ayabaca Sarria, “Análisis del almacenamiento en sistemas de gas licuado de petróleo: tanques estacionarios vs. cilindros,” *Ingenius, Revista de Ciencia y Tecnología*, no. 22, pp. 113–122, 2019. [Online]. Available: <https://doi.org/10.17163/ings.n22.2019.11>
- [33] NFPA, *National Fuel Gas Code: NFPA 54 ANSI Z223*. National Fire Protection Association, 2020. [Online]. Available: <https://bit.ly/3ZmRuOV>
- [34] D. Venegas Vásconez, C. Ayabaca Sarria, S. Ortega, J. Rocha Hoyos, and E. Mena Mena, “Optimización en el dimensionamiento de un sistema industrial de gas licuado de petróleo,” *I+D Tecnológico*, vol. 14, no. 1, pp. 41–48, 2018. [Online]. Available: <https://doi.org/10.33412/idt.v14.1.1801>
- [35] Ministerio de Economía, *Decreto 66 Reglamento de Instalaciones Interiores y Medidores de Gas*. Biblioteca del Congreso Nacional de Chile, 2007. [Online]. Available: <https://bit.ly/3Lvs5Ns>
- [36] J. E. López Sopena, *Manual de instalaciones de GLP*. CEPESA, 2001. [Online]. Available: <https://bit.ly/3ZsajAr>
- [37] E. A. Hernández Martín and A. M. García Gascó, *Especificaciones técnicas CONAIF-SEDIGAS para la certificación de instaladores de gas. Materias comunes tipos A, B y C. Cálculo de instalaciones receptoras*. CONAIF-SEDIGAS Certificación, 2008. [Online]. Available: <https://bit.ly/45XmiIF>
- [38] D. Venegas Vásconez, “Falencias en el almacenamiento de GLP en Chile,” in *Congreso Panamericano COPIMERA XXVI 2017*, 10 2017. [Online]. Available: <https://bit.ly/3ZtJ7B5>
- [39] —, “Ubicación de recipientes para GLP en terrazas,” *Construcción y Servicios*, vol. 1, 01 2018. [Online]. Available: <https://bit.ly/3PLQr85>
- [40] M. Bestratén Bellovi and E. Turmo Sierra, *NTP 293: Explosiones BLEVE (I): Evaluación de la radiación térmica*. Instituto Nacional de Seguridad e Higiene en el Trabajo, s/n. [Online]. Available: <https://bit.ly/3LxrPgS>
- [41] ASME, *ASME A13.1 - 2020: Scheme for the Identification of Piping Systems*. The American Society of Mechanical Engineers, 2020. [Online]. Available: <https://bit.ly/3sYMXGd>

- [42] INEN, *NTE INEN 439:1984 Colores, señales y símbolos de seguridad*. Instituto Ecuatoriano de Normalización, 1984. [Online]. Available: <https://bit.ly/3rlJYY1>
- [43] D. Venegas-Vásconez, C. Ayabaca-Sarria, R. Reina-Guzmán, and O. Farías-Fuentes, “Optimización dimensional de tuberías de gas licuado de petróleo en sistemas industriales,” in *XV Congreso Iberoamericano de Ingeniería Mecánica*, 2022. [Online]. Available: <https://bit.ly/3EMMn11>
- [44] P. M. Coelho and C. Pinho, “Considerations about equations for steady state flow in natural gas pipelines,” *Journal of the Brazilian Society of Mechanical Sciences and Engineering*, vol. 29, no. 3, pp. 262–273, Jul 2007. [Online]. Available: <https://doi.org/10.1590/S1678-58782007000300005>
- [45] D. Venegas Vásconez, “Materiales para instalaciones de gas licuado de petróleo según NFPA,” in *Congreso Internacional de Metalurgia y Materiales 16 SAM CONAMET*, 11 2016. [Online]. Available: <https://bit.ly/460zwUO>
- [46] UNE, *UNE 60670-6:2014 Instalaciones receptoras de gas suministradas a una presión máxima de operación (MOP) inferior o igual a 5 bar*. Asociación Española de Normalización, 2014. [Online]. Available: <https://bit.ly/3rreU99>
- [47] NFPA, *NFPA 58 Código del Gas Licuado de Petróleo, edición 2014*. National Fire Protection Association, 2020. [Online]. Available: <https://bit.ly/48yVwrM>
- [48] D. Venegas, C. Ayabaca, S. Celi, J. Rocha, and E. Mena, “Factores para seleccionar tuberías de conducción de gas licuado de petróleo en el Ecuador,” *Ingenius, Revista de Ciencia y Tecnología*, no. 19, pp. 51–58, 2018. [Online]. Available: <https://doi.org/10.17163/ings.n19.2018.05>
- [49] REGO, *Catálogo L-102-SV. Equipo de GLP y amoníaco anhidro*. REGO Products, 2023. [Online]. Available: <https://bit.ly/44ZY11S>
- [50] INDECOPI, *Instalaciones internas de GLP para consumidores directos y redes de distribución interna*. Norma Técnica Peruana, 2008. [Online]. Available: <https://bit.ly/3ENsyqe>
- [51] J. Landete Morato and M. Enguidanos Javega, *Guía Instalaciones de gas*. Generalitat Valenciana, 2007. [Online]. Available: <https://bit.ly/46dTCvb>
- [52] REGO, *L-500 Catalog Regulators and Accessories*. REGO Products, 2023. [Online]. Available: <https://bit.ly/3ELXpnb>
- [53] UNE, *UNE 60621-1:1996 Instalaciones receptoras de gas para usos industriales suministradas en media y baja presión. Parte 1: Generalidades*. Asociación Española de Normalización, 1996. [Online]. Available: <https://bit.ly/48z9LwK>
- [54] D. Venegas Vásconez, “La importancia de la prueba de hermeticidad en las tuberías de gas,” *Construcción y Servicios*, vol. 1, 01 2018. [Online]. Available: <https://bit.ly/2Yc9pY1>



REUSE OF ELECTRICAL VEHICLE BATTERIES FOR SECOND LIFE APPLICATIONS IN POWER SYSTEMS WITH A HIGH PENETRATION OF RENEWABLE ENERGY: A SYSTEMATIC LITERATURE REVIEW

REUTILIZACIÓN DE BATERÍAS DE VEHÍCULOS ELÉCTRICOS PARA APLICACIONES DE SEGUNDA VIDA EN SISTEMAS ELÉCTRICOS DE POTENCIA CON UNA ALTA PENETRACIÓN DE ENERGÍA RENOVABLE: UNA REVISIÓN SISTEMÁTICA DE LA LITERATURA

Jorge Campoverde-Pillco¹ , Danny Ochoa-Correa^{2,*} ,
 Edisson Villa-Ávila³ , Patricio Astudillo-Salinas¹ 

Received: 12-05-2023, Received after review: 17-10-2023, Accepted: 26-10-2023, Published: 01-01-2024

Abstract

This article presents a systematic literature review on the reuse of electric vehicle batteries (EVV) for second-life applications in power systems. The end-of-life of these batteries represents a major environmental problem due to their composition and materials. The study aims to analyze the reuse of EVVs as a sustainable alternative for the environment. Additionally, it seeks to provide complementary services to facilitate the incorporation of intermittent unconventional renewable generation into the electrical grid. Through an exhaustive search of scientific publications indexed in prestigious digital catalogs and their subsequent systematic treatment, a selected group of 49 scientific articles published between 2018 and 2023 have been found in which the different opportunities, benefits and limitations of second-life energy storage systems oriented to boost a circular economy have been identified. The study concludes that, although the reuse of batteries has not yet been fully addressed or implemented due to existing challenges in terms of technology, costs, and regulations, it is of utmost importance to delve deeper into its analysis to improve efficiency and reduce the environmental impacts associated with the manufacturing, use, and disposal of such batteries.

Keywords: Battery energy storage system, Electrical vehicle, Second-life applications, Power systems, Renewable energy

Resumen

Este artículo presenta una revisión sistemática de literatura relativa al tópico reutilización de baterías de vehículos eléctricos (BVE) para aplicaciones de segunda vida en sistemas eléctricos de potencia. El fin del ciclo de vida de estas baterías representa un gran problema ambiental debido a su composición y materiales. El estudio tiene por objeto analizar la reutilización de las BVE como una alternativa sostenible para el medioambiente y, además, para brindar servicios complementarios que faciliten la incorporación de generación renovable no convencional de carácter intermitente a la red eléctrica. A través de una búsqueda exhaustiva de publicaciones científicas indexadas en catálogos digitales prestigiosos y de su posterior tratamiento sistemático, se ha llegado a un número selecto de 49 artículos científicos publicados entre 2018 y 2023. En ellos ha sido posible identificar las diferentes oportunidades, beneficios y limitaciones de los sistemas de almacenamiento de energía de segunda vida orientadas a impulsar una economía circular. El estudio concluye que, si bien la reutilización de baterías no está plenamente tratada ni implementada, debido a que aún enfrenta desafíos en términos de tecnología, costos y regulaciones, es de gran importancia profundizar su análisis para mejorar la eficiencia y disminuir los impactos ambientales que provocan su fabricación, uso y desecho.

Palabras clave: Sistemas de almacenamiento de energía en baterías, vehículos eléctricos, aplicaciones de segunda vida, sistemas eléctricos de potencia, energía renovable

¹Facultad de Ingeniería, Universidad de Cuenca, Ecuador.

^{2,*}Departamento de Ingeniería Eléctrica, Electrónica y Telecomunicaciones (DEET), Universidad de Cuenca, Ecuador. Corresponding author ✉: danny.ochoac@ucuenca.edu.ec.

³Laboratorio de Micro-Red, Universidad de Cuenca, Ecuador.

Suggested citation: Campoverde-Pillco, J.; Ochoa-Correa, D.; Villa-Ávila, E. y Astudillo-Salinas, P. "Reuse of Electrical Vehicle Batteries for Second Life Applications in Power Systems with a High Penetration of Renewable Energy: A Systematic Literature Review," *Ingenius, Revista de Ciencia y Tecnología*, N.º 31, pp. 95-105, 2024, DOI: <https://doi.org/10.17163/ings.n31.2024.08>.

1. Introduction

The concerning statistics outlining the decline of fossil fuels and the consequences the world faces due to climate change have driven the development of new technologies. Among these innovations, the electric vehicle (EV) has emerged as a standout solution [1]. The escalating focus on decarbonizing transportation has resulted in a surge of electric vehicles on our roads, necessitating a continuous supply of charging infrastructure. As electromobility (EM) becomes more relevant for users, the demand for secondary batteries, also called rechargeables [2], increases. Among all the currently available options, lithium-ion batteries play a prominent role in the application of electric vehicles [1].

The demand for lithium-ion batteries has significantly increased in recent years due to the growth of the electric vehicle market. Although these batteries can last several years, they eventually lose their ability to hold a charge and must be replaced. Proper disposal of these batteries is crucial to prevent the release of toxic chemicals and reduce environmental impact [3]. In this context, electric vehicle battery reuse has emerged as a sustainable and cost-effective alternative [4]. Although the batteries may not be suitable for vehicles after losing their capacity, they can still have significant value for energy storage applications within a power system, as reported in studies in [5–8].

Beyond the environmental benefits, battery reuse can also be economically profitable [9] since a significant reduction in the cost of energy storage systems (ESS) and other products relying on lithium-ion batteries can be achieved for secondary applications. This becomes particularly important as the demand for ESS increases to support the integration of intermittent renewable energy sources into power systems.

Regarding electric vehicles (EVs), a battery is considered to have reached the end of its useful life when its charging capacity falls below 80% of its nominal capacity [10]. As a result, it is foreseen that in a few years, the storage of used EV batteries will become a significant problem from various perspectives. Finding an efficient way to recycle or reuse them is a sensitive environmental issue. However, the fate of EV batteries will depend mainly on charging habits and the temperatures to which they have been exposed. If a battery is in good condition, its components could be used as spare parts for other similar systems [11, 12]. A battery in good condition should maintain an acceptable storage capacity (generally above 80% of its nominal capacity), be physically intact without significant damage, have remaining life cycles, maintain proper chemical condition, have been operated under suitable temperature and charging conditions, and be equipped with effective battery management and communication systems. Otherwise, they could be used as a means to store energy in conjunction with distributed

generation systems [13], such as photovoltaic [14] or wind generation [15]. With the notable increase in the use of renewable energies worldwide [16], the need to store surplus generated energy has become crucial. Currently, ESS play a pivotal role in ensuring stability in distribution systems (DS) during periods of high or low demand. For this reason, in the future, the inclusion of battery systems in DS should be considered, which could contribute significantly to reducing energy costs and improving specific quality indicators of the electric supply affected by the massive integration of renewable generation with high variability [17, 18].

The planet's resources are limited, and their extraction from nature often involves complex engineering processes. Therefore, it is necessary for all engineering fields that have contributed to the development of EVs to collaborate to find the most suitable environmental solution, considering the construction, maintenance, and recycling of batteries [19]. To address this issue, this article presents a systematic literature review focused on searching for technological solutions to reuse EV batteries for energy storage applications and providing ancillary services to power systems to facilitate the widespread integration of renewable energy. This review considers research conducted in the last five years by scientists and researchers worldwide.

2. Materials and methods

The systematic process of searching for literary sources that enrich the content of this research is carried out using the documented bibliographic review methodology, according to Codina [20]. The final result will be a systematic review based on high-quality scientific articles published, focusing on the reuse of EV batteries. Prestigious databases such as Web of Science, Scopus, and IEEE Xplore have been used as sources for searching bibliographic resources. Figure 1 shows a flowchart illustrating the procedure followed for selecting the studies.

2.1. Inclusion criteria

The literature review encompasses the search period from 2018 to 2023, employing the keywords: "second-life electric vehicle batteries," "renewable energy," and "grid support." Articles in English that are fully available online and address the reuse and/or recycling of EV batteries have been selected. The digital databases considered in this study are recognized for their prestige in the academic and research domains and for being subscribed to by many academic and research institutions worldwide. This makes them essential sources of information for a broad community of researchers, professors, and students. Therefore, accessibility to these resources is a crucial factor that must be considered in a systematic literature review Table 1 provides

a concise summary of the selection criteria employed in the systematic review.

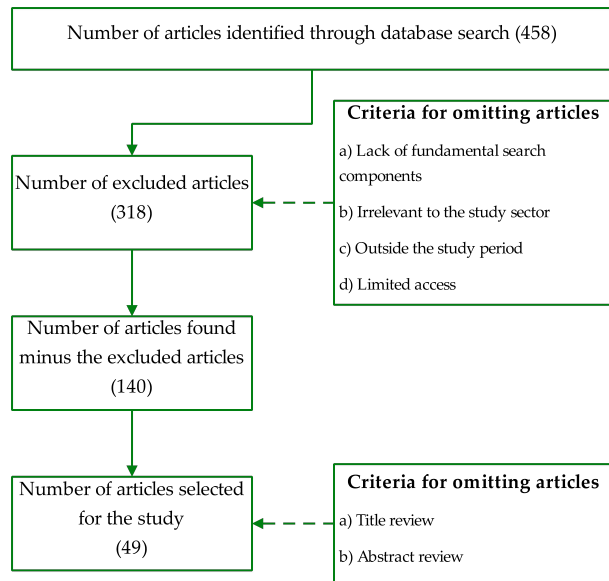


Figure 1. Flowchart of the process followed for study selection

Table 1. Criteria for article selection

Article	Selection criteria
Sector	Electrical engineering, renewable energy, sustainable technology
Language	English
Sources	Web of Science, Scopus, IEEE Xplore
Year of publication	2018-2023
Accessibility	Online access, full text
Relevance	Reuse of EV batteries with renewable energy
Search string	"Second-life electric vehicle batteries" AND "Renewable energy" AND "Grid support"

2.2. Study selection

The initial search yielded a comprehensive set of 458 scientific works. Subsequently, 318 articles were excluded due to the lack of fundamental search components (title, abstract, and keywords) and because they were outside the study period or had limited access, thus reducing the number of articles to a total of 140 with the characteristics shown in Figures 2 and 3. After reviewing the title and abstract of each article, 49 articles were selected to serve as the foundation for this study. This meticulous curation represents the essence of a systematic literature review, ensuring the incorporation of studies characterized by quality, relevance, and accessibility.

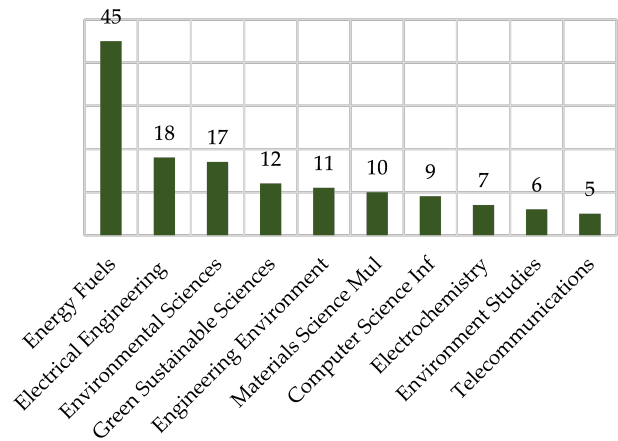


Figure 2. Classification of articles by areas Source: Web of Science

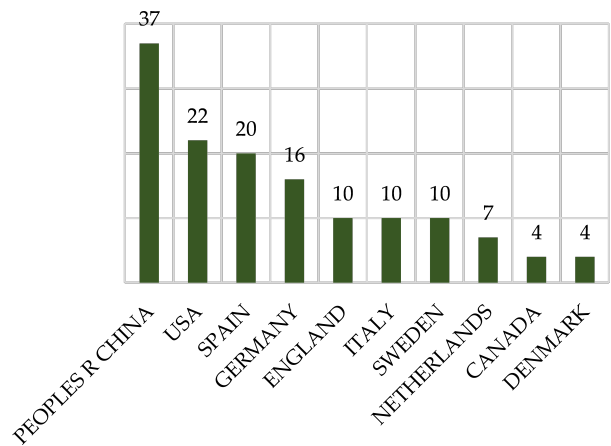


Figure 3. Classification of articles by country Source: Web of Science

2.3. Bibliometric analysis

Once the articles that meet the inclusion criteria defined in section 2.1 are selected, bibliometric analyses are conducted using the open-access program VOSviewer. This allows for exploring the relationships between the articles and presenting a graphical analysis showing nodes represented by keywords and the links or connections between each article. The position of the nodes in the visualization is determined by the clustering algorithm used by VOSviewer.

After selecting the articles for the study, they were imported into VOSviewer (version 1.6.19) [21], where a co-occurrence analysis was conducted to assess the relationships between the articles based on keywords. Finally, a network visualization was generated to facilitate the scientific literature’s exploration and analysis of patterns.

Figure 4 shows the network visualization identifying four emerging groups. Four main clusters related to lithium-ion batteries, electric vehicles, second life, and energy-storage can be observed.

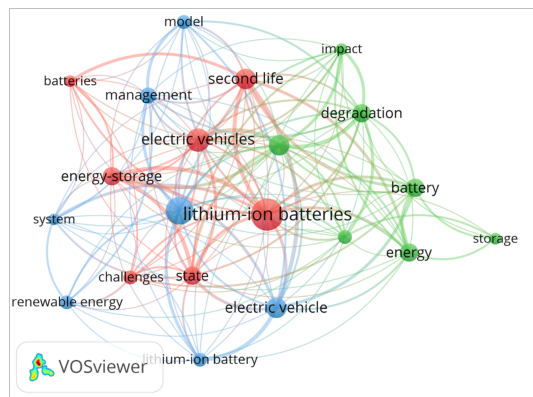


Figure 4. Network of words obtained through bibliometric analysis using the open-access program VOSviewer

3. Results and discussion

Figure 5 illustrates the evolution of bibliographic material related to the reuse of EV batteries between 2018 and 2023. The selection of studies to support this systematic review revealed a significant increase in publications starting in 2018, further escalating in 2022. This upward trend continues in 2023, considering the substantial number of articles published in the early months of this year. This indicator demonstrates the current relevance of the topic addressed in this study, whose fundamental aspects will be discussed in this section.

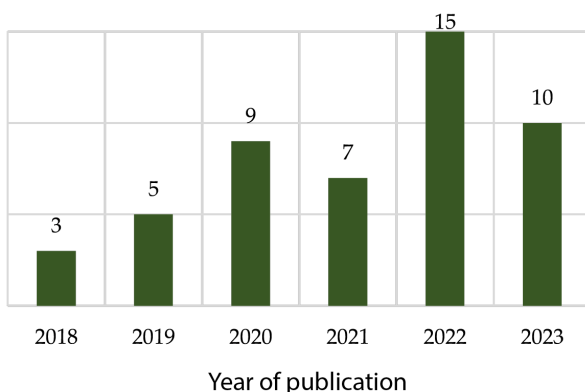


Figure 5. Classification by year of the selected publications

The following is a critical analysis based on the comprehensive review of the 49 selected articles, which address the challenges or barriers currently faced by reusing electric vehicle batteries. Additionally, some

benefits offered by reusing to various stakeholders are highlighted, as well as the sectors interested in providing second-life to these batteries. Finally, the results obtained through the literature review on renewable energy storage in the second-life of EV batteries are presented.

3.1. Barriers and benefits of the reuse of EV batteries

In practice, projects involving the reuse of EV batteries seek to reduce dependence on fossil fuels [1], enhance the electrical grid's stability, reduce energy costs, etc. The inclusion criteria for renewable energies may vary depending on the specific focus and objectives of the study or project.

3.1.1. Barriers or limitations

- Battery Type:** Not all available batteries are suitable for reuse projects. Primarily lithium-ion batteries will be reused because among their fundamental characteristics, they exhibit high specific energy and energy density, enabling them to operate in extreme temperatures and for more extended periods. This is in contrast, for example, to nickel-cadmium or lead-acid batteries, which tend to be discarded. Additionally, lithium-ion batteries are manufactured with more environmentally friendly materials [22].
- Battery condition:** The condition and functionality of a battery must be determined [8–10]. Batteries in good condition can be reused for energy purposes, while those in poor condition may require repair or recycling processes.
- Scale of use:** It is necessary to define the scale of use for the batteries, determining whether they will be used in small or large-scale projects [5]. This can influence the choice of storage technology and how the batteries will be integrated into the power system.
- Storage technology:** It is necessary to determine the storage technology that will be used to reuse batteries, such as stationary or mobile storage [23]. Each technology has its specific characteristics and requirements, so it must be determined which one is most suitable based on the requirements of the final application.
- Regulatory framework and Grid Code:** There should be a regulatory framework and Grid Code governing the reuse of EV batteries in the context of renewable energies. These regulations could include incentives or subsidies. In the European Union, new battery-use measures were implemented at the end of 2022 to increase

the recycling of all types of batteries. The aim is to achieve recycling rates of 45% by 2023, 63% by 2027, and 73% by 2030 [24, 25]. On the other hand, in Spain, Real Decreto 265/2021 was enacted in April 2021, addressing the treatment of EVs at the end of their useful life and the handling of all their parts [26]. This aspect is crucial for fostering project initiatives in this field.

3.1.2. Benefits

- **Environmental impact:** It is essential to assess the environmental impact arising from the reuse of electric vehicle batteries in the context of renewable energies [5], emphasizing benefits such as reducing greenhouse gas emissions and decreasing carbon footprint. Likewise, it is crucial to consider the environmental impact associated with the production, repair, and recycling processes of these batteries.
- **Economic viability:** Acquiring a second-life battery will always be more economical than acquiring a new one [27]. Therefore, it is necessary to assess the project's economic viability, considering the costs associated with the acquisition, transportation, installation, and maintenance of the batteries, as well as the potential income generated from the sale of energy.

3.2. Main sectors interested in the reuse of EV batteries

Various sectors show potential interest in reusing and recycling the EV batteries. Among them are electric vehicle manufacturers, who could benefit from reducing production costs. Owners of electric vehicles with environmental awareness might also be interested, as it would provide peace of mind by ensuring proper handling of waste and hazardous materials and offering savings when acquiring a new battery. Recycling companies are also interested due to the growing demand for these types of batteries and the rising prices of raw materials used in their production. Governments concerned about environmental and safety issues could promote battery reuse to support the transition to a circular economy [28–30] and reduce the exploitation of natural resources.

A solution to minimize waste and maximize the reuse and recycling of resources is to implement a circular economy [28] in producing and recycling EV batteries. This involves designing batteries with easily removable and reusable components. It also entails using recycled and recyclable materials in manufacturing new batteries, which would significantly contribute to reducing the carbon footprint and decreasing the need to extract and process raw materials from nature [27].

Figure 6 provides a perspective of a circular economy applied to EV batteries.

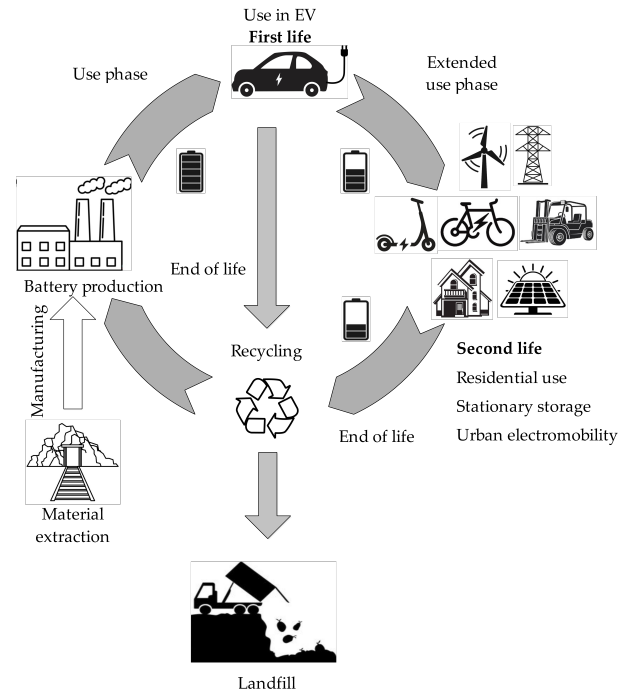


Figure 6. Circular economy perspective of the life of an EV battery. Illustration modified from [30]

3.3. Applications of EV battery reuse for renewable energy storage

The efforts invested in the literature review documented in this article have been primarily focused on presenting the main applications of the reuse of EV batteries in the field of renewable energy storage in an electrical grid. By addressing the established objective of the study and conducting a thorough search based on inclusion criteria, a total of 49 articles were gathered to analyze EV battery reuse in renewable energy storage. Of these, 26 articles specifically discuss the second-life of EV batteries.

The storage capacity retained by an EV battery at the end of its useful life, combined with the urgency to address global warming and environmental pollution, promotes the development of efficient and alternative technologies for the second-life application of EV batteries [31].

With the expansion of renewable energies worldwide, it becomes imperative to have energy storage systems [32], and the use of second-life EV batteries emerges as one of the viable solutions.

Stationary energy storage [23], involving the use of a bank of EV batteries on platforms located on a fixed surface, represents one of the most common applications for the reuse of EV batteries, especially

those storing energy from renewable sources such as photovoltaic and wind [33]. This energy could meet demand when generation experiences significant variations due to the intermittent nature of solar or wind energy. This could be achieved by injecting energy into the grid or directly delivering surplus energy to users to cover their total or partial demand. Users representing a substantial load would be crucial to justify the implementation of storage systems, such as integrating battery systems in buildings [34–36] or educational institutions. A specific example of this application is the installation of solar panels and batteries in elementary schools in Kenya [37].

For residential users, low consumption implies reduced savings when using storage systems; therefore, their installation is only viable if they serve community installations [38]. Another published case study focused on a collective system of four homes. The electrical consumption behavior was analyzed over a week with the incorporation of a storage system using second-life electric vehicle batteries integrated with a photovoltaic system. As a result, a self-consumption rate of 69% was achieved, along with a reduction in peak power from 10.8 to 6.9 kW [39].

It is estimated that, from electric vehicles sold until 2020, there will be a storage capacity of retired batteries by 2028 ranging between 120 and 549 GWh. This availability can be utilized in implementing projects for small, decentralized and autonomous rural networks, contributing to developing rural communities in developing countries [40].

Research conducted on the island of Tenerife, Spain, estimates that by 2031, up to 83.2 MWh could be collected using second-life electric vehicle batteries integrated into wind power generation [5]. A study related to wind farms has developed a stochastic economic dispatch model for renewable energy at the megawatt level based on data from NASA batteries. This model assesses the temperature conditions and charging and discharging currents to which the batteries are subjected in a power system with ten generation units [41].

A study conducted in California, United States, demonstrated that economically, a project using second-life batteries is more advantageous than one considering new batteries in a combined photovoltaic energy project [27]. At the University of California, Davis, a microgrid was designed and built to investigate the effectiveness of second-life electric vehicle (EV) batteries in conjunction with commercial-scale photovoltaic generation. The first study's results, conducted over a year, indicate that EV batteries help reduce the load on an electrical grid and provide stability during peak hours, thus supporting the reuse of EV batteries [42]. In California, it is estimated that by 2050, the energy stored by second-life EV battery systems will represent 15 TWh per year, equivalent to 5% of the currently used energy [32].

An innovative and sustainable application for second-life EV batteries is fast-charging stations for EVs, where the batteries receive energy from renewable sources and then supply it to the EVs [43, 44]. In China, EV batteries were used as a backup for a communication station, supported by a technical-economic study endorsing their use [45].

Electric vehicle batteries reused in stationary storage can contribute to stabilizing the frequency of power systems [9], especially in those with a high percentage of unconventional renewable energy penetration or in weak systems such as island grids. The frequency of the electrical network depends on the variability of the load: when the demand for energy increases, the frequency of the electrical system decreases, and vice versa. In these systems, batteries play a crucial role in regulating the variability between demand and generation, providing energy to the system when demand increases and storing surplus generation during periods of low demand. This reduces the need for fossil generation sources, contributing significantly to reducing carbon emissions.

Another interesting application is power smoothing, which refers to the technique used to reduce fluctuations in electrical power production [46, 47]. Its goal is to improve the quality and stability of the energy source, which is crucial for sectors like industry or healthcare, where a power outage could lead to significant losses or severe consequences for human health. There are various methods to implement power smoothing in electrical generation systems, including using batteries or other energy storage systems, employing energy converters, or implementing advanced control and monitoring systems [48, 49]. Power smoothing, through the use of EV batteries, optimizes the utilization of second-life EV batteries as stationary energy storage systems [50, 51], thereby reducing fluctuations in electrical power production. This application is handy in renewable energy generation, such as wind or solar power [48], [52, 53], where power production is stochastically modeled and varies based on weather conditions. This technique contributes to improving the quality and stability of the energy source and represents a cost-effective and sustainable solution for reusing EV batteries [54].

The application of mobile energy storage considers using second-life batteries for smaller electric vehicles. This application can make urban electromobility more sustainable and reduce carbon emissions into the environment [23].

4. Conclusions

This study presents the results obtained by applying a systematic literature review methodology related to reusing electric vehicle (EV) batteries. The review pro-

cess involved a thorough exploration conducted across reputable databases, including Web of Science, Scopus, and IEEE Xplore. In the initial stage, 458 relevant scientific papers were identified. Nevertheless, following an exclusion process that factored in criteria such as the availability of key components in the search, document accessibility, and inclusion within the study period (2018-2023), only 140 articles were selected. Finally, after a thorough review of titles and abstracts, 49 articles were carefully chosen as the foundation for this study.

The results indicate that, over the last five years, there has been a steady increase in the number of scientific works published in indexed journals addressing the concept of the second-life of electric vehicle batteries to provide energy support to power systems incorporating unconventional renewable generation.

The reuse of electric vehicle batteries has significant potential to reduce the carbon footprint of the transportation industry, contribute to the decarbonization of energy matrices, and support the stability and quality of energy in electrical systems. For this reason, research and development in this field must continue to advance to increase the energy efficiency of generation systems that utilize unconventional renewable energies. The ultimate goal should be establishing a circular economy system where electric vehicle batteries are reused in various applications, extending their lifespan to the maximum. This approach will help reduce the need for new batteries and, in turn, decrease the ecological impact of raw material extraction processes.

Acknowledgments

The authors would like to express their gratitude to the University of Cuenca, Ecuador, for providing access to the facilities of the Micro-Grid Laboratory at the Centro Científico, Tecnológico y de Investigación Balzay (CCTI-B), whose collaboration has been essential for the completion of this work. The findings presented in this article are part of the activities carried out in the project Movilidad Eléctrica: retos, limitaciones y plan de implementación en el régimen especial de la provincial de Galápagos, enfocada en el desarrollo sostenible y su factibilidad en la Ciudad de Cuenca. This project was co-directed by the author D. Ochoa-Correa and was conducted in the context of the II Concurso de Proyectos de Investigación-Vinculación organized by the Vice-Rectoría of Research and the Directorate of Engagement with Society at the University of Cuenca.

References

[1] S. Sharma, A. K. Panwar, and M. Tripathi, "Storage technologies for electric vehicles," *Journal of Traffic and Transportation Engineering*

(*English Edition*), vol. 7, no. 3, pp. 340–361, 2020, special Issue: Clean Alternative Fuels for Transport Vehicles. [Online]. Available: <https://doi.org/10.1016/j.jtte.2020.04.004>

[2] C. Peña Ordóñez and J. Pleite Guerra, *Estudio de baterías para vehículos eléctricos*. Departamento de Tecnología Electrónica, Universidad Carlos III de Madrid, 2011. [Online]. Available: <https://bit.ly/46ka8Jd>

[3] W. Wu, B. Lin, C. Xie, R. J. Elliott, and J. Radcliffe, "Does energy storage provide a profitable second life for electric vehicle batteries?" *Energy Economics*, vol. 92, p. 105010, 2020. [Online]. Available: <https://doi.org/10.1016/j.eneco.2020.105010>

[4] J. Zhu, I. Mathews, D. Ren, W. Li, D. Cogswell, B. Xing, T. Sedlatschek, S. N. R. Kantareddy, M. Yi, T. Gao, Y. Xia, Q. Zhou, T. Wierzbicki, and M. Z. Bazant, "End-of-life or second-life options for retired electric vehicle batteries," *Cell Reports Physical Science*, vol. 2, no. 8, p. 100537, 2021. [Online]. Available: <https://doi.org/10.1016/j.xcrp.2021.100537>

[5] A. López, A. Ramírez-Díaz, I. Castilla-Rodríguez, J. Gurriarán, and J. Méndez-Pérez, "Wind farm energy surplus storage solution with second-life vehicle batteries in isolated grids," *Energy Policy*, vol. 173, p. 113373, 2023. [Online]. Available: <https://doi.org/10.1016/j.enpol.2022.113373>

[6] Y. Li, S. Arnold, S. Husmann, and V. Presser, "Recycling and second life of mxene electrodes for lithium-ion batteries and sodium-ion batteries," *Journal of Energy Storage*, vol. 60, p. 106625, 2023. [Online]. Available: <https://doi.org/10.1016/j.est.2023.106625>

[7] D. Galatro, D. A. Romero, C. Da Silva, O. Trescases, and C. H. Amon, "Impact of cell spreading on second-life of lithium-ion batteries," *The Canadian Journal of Chemical Engineering*, vol. 101, no. 3, pp. 1114–1122, 2023. [Online]. Available: <https://doi.org/10.1002/cjce.24570>

[8] C. H. Illa Font, H. V. Siqueira, J. E. Machado Neto, J. L. Ferreira dos Santos, S. L. Stevan, A. Converti, and F. C. Corrêa, "Second life of lithium-ion batteries of electric vehicles: A short review and perspectives," *Energies*, vol. 16, no. 2, p. 953, 2023. [Online]. Available: <https://doi.org/10.3390/en16020953>

[9] L. Janota, T. Králík, and J. Knápek, "Second life batteries used in energy storage for frequency containment reserve service," *Energies*, vol. 13, no. 23, p. 6396, 2020. [Online]. Available: <https://doi.org/10.3390/en13236396>

- [10] M. Shahjalal, P. K. Roy, T. Shams, A. Fly, J. I. Chowdhury, M. R. Ahmed, and K. Liu, “A review on second-life of Li-ion batteries: prospects, challenges, and issues,” *Energy*, vol. 241, p. 122881, 2022. [Online]. Available: <https://doi.org/10.1016/j.energy.2021.122881>
- [11] E. Braco, I. San Martín, P. Sanchis, and A. Ursúa, “Fast capacity and internal resistance estimation method for second-life batteries from electric vehicles,” *Applied Energy*, vol. 329, p. 120235, 2023. [Online]. Available: <https://doi.org/10.1016/j.apenergy.2022.120235>
- [12] M. F. Börner, M. H. Frieges, B. Späth, K. Spütz, H. H. Heimes, D. U. Sauer, and W. Li, “Challenges of second-life concepts for retired electric vehicle batteries,” *Cell Reports Physical Science*, vol. 3, no. 10, p. 101095, 2022. [Online]. Available: <https://doi.org/10.1016/j.xcrp.2022.101095>
- [13] G. Pepermans, J. Driesen, D. Haeseldonckx, R. Belmans, and W. D’haeseleer, “Distributed generation: definition, benefits and issues,” *Energy Policy*, vol. 33, no. 6, pp. 787–798, 2005. [Online]. Available: <https://doi.org/10.1016/j.enpol.2003.10.004>
- [14] J. Pastuszak and P. Węgierek, “Photovoltaic cell generations and current research directions for their development,” *Materials*, vol. 15, no. 16, 2022. [Online]. Available: <https://doi.org/10.3390/ma15165542>
- [15] P. Pijarski, M. Wydra, and P. Kacejko, “Optimal control of wind power generation,” *Advances in Science and Technology Research Journal*, vol. 12, no. 1, pp. 9–18, 2018. [Online]. Available: <https://doi.org/10.12913/22998624/81448>
- [16] H. Lund, “Renewable energy strategies for sustainable development,” *Energy*, vol. 32, no. 6, pp. 912–919, 2007, third Dubrovnik Conference on Sustainable Development of Energy, Water and Environment Systems. [Online]. Available: <https://doi.org/10.1016/j.energy.2006.10.017>
- [17] S. Chai, N. Z. Xu, M. Niu, K. W. Chan, C. Y. Chung, H. Jiang, and Y. Sun, “An evaluation framework for second-life EV/PHEV battery application in power systems,” *IEEE Access*, vol. 9, pp. 152 430–152 441, 2021. [Online]. Available: <https://doi.org/10.1109/ACCESS.2021.3126872>
- [18] D. Ochoa, E. Villa, V. Iñiguez, C. Larco, and R. Sempértegui, “Uso de supercondensadores para brindar soporte de frecuencia en una microrred aislada,” *RTE*, vol. 34, no. 4, pp. 174–185, 2022. [Online]. Available: <https://doi.org/10.37815/rte.v34n4.961>
- [19] N. Horesh, C. Quinn, H. Wang, R. Zane, M. Ferry, S. Tong, and J. C. Quinn, “Driving to the future of energy storage: Techno-economic analysis of a novel method to recondition second life electric vehicle batteries,” *Applied Energy*, vol. 295, p. 117007, 2021. [Online]. Available: <https://doi.org/10.1016/j.apenergy.2021.117007>
- [20] L. Codina, “Cómo hacer revisiones bibliográficas tradicionales o sistemáticas utilizando bases de datos académicas,” *ORRL*, vol. 11, no. 2, pp. 139–153, 2020. [Online]. Available: <https://doi.org/10.14201/orl.22977>
- [21] N. Jan van Eck and L. Waltman, *VOSviewer Manual*. Universiteit Leiden, Meaningful metrics, 2018. [Online]. Available: <https://bit.ly/3R2P8IF>
- [22] T. Montes, M. Etxandi-Santolaya, J. Eichman, V. J. Ferreira, L. Trilla, and C. Corchero, “Procedure for assessing the suitability of battery second life applications after EV first life,” *Batteries*, vol. 8, no. 9, 2022. [Online]. Available: <https://doi.org/10.3390/batteries8090122>
- [23] H. S. Hayajneh, M. Lainfiesta Herrera, and X. Zhang, “Design of combined stationary and mobile battery energy storage systems,” *PLOS ONE*, vol. 16, no. 12, pp. 1–21, 12 2021. [Online]. Available: <https://doi.org/10.1371/journal.pone.0260547>
- [24] E. Commission, *Concerning batteries and waste batteries, repealing Directive 2006/66/EC and amending Regulation (EU) No 2019/1020*. EU Monitor, 2020. [Online]. Available: <https://bit.ly/3MO2obv>
- [25] Parlamento Europeo, *Nuevas medidas europeas para que las baterías sean más sostenibles y éticas*. Parlamento Europeo, 2022. [Online]. Available: <https://bit.ly/3MMtobs>
- [26] M. de la Presidencia, *Real Decreto 265/2021 Reglamento General de Vehículos*. Agencia Estatal Boletín General del Estado, 2021. [Online]. Available: <https://bit.ly/47neIb2>
- [27] I. Mathews, B. Xu, W. He, V. Barreto, T. Buonassisi, and I. M. Peters, “Technoeconomic model of second-life batteries for utility-scale solar considering calendar and cycle aging,” *Applied Energy*, vol. 269, p. 115127, 2020. [Online]. Available: <https://doi.org/10.1016/j.apenergy.2020.115127>
- [28] J. Ahuja, L. Dawson, and R. Lee, “A circular economy for electric vehicle batteries: driving the change,” *Journal of Property, Planning and Environmental Law*, vol. 12, no. 3, pp. 235–250, Jan 2020. [Online]. Available: <https://doi.org/10.1108/JPEL-02-2020-0011>

- [29] B. M. Sopha, D. M. Purnamasari, and S. Ma'mun, "Barriers and enablers of circular economy implementation for electric-vehicle batteries: From systematic literature review to conceptual framework," *Sustainability*, vol. 14, no. 10, 2022. [Online]. Available: <https://doi.org/10.3390/su14106359>
- [30] Y. Kotak, C. Marchante Fernández, L. Canals Casals, B. S. Kotak, D. Koch, C. Geisbauer, L. Trilla, A. Gómez-Núñez, and H.-G. Schweiger, "End of electric vehicle batteries: Reuse vs. recycle," *Energies*, vol. 14, no. 8, 2021. [Online]. Available: <https://doi.org/10.3390/en14082217>
- [31] S. I. Sun, A. J. Chipperfield, M. Kiaee, and R. G. Wills, "Effects of market dynamics on the time-evolving price of second-life electric vehicle batteries," *Journal of Energy Storage*, vol. 19, pp. 41–51, 2018. [Online]. Available: <https://doi.org/10.1016/j.est.2018.06.012>
- [32] R. Sathre, C. D. Scown, O. Kavvada, and T. P. Hendrickson, "Energy and climate effects of second-life use of electric vehicle batteries in california through 2050," *Journal of Power Sources*, vol. 288, pp. 82–91, 2015. [Online]. Available: <https://doi.org/10.1016/j.jpowsour.2015.04.097>
- [33] J. Mendoza-Vizcaíno, A. Sumper, A. Sudria-Andreu, and J. Ramírez, "Renewable technologies for generation systems in islands and their application to Cozumel island, Mexico," *Renewable and Sustainable Energy Reviews*, vol. 64, pp. 348–361, 2016. [Online]. Available: <https://doi.org/10.1016/j.rser.2016.06.014>
- [34] L. Canals Casals, M. Barbero, and C. Corchero, "Reused second life batteries for aggregated demand response services," *Journal of Cleaner Production*, vol. 212, pp. 99–108, 2019. [Online]. Available: <https://doi.org/10.1016/j.jclepro.2018.12.005>
- [35] J. Thakur, C. Martins Leite de Almeida, and A. G. Baskar, "Electric vehicle batteries for a circular economy: Second life batteries as residential stationary storage," *Journal of Cleaner Production*, vol. 375, p. 134066, 2022. [Online]. Available: <https://doi.org/10.1016/j.jclepro.2022.134066>
- [36] F. Salek, A. Azizi, S. Resalati, P. Henshall, and D. Morrey, "Mathematical modelling and simulation of second life battery pack with heterogeneous state of health," *Mathematics*, vol. 10, no. 20, 2022. [Online]. Available: <https://doi.org/10.3390/math10203843>
- [37] N. Kebir, A. Leonard, M. Downey, B. Jones, K. Rabie, S. M. Bhagavathy, and S. A. Hirmer, "Second-life battery systems for affordable energy access in kenyan primary schools," *Scientific Reports*, vol. 13, no. 1, p. 1374, Jan 2023. [Online]. Available: <https://doi.org/10.1038/s41598-023-28377-7>
- [38] L. Colarullo and J. Thakur, "Second-life EV batteries for stationary storage applications in local energy communities," *Renewable and Sustainable Energy Reviews*, vol. 169, p. 112913, 2022. [Online]. Available: <https://doi.org/10.1016/j.rser.2022.112913>
- [39] A. Soto, A. Berrueta, P. Zorrilla, A. Iribarren, D. H. Castillo, W. E. Rodríguez, A. J. Rodríguez, D. T. Vargas, I. R. Matias, P. Sanchis, and A. Ursúa, "Integration of second-life battery packs for self-consumption applications: analysis of a real experience," in *2021 IEEE International Conference on Environment and Electrical Engineering and 2021 IEEE Industrial and Commercial Power Systems Europe (EEEIC / I&CPS Europe)*, 2021, pp. 1–6. [Online]. Available: <https://doi.org/10.1109/EEEIC/ICPSEurope51590.2021.9584809>
- [40] H. Ambrose, D. Gershenson, A. Gershenson, and D. Kammen, "Driving rural energy access: a second-life application for electric-vehicle batteries," *Environmental Research Letters*, vol. 9, no. 9, p. 094004, sep 2014. [Online]. Available: [//dx.doi.org/10.1088/1748-9326/9/9/094004](https://dx.doi.org/10.1088/1748-9326/9/9/094004)
- [41] S. Hu, H. Sun, F. Peng, W. Zhou, W. Cao, A. Su, X. Chen, and M. Sun, "Optimization strategy for economic power dispatch utilizing retired EV batteries as flexible loads," *Energies*, vol. 11, no. 7, 2018. [Online]. Available: <https://doi.org/10.3390/en11071657>
- [42] J. Lacap, J. W. Park, and L. Beslow, "Development and demonstration of micro-grid system utilizing second-life electric vehicle batteries," *Journal of Energy Storage*, vol. 41, p. 102837, 2021. [Online]. Available: <https://doi.org/10.1016/j.est.2021.102837>
- [43] L. C. Casals, B. Amante García, and C. Canal, "Second life batteries lifespan: Rest of useful life and environmental analysis," *Journal of Environmental Management*, vol. 232, pp. 354–363, 2019. [Online]. Available: <https://doi.org/10.1016/j.jenvman.2018.11.046>
- [44] G. Graber, V. Calderaro, V. Galdi, and A. Piccolo, "Battery second-life for dedicated and shared energy storage systems

- supporting EV charging stations,” *Electronics*, vol. 9, no. 6, 2020. [Online]. Available: <https://doi.org/10.3390/electronics9060939>
- [45] C. Zhu, J. Xu, K. Liu, and X. Li, “Feasibility analysis of transportation battery second life used in backup power for communication base station,” in *2017 IEEE Transportation Electrification Conference and Expo, Asia-Pacific (ITEC Asia-Pacific)*, 2017, pp. 1–4. [Online]. Available: <https://doi.org/10.1109/ITEC-AP.2017.8080810>
- [46] J. W. Shim, H. Kim, and K. Hur, “Incorporating state-of-charge balancing into the control of energy storage systems for smoothing renewable intermittency,” *Energies*, vol. 12, no. 7, 2019. [Online]. Available: <https://doi.org/10.3390/en12071190>
- [47] S.-S. Shin, J.-S. Oh, S.-H. Jang, J.-H. Cha, and J.-E. Kim, “Active and reactive power control of ESS in distribution system for improvement of power smoothing control,” *Journal of Electrical Engineering and Technology*, vol. 12, no. 3, pp. 1007–1015, 2017. [Online]. Available: <https://doi.org/10.5370/JEET.2017.12.3.1007>
- [48] M. Lei, Z. Yang, Y. Wang, H. Xu, L. Meng, J. C. Vásquez, and J. M. Guerrero, “An MPC-based ESS control method for PV power smoothing applications,” *IEEE Transactions on Power Electronics*, vol. 33, no. 3, pp. 2136–2144, 2018. [Online]. Available: <https://doi.org/10.1109/TPEL.2017.2694448>
- [49] J.-C. Wu, H.-L. Jou, W.-C. Wu, and C.-H. Chang, “Solar power generation system with power smoothing function,” *IEEE Access*, vol. 10, pp. 29 982–29 991, 2022. [Online]. Available: <https://doi.org/10.1109/ACCESS.2022.3159801>
- [50] A. Zulueta, D. A. Ispas-Gil, E. Zulueta, J. García-Ortega, and U. Fernández-Gamiz, “Battery sizing optimization in power smoothing applications,” *Energies*, vol. 15, no. 3, 2022. [Online]. Available: <https://doi.org/10.3390/en15030729>
- [51] D. Benavides, P. Arévalo, J. A. Aguado, and F. Jurado, “Experimental validation of a novel power smoothing method for on-grid photovoltaic systems using supercapacitors,” *International Journal of Electrical Power & Energy Systems*, vol. 149, p. 109050, 2023. [Online]. Available: <https://doi.org/10.1016/j.ijepes.2023.109050>
- [52] Y. Zhu, H. Zang, L. Cheng, and S. Gao, “Output power smoothing control for a wind farm based on the allocation of wind turbines,” *Applied Sciences*, vol. 8, no. 6, 2018. [Online]. Available: <https://doi.org/10.3390/app8060980>
- [53] A. Atif and M. Khalid, “Savitzky–golay filtering for solar power smoothing and ramp rate reduction based on controlled battery energy storage,” *IEEE Access*, vol. 8, pp. 33 806–33 817, 2020. [Online]. Available: <https://doi.org/10.1109/ACCESS.2020.2973036>
- [54] X. Li, D. Hui, and X. Lai, “Battery energy storage station (BESS)-based smoothing control of photovoltaic (PV) and wind power generation fluctuations,” *IEEE Transactions on Sustainable Energy*, vol. 4, no. 2, pp. 464–473, 2013. [Online]. Available: <https://doi.org/10.1109/TSTE.2013.2247428>



IMPROVEMENT PROPOSAL IN THE STRUCTURAL SYSTEM OF A15" R29 RIGID MOUNTAIN BIKE FRAME, WITH FEA AND GEOMETRIC OPTIMIZATION

PROPUESTA DE MEJORA EN EL SISTEMA ESTRUCTURAL DE UN CUADRO RÍGIDO DE BICICLETA DE MONTAÑA DE 15" R29, MEDIANTE FEA Y OPTIMIZACIÓN GEOMÉTRICA

Juan P. Guamán^{1,*} , Hugo E. Crespo¹ ,
 César A. Paltán² , Jorge I. Fajardo² 

Received: 13-03-2023, Received after review: 06-06-2023, Accepted: 21-09-2023, Published: 01-01-2024

Abstract

Currently, cycling has increased significantly, along with the implementation of mountain bikes (MTB) with rigid frames, which are employed both as a means of transportation and for competitions due to their affordable cost. Since these bikes serve various purposes, they present varying stresses on their frames, surpassing design requirements and leading to failures in the upper chainstays. This study analyzes this type of failure, for which information regarding the frame material, acting loads, and 3D modeling is collected. Subsequently, a failure homologation analysis is conducted, and a proposal for improvement is generated by applying geometric optimization, determining a thickness of 3.50 mm in the upper chainstays and guaranteeing the resistance of the bike frame under the study conditions; that is, a drop of 60 cm and a load of 74 kg. This modification ensures that the stress in the upper chainstays does not exceed the ultimate stress of the material of 890,94 MPa.

Keywords: rigid frame, MTB, chainstay, geometric optimization, ultimate stress, drop.

Resumen

En la actualidad la práctica del ciclismo ha tenido un incremento considerable, así como el uso de bicicletas de montaña (Mountain Bike, MTB, en inglés), de cuadro rígido, utilizadas como medio de transporte y para competencia, debido a su costo asequible. Este tipo de bicicletas, al ser utilizadas para varios propósitos, presentan esfuerzos variados en su cuadro, que conllevan a sobrepasar las exigencias de diseño, presentándose fallos en las vainas superiores. Este tipo de fallo es analizado en este estudio, motivo por el cual se levanta la información referente al material del cuadro, cargas actuantes y modelado 3D. Posterior se genera un análisis de homologación del fallo y se determina una propuesta de mejora aplicando optimización geométrica, donde se determina un espesor de 3,50 mm en las vainas superiores, garantizando la resistencia del cuadro de bicicleta bajo las condiciones de estudio; es decir, un drop de 60 cm y carga de 74 kg, con la cual se garantiza que el esfuerzo en las vainas superiores no sobrepase el esfuerzo último del material de 890,94 MPa.

Palabras clave: cuadro rígido, MTB, vainas superiores, optimización geométrica, esfuerzo último, drop.

^{1,*}Mechanical Engineering, Universidad Politécnica Salesiana, Cuenca, Ecuador.

²New Materials and Transformation Processes Research Group GiMaT, Universidad Politécnica Salesiana, Cuenca, Ecuador. Corresponding author ✉: cpaltan@ups.edu.ec.

Suggested citation: Guamán, J. P.; Crespo, H. E.; Paltán, C. A. y Fajardo, J. I. "Improvement proposal in the structural system of a15" R29 rigid mountain bike frame, with fea and geometric optimization," *Ingenius, Revista de Ciencia y Tecnología*, N.º 31, pp. 106-114, 2024, DOI: <https://doi.org/10.17163/ings.n30.2024.09>.

1. Introduction

The bicycle has become one of the most widely used alternative means of transportation, experiencing a significant increase in recent years [1,2]. In addition to promoting health and being environmentally friendly, its accessibility makes it an affordable option for society [3,4].

Considering the wide variety of bicycles, MTBs are the most commonly used due to their versatility and ability to ride on both roads and mountainous terrains [5]. These bicycles have front suspension, and their frame is rigid. Over time, bicycles have undergone a significant technological evolution, with a considerable reduction in weight and an increase in resistance, transitioning from the use of steel to composite materials reinforced with carbon fiber in most bicycle components and experiencing improvements in their transmission system [6].

Carbon Fiber Reinforced Polymer (CFRP) composites are used in manufacturing bicycle frames due to their advantages in lightweight, mechanical strength, and corrosion resistance [7]. It is worth noting that aluminium alloy inserts are incorporated in the interface areas with other bicycle components due to the type of connection [1]. The application of composite material in MTB bicycles is based on the arrangement or orientation of the fibers, using proposed filament braiding, which avoids excessive stiffness [8].

This vehicle comprises various components, one of the most important being the frame, as it holds the primary interfaces and is the point where stresses converge. Consequently, the frame is predisposed to failure due to the concentration of loads transmitted during operation [9].

Besides occurring at the joints and interfaces, the most common failures in rigid frames of MTB bicycles manifest in the upper and lower chainstays [10, 11]. This is due to overload caused by jumps or steep descents. Additionally, there are cases caused by falls, which are not considered failures in normal operation [12]. The analysis specifically focuses on the failure in the upper chainstays due to the physical configuration of a rigid frame.

It is essential to present a solution proposal since the failures are directly proportional to the increased use of rigid carbon fiber frame bicycles. This leads to greater customer dissatisfaction, resulting in a direct discredit of bicycle brands and, consequently, causing losses in sales [13].

By determining an improvement proposal through the geometric optimization of the upper chainstays [14], mechanical strength is ensured according to the design requirements of this type of bicycle, considering the desired input and output parameters [15], in line with the provisions of ISO 4210-6 2019 and its application [16].

In this article, the failure load and the configu-

ration of the material used are determined. Then, a validation of the failure is carried out using engineering software. Subsequently, a solution proposal is presented through the geometric optimization of the upper chainstays [17].

2. Materials and Methods

2.1. Laminate configuration

An MTB bicycle manufactured with CFRP of dimensions 15" R29, was used, exhibiting a failure in the upper chainstays, as illustrated in Figure 1.



Figure 1. Failure in the upper chainstays

In this case, for the application of the bicycle frame, a quasi-isotropic laminate is used, with layers oriented in $[0^\circ, 45^\circ, -45^\circ, 90^\circ]$. This quasi-isotropic carbon fiber laminate offers several significant advantages, such as good performance in terms of strength and stiffness in multiple planes. It also provides greater durability due to better load distribution, increasing the material's resistance to fatigue. This is especially valuable in applications where the laminate is subject to variable or cyclic loads over time. Another factor is the reduction in sensitivity to cracks, as it is less prone to crack propagation or localized damage, in addition to better vibration absorption. These characteristics result from its structure and uniform distribution of carbon fibers in multiple directions [18].

Carbon fiber sheets are composed of filaments containing a percentage between 80 and 95% carbon, with a diameter usually around 8 μm . A resin or polymeric matrix is used to position and bond these filaments and protect them from external agents [19,20].

Figure 2 illustrates the orientation system of carbon fibers subjected to tensile and compressive stress, considering fiber orientation [19,21].

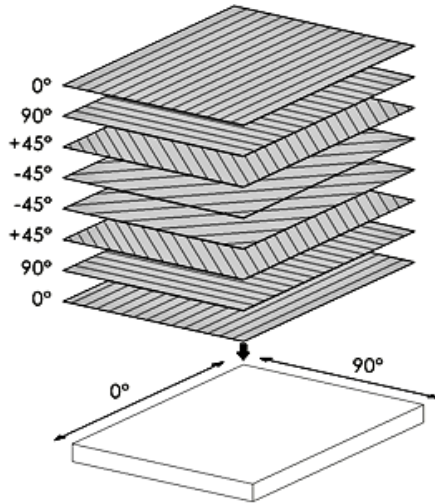


Figure 2. Quasi-isotropic laminate [20]

Table 1 shows the epoxy/carbon composite material constants.

Table 1. Composite material constants

	E_{xy}	E_{yz}	E_{xz}
Young's Modulus (GPa)	123.3	7.78	7.78
	ν_{xy}	ν_{yz}	ν_{xz}
Poisson's Ration	0.27	0.42	0.27
	G_{xy}	G_{yz}	G_{xz}
Shear Modulus (GPa)	5	3.8	5

2.2. Methods of analysis

To analyze carbon fiber bicycle frames, a quasi-isotropic laminate is used with the following fiber orientation and arrangement angles: $0^\circ / 90^\circ / +45^\circ / -45^\circ / -45^\circ / +45^\circ / 90^\circ / 0^\circ$, which are loaded into the program configuration as layers before conducting simulations.

Furthermore, in the material analysis, orthotropic symmetry is taken as a reference, and the material constitutive equation in equation (1) is considered for a Cartesian system with three mutually perpendicular directions, where the stresses (σ) are equal to the product of the stiffness matrix (C) and the deformations (ε) [19].

$$\begin{Bmatrix} \sigma_1 \\ \sigma_2 \\ \sigma_3 \\ \tau_{23} \\ \tau_{31} \\ \tau_{12} \end{Bmatrix} = \begin{bmatrix} C_{11} & C_{12} & C_{13} & 0 & 0 & 0 \\ C_{21} & C_{22} & C_{23} & 0 & 0 & 0 \\ C_{31} & C_{32} & C_{33} & 0 & 0 & 0 \\ 0 & 0 & 0 & C_{44} & 0 & 0 \\ 0 & 0 & 0 & 0 & C_{55} & 0 \\ 0 & 0 & 0 & 0 & 0 & C_{66} \end{bmatrix} \begin{Bmatrix} \varepsilon_1 \\ \varepsilon_2 \\ \varepsilon_3 \\ \gamma_{23} \\ \gamma_{31} \\ \gamma_{12} \end{Bmatrix} \quad (1)$$

Where:

- $\sigma_{1,2,3}$ = Stresses in the x, y, and z directions
- $\tau_{1,2,3}$ = Shear in the x, y, and z directions
- $[C]$ = Stiffness matrix
- $\varepsilon_{1,2,3}$ = Deformations in x, y, and z
- $\gamma_{1,2,3}$ = Angular deformation in x, y, and z

2.3. Finite element model used

The finite element model used in this study is the Von Mises model, which determines the deformations generated on the chainstays. The analysis is static, as the loads influencing the bicycle frame and the correlation of dynamic loads are known. Tetrahedral elements are employed for meshing due to the complexity of the model, and the element order number is quadratic, contributing to convergence [9]. Regarding the type of laminate bonding in practical cases, Bonded is used due to its process, and for the simulation, a laminate was loaded as a Layered Section, allowing the specification of the thickness and angles of each layer.

2.4. Failure criterion

The failure criterion is based on the maximum normal stress since the material is brittle; in this case, the bicycle frame, made of carbon fiber, undergoes minimal deformation before breaking. For validation, failure occurs when one of the stress components in the three orthogonal directions is greater than or equal to the material's stress limit in the corresponding direction, as indicated in equation (2).

$$\sigma_{max} = \max(|\sigma_1|, |\sigma_2|, |\sigma_3|) \geq \sigma_u \quad (2)$$

Where:

- σ_{max} = Maximum stress
- $\sigma_1, \sigma_2, \sigma_3$ = Stress in x and z
- σ_u = Ultimate stress

2.5. Geometric optimization

The objective of the geometric optimization in this case study is to maximize the thickness of the upper chainstays to increase resistance and thereby withstand the stresses generated by the load acting on the bicycle frame. It is crucial to identify the input and output parameters or conditions necessary to obtain the appropriate values according to the established requirements.

The input condition is:

- **P4:** Thickness

The output conditions are:

- **P2:** Restriction of the ultimate material stress (890 MPa) and thickness range from 1 to 5 mm
- **P3:** Maximize the volume

2.6. Characterizations

2.6.1. Microscopy analysis

To determine the thickness of the laminate, a sample was taken from the area near the break in the upper chainstay, which was prepared following the metallographic procedure [22]. The micrograph of the analyzed region provided the image shown in Figure 3.



Figure 3. Microscopy 5x (a) and 20x (b)

With the microscopic analysis at 20x, it is determined that the thickness of the laminate is $125 \mu\text{m}$ [23], indicating that, according to the raised thickness of 1 mm in the upper chainstay, there are 8 sheets, as mentioned in [24–26].

2.6.2. Data sensor

The bicycle user, using a Mobvoi Ticwatch E3 sports bracelet equipped with GPS, gyroscope, accelerometer, and heart rate monitor sensors, recorded data such as bicycle speed, terrain slope, and jump height.

2.6.3. Thickness analysis

To determine the thickness of the laminate in the upper chainstays of the bicycle frame, An Olympus BX51M metallographic microscope with a DP72 digital camera was used, along with the OLYMPUS Stream Essential® software, which allows capturing images at magnifications of 5x and 20x.

2.7. Bicycle frame geometry

The geometry of the bicycle frame is modeled as a 1:1 scale surface, allowing the loading of the laminates with their respective orientation of quasi-isotropic fibers. Figure 4 displays the model of the rigid bicycle frame.



Figure 4. 3D frame geometry

2.8. Meshing

A meshing of the geometry surface is performed, using the Capture Proximity and Curvature mesh enhancement method. 81786 nodes and 82487 elements were obtained (Figure 5).

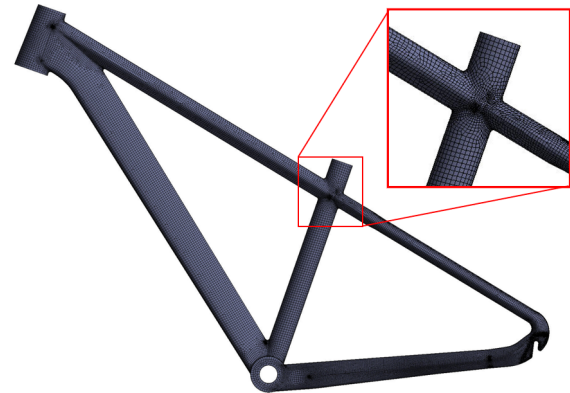


Figure 5. Bicycle frame meshing

In the mesh quality verification, average values of Orthogonal Quality: 0.97 and Skewness: 0.14 are obtained. These results indicate a high mesh quality [26], ensuring an appropriate approximation of the simulation values.

2.9. Determination of failure factors

The data collected from the sports bracelet used by the cyclist on the day of the event include a speed of 35 km/h, a route slope of -2° , and a drop or jump of 0.60 m in height. Additionally, it is known that the mass of the cyclist is 74 kg, which acted on the bicycle saddle.

2.10. Determination of the ultimate tensile stress of the laminate

With the information on the layers thickness with its respective orientation and the acting load, the ultimate tensile stress of the bicycle frame laminate can be determined.

To simulate the tensile test, a specimen model measuring 25 mm wide x 150 mm long and 2.50 mm thick with eight layers of laminate with quasi-isotropic configuration is generated. The boundary conditions include a fixed end and a displaced end, where a displacement of 4 mm is applied in the longitudinal direction of the specimen, following the standards established in ASTM D3090 [27]. The analysis was conducted using Explicit Dynamics, obtaining the maximum equivalent Von Mises stress (514,87 MPa), as shown in Figure 6.

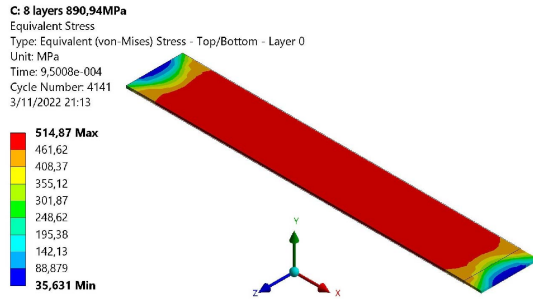


Figure 6. Tensile test specimen simulation

After performing the simulation of the tensile test specimen, a maximum tensile stress of 890,94 MPa is obtained.

2.11. Numerical simulation of vertical load

The vertical load test method of UNE ISO 4210-6 [16] describes boundary conditions that apply to this analysis, thus complementing the information described in the failure mode determination section (Figure 7).

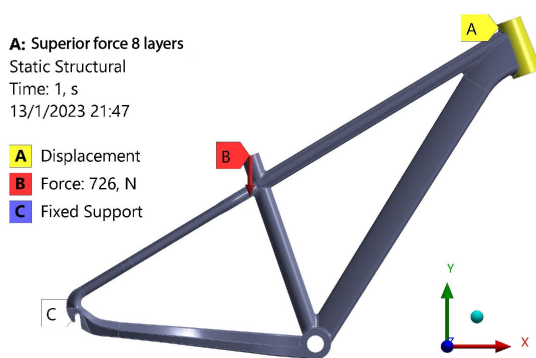


Figure 7. Initial and boundary conditions

Additionally, the standard specifies that the tests to be applied are dynamic; however, the analysis of this bicycle frame will be carried out statically, applying values relative to dynamic loads to achieve the same effect [28, 29].

Equation (3) is used to calculate the dynamic coefficient. Then, the dynamic force is calculated using equation (4).

$$K_d = 1 + \sqrt{1 + \frac{2 * H}{\delta_{est}}} = 46,119 \quad (3)$$

Where:

- H= Bicycle drop height (mm)
- δ_{est} = Static displacement of the point of application of the static force (mm)

To determine the static displacement at the load application point, a preliminary simulation is conducted, applying a load of 74 kg, and resulting in a displacement of 0.52 mm (Figure 8).

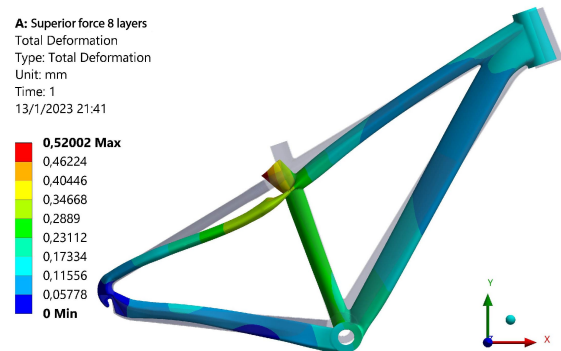


Figure 8. Maximum displacement with a static load of 74 kg

Thus, the dynamic load is determined.

$$P_d = P_e * K_d = 3412,80 \text{ kg} \quad (4)$$

Where:

- P_e = Static force

The P_d value is the new load applied to carry out a second simulation, considering the impact of the initial load of 74 kg, with a drop height of 0.60 m.

3. Results and Discussion

3.1. Rupture of the upper chainstays

To determine the equivalent Von Mises stress acting on the upper chainstays to homologate the failure mode, a load of $-3412,80$ kg (P_d) is applied to the “Y” axis of the seat tube, representing the cyclist’s load. After post-processing, values exceeding the ultimate stress of 890.94 MPa (determined with the specimen) are obtained, as shown in Figure 9. The failure mechanism occurs due to impact and repetitive stress; cracks that are not detected in time and that can propagate and weaken the bicycle structure may appear. In this study, no delamination is observed because the carbon fiber layers do not separate or detach, as demonstrated in the bicycle frame inspection using microscopy. Impact damage weakens the structure and reduces its strength. A forceful impact against a hard object or a significant

fall can cause internal damage not visible to the naked eye. Additionally, the overload from the jump exceeded the design limits.

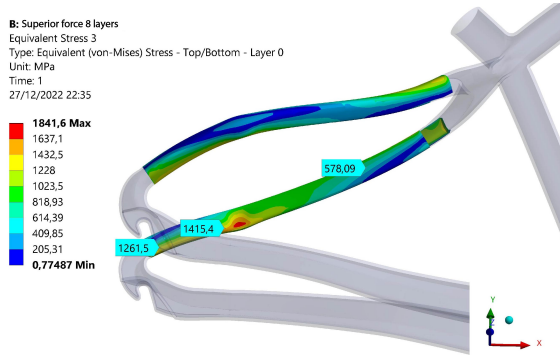


Figure 9. Stresses generated in the upper chainstays

3.2. Analysis through geometric optimization

3.2.1. Optimization of the bicycle frame thickness

Considering the ultimate stress of the laminated material specimen of 890.94 MPa, the stress obtained in the rupture zone of the upper chainstays of 1415.40 MPa, and maximum stress of 1841.60 MPa displaced towards the rupture zone, located in the subsequent left zone, as shown in Figure 9, an optimization is performed to prevent this stress from affecting the upper chainstays.

After the first iteration, three candidate points are obtained as a solution, as shown in Table 2. These points represent the three possible thickness options for the bicycle frame laminate. Candidate point 1 corresponds to a thickness of 5 mm, representing a 400% increase in thickness; candidate point 2 corresponds to a thickness of 4.60 mm, representing a 360% increase; and candidate point 3 corresponds to a thickness of 4.16 mm, representing a 316% increase. Point 3 shows the smallest increase among all; therefore, it can be considered for the simulation with the new thickness.

Table 2. Geometric optimization results. First optimization.

Name	P4-SYS \ Surface Thickness (mm)		P2 - Equivalent Stress 3 Máximum (MPa)		P3 - SYS \ Surface Volume (mm ³)	
	Surface Thickness (mm)	Parameter value	Variation in relation to the reference	Parameter value	Variation in relation to the reference	
Candidate point 1	5	2167,6	0,45 %	1,93E+0,6	20,09 %	
Candidate point 2	4,6	2164,1	0,29 %	1,78E+0,6	10,48 %	
Candidate point 3	4,16	2157,8	0,00 %	1,61E+0,6	0,00 %	

By conducting another simulation with the new thickness of 4.16 mm throughout the bicycle frame, a stress of 478.68 MPa is obtained in the failure zone,

and a maximum stress of 665 MPa in the subsequent left zone. See Figure 10a.

3.2.2. Optimization of the upper chainstays thickness

The second iteration focuses exclusively on the thickness of the upper chainstays, using the results from the first run and referencing the maximum stress of 665 MPa. As a result, three candidate points with new thickness values are obtained, as shown in Table 3. The objective of this second iteration is to reduce the thickness of the upper chainstays compared to the thickness found for the rest of the frame. Candidate point 1 was discarded because it has a value of 4.16 mm. From the remaining candidate points, the one with the least thickness was selected, which was point 3 with a value of 3.50 mm.

A new simulation was conducted with the new thickness value of 3.50 mm in the upper chainstays of the bicycle frame, resulting in a stress of 604.60 MPa in the failure zone and a maximum stress of 714.94 MPa in the subsequent left zone. See Figure 10b.

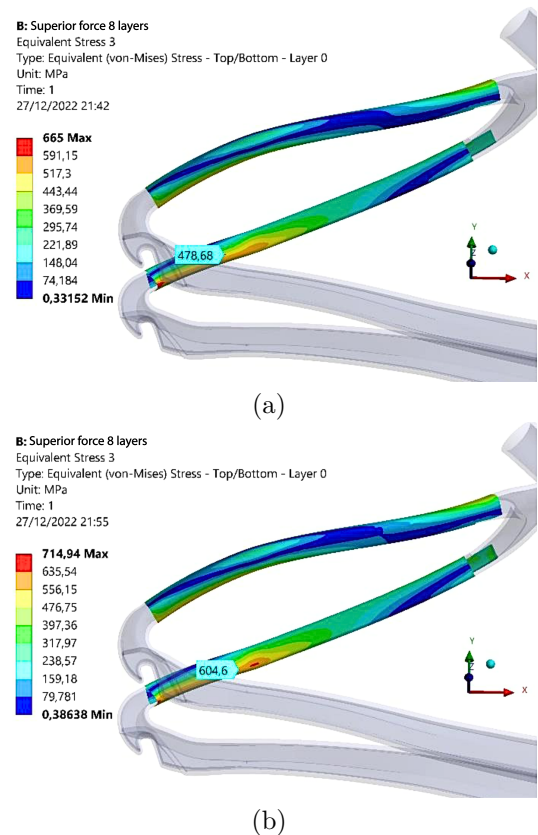


Figure 10. Stresses generated in the upper chainstays in the first iteration (a). Stresses generated in the upper chainstays in the second iteration (b).

Table 3. Geometric optimization results. Second optimization

Name	P4-SYS\ Surface Thickness (mm)	P2 – Equivalent Stress 3 Máximum (MPa)		P3 - SYS \Surface Volume (mm^3)	
		Parameter value	Variation in relation to the reference	Parameter value	Variation in relation to the reference
Candidate point 1	4,16	664,97	0,00 %	1,61E+0,6	18,89 %
Candidate point 2	3,84	664,97	0,00 %	1,491E+0,6	9,85 %
Candidate point 3	3,5	664,97	0,00 %	1,358E+0,6	0,00 %

3.2.3. Final proposal

Table 4 shows the final results of the optimizations:

Table 4. Final results of the optimizations

Parameters	Initial state	Optimized state	Variation
Stress in the upper chainstays	1766 MPa	619,54 MPa	-64,92 %
Material thickness	1 mm	3,50 mm	250,20 %

4. Conclusions

Currently, rigid-frame mountain bikes are widely used, both as a means of transportation and in competitions. Often, users tend to overuse them due to their versatility and affordability, disregarding their application limits and employing them in situations for which they were not originally designed.

The study allowed identifying the mechanisms to determine failures in carbon fiber bicycle frames, analyzing the failure mode of the upper chainstays after a 60 cm drop, based on the UNE ISO 4210-6 standard and collecting user data. Validation was carried out through Finite Element Analysis (FEA).

Microscopy analysis allowed determining the thickness and number of layers, as well as the total thickness of the laminate.

It is valid to note the determination of the number of layers (8 layers) and, considering previous studies on the standard laminate of commercial carbon fiber bicycle frames (quasi-isotropic), a tensile analysis is performed. In this analysis, ultimate load values are obtained, and a stress-deformation curve is generated for a brittle material.

To perform the analysis in the numerical simulation program, the Layered Section laminate is loaded, configuring the number of layers and their orientation. This allows for establishing a similarity with the

"bonded" laminate used in the manufacture of carbon fiber bicycle frames.

The failure of the bicycle frame components, specifically in the upper chainstays, occurs when the generated stresses exceed the ultimate stress of the composite material, which is 890.94 MPa, according to the simulation conducted on the laminate specimen.

The geometric optimization is based on the proposal of new thickness values for the laminated material and not on the variation of its geometry. Furthermore, the improvement proposal guarantees the stresses generated by the cyclist's load, considering a weight of 74 kg and a drop of 60 cm.

Optimization proposes a thickness of 3.50 mm for the upper chainstays. Additionally, a thickness of 4.16 mm is proposed for the rear wheel attachment area, as it directly impacts the upper chainstays.

The rupture of the system under study is due to the inherent fragility of the material. The observed deformation is characteristic of a fragile system, and the rupture occurs because of the fragility of the carbon fiber. By proposing a thickness of 3.5 mm through optimization, it is possible to prevent breakages caused by impacts when the bicycle falls to the ground during the analyzed jumps. This result is attributed to the increased area, thus avoiding exceeding the stress limit of the composite material.

References

- [1] S. M. Martín Mozas, *Desarrollo de guía metodológica y ejemplo de análisis estático y a fatiga de cuadro de bicicleta*. E. T. S. I. Industriales. Universidad Politécnica de Madrid, 2021. [Online]. Available: <https://bit.ly/48wefnU>
- [2] J. Freire, *El sector de la bicicleta en cifras 2020*. 30 Días en Bici, 2020. [Online]. Available: <https://bit.ly/3ruvJAF>
- [3] W. J. Jara Lupercio and M. A. Dunia Pauta, *Beneficios sobre la salud derivados del uso de la bicicleta, frente a la contaminación ambiental y la pandemia SARS CoV-2. Revisión bibliográfica*. Carrera de Cultura Física. Universidad de Cuenca, 2021. [Online]. Available: <https://bit.ly/48rqrpO>
- [4] J. Sanín Eastman, "El uso de la bicicleta como promotor de la movilidad sostenible: acciones y efectos en la movilidad cotidiana, el mejoramiento de la calidad del aire y el transporte público de las ciudades," *Revista Kavilando*, vol. 12, no. 1, pp. 118–126, jun. 2020. [Online]. Available: <https://bit.ly/45a030G>
- [5] P. Cañizares Gómez de Terreros, *Prediseño y análisis numérico de un prototipo de cuadro de*

- bicicleta en CFRP*. Universidad de Sevilla, 2016. [Online]. Available: <https://bit.ly/3Pt8DSx>
- [6] P. Navarro, J. Rui-Wamba, A. Campos, O. Antisench, C. Bañuelos, and M. Jordi, J. Rui-Wamba, *Ingeniería de la Bicicleta*. Fundación Esteyco, 2009. [Online]. Available: <https://bit.ly/466mHIC>
- [7] P. Bajpai, *Carbon Fiber*. Second edition. Cambridge, Elsevier, 2020. [Online]. Available: <https://bit.ly/453CAOU>
- [8] A. Paz Carvajal, L. M. Ríos Gamboa, G. F. Casanova García, A. Leyton, and J. J. García Álvarez, “Fabricación y caracterización mecánica de un laminado de fibra de carbono en matriz de resina epoxi,” *Scientia et Technica*, vol. 22, no. 3, pp. 262–267, 2017. [Online]. Available: <https://bit.ly/465xoev>
- [9] K. Khutal, G. Kathiresan, K. Ashok, B. Simhachalam, and D. Davidson Jebaseelan, “Design validation methodology for bicycle frames using finite element analysis,” *Materials Today: Proceedings*, vol. 22, pp. 1861–1869, 2020, 2nd International Conference on Materials Manufacturing and Modelling, ICMMM – 2019, VIT University, Vellore, 29th - 31st March 2019. [Online]. Available: <https://doi.org/10.1016/j.matpr.2020.03.085>
- [10] Aszahara. (2010) Rotura tirante carbono Orbea Oiz, garantía. Foro MTB. Foro MTB. [Online]. Available: <https://bit.ly/3ZvqFbf>
- [11] NazcaCarbono. (2020) Caso de éxito: Reparación de una vaina totalmente seccionada. Nazca Carbono. [Online]. Available: <https://bit.ly/3rsOqnP>
- [12] UvesBikes. (2023) Reparar cuadro de bicicleta. Uves Bikes. Uves Bikes. [Online]. Available: <https://bit.ly/3rAvt2u>
- [13] C. Carlson Morales and A. L. Villarreal-Gómez, “Análisis de las 5 fuerzas de Porter aplicado a una refaccionaria de bicicletas y motocicletas,” *Boletín Científico de las Ciencias Económico Administrativas del ICEA*, vol. 8, no. 16, pp. 44–47, jun. 2020. [Online]. Available: <https://doi.org/10.29057/icea.v8i16.5832>
- [14] M. A. Guzmán and A. Delgado, “Optimising a shaft’s geometry by applying genetic algorithms,” *Ingeniería e Investigación*, vol. 25, no. 2, pp. 15–23, 2005. [Online]. Available: <https://doi.org/10.15446/ing.investig.v25n2.14631>
- [15] U. Khalid, O. M. A. Mustafa, M. A. Naeem, M. Y. M. Alkhateeb, and B. M. A. E. Awad, “Direct optimization of an automotive sheet metal part using ANSYS,” *International Journal of Engineering and Management Sciences*, vol. 5, no. 3, pp. 134–142, 2020. [Online]. Available: <https://doi.org/10.21791/IJEMS.2020.3.14>
- [16] ISO, *ISO 4210-6:2023 Cycles – Safety requirements for bicycles – Part 6: Frame and fork test methods*. International Organization for Standardization, 2023. [Online]. Available: <https://bit.ly/3LCmg0m>
- [17] L. Parras, “Métodos alternativos de optimización de la geometría de estructuras articuladas,” *Informes de la Construcción*, vol. 35, no. 351–352, pp. 77–82, 1983. [Online]. Available: <https://bit.ly/3Zy91DG>
- [18] J. Fajardo, M. Villa, J. Pozo, and D. Urgilés, “Characterization of the tensile properties of an epoxy-carbon laminated composite used in the development of a single-seater Formula SAE type,” *Enfoque UTE*, vol. 10, no. 3, pp. 1–12, 2019. [Online]. Available: <https://doi.org/10.29019/enfoque.v10n3.381>
- [19] A. F. Rivas Bolívar, *Análisis estructural de un marco rígido de bicicleta de montaña mediante el modelamiento de elemento finitos en el software ANSYS*. Facultad de Ingeniería. Universidad de los Andes, 2019. [Online]. Available: <https://bit.ly/48wxep9>
- [20] L. A. Vargas Martínez and J. M. Martínez Benavides, *Estudio de propiedades mecánicas en láminas de fibra de carbono fabricadas mediante el proceso de laminación para elementos aeronáuticos*. Universidad Tecnológica de Pereira, 2019. [Online]. Available: <https://bit.ly/3PwqDvd>
- [21] R. M. Jones, *Mechanics of composite materials*. Taylor and Francis, 1999. [Online]. Available: <https://bit.ly/3ro9DiT>
- [22] Facultad de Ingeniería, *Metalografía Protocolo. Curso de Materiales*. Escuela Colombiana de Ingeniería Julio Garavito, Colombia, 2011. [Online]. Available: <https://bit.ly/3t5aw0i>
- [23] S. K. García Castillo, *Análisis de laminados de materiales compuestos con precarga en su plano y sometidos a impacto*. Departamento de Mecánica de Medios Continuos y Teoría de Estructuras. Universidad Carlos III de Madrid, 2007. [Online]. Available: <https://bit.ly/46ooad5>
- [24] E. Monsalvo Barrera and J. Cortés Rico, *Propuesta de diseño de una masa soporte en fibra de carbono para un vehículo mini-baja*. Facultad de Ingeniería. Universidad Nacional Autónoma de México, 2012. [Online]. Available: <https://bit.ly/3ZsUl93>

- [25] A. Solana Rodríguez, *Cuadro de bicicleta en material compuesto*. Departamento de Ingeniería Mecánica, Energética y de Materiales. Universidad Pública de Navarra, 2014. [Online]. Available: <https://bit.ly/3ZzFkSP>
- [26] ANSYS, *Mesh Quality*. ANSYS Workbench, 2023. [Online]. Available: <https://bit.ly/3RBFMyC>
- [27] ASTM, *ASTM D3039/D3039M-08 Standard Test Method for Tensile Properties of Polymer Matrix Composite Materials*. ASTM International, 2014. [Online]. Available: <https://bit.ly/3PzA6SJ>
- [28] Y. Lugo Pérez, *Modelación de un cuadro de bicicleta “Minerva” para la utilización de un nuevo material aplicando el MEF*. Ingeniería Mecánica, 2006. [Online]. Available: <https://bit.ly/3rtgUxQ>
- [29] D. Vdovin, Y. Levenkov, and V. Chichekin, “Light frame design for quad bike using topology optimization,” *IOP Conference Series: Materials Science and Engineering*, vol. 589, no. 1, p. 012026, 2019. [Online]. Available: <https://dx.doi.org/10.1088/1757-899X/589/1/012026>



INCIDENCE OF AUTOMOTIVE AIR CONDITIONING ON THE INDEX OF FUEL CONSUMPTION IN SPARK IGNITION VEHICLE ON A ROUTE IN THE ECUADORIAN AMAZON

INCIDENCIA DEL AIRE ACONDICIONADO AUTOMOTRIZ EN EL ÍNDICE DE CONSUMO DE COMBUSTIBLE EN VEHÍCULO DE ENCENDIDO PROVOCADO EN UNA RUTA DE LA AMAZONÍA ECUATORIANA

Edilberto Antonio Llanes-Cedeño^{1,*} , Shayan Fredy Grefa Shiguango¹ , Jaime Vinicio Molina-Osejos¹ , Juan Carlos Rocha-Hoyos² 

Received: 24-01-2023, Received after review: 07-12-2023, Accepted: 11-12-2023, Published: 01-01-2024

Abstract

In recent years the environment has been affected by pollution produced by vehicles. The objective of this research project was to determine the incidence of air conditioning (A/C) in the vehicular fuel consumption index in the Shushufindi canton, through real traffic tests, Efficient driving mode and the use of Extra and Super gasoline, for the selection of the best alternative. The study was carried out on a route with a greater flow of vehicles, especially during normal (9:00 am) and peak (5:00 pm) hours, which comprises 16.17 km; for which used gasoline Extra (85 octane) and Super (92 octane). Data collection was carried out using an OBD2 ELM 327 system. The results obtained in the characterization of the representative mixed cycle at 9:00 am, a maximum speed of 81 km/h and an average speed of 39 km/h were obtained in a time of 1446 s route; while the mixed cycle at 5:00 pm the maximum speed is 70 km/h and an average speed of 37 km/h with a travel time of 1632 s. The lowest fuel consumption index was evidenced in normal hours, without A/C and Extra fuel (T3) with values between 0.0584 - 0.060 (L/km), and in normal hours, without A/C and super fuel (T7) that are between 0.0561-0.0585 (L/km).

Keywords: fuel consumption index, air conditioning, efficient driving, fuel, schedule, driving cycle

Resumen

En los últimos años, el ambiente se ha visto afectado a causa de la contaminación producida por los vehículos. El presente proyecto de investigación tuvo como objetivo determinar la incidencia del aire acondicionado (A/C) en el índice de consumo de combustible vehicular en el cantón Shushufindi, por medio de pruebas reales de tráfico, modo de conducción eficiente y empleo de gasolina extra y súper, para la selección de la mejor alternativa. El estudio se realizó en una ruta de mayor flujo de vehículos, especialmente en la hora normal (9 a. m.) y pico (5 p. m.) que comprende 16.17 km, para ello se utilizó el combustible Extra (85 octanos) y Súper (92 octanos). La toma de datos se ejecutó mediante un sistema OBD2 ELM 327. Los resultados obtenidos en la caracterización del ciclo mixto representativo de 9 a. m. se obtuvo una velocidad máxima de 81 km/h y una velocidad media de 39 km/h en un tiempo de recorrido de 1446 s; mientras que el ciclo mixto de 5 p. m. la velocidad máxima es de 70 km/h y una velocidad media de 37 km/h con un tiempo de recorrido de 1632 s. El menor índice de consumo de combustible se evidenció en el horario normal, sin A/C y combustible extra (T3) siendo sus valores entre 0.0584 – 0.060 (L/km), y en el horario normal, sin A/C y combustible súper (T7) que se encuentran entre 0.0561-0.0585 (L/km).

Palabras clave: índice de consumo de combustible, aire acondicionado, conducción eficiente, combustible, horario, ciclo de conducción

^{1,*}Grupo de Investigación Eficiencia, Impacto Ambiental e Innovación en la Industria y el Transporte, Facultad de Ingeniería y Ciencias Aplicadas, Carrera de Ingeniería Automotriz, Universidad Internacional SEK, Quito-Ecuador.
Corresponding author ✉: antonio.llanes@uisek.edu.ec.

²Grupo de Investigación INVELECTRO, Facultad de Mecánica, Carrera de Ingeniería Automotriz, Escuela Superior Politécnica de Chimborazo, Riobamba, Ecuador.

Suggested citation: Llanes-Cedeño, E.A.; Grefa Shiguango, S.F.; Molina-Osejos, J.V. and Rocha-Hoyos, J.C. "Incidence of automotive air conditioning on the index of fuel consumption in spark ignition vehicle on a route in the ecuadorian amazon," *Ingenius, Revista de Ciencia y Tecnología*, N.º 31, pp. 115-126, 2024, DOI: <https://doi.org/10.17163/ings.n31.2024.10>.

1. Introduction

According to AEADE [1], in Ecuador, an annual sale of 132,000 vehicles is recorded, representing a high sales rate in the market that varies according to the country's economic situation. However, the number of cars directly influences environmental pollution. For this reason, Ecuador has adopted Euro 3 regulations to control pollution. Nevertheless, due to the poor fuel quality, the pollution index of vehicles has directly impacted the environment.

Air pollution is one of the most severe global environmental issues today. Gas emissions are linked to the hydrocarbons found in the fuel used for vehicles. These vehicular emissions manifest through the combustion of hydrocarbons (HC), nitrogen oxides (NO_x), carbon monoxide (CO), and carbon dioxide (CO₂), directly impacting the public health of the country [2]. Climate change has been observable for many years, increasingly evoking heightened concern. The greenhouse gas emissions produced have intensified vulnerability in the natural regions of Ecuador [3].

Según Guzmán et al. [4] and Llanes et al. [2] assert that Super gasoline produces low emissions and relatively lower fuel consumption than Extra gasoline. Ecopais fuel was introduced in Guayaquil in 2010 as the primary choice for consumers due to its cost-effectiveness compared to other fuels [5]. Initially proposed with an octane rating of 80, it has recently been regulated between 85 and 87 octane. In contrast to Extra gasoline, it contains 5% ethanol, derived from corn and sugarcane.

At present, there is considerable interest in driving cycles, represented by driving patterns and utilized to comprehend energy consumption, fuel consumption, and exhaust gas emissions in vehicles [6]. According to Tong & Hung [7], the driving cycle is a time series of speeds that describes the driving pattern; thus, the driving pattern plays a crucial role in a driving cycle.

In 1960, the Federal Test Procedure (FTP) cycle was conducted through a conventional driving route in Los Angeles, California. Established parameters included vehicle speed, engine speed, and intake manifold pressure. A 1964 Chevrolet was used for the 12-mile route. In 2002, Ecuador adopted the FTP 75 test cycle following the NTE INEN 2204 standard, designed for light and medium vehicles using gasoline [8].

The New European Driving Cycle (NEDC) is used for homologating vehicles that comply with Euro 6 regulations in Europe and other countries. Commonly referred to as ECE for urban areas, repeated four times, and EUDC for extra-urban regions, it serves as a standardized procedure. According to Romain [9], the main characteristics of the cycle are distance: 11,023 m, duration: 1180 s, and an average speed: 33.6 km/h.

The European cycle has been criticized for not accurately representing real driving conditions in recent

years. It features very smooth accelerations, constant-speed cruising, and periods of inactivity, posing a challenge in obtaining a certificate that genuinely reflects the vehicle's performance in real-world conditions [9].

Wang et al. [10] mention the use of specially designed instruments for recording speed and travel time, incorporating a GPS and a speed sensor to monitor data quality. Conversely, Morey, Limanond, & Niemeier [11] emphasize that overrepresenting driving data during peak hours compared to non-peak hours may compromise their representativeness of real driving conditions. Hence, they highlight the significance of conducting route tests during peak hours, as they yield valid data corresponding to the specific situation of the city or study area.

The analysis of driving patterns proposed by Joumard et al. [12] covers speed, acceleration, and braking rates, ranging from highly congested urban driving to highway conditions. The research results reveal variations between 10% and 20% in pollutant emissions in urban areas, with rural emissions experiencing a slight decrease. According to Urbina et al. [13], the On-Board cycle enables on-road tests under real traffic conditions, measuring emission concentrations, fuel consumption, and distance traveled. To achieve this, a mixed cycle in city and highway settings was utilized, demonstrating lower CO emission factors than the IM240 cycle. Jiménez, Román & López [14] highlight global parameters influencing driving dynamics, including maximum speed (km/h), average speed (km/h), average acceleration (m/s^2), average deceleration (m/s^2), duration (s), among others. The selection of driving patterns depends on the vehicle, terrain, traffic data, and other factors, underscoring the importance of defining routes that represent typical driving patterns to gather relevant data for the vehicle study.

Ternz & Ternz [15] and Huang et al. [16] mention the following list of techniques associated with eco-friendly driving: (1) moderate acceleration with shifts between 2000-2500 revolutions for manual transmissions; (2) anticipate traffic flow and signals, avoiding constant starts and stops; (3) maintain a constant speed; (4) avoid high speeds; (5) vehicle maintenance according to the manufacturer's manual; (6) turn off the engine during prolonged stops; (7) maintain optimal tire pressure and regularly change the air filter.

According to Barkenbus [17], eco-friendly driving reduces fuel consumption by an average of 10%, thereby gradually lowering CO₂ emissions from driving by an equivalent percentage. Additionally, Mensing et al. [18] found that emissions and fuel consumption increase due to the extended time spent in high-acceleration engine operation.

The air conditioning (A/C) system in cars has enhanced people's comfort and, to some extent, their safety when driving in adverse weather conditions [19]. However, using A/C results in energy loss and an

increase in fuel consumption and polluting gas emissions [20].

In the study conducted in the highland and coastal regions, Acosta & Tello [21] state that the thermal comfort in the cabin ranges between 22 and 27 °C, with a relative humidity between 45% and 65%. In contrast, Pérez & Córdova [22] mention that, for the coastal region, the comfortable temperature ranges between 20 and 24 °C, attributed to the climate characteristic of cities located at sea level.

The A/C has the most significant impact on fuel consumption. Tamura, Yakumaru, & Nishiwaki [23] reported additional fuel consumption ranging between 2.5% and 7.5% due to the performance of the air conditioning, considering factors such as climatic conditions, engine type, and user profile.

It is known that the use of air conditioning affects emission factors and the fuel consumption index in driving conditions in the Amazonian regions. However, there is insufficient information available regarding the driving cycle. Therefore, this study aimed to assess the incidence of air conditioning on the vehicular fuel consumption index in the Shushufindi canton through accurate traffic tests, implementing Eco driving mode and using Extra and Super gasoline to choose the best alternative.

2. Materials and methods

The study adopts a quantitative approach, focusing on characterizing a specific route to evaluate the fuel consumption index in the Ecuadorian Amazon region through experimental calculations and statistical operations. The research can be classified as exploratory and field-based, involving the review of various types of studies and the execution of an on-board driving cycle on a real route that spans urban and rural environments, including roads.

2.1. Study area

The Shushufindi canton, situated in the province of Sucumbíos in the Amazon Region of Ecuador, was selected, as illustrated in Figure 1 (marked with a red point). This location sits at an elevation of 240 meters above sea level and shares borders with the cantons of Lago Agrio and Cuyabeno to the north, the province of Orellana to the south and west, and the canton of Cuyabeno to the east. The ambient temperature in this area ranges between 26 and 30 °C.



Figure 1. Map of the study area. Shushufindi Canton (Google Maps [24])

2.2. Route characterization

For the selection of the route, various criteria were taken into account. These criteria included roads with higher traffic flow, slow acceleration lanes, free acceleration lanes, and the type of road [12].

The altitude and coordinate data for the study were obtained using a GPSMAP 62s. The information collection was conducted directly with the vehicle. The stored data was then filtered in Excel to perform statistical analysis and obtain the driving cycle. Figure 2 displays the points obtained through Google Earth, covering a route that includes urban and rural environments (roads).

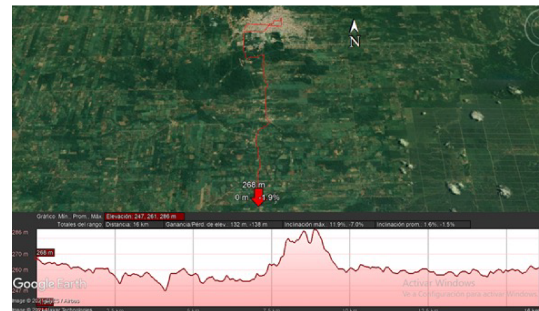


Figure 2. Established urban-rural route. Shushufindi Canton

This study encompasses a route of 16.17 km that includes the urban area with streets and avenues with heavy traffic, such as Perimetral Avenue, Policía Nacional Avenue, Unidad Nacional Avenue, Aguarico 3 Avenue, 11 de Julio Avenue, Napo Avenue, Siona Street, Oriental Street, and Naciones Unidas Avenue. On the other hand, the rural part of the route includes the Shushufindi-Limoncocha Road and San Mateo Avenue.

According to Safety Enforcement Seguridad Vial S. A. [25], speed limits for light vehicles in urban areas are 50 km/h, with a maximum of 60 km/h. The speed range for straight sections on the road is from 100 to 135 km/h, while for curves on the road, the speed is 60 km/h, with a maximum of 75 km/h. The ELM 327 (OBD2) device was used to obtain speed, acceleration, and time data.

Based on the proposals of Tong & Hung [7] and Quinchimbla & Solís [26], the following parameters are deduced for this study: distance traveled (km), maximum speed (km/h), average speed (km/h), travel time (s), average positive acceleration (m/s^2), time with positive acceleration (s), and, finally, the number of stops.

The driving cycle was established through weightings. Gómez [27] developed the driving cycle for the central-western metropolitan area in Colombia, determined by weighted parameters. Valdez [28] developed vehicle driving cycles in Naucalpan, Mexico City, and the United States, among other locations. This is represented by the result of a sample of experimental curves obtained by comparing the most influential variables of each experiment. The variables are identified based on their relevance to each parameter. The weighting is set on a scale from 0 to 1, and the value of each parameter is composed of multiples of 0.25 [28,29]. Table 1 displays the weighting assigned to each previously established parameter.

Table 1. Weighting table for each parameter

PARAMETERS	WEIGHTING COEFFICIENT W_i
Distance traveled (km)	1
Maximum speed (km/h)	0.25
Average speed (km/h)	1
Total travel time (s)	1
Average positive acceleration (m/s^2)	1
Time with positive acceleration (s)	1
Number of stops	0.25
Total	5.5

Equation (1) considers the smaller value Y , representing a lesser deviation from the mean. In this equation, Y corresponds to the weighted average, W_i is the weighting coefficient for each average, $P_{i,j}$ is the parameter value, \bar{P} is the average of the parameter, and $\frac{|P_{i,j}-\bar{P}|}{\bar{P}}$ is the deviation from the mean expressed in dimensionless terms.

$$Y = \frac{W_i * \frac{|P_{i,j}-\bar{P}|}{\bar{P}}}{Total\ weightings} \quad (1)$$

2.3. Test vehicle. Fuels

For this study, the chosen vehicle is the BEAT PREMIER AC 1.2 4P 4X2 TM, as depicted in Figure 3. According to the Association of Automotive Companies of Ecuador, this vehicle was among the top-selling models in 2019, with over 4,125 units sold, and its commercial availability extends through 2021. This car is recognized for its comfort, safety features, stylish design, and advanced technology. Additionally, it is noteworthy for its low fuel consumption and spare parts utilization [30]. In the Amazon region, it is one of the most in-demand vehicles due to its cost-effectiveness and accessibility.



Figure 3. Chevrolet BEAT

In the chosen test, the vehicle underwent preventative maintenance, encompassing the ABC of the engine (oil changes, air filter, and fuel filter). Additionally, the proper functioning of the electronic injection system was verified, and an electronic examination was conducted using a scanner. Likewise, the tire pressure was ensured to align with the manufacturer's specifications, set at 30 PSI of air in each tire. These procedures validated the correct vehicle operation for the respective study test.

The fuel consumption (Extra and Super) on the established route was determined using the OBD2 ELM327. According to Cortez and Alejandro [31], the OBD2 is an electronic device capable of automatically identifying the communication protocol of the ECU and enables the reading and clearing of codes. The "Car Scanner ELM OBD2" application was used for data collection, allowing the user to read and record real-time operating data of the car's variables. Additionally, it facilitates the wireless transmission of ECU information to the mobile phone using Bluetooth technology.

Table 2 displays the primary characteristics of the utilized fuels.

Table 2. Fuel properties. Note: Taken from the study conducted by Taipe-Defaz et al. [32]

PARAMETERS	SUPER	EXTRA
Octane number (RON)	92	87
Sulfur content (%)	0.065	0.065
Gum content (mg/100 ml)	4	3
Aromatic content (% vol.)	35	30
Olefin content (% vol.)	18	18
Final evaporation point (°C)	220	220
Density (kg/m^3)	722	723
PCI (kJ/kg)	48345	45124

Figure 4 illustrates the air conditioning system's components [21]; the refrigerant employed is R-134a.

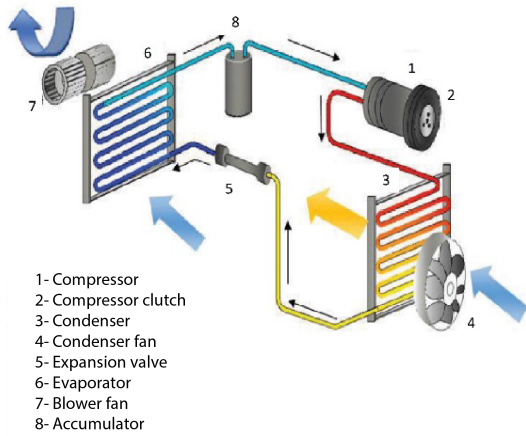


Figure 4. Automotive air conditioning components

2.4. Efficient driving protocol

Efficient driving requires the driver to adhere to a set of parameters while operating the vehicle. The guidelines, as proposed by Ternz and Ternz [15] and Mensing et al. [18], are as follows: (1) execute gear changes between 2000 and 2500 rpm, (2) utilize the first gear solely to initiate vehicle movement, (3) apply smooth acceleration without excessive pedal pressure, (4) shift to second gear at the earliest opportunity, (5) capitalize on the vehicle’s gravity and inertia when descending slopes (avoid fully depressing the accelerator), (6) anticipate traffic to minimize frequent starts and stops, (7) prioritize braking using the engine brake, (8) when using air conditioning on routes, keep all windows completely closed; for routes without A/C, keep the windows down, (9) avoid sudden braking and acceleration, (10) maintain a consistent speed (80 km/h-90 km/h maximum in perimeter areas and 45 km/h in urban areas), (11) refrain from high speeds on highways and urban routes, (12) consistently attempt to use the highest possible gear, and (13) ultimately, turn off the engine during prolonged stops.

2.5. Experimental Design

A factorial multilevel design was created to evaluate the fuel consumption index using STATGRAPHICS Centurion XVI software. For this purpose, the factors of fuel, air conditioning, and schedule were established, each represented by two levels, as detailed in Table 3.

Table 3. Design of the factors and levels to be considered

FACTORS	LEVELS	DESIGNATION
Fuel	Extra	1
	Súper	2
Air conditioning	Without A/C	1
	With A/C	2
Schedule	Regular	1
	Hour	
	Peak Hour	2

Table 4 displays the response variables: Fuel consumption index (L/km) of the experimental design.

Table 4. Response variables of the experimental design

RESPONSE	UNITS
Fuel consumption index	L/km

The Statgraphics Centurión XVI software was used to analyse and compare the results. A simple ANOVA was conducted for the different treatments (combinations) detailed in Table 5. In this analysis, the Fisher’s Least Significant Difference (LSD) procedure was applied with a confidence level of 95.0%. Three repetitions were carried out for each treatment, following the guidelines of the NTE INEN 2205 standard in Section 6 on test methods. Section 6.1.5.4 specifies: "Record and average a minimum of 3 readings for each test" (24 tests were conducted) [33].

Table 5. Treatment for response surface analysis

FORMATION OF TREATMENTS			
N.º	Fuel	Air Conditioning	Schedule
T1	Extra (1)	With A/C (2)	Regular H (1)
T2	Extra (1)	With A/C (2)	Peak H (2)
T3	Extra (1)	Without A/C (1)	Regular H (1)
T4	Extra (1)	Without A/C (1)	Peak H (2)
T5	Súper (2)	With A/C (2)	Regular H (1)
T6	Súper (2)	With A/C (2)	Peak H (2)
T7	Súper (2)	Without A/C (1)	Regular H (1)
T8	Súper (2)	Without A/C (1)	Peak H (2)

2.6. Test protocol

A driver was chosen to carry out 24 route tests. This driver was provided with information about the efficient driving pattern and the route to follow, considering the recommendations of Milla, Cedeño and Hoyos [34].

The proposed route covers 16.17 kilometers and is conducted under the following conditions: (1) two initial scenarios are considered for the test, one during regular hours (9 a.m.) and another during peak hours (5:00 p.m.); (2) tests are performed using two types of fuel (Extra and Super). For the test with Extra fuel, the vehicle’s fuel tank is filled completely at the beginning and end of the route. The same procedure is applied for the test with Super fuel; (3) the OBD2 connector is connected to the ELM 327 measurement equipment (Figure 5); (4) the Car Scanner ELM OBD2 application is activated to record information on fuel consumption, speed, acceleration, and time; (5) the test is initiated after verifying the proper connection of all equipment; (6) the established route is followed until completion with the same driver; (7) upon completing the route, the information is saved in a file and exported to Excel software for analysis and tabulation of results. These steps are repeated for treatments according to the established levels: regular hours, peak

hours, with A/C, without A/C, Extra fuel, and Super fuel.



Figure 5. OBD2 ELM 327 Mini Module and Car Scanner Application

3. Results and discussion

This section presents the results obtained by executing tests at different times (regular and peak hours) on a predetermined route, as detailed in the methodology. The weighting formula was applied to determine the estimated results of route characterization, selecting the value with the least variability and the result that most accurately represents the collected data.

3.1. Mixed cycle. Regular hours (9 a.m.)

The first established route was carried out during regular hours with less traffic congestion. In this case, three complete trips were conducted. The values were obtained through everyday driving with a weighting of $Y = 0.0316$.

Figure 6 illustrates that the maximum speed reached 81 km/h, with an average speed of 39 km/h over a travel time of 1446 s (24.1 min). Throughout the journey, 4 stops were made, with an average positive acceleration of 0.479 m/s^2 and a positive acceleration time of 520 s. Additionally, there is evidence of speed variability corresponding to rural and urban routes. In the study conducted by Pérez y Quito [29], a weighted mean of $Y = 0.097$ was recorded in a combined cycle conducted in Cuenca, demonstrating less deviation in the proposed results, with a 31% lower variability compared to the study. Table 6 presents the values corresponding to the driving cycle.

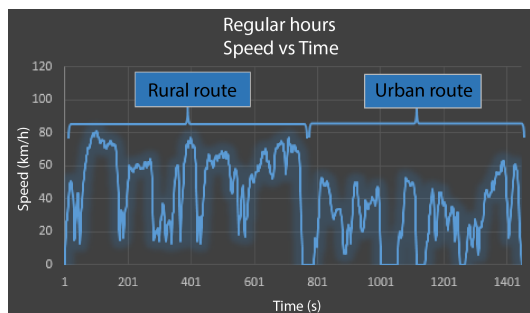


Figure 6. Graph illustrating data during regular hours

Table 6. Characteristic parameters corresponding to regular hours (9 a.m.)

PARAMETERS	VALUE	UNIT
Maximum speed	81	km/h
Average speed	39	km/h
Distance traveled	16.17	km
Total travel time	1446	s
Average positive acceleration	0.479	m/s^2
Time with positive acceleration	520	s
Number of stops	4	–

3.2. Mixed cycle. Peak hours (5 p.m.)

Figure 7 depicts the peak hours with increased vehicular traffic, primarily due to the presence of businesses and factories along the route. The lowest weighted mean of $Y = 0.0241$ was obtained. The values were determined through everyday driving.

Figure 7 illustrates that the maximum speed reached 70 km/h, with an average speed of 37 km/h over a travel time of 1632 s (27.2 min). Throughout the journey, 5 stops were made, with an average positive acceleration of 0.427 m/s^2 and a positive acceleration time of 452 s. Additionally, there is evidence of speed variability corresponding to the urban area, reaching a speed of 48 km/h. The cycle proposed by Quinchimbla y Solís [26] records a weighted mean of $Y = 0.1168$ in a combined route conducted in Quito, exhibiting a 9% variability compared to the proposed study and a maximum 72 km/h speed. This demonstrates an acceptable correlation with the proposed cycle. Table 7 presents the parameters corresponding to the representative peak hours.

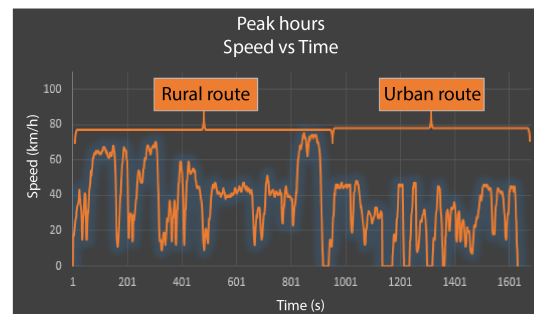


Figure 7. Graph illustrating data during peak hours

Table 7. Characteristic parameters corresponding to peak hours (5 p. m.)

PARAMETERS	VALUE	UNIT
Maximum speed	70	km/h
Average speed	37	km/h
Distance traveled	16.17	km
Total travel time	1632	s
Average positive acceleration	0.427	m/s^2
Time with positive acceleration	452	s
Number of stops	5	–

3.3. Comparison between Regular Hours and Peak Hours

Figure 8 shows the representative cycle corresponding to the journey during regular and peak hours, with a weighted mean value of $Y = 0.0316$ at 9 a.m. and $Y = 0.0241$ at 5 p.m.

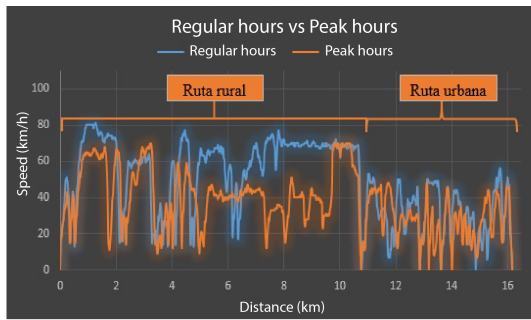


Figure 8. Comparative graph of representative mixed cycles

It can be observed that the maximum speed is 81 km/h during regular hours and 70 km/h during peak hours. Additionally, speed variability in urban and rural areas is attributed to vehicular congestion within the allowed limits for each sector. For example, the average speed was 39 km/h during regular hours, whereas it was 34 km/h during peak hours. Similarly, the travel time during regular hours was 1446 s, whereas during peak hours, it was 1632 s. Thus, it is evident that the highest congestion occurs on the urban route, particularly during peak hours due to traffic lights and vehicle stops. The findings align with the study conducted by Quinchimbla y Solís [26], where the distance covered in combined cycles from various research was compared, resulting in an average distance of 15973.75 m. Given that the proposed study covers 1600.17 m, it is validated to fall within the allowed limits. Additionally, the driving parameters of the combined cycle are compared with various studies, determining that the cycle is highly variable due to geographical conditions, traffic density, and road infrastructure, which can influence the obtained driving parameters. Therefore, the obtained values vary compared to European, American, or other cycles.

3.4. Fuel consumption index

The fuel consumption index (FCI) was calculated following the test protocols mentioned in the methods. The FCI was evaluated using the STATGRAPHICS Centurion XVI software, entering the values corresponding to the fuel consumption obtained in the tests conducted on the vehicle.

Figure 9 illustrates that the factors influencing the fuel consumption index include air conditioning (A/C), fuel type, schedule, and the combination of fuel and

schedule. Conversely, the BC and AB combinations do not impact fuel consumption. According to the analysis of variance for the fuel consumption index (FCI), the adjusted model accounts for 98.8% of the variability in FCI with a confidence level of 95%.

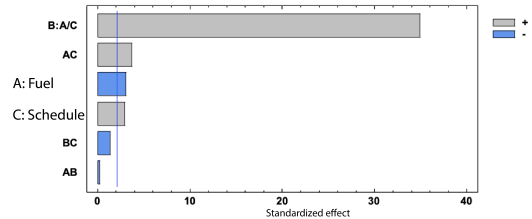


Figure 9. Standardized Pareto diagram for FC

Figure 10 shows the main effects for the fuel consumption index (FCI). When using Extra fuel (1), FCI increases. Conversely, when using Super fuel (2), FCI improves. Using air conditioning (2) significantly increases FCI, while FCI (1) without air conditioning is relatively lower. Additionally, FCI increases during peak hours (2) and decreases during regular hours. Thus, the optimal minimum value is 0.057 (L/km), obtained with the combination 2-1-1 (Super-Reg. Hours- No A/C).

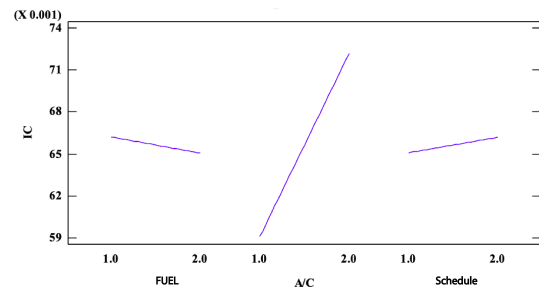


Figure 10. Main effects graph for FC

Figure 11 illustrates that the fuel consumption index (FCI) is lower when A/C = 1 (no A/C); however, the time factor does not exert an impact. The influential value for fuel = 1 (Extra) is obtained when A/C is not in use, yielding an optimal value of 0.06 L/km, with time not significantly impacting. Lower values are observed during regular hours, even when time, based on observed shading, does not exert a considerable impact; nevertheless, it is evident that the most favourable results are obtained for time 1 (regular). When using fuel = 2 (Super), the lowest values are achieved when not employing air conditioning, resulting in an optimal value of 0.058 L/km, with time not significantly influencing. Lower values are obtained during regular hours, even though regular hours do not exert a significant impact, leading to the lowest results compared to peak hours. Consequently, Super fuel exhibits lower fuel consumption indices without air conditioning and under regular time conditions. This

study aligns with Andrade [35], who conducted research with the Chevrolet Aveo vehicle under sea-level conditions, concluding that Super gasoline yields lower fuel consumption indices, demonstrating better mileage performance and representing a lower long-term cost. In the study conducted by García and Villalba [36], it is observed that the fuel consumption index decreases with efficient driving, achieving a fuel optimization of 28.34%; nevertheless, the proposed study is based on regular time conditions.

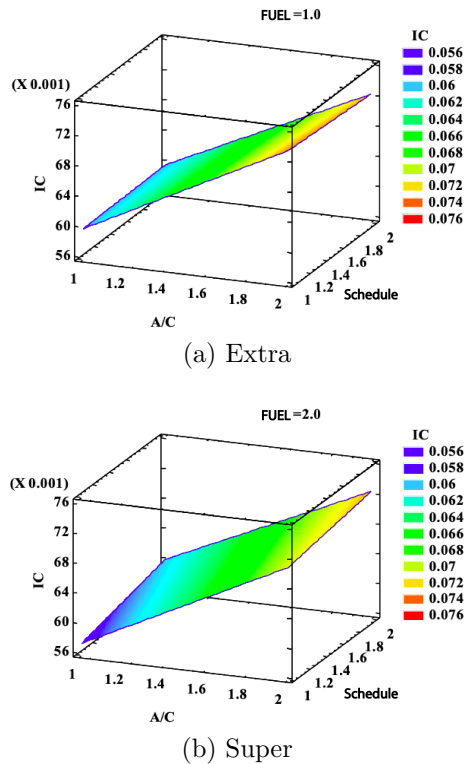


Figure 11. Estimated response surface FC. a) Extra fuel vs. b) Super gasoline

Figure 12 illustrates the behavior of the Fuel Consumption Index (FCI) concerning the type of fuel utilized and the activation of air conditioning (A/C) when the schedule is set to 1 (regular). In this context, it is observed that the lowest CI values are attained with Super fuel (2) and without A/C (1), resulting in a value of 0.057 L/km. Conversely, when the schedule is adjusted to 2 (peak), the lowest CI values are derived from Super fuel, Extra fuel, and the absence of A/C. While the fuel factor does not exert a direct influence based on the observed hue, it is perceived that Super fuel yields lower outcomes. In summary, using air conditioning during peak hours corresponds to an elevation in the fuel consumption index. These findings align with the results of a study conducted by Arias and Ludeña [37] involving the Chevrolet Aveo Activo vehicle in Cuenca. Their study concluded that fuel consumption increases during peak hours, whereas it decreases during regular hours. This implies that peak

hours, characterized by heightened traffic congestion, are associated with a higher fuel consumption index irrespective of the day.

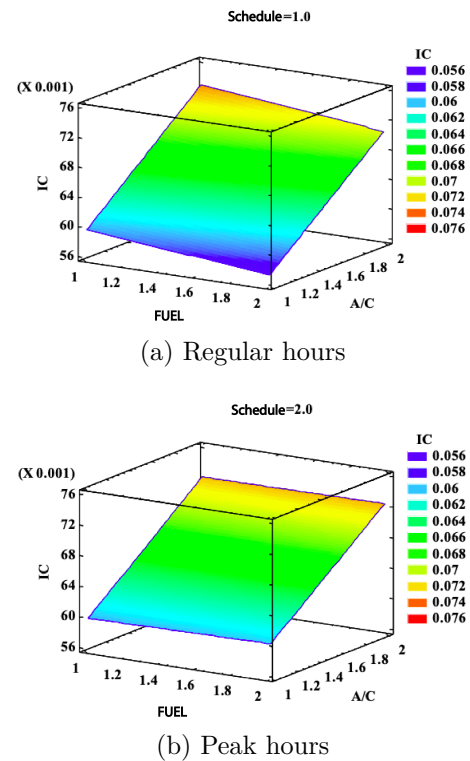


Figure 12. Estimated response surface FC. a) Regular hours and b) Peak hours

Figure 13 illustrates the behavior of the Fuel Consumption Index (FCI) concerning the type of fuel used and the travel schedule. When A/C = 1 (without A/C), it is observed that the lowest CI values are achieved with Super fuel (2) during regular hours (1), reaching a value of 0.057 L/km. As the quality of the fuel increases, more favorable results are obtained in the CI, and less traffic on the route also positively influences the CI. However, the schedule and fuel type are insignificant, although lower results are noted for regular hours and Super fuel based on the observed hue. When A/C = 2 (with A/C), it is observed that the lowest CI values are obtained with fuel type 2 (Super) during schedule 1 (regular), signifying that the lowest CI values are attained with higher-quality fuel. As the fuel quality improves, the CI results also show improvement, and the traffic reduction on the route positively impacts the CI. The study conducted by Chancafe [38] confirms that using air conditioning increases vehicle fuel consumption. According to Acosta & Tello [21], the highest fuel consumption rates were recorded on the road using air conditioning. It is noteworthy that as one descends to lower altitudes, consumption increases due to the correction made for the higher levels of oxygen present.

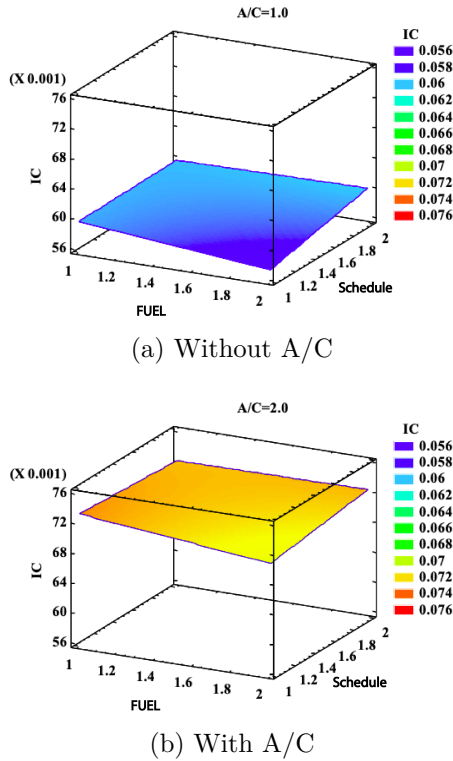


Figure 13. Estimated response surface FC. a) Regular hours and b) Peak hours

Figure 14 illustrates the box and whisker plot of the fuel consumption index. It is observed that treatments T7 (Super-without AC-H. regular) and T3 (Extra-without AC-H. regular) fall within the range of 0.057 to 0.073 L/km, with T7 exhibiting the least significant difference. This is attributed to the use of Super fuel, which has an octane rating of 92, promoting engine combustion. Furthermore, the absence of air conditioning (A/C) reduces the fuel consumption index (FCI). Treatment T3 also complies with the permitted usage limits, indicating that both T3 and T7 exhibit optimal responses. Conversely, treatments T1, T2, T4, T5, T6, and T8 demonstrate elevated fuel consumption indices.

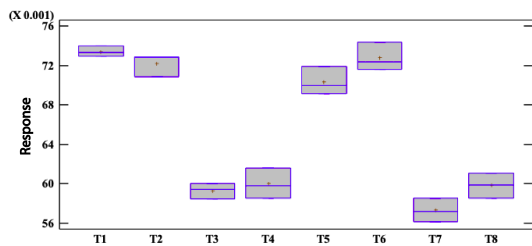


Figure 14. FC Box and whisker graph

Table 8 presents the results obtained from applying the LSD (Fisher) test with a 95% confidence level. It is evident that in treatments T7 (Super-Without A/C-Regular Schedule) and T3 (Extra-Without A/C-Regular Schedule), no significant differences are observed. These findings align with the conclusions of

Andrade [35], who asserts that the use of Super gasoline is associated with lower fuel consumption indices. Additionally, Arias and Ludeña [37] determine that the fuel consumption index tends to be lower during regular schedules. Chancafe [38] confirms that the absence of air conditioning results in lower fuel consumption indices. Therefore, it is suggested that the most suitable treatment for the Amazon region is T7, with an average efficiency of 17.45 km/L. However, due to the cost of Super gasoline, it is recommended to use treatment T3, which provides an efficiency of 16.86 km/L. This treatment includes Extra fuel, no A/C, and a regular schedule, as it does not exhibit significant differences. It is crucial to adopt efficient driving practices since, under normal conditions, the impact on fuel consumption significantly increases. In contrast, treatments T1, T2, T4, T5, T6, and T8 exhibit significant differences, emphasizing peak hour factors and A/C usage, resulting in an increased fuel consumption index.

Table 8. Multiple range tests

	Cases	Mean	Homogeneous groups	
T7	3	0.0573078	X	
T3	3	0.0593074	X	X
T8	3	0.0598433		X
T4	3	0.0599876		X
T5	3	0.070336		X
T2	3	0.0721707		X X
T6	3	0.0727685		X
T1	3	0.0734075		X

4. Conclusions

The statistical method, chosen by applying weighting criteria on each established route, facilitated the identification of representative journeys characterized by minimal deviations from the average. During regular hours, a Y value of 0.0316 was obtained, while during peak hours, a Y value of 0.0241 was achieved, indicating a 31% reduction compared to the literature under investigation. In regular hours (9 a.m.), the recorded data included a maximum speed of 81 km/h and an average speed of 39 km/h, with a travel time of 1446 s (24.1 minutes). Conversely, during peak hours (5 p.m.), the maximum speed reached 70 km/h, with an average speed of 37 km/h and a travel time of 1632 s (27.2 minutes), resulting in a 10% difference.

The road test conducted with the Chevrolet Beat vehicle determined that the optimal lowest value of the fuel consumption index (FCI) is attained during regular hours, without A/C, and using Super fuel. Consequently, it is concluded that the significant factors influencing the FCI include the use of air conditioning (A/C), Extra gasoline, and peak hours in the Shushufindi canton, situated in the Eastern region of Ecuador.

In the study of the fuel consumption index (FCI), it was determined through the LSD test with a 95% confidence level that treatment T3 (regular schedule, without A/C and Extra fuel), with values ranging from 0.0584 to 0.060 L/km and treatment T7 (regular schedule, without A/C, and Super fuel), with values between 0.0561 and 0.0585 L/km, demonstrate optimal savings in the fuel consumption index when applying efficient driving practices.

Further research encompassing various vehicles, brands, and models is recommended. This will facilitate a comprehensive understanding of the dynamics associated with fuel, air conditioning, and regular and peak schedules.

References

- [1] AEADE, *Anuario 2019*. Asociación de Empresas Automotrices del Ecuador, 2019. [Online]. Available: <https://bit.ly/3Rl41yA>
- [2] E. A. Llanes Cedeño, J. C. Rocha-Hoyos, D. B. Peralta Zurita, and J. C. Leguísamo Milla, “Evaluation of gas emissions in light gasoline vehicles in height conditions. case study quito, ecuador,” *Enfoque UTE*, vol. 9, no. 2, pp. 149–158, Jun. 2018. [Online]. Available: <https://doi.org/10.29019/enfoqueute.v9n2.201>
- [3] FLACSO, *GEO Ecuador 2008 Informe sobre el estado del arte del medio ambiente*. FLACSO, MAE, PNUMA, 2008. [Online]. Available: <https://bit.ly/4aC6v4K>
- [4] A. R. Guzmán, E. Cueva, A. Peralvo, M. Revelo, and A. Armas, “Study of the dynamic performance of an otto engine using mixtures two types of extra and super gasolines,” *Enfoque UTE*, vol. 9, no. 4, pp. 208–220, Dec. 2018. [Online]. Available: <https://doi.org/10.29019/enfoqueute.v9n4.335>
- [5] D. G. Perez Darquea, “Estudio de emisiones contaminantes utilizando combustibles locales,” *INNOVA*, vol. 3, no. 3, pp. 23–34, 2018. [Online]. Available: <https://doi.org/10.33890/innova.v3.n3.2018.635>
- [6] L. F. Quirama, M. Giraldo, J. I. Huertas, and M. Jaller, “Driving cycles that reproduce driving patterns, energy consumptions and tailpipe emissions,” *Transportation Research Part D: Transport and Environment*, vol. 82, p. 102294, 2020. [Online]. Available: <https://doi.org/10.1016/j.trd.2020.102294>
- [7] H. Y. Tong and W. T. Hung, “A framework for developing driving cycles with on-road driving data,” *Transport Reviews*, vol. 30, no. 5, pp. 589–615, 2010. [Online]. Available: <https://doi.org/10.1080/01441640903286134>
- [8] INEN, *NTE INEN 2204 Gestión ambiental. Aire. Vehículos automotores. Límites permitidos de emisiones producidas por fuentes móviles terrestres que emplean gasolina*. Instituto Ecuatoriano de Normalización, 2017. [Online]. Available: <https://bit.ly/3ROTgpG>
- [9] N. Romain. (2013) The different driving cycles. Car Engineer. Car Engineer. [Online]. Available: <https://bit.ly/3RrVZ7e>
- [10] Q. Wang, H. Huo, K. He, Z. Yao, and Q. Zhang, “Characterization of vehicle driving patterns and development of driving cycles in chinese cities,” *Transportation Research Part D: Transport and Environment*, vol. 13, no. 5, pp. 289–297, 2008. [Online]. Available: <https://doi.org/10.1016/j.trd.2008.03.003>
- [11] J. E. Morey, T. Limanond, and D. A. Niemeier, “Validity of chase car data used in developing emissions cycles,” *Statistical Analysis and Modeling of Automotive Emissions*, vol. 3, no. 2, pp. 15–28, Sep 2000, journal Article. [Online]. Available: <https://bit.ly/3RN5wXO>
- [12] M. André, R. Joumard, R. Vidon, P. Tassel, and P. Perret, “Real-world european driving cycles, for measuring pollutant emissions from high- and low-powered cars,” *Atmospheric Environment*, vol. 40, no. 31, pp. 5944–5953, 2006, 13th International Symposium on Transport and Air Pollution (TAP-2004). [Online]. Available: <https://doi.org/10.1016/j.atmosenv.2005.12.057>
- [13] A. Urbina, L. Tipanluisa, and A. Portilla, “Estudio de las emisiones vehiculares en pruebas con dinamómetro y en ruta,” in *VIII Congreso Internacional de Ingeniería Mecánica y Mecatrónica*, 04 2017. [Online]. Available: <https://bit.ly/41prHGZ>
- [14] F. Jiménez Alonso, A. Román, and J. M. López Martínez, “Determinación de ciclos de conducción en rutas urbanas fijas,” *DINA Ingeniería e Industria*, vol. 88, pp. 681–688, 2013. [Online]. Available: <https://doi.org/10.6036/5751>
- [15] R. Luther and P. Baas, *Eco-Driving Scoping Study*. Energy Efficiency and Conservation Authority, 2011. [Online]. Available: <https://bit.ly/41wjq3T>
- [16] Y. Huang, E. C. Ng, J. L. Zhou, N. C. Surawski, E. F. Chan, and G. Hong, “Eco-driving technology for sustainable road transport: A review,” *Renewable and Sustainable Energy Reviews*, vol. 93, pp. 596–609, 2018. [Online]. Available: <https://doi.org/10.1016/j.rser.2018.05.030>

- [17] J. N. Barkenbus, "Eco-driving: An overlooked climate change initiative," *Energy Policy*, vol. 38, no. 2, pp. 762–769, 2010. [Online]. Available: <https://doi.org/10.1016/j.enpol.2009.10.021>
- [18] F. Mensing, E. Bideaux, R. Trigui, J. Ribet, and B. Jeanneret, "Eco-driving: An economic or ecologic driving style?" *Transportation Research Part C: Emerging Technologies*, vol. 38, pp. 110–121, 2014. [Online]. Available: <https://doi.org/10.1016/j.trc.2013.10.013>
- [19] B. A. Cuaical Angulo and E. Torres Tamayo, "Caracterización de la eficiencia energética en los sistemas de refrigeración aplicados en el área automotriz," *INVPOS*, vol. 1, no. 1, pp. 1–16, 2018. [Online]. Available: <https://bit.ly/41qG3H7>
- [20] M. d. J. Guananga Totoy, *Diseño y construcción de un simulador de climatización automotriz*. Universidad Internacional del Ecuador, 2013. [Online]. Available: <https://bit.ly/3TrvRfr>
- [21] M. A. Acosta Corral and W. P. Tello Flores, *Estudio del aire acondicionado en el consumo de combustible, potencia del motor y confort térmico en la cabina de un vehículo liviano*. Escuela Politécnica Nacional, 2016. [Online]. Available: <https://bit.ly/3NBhuBw>
- [22] M. A. Córdova Suárez and C. F. Pérez Salinas, *El gasto metabólico y la temperatura WBGT en el sistema de trabajo de conductor de bus tipo volkswagen 17210 de la carrocería Modelo Orión Marca Imce y su incidencia en el estrés térmico*. Universidad Técnica de Ambato, 2014. [Online]. Available: <https://bit.ly/3Rmp3bm>
- [23] T. Tamura, Y. Yakumaru, and F. Nishiwaki, "Experimental study on automotive cooling and heating air conditioning system using CO₂ as a refrigerant," *International Journal of Refrigeration*, vol. 28, no. 8, pp. 1302–1307, 2005, cO2 as Working Fluid - Theory and Applications. [Online]. Available: <https://doi.org/10.1016/j.ijrefrig.2005.09.010>
- [24] Google. (2023) Shushufindi. Google Maps. Google Maps. [Online]. Available: <https://bit.ly/475PMDF>
- [25] SES. (2018) Los limites de velocidad en el Ecuador. Safety Enforcement Seguridad Vial S.A. (SES). Safety Enforcement Seguridad Vial S.A. (SES). [Online]. Available: <https://bit.ly/3RPAiyn>
- [26] F. E. Quinchimbla Pisuña and J. M. Solís Santamaría, *Desarrollo de ciclos de conducción en ciudad, carretera y combinado para evaluar el rendimiento real del combustible de un vehículo con motor de ciclo Otto en el Distrito Metropolitano de Quito*. Escuela Politécnica Nacional, 2017. [Online]. Available: <https://bit.ly/3TrKtvi>
- [27] A. Hurtado Gómez, *Desarrollo de ciclos de conducción para el área metropolitana Centro Occidente-AMCO*. Universidd Tecnológica de Pereira, 2014. [Online]. Available: <https://bit.ly/41thLvY>
- [28] A. Valdéz Aguilera, *Desarrollo de Ciclos de Conducción Vehicular en el Municipio de Naucalpan*. Tecnológico de Monterrey, 2004. [Online]. Available: <https://bit.ly/3RQEDSM>
- [29] P. S. Pérez Llanos and C. O. Quito Sinchi, *Determinación de los ciclos de conducción de un vehículo categoría M1 para la ciudad de Cuenca*. Universidd Politécnica Salesiana, 2018. [Online]. Available: <https://bit.ly/3ROiIf0>
- [30] Chevrolet, *Datasheet Chevrolet Beat 2021*. Chevrolet Ecuador, 2021. [Online]. Available: <https://bit.ly/4aqb6H0>
- [31] M. A. Pinto Cortez, *Investigación de los parámetros característicos de desempeño del motor de combustión interna efi al utilizar la interfase ECO-OBD2*. Universidad de las Fuerzas Armadas, 2019. [Online]. Available: <https://bit.ly/3v8TgZ1>
- [32] V. A. Taípe-Defaz, E. A. Llanes Cedeño, C. F. Morales-Bayetero, and A. E. Checa-Ramírez, "Evaluación experimental de un motor de encendido provocado bajo diferentes gasolinas," *Ingenius*, no. 26, pp. 17–29, 2021. [Online]. Available: <https://doi.org/10.17163/ings.n26.2021.02>
- [33] INEN, *NTE INEN 2205:2010, Vehículos Automotores. Bus Urbano. Requisitos*. Instituto Ecuatoriano de Normalización, 2010. [Online]. Available: <https://bit.ly/3TWXl36>
- [34] J. C. Leguísamo Milla, E. Llanes Cedeño, and J. Rocha Hoyos, "Impact of ecodriving on fuel emissions and consumption on road of quito," *Enfoque UTE*, vol. 11, no. 1, pp. 68–83, Jan. 2020. [Online]. Available: <https://doi.org/10.29019/enfoque.v11n1.500>
- [35] F. L. Morquecho Andrade, "Análisis de rendimiento y costo de los combustibles Ecopaís y súper," *Innova*, vol. 3, no. 1, pp. 135–149, 2018. [Online]. Available: <https://doi.org/10.33890/innova.v3.n10.1.2018.899>
- [36] N. G. García Jaramillo and J. R. Villalba Arteaga, *Estudio del efecto de la conducción eficiente sobre el consumo y las emisiones*. Universidad Internacional del Ecuador, 2016. [Online]. Available: <https://bit.ly/3RRXTzD>

- [37] E. I. Arias Montaña and J. A. Ludeña Ayala, *Estimación del consumo de combustible y niveles de emisiones contaminantes de un vehículo de categoría M1 en rutas con mayor grado de saturación en la ciudad de Cuenca*. Universidad Politécnica Salesiana, 2018. [Online]. Available: <https://bit.ly/48heD8U>
- [38] J. E. Chancafe Zarpan, *Evaluación Del Aire Acondicionado En Vehículos De 1300cc Utilizando R-134a Y R-12 Para Determinar El Consumo De Combustible*. Universidad César Vallejo, 2017. [Online]. Available: <https://bit.ly/3GQPwxH>

GUIDELINES FOR PUBLICATION IN INGENIUS JOURNAL

1. General Information

INGENIUS is a scientific publication of the *Universidad Politécnica Salesiana* of Ecuador, published since January 2007, with a fixed biannual periodicity, specialized in Mechanical Engineering, Electrical Engineering, Electronics, Computer Science and its integration in what is now known as Mechatronics; these lines of action strengthen areas such as automation, control, robotics, among others..

It is a scientific journal, which uses the peer-review system, under double-blind review methodology, according to the publication standards of the Institute of Electrical and Electronics Engineers (IEEE). Compliance with this system allows authors to guarantee an objective, impartial and transparent review process, which facilitates the publication of their inclusion in reference databases, repositories and international indexing.

INGENIUS is indexed in the directory and selective catalog of the Regional Online Information System for Scientific Journals of Latin America, the Caribbean, Spain and Portugal (Latindex), in the Directory of Journals of Open Access DOAJ, In the Information Matrix for the Analysis of Journals, MIAR, In the Ibero-American Network of Innovation and Scientific Knowledge, REDIB and in repositories, libraries and specialized catalogs of Latin America.

The journal is published in a double version: printed (ISSN: 1390-650X) and digital (e-ISSN: 1390-860X), in Spanish, each work being identified with a DOI (Digital Object Identifier System). The articles sent to INGENIUS magazine must comply with the following criteria:

2. Scope and policy

2.1. Theme

Original contributions in Mechanical Engineering, Electrical and Electronic Engineering, Computer Science and its integration in what is now known as Mechatronics, as well as related areas: Automation, Control, Domotics, Robotics in their different fields of action and all those related disciplines with the same central theme.

All the work carried out by national or foreign researchers may be published once they meet the required scientific quality criteria.

2.2. Contributions

INGENIUS Journal preferably publishes articles related to empirical research, and also reports of technological development, proposals for models and innovations, products for the elaboration of graduate and postgraduate thesis that contribute to the field of science and technology, as well as select revisions of literature. (state-of-the-art).

- **Research:** 5,000 to 6,500 words of text, including title, abstracts, descriptors, charts and references.
- **Reports:** 5,000 to 6,500 words of text, including title, abstracts, charts and references.
- **Reviews:** 6,000 to 7,000 words of text, including charts and references. Current, selective and justified references, would be specially valued from among 40 works

The INGENIUS Journal publishes original and unpublished works written in Spanish and English, they may not have been published

through any printed or electronic media, nor be in the process of arbitration or publication.

Every article will be subjected to a rigorous arbitration process; the evaluation of the article will be made according to criteria of originality, relevance, relevance, contributions, scientific rigor and compliance with established editorial guidelines.

Being an arbitrated publication, the Editorial Board approves its publication based on the concept of specialized pairs. The reception of a document does not imply commitment of publication.

It is essential to present a letter of presentation and grant of rights which can be downloaded from: [urlhttps://goo.gl/ZNkMRD](https://goo.gl/ZNkMRD).

Contributions must be exclusively sent and through the OJS (Open Journal System) <https://goo.gl/JF7dWT>. In which all authors must previously register as a user. For any consultation of the procedure you should contact:

revistaingenius@ups.edu.ec,
jcalles@ups.edu.ec ó
mquinde@ups.edu.ec.

To promote diversity in publications, the author(s) may not publish more than one (1) article per issue, nor in consecutive issues. In order for the author(s) to submit their research again to Ingenius, a minimum of 3 published issues must have elapsed.

3. Presentation and structure of the manuscripts

For those works that are empirical investigations, the manuscripts will follow the IMRDC structure (Introduction, Materials and Methods, Results and Discussion and Conclusions), being optional the Notes and Supports. Those papers that, on the contrary, deal with reports, studies, proposals and reviews may be

more flexible in their epigraphs, particularly in material and methods, analysis, results, discussion and conclusions. In all typologies of works, references are mandatory.

Articles may be written on Microsoft Word (.doc or .docx) or L^AT_EX(.tex). The template to be used can be downloaded from the journal's website, a, <https://goo.gl/gtCg6m>, while for L^AT_EX in <https://goo.gl/hrHzzQ>, it is necessary that the file be anonymised in Properties of File, so that the author(s) ID is not displayed.

Figures, Graphs and/or Illustrations, as well as Charts shall be numbered sequentially including an explanatory description for each. The equations included in the article must also be numbered; the figures, charts and equations must be cited in the text.

Use space after point, commas and question marks.

Use "enter" at the end of each paragraph and title heading. Do not use .^{enter}.anywhere else, let the word processor program automatically break the lines.

Do not center headings or subheadings as they should be aligned to the left.

Charts must be created in the same program used for the document body, but must be stored in a separate file. Use tabs, not spaces, to create columns. Remember that the final size of printed pages will be 21 x 28 cm, so the tables must be designed to fit the final print space.

3.1. Structure of the manuscripts

3.1.1. Presentation and cover letter

1. **Título (español) / Title (inglés):** Concise but informative, in Spanish on the front line and in English on the second, when the article is written in Spanish and vice versa if it is written in English.

2. **Authors and affiliations:** Full name and surname of each author, organized by order of priority and their institutional affiliation with reference to the end of the first sheet, where it must include: Dependency to which belongs within the institution, Institution to which he/she belongs, country, ORCID. A maximum of 5 authors will be accepted, although there may be exceptions justified by the complexity and extent of the topic.
 3. **Abstract (Spanish) / Abstract (English):** It will have a maximum extension of 230 words, first in Spanish and then in English. : 1) Justification of the topic; 2) Objectives; 3) Methodology and sample; 4) Main results; 5) Main conclusions.
 4. **Keywords (Spanish) / Keywords (English):** 6 descriptors must be presented for each language version directly related to the subject of the work. The use of the key words set out in UNESCO's Thesaurus will be positively valued.
 5. **Presentation (Cover Letter):** A statement that the manuscript is an original contribution, not submission or evaluation process in another journal, with the confirmation of the signatory authors, acceptance (if applicable) of formal changes in the manuscript according to the guidelines and partial assignment of rights to the publisher, according to the format established in: <<https://goo.gl/ZNkMRD>>
- nal affiliation with reference to the end of the first sheet, where it must include: Dependency to which belongs within the institution, Institution to which he/she belongs, country, ORCID. A maximum of 5 authors will be accepted, although there may be exceptions justified by the complexity and extent of the topic.
3. **Abstract (Spanish) / Abstract (English):** It will have a maximum extension of 230 words, first in Spanish and then in English. : 1) Justification of the topic; 2) Objectives; 3) Methodology and sample; 4) Main results; 5) Main conclusions.
 4. **Keywords (Spanish) / Keywords (English):** 6 descriptors must be presented for each language version directly related to the subject of the work. The use of the key words set out in UNESCO's Thesaurus will be positively valued.
 5. **Introduction:** It should include the problem statement, context of the problem, justification, rationale and purpose of the study, using bibliographical citations, as well as the most significant and current literature on the topic at national and international level.
 6. **Material and methods:** It must be written so that the reader can easily understand the development of the research. If applicable, it will describe the methodology, the sample and the form of sampling, as well as the type of statistical analysis used. If it is an original methodology, it is necessary to explain the reasons that led to its use and to describe its possible limitations.
 7. **Analysis and results:** It will try to highlight the most important observations, describing, without making value judgments, the material and methods used. They will appear in a logical sequence

3.1.2. Manuscript

1. **Título (español) / Title (inglés):** Concise but informative, in Spanish on the front line and in English on the second, when the article is written in Spanish and vice versa if it is written in English.
2. **Authors and affiliations:** Full name and surname of each author, organized by order of priority and their institutio-

in the text and the essential charts and figures avoiding the duplication of data.

8. **Discussion and Conclusions:** It will summarize the most important findings, relating the observations themselves to relevant studies, indicating contributions and limitations, without adding data already mentioned in other sections. It should also include deductions and lines for future research.
9. **Supports and acknowledgments (optional):** The Council Science Editors recommends the author (s) to specify the source of funding for the research. Priority will be given to projects supported by national and international competitive projects.
10. **The notes (optional):** will go, only if necessary, at the end of the article (before the references). They must be manually annotated, since the system of footnotes or the end of Word is not recognized by the layout systems. The numbers of notes are placed in superscript, both in the text and in the final note. The numbers of notes are placed in superscript, both in the text and in the final note. No notes are allowed that collect simple bibliographic citations (without comments), as these should go in the references.
11. **References:** Bibliographical citations should be reviewed in the form of references to the text. Under no circumstances should references mentioned in the text not be included. Their number should be sufficient to contextualize the theoretical framework with current and important criteria. They will be presented sequentially in order of appearance, as appropriate following the format of the IEEE.

3.2. Guidelines for Bibliographical references

Journal articles:

- [1] J. Riess, J. J. Abbas, "Adaptive control of cyclic movements as muscles fatigue using functional neuromuscular stimulation". IEEE Trans. Neural Syst. Rehabil. Eng vol. 9, pp.326–330, 2001. [Online]. Available: <https://doi.org/10.1109/7333.948462>

Books:

- [1] G. O. Young, "Synthetic structure of industrial plastics" in *Plastics*, 2nd ed., vol. 3, J. Peters, Ed. New York: McGraw–Hill, 1964, pp. 15–64.

Technical reports:

- [1] M. A. Brusberg and E. N. Clark, "Installation, operation, and data evaluation of an oblique–incidence ionosphere sounder system," in "Radio Propagation Characteristics of the Washington–Honolulu Path," Stanford Res. Inst., Stanford, CA, Contract NOBSR–87615, Final Rep., Feb. 1995, vol. 1

Articles presented in conferences (unpublished):

- [1] Vázquez, Rolando, Presentación curso "Realidad Virtual". National Instruments. Colombia, 2009.

Articles of memories of Conferences (Published):

- [1] L. I. Ruiz, A. García, J. García, G. Tafoada. "Criterios para la optimización de sistemas eléctricos en refinerías de la industria petrolera: influencia y análisis en el equipo eléctrico," IEEE CONCAPAN XXVIII, Guatemala 2008.

Thesis:

- [1] L.M. Moreno, "Computación paralela y entornos heterogéneos," Tesis doctoral, Dep. Estadística, Investigación Operativa y Computación, Universidad de La Laguna, La Laguna, 2005.

Guidelines:

- [1] IEEE Guide for Application of Power Apparatus Bushings, IEEE Standard C57.19.100–1995, Aug. 1995.

Patents:

- [1] J. P. Wilkinson, “Nonlinear resonant circuit devices,” U.S. Patent 3 624 125, July 16, 1990.

Manuals:

- [1] Motorola Semiconductor Data Manual, Motorola Semiconductor Products Inc., Phoenix, AZ, 1989.

Internet resources:

- [1] E. H. Miller, “A note on reflector arrays” [Online]. Available. <https://goo.gl/4cJkCF>

3.3. Epigraphs, Figures and Charts

The epigraphs of the body of the article will be numbered in Arabic. They should go without a full box of capital letters, neither underlined nor bold. The numbering must be a maximum of three levels: 1. / 1.1. / 1.1.1. At the end of each numbered epigraph will be given an enter to continue with the corresponding paragraph.

The charts must be included in the text according to order of appearance, numbered in Arabic and subtitled with the description of the content, the subtitle should go at the top of the table justified to the left.

Figures can be linear drawings, maps or black and white halftone or color photographs in 300 dpi resolution. Do not combine photographs and line drawings in the same figure.

Design the figures so that they fit eventually to the final size of the journal 21 x 28 cm. Make sure inscriptions or details, as well as lines, are of appropriate size and thickness so that they are not illegible when they are reduced to their final size (numbers, letters and symbols must be reduced to at least 2.5 mm in height After the illustrations have

been reduced to fit the printed page). Ideally, the linear illustrations should be prepared at about a quarter of their final publication size.

Different elements in the same figure should be spelled a, b, c, etc.

Photographs should be recorded with high contrast and high resolution. Remember that photographs frequently lose contrast in the printing process. Line drawings and maps should be prepared in black.

The text of the figures and maps must be written in easily legible letters.

If the figures have been previously used, it is the responsibility of the author to obtain the corresponding permission to avoid subsequent problems related to copyright.

Each figure must be submitted in a separate file, either as bitmap (.jpg, .bmp, .gif, or .png) or as vector graphics (.ps, .eps, .pdf).

4. Submission process

The manuscript must be sent through the OJS system of the journal, <<https://goo.gl/JF7dWT>>, the manuscript should be uploaded as an original file in .pdf without author data and anonymized according to the above; In complementary files the complete manuscript must be loaded in .doc or .docx (Word file), that is to say with the data of the author (s) and its institutional ascription; Also the numbered figures should be uploaded in independent files according to the corresponding in the manuscript (as bitmap .jpg, .bmp, .gif, or .png or as vector graphics .ps, .eps, .pdf). It is also obligatory to upload the cover letter and grant of rights as an additional file.

All authors must enter the required information on the OJS platform and only one of the authors will be responsible for correspondence.

Once the contribution has been sent the system will automatically send the author for correspondence a confirmation email of receipt

of the contribution.

5. Editorial process

Once the manuscript has been received in OJS, a first check by the editorial team of the following points:

- The topic is in accordance with the criteria of the journal.
- Must have the IMRDC structure.
- Must be in the INGENIUS format.
- Must use the IEEE citation format.
- All references should be cited in the text of the manuscript as well as charts, figures and equations.
- The manuscript is original; for this, software is used to determine plagiarism.

The assessment described above can take up to 4 weeks.

If any of the above is not complete or there is inconsistency, an email will be sent to the author to make the requested corrections.

The author will make the corrections and resend the contribution through an email in response to the notification and will also upload the corrected manuscript into OJS supplementary files.

The editorial team will verify that the requested corrections have been incorporated, if it complies, the manuscript will start the second part of the process that may be followed by the author through OJS, otherwise the author will be notified and the manuscript will be archived.

The second phase of the process consists of the evaluation under the methodology of double-blind review, which includes national and foreign experts considering the following

steps:

- The editor assigns two or more reviewers for the article.
- After reviewing the article, the reviewers will submit the evaluation report with one of the following results.
 - Publishable
 - Publishable with suggested changes
 - Publishable with mandatory changes
 - Non publishable
- The editor once received the evaluation by the reviewers will analyze the results and determine if the article is accepted or denied.
- If the article is accepted, the author will be notified to make corrections if required and the corresponding editorial process will be continued.
- If the article is denied, the author will be notified and the manuscript will be archived.
- In the two previous cases the result of the evaluation of the reviewers and their respective recommendations will be sent.

The second phase of the process lasts at least 4 weeks, after which they will be notified to the author giving instructions to continue with the process.

6. Publication

The INGENIUS Journal publishes two issues per year, on January 1st and July 1st, so it is important to consider the dates for sending the articles and their corresponding publication. Articles received until October will be considered for the January publication and those received until April for the July publication.

UNIVERSIDAD POLITÉCNICA SALESIANA DEL ECUADOR

Juan Cárdenas Tapia, sdb,
Rector

©Universidad Politécnica Salesiana
Turuhuayco 3-69 y Calle Vieja
Postal code 2074
Cuenca, Ecuador
Teléfono: (+593 7) 205 00 00
Fax: (+593 7) 408 89 58
Email: srector@ups.edu.ec

Exchange

Exchange with other periodicals is accepted.

Address:

Secretaría Técnica de Comunicación
Universidad Politécnica Salesiana
Turuhuayco 3-69 y Calle Vieja
Postal code 2074
Cuenca, Ecuador
Phone: (+593 7) 205 00 00 Ext. 1182
Fax: (+593 7) 408 89 58
Email: rpublicas@ups.edu.ec
www.ups.edu.ec
Cuenca – Ecuador

INGENIUS, Journal Science of Technology,
Special Issue 31: Additive Manufacturing
january/june 2024

John Calle Sigüencia, Editor in chief
revistaingenius@ups.edu.ec

Thematic Editors

Christian Cobos Maldonado, PhD
José J. G. Moura, PhD
Santiago Ferrandiz, PhD
Miguel Fernandez Vicente, PhD

Printed

Centro Gráfico Salesiano: Antonio Vega Muñoz 10-68 y General Torres.
Phone: (+593 7) 283 17 45
Cuenca – Ecuador
Email: centrograficosalesiano@lms.com.ec

OTHER PERIODIC PUBLICATIONS OF THE UNIVERSITY

UNIVERSITAS, Journal of Social and Human Sciences.

LA GRANJA, Journal of the Sciences.

ALTERIDAD, Journal of Education.

RETOS, Journal of Administration Sciences and Economics.

UTOPIA, University Youth Ministry Magazine.

SOPHIA, Collection of Philosophy of Education.



**ABYA
YALA** | UNIVERSIDAD
POLITÉCNICA
SALESIANA

